UNCLASSIFIED

JPL
TM 33-34
Cy 86

[redacted]

Downg[redacted]
[redacted] 12 years

Technical Memorandum No. 33-34

Mariner B Study Report

March, 1961

JET PROPULSION LABORATORY
LIBRARY
APR 11 1961

CALIFORNIA INSTITUTE OF TECHNOLOGY

jpl

JET PROPULSION LABORATORY
CALIFORNIA INSTITUTE OF TECHNOLOGY
PASADENA, CALIFORNIA

April 1, 1961

Classification Changed
UNCLASSIFIED
Authority
Executive Order #11652
Date 7-30-1975 By R. Castain

[redacted]

191496
[redacted]
CRIMINAL SANCTIONS
LOG-M01087

UNCLASSIFIED

UNCLASSIFIED

[redacted]

NATIONAL AERONAUTICS AND SPACE ADMINISTRATION
CONTRACT NO. NASw-6

Technical Memorandum No. 33-34

Mariner B Study Report

March, 1961

Classification changed to
UNCLASSIFIED
Authority
Executive Order #11652
Date
7-30-1975 G. Castain

JET PROPULSION LABORATORY
LIBRARY
APR 11 1961
CALIFORNIA INSTITUTE OF TECHNOLOGY

Copy No. 86
This document consists of
covers and 90 leaves.

JET PROPULSION LABORATORY
CALIFORNIA INSTITUTE OF TECHNOLOGY
PASADENA, CALIFORNIA

April 1, 1961

NATIONAL [redacted] INFORMATION
[redacted] DISCLOSURE [redacted] SUBJECT TO
CRIMINAL SANCTIONS

LOG-M01687

[redacted]

UNCLASSIFIED

UNCLASSIFIED

Copyright © 1961
Jet Propulsion Laboratory
California Institute of Technology

[redacted] information affecting the [redacted] of the defense of the United [redacted] of the Espionage Laws, Title [redacted] 794, the transmission or revelation of which in any manner to an unauthorized person is prohibited by law.

UNCLASSIFIED

UNCLASSIFIED

CONTENTS

I. Introduction 1

II. Mission Selection 5

A. Competing Missions 7

B. Scientific Critique of *Mariner B* 9

C. Mars Orbiter 11

D. Mars Lander 13

III. The Split Capsule 15

A. Mission Description 17

B. Spacecraft 19

1. Trajectories 19

2. Space Science 30

3. Midcourse-Guidance Analysis 34

4. Guidance and Control 39

5. Communications 77

6. Power 79

7. Propulsion 85

8. Configuration 89

C. Capsule 95

1. Approach Trajectory and Accuracy Analysis 95

2. Entry Dynamics and Heating 108

3. Space Science 133

4. Communications 135

5. Power 139

6. Configuration 140

Appendixes

A. Capsule Propulsion 151

B. Alternate Spacecraft Configurations 153

UNCLASSIFIED

UNCLASSIFIED

FIGURES

1. Impulse-velocity requirements for Mars orbit 11
2. Mars 1964, time of flight vs launch date 20
3. Mars 1964, declination of near-Earth conic asymptote vs launch date 21
4. Mars 1964, heliocentric central angle vs launch date 21
5. Mars 1964, Earth–Mars communication distance vs launch date . . 22
6. Mars 1964, asymptotic velocity of probe with respect to Mars vs launch date 22
7. Mars 1964, angles between hyperbolic excess-velocity vector and arrival planet's orbital plane vs launch date 23
8. Mars 1964, angles between arrival hyperbolic excess-velocity vector and Mars–Sun vector vs launch date 23
9. Allowable separated spacecraft weight C_3 24
10. C_3 vs launch date (for Mars encounter) 24
11. Allowable separated spacecraft weight vs firing period to Mars . . 24
12. Parking-orbit coast time vs launch date (arrival date, 14 July 1965) 25
13. Launch time (E.S.T.) vs launch date (arrival date, 14 July 1965) . . . 26
14. Mars 1964 Earth track (launch date, 15 November 1964; arrival date, 14 July 1965) 26
15. Heliocentric transfer orbit (launch date, 15 November 1964; arrival date, 14 July 1965) 27
16. Heliocentric transfer orbit (launch date, 6 December 1964; arrival date, 14 July 1965) 27
17. Earth–probe communication distance (arrival date, 14 July 1965) . . 28
18. Earth–probe–Sun angle vs calendar date (arrival date, 14 July 1965) 29
19. Earth–probe–Mars angle vs calendar date (arrival date, 14 July 1965) 29
20. Sun–probe–Mars angle vs calendar date (arrival date, 14 July 1965) 30
21. Guidance-analysis coordinate system 34
22. Approach-guidance geometry 38
23. Probability of miss-maneuver capability 39
24. Autopilot diagram 43
25. Approach-guidance loop 47
26. Single-plane approach guidance, two-correction maneuver 47
27. Effect of yaw pointing error 51

UNCLASSIFIED

UNCLASSIFIED

FIGURES (Cont'd)

28. Spacecraft-centered celestial triangles 51
29. Planet-centered coordinate system for approach guidance 52
30. Sun–spacecraft–planet plane 52
31. Spacecraft-centered celestial triangle 53
32. Secondary-reference roll search and acquisition modes 59
33. Directional-antenna control 61
34. Planetary horizontal-platform control loop 63
35. Optimum reaction-sphere weight and radius for $i = 2$ 65
36. Optimum reaction-sphere weight and radius for $i = 3$ 65
37. Pitch- and yaw-control loop 67
38. Schedule of operations, spacecraft power system 80
39. Battery-charge status 82
40. Segmented concentrator 84
41. Midcourse and approach-correction propulsion system 86
42. Total propulsion-system mass as a function of injected gross spacecraft mass 88
43. *Mariner B* spacecraft, incorporating solar panels 90
44. *Mariner B* spacecraft, incorporating a solar collector 91
45. Estimated weights of Table 23 compared with firing period 92
46. Earth–Mars solar geometry 96
47. Typical Mars 1964 trajectory 96
48. Approach geometry for split-capsule Mars trajectory 97
49. Description of miss-distance coordinates 97
50. Reference-vector traces on a Mars-centered celestial sphere . . . 98
51. Mars seen from spacecraft as it will appear for a 14 July 1965 arrival 99
52. Spacecraft aiming points 99
53. Sun–probe–near-Mars-limb angle vs time 100
54. Earth–probe–near-Mars-limb angle vs time 100
55. Canopus–probe–near-Mars-limb angle vs time 101
56. Mars angular diameter vs time 101
57. Spacecraft altitude-reference system 102
58. Mars cone angle β vs time 103
59. Mars clock angle α vs time 103
60. Earth–probe–Sun angle during transit 104
61. Mars split-capsule trajectories—effect of miss-maneuver magnitude ΔV 104
62. Mars split-capsule trajectories—communication time for 90-deg flyby impulse 105

UNCLASSIFIED

UNCLASSIFIED

FIGURES (Cont'd)

63. Mars split-capsule trajectories—effect of flyby impulse direction θ 106
64. Mars split-capsule trajectories—effect of impulse direction on "eclipse" time for a 20-deg entry angle 107
65. Mars split-capsule trajectories—effect of impulse direction on "eclipse" time for a 40-deg entry angle 107
66. Mars split-capsule trajectories—effect of impulse direction on "eclipse" time for a 52-deg entry angle 107
67. Entry angle vs miss distance, Mars 110
68. Central angle vs miss distance, Mars 110
69. Mars entry, velocity history—effect of entry angle 112
70. Mars entry, altitude history—effect of entry angle 113
71. Mars entry, path-angle history—effect of entry angle 114
72. Mars entry, trajectory geometry—effect of entry angle 115
73. Mars entry, velocity history—effect of entry velocity 115
74. Mars entry, altitude history—effect of entry velocity 116
75. Mars entry, path-angle history—effect of entry velocity 116
76. Mars entry, trajectory geometry—effect of entry velocity 116
77. Mars entry, heating rate and total heat—effect of entry angle . . . 117
78. Mars entry, heating rate and total heat—effect of ballistic coefficient 117
79. Mars entry, heating rate—effect of entry velocity 118
80. Mars entry, Reynolds number—effect of entry angle 119
81. Mars entry, Reynolds number—effect of ballistic coefficient . . . 119
82. Mars entry, Reynolds number—effect of entry velocity 119
83. Mars entry, deceleration—effect of entry angle 120
84. Mars entry, deceleration—effect of ballistic coefficient 120
85. Mars entry, deceleration—effect of entry velocity 121
86. Entry-attitude-envelope function for large entry angles 121
87. *Mariner B* entry capsule—heat-shield weights 123
88. *Mariner B* typical-entry body configuration 125
89. Time for a terminal-velocity descent on Mars 126
90. Parachute-opening load constraint 127
91. Mars-atmosphere model temperature vs altitude 129
92. Mars-atmosphere model density vs altitude 129
93. Communications sequence of events 136
94. Capsule-to-spacecraft communication system 137
95. Null probability for a randomly oriented dipole-antenna pattern . . 138
96. Available capsule noise bandwidth 138

UNCLASSIFIED

UNCLASSIFIED

FIGURES (Cont'd)

97. Three-hundred-pound entry capsule 142
98. Artist's rendition of capsule 143
99. Aerodynamic profile of entry capsule 144
100. Configuration schematic of 80-lb entry capsule 146
A-1. Typical capsule configuration with solid-propellant spin and deflection rockets 152
B-1. Capsule aft 154
B-2. Capsule forward, antenna on centerline, four motors 155
B-3. Capsule forward, antenna on centerline, single motor, panels with reflectors 156
B-4. Antenna off centerline, electronics on centerline 157
B-5. Foldable feed on antenna 158
B-6. Largest electronics volume 159
B-7. Antenna forward, four motors 160
B-8. Triangular structure with solar panels 161
B-9. Triangular structure with single fixed solar concentrator 162
B-10. Modified *Mariner A* 163
B-11. Triangular structure with single fixed solar concentrator and motor on capsule 164
B-12. Modified *Mariner A* with motor on capsule 165
B-13. Two large movable solar concentrators 166
B-14. Four movable solar concentrators 167
B-15. Triangular structure with elliptic paraboloid concentrators and antenna 168
B-16. Solar panels stowed along centerline 169

TABLES

1. Mars-orbiter data 12
2. Compilation of spacecraft scientific experiments 33
3. Standard coordinate deviations and correlations for four Mars trajectories 35
4. Uncorrected 1-σ Mars miss 36
5. Required 1-σ midcourse capability 36
6. Midcourse-error coefficients 37
7. Miss at Mars due to midcourse errors 37
8. Time-of-flight variation due to midcourse errors 37
9. Approach-maneuver velocity requirements 39

UNCLASSIFIED

UNCLASSIFIED

TABLES (Cont'd)

10. Summary of guidance-control instrument-configuration discussion with accuracy estimates 70
11. Estimated approach-guidance measurement errors vs error sources and types 72
12. Example of Sun–probe–planet angle measurement errors 73
13. Spacecraft-to-Earth link (at Mars) 78
14. Earth-to-spacecraft link (at Mars) 78
15. Spacecraft communication-system weights 79
16. Regulated and raw-power requirements 80
17. Spacecraft power-system characteristics 83
18. Assumed mission parameters 87
19. Maneuver requirements 87
20. Propulsion-system description 87
21. Comparison of midcourse-propulsion systems 88
22. Elements of configuration 90
23. Weight summary, lb 92
24. Capsule–spacecraft communication optimization 104
25. Typical *Mariner B* encounter sequence 105
26. Comparison of typical entry situations 109
27. Approach- and entry-parameter summary 111
28. Typical quantities during capsule entry 123
29. Typical low-temperature-ablation material characteristics 125
30. Final-descent quantities 126
31. Errors for altitude-controlled parachute deployment 127
32. Errors for velocity-controlled parachute deployment 128
33. Mars-atmosphere model 130
34. Compilation of capsule scientific experiments 134
35. Capsule-to-spacecraft link (at impact) 136
36. Capsule communications-weight breakdown 138
37. Power-sytem characteristics 139
38. Capsule weight breakdown 144
39. Minimal capsule weight breakdown 146
40. Effect of atmospheric uncertainties on ablation plus insulation weights 146

UNCLASSIFIED

UNCLASSIFIED

PART I
INTRODUCTION

UNCLASSIFIED

INTRODUCTION

C. R. GATES

(This Part is UNCLASSIFIED)

In August, 1960, the Planetary Program Office, Jet Propulsion Laboratory (JPL), commissioned a study of the *Mariner B* mission, which mission is directed toward sending a spacecraft to Mars in 1964 using the *Centaur* vehicle as a booster. The study group included members from the various technical disciplines at JPL, and the results of the study are presented in this Report.

The purposes of the study were to (a) examine and assess the feasibility of possible missions, (b) select and recommend a most promising mission, and (c) describe means for accomplishing the recommended mission. Thus, the study is intended to establish a framework from which detailed preliminary design of the spacecraft can proceed. Certain areas were deliberately excluded from the study, including manpower and funding considerations, launch-vehicle and launch-facility availability, and the ground complex of data-processing equipments.

In Part II of the Report an examination of the various missions which were considered is presented, together with the reasons for selecting the recommended mission. In Part III the recommended mission is described in detail.

The essential conclusion of the study is that the *Mariner B* mission should involve a split capsule, in which the main body of the spacecraft passes by the planet and a small, passive capsule separates from the spacecraft and impacts the planet.

UNCLASSIFIED

A. COMPETING MISSIONS

C. R. GATES

(This Section is CONFIDENTIAL)

1. Planning Considerations

In planning for future spacecraft experiments, one is usually confronted with three considerations: (a) The experiment should be conservative and should be based, to the maximum extent possible, on previous experience, technology, and components; (b) the experiment should, in its own right, be significant in the contributions that it makes to technology and scientific knowledge; and (c) the experiment should be daring and imaginative, should take a substantial stride forward, and should bridge the gap between our present state of knowledge and the more distant future. It is rare for these considerations not to lead in diverse directions.

For the *Mariner B* study, the present state of technology may be typified by the *Mariner A* spacecraft. The *Mariner A* spacecraft is intended to accomplish a Venus fly-by mission, with launching in mid-1962 and arrival at Venus in late 1962. This spacecraft is fully attitude-stabilized, using the Sun and the Earth as references; it has Sun-oriented solar panels with batteries for backup and intermittent operation; it has a propulsion system and can execute midcourse corrective maneuvers; it has a two-way communication system with a directional antenna which can be oriented in the direction of the Earth; and, it has a "horizontal platform" on which are mounted a variety of scientific instruments and which can be oriented in the direction of the target planet when the spacecraft is near the planet. The *Mariner A* spacecraft has neither approach nor terminal guidance, and its dispersion is too large to hit the planet reliably.

The goal of the *Mariner B* spacecraft is to accomplish a Mars mission, with launching late in 1964 and arrival in mid-1965, utilizing the *Centaur* vehicle as booster. Looking beyond the *Mariner B* in order to gage the gap which the *Mariner B* should fill, the *Voyager* series of spacecraft is seen* with launchings in the interval from 1966 to 1970. The missions of the *Voyager* spacecraft are to accomplish landings and to place precision orbiters about Mars and Venus. Thus, among the technological accomplishments that will be needed for the *Voyager* missions are: (a) approach guidance which will place the spacecraft into desired relation with respect to the planet; (b) techniques for aerodynamic entry into a planetary atmosphere; and (c) propulsion systems for the addition of the relatively large velocity increments required by the planetary orbiters.

2. Morphology

It will be instructive to examine those missions which might be feasible and to measure these missions against the goals and the technological developments discussed in the preceding Section.

First, the return experiment will be investigated. It has been variously proposed that a spacecraft be directed toward Mars, pass by Mars at a relatively close distance while obtaining scientific information, and subsequently return to the Earth where entry and recovery would be accomplished in order that the scientific information, particularly photographic plates, might be physically recovered. Trajectories are available for such a mission with modest midcourse requirements, although the flight times are very long. Such a mission is unattractive, since the quality and quantity of data which can be transmitted over the radio link from the spacecraft to the Earth is entirely adequate. Experience on Earth-entry and recovery of the spacecraft would be valuable, but such experience can be obtained more directly than by sending the spacecraft to Mars and back.

A second mission to consider is the "flyby," in which the spacecraft simply passes by the planet. That such a mission appears to be only a repetition of the *Mariner A* mission lessens its attractiveness. However, approach guidance could be added in order to position the spacecraft more precisely with respect to the planet, and since

*"Ten-Year Plan," Planning Report No. 35-1, Jet Propulsion Laboratory, Pasadena, Calif., September 1, 1960 (CONFIDENTIAL).

UNCLASSIFIED

the spacecraft at encounter is further from the Earth and from the Sun, new demands will be put on the communications and power subsystems.

A third mission to be considered is the planetary orbiter. With the exception of the scientific-instruments area, an orbiting planetary spacecraft would require, in addition to the propulsion system needed for the retromaneuver to place the vehicle in orbit, virtually all of the subsystems needed for the fly-by mission. Thus, such a mission might be difficult to attain, particularly since the velocity increments required for the retromaneuver are large. It would be possible, in principle, to remove part of the vehicle's approach velocity by grazing the atmosphere of the target planet. However, such a procedure requires control of the "miss" distance of the vehicle to only a few kilometers, and, as will be shown in Part III, the approach-guidance system which may be expected in 1964 will not possess this accuracy.

A fourth mission for consideration is that of landing upon the surface of the planet. The remarks made above regarding the accuracy required for a grazing encounter are again applicable, and the shallow type of re-entry which has been proposed for manned entry to the Earth could not be considered; a relatively direct entry into the atmosphere would be required. Moreover, with the exception of the scientific instruments, virtually all of those subsystems needed for the fly-by mission would be required simply to get the vehicle to Mars. In addition, protection during the entry phase would be required, and the landed vehicle would be confronted with the formidable problem of communicating with the Earth from the surface of the planet.

The above four missions appear to exhaust the morphological treatment. Either the spacecraft returns to the Earth, or it flies by the planet, or it remains in the vicinity of the planet; if it remains in the vicinity of the planet, it can either go into orbit or land upon the surface of the planet. However, as on the *Ranger* program, it may be profitable to combine two of these missions. For example, one might (a) place the main body of the spacecraft in orbit around the planet and subsequently direct a small capsule to enter the atmosphere and land upon the surface; (b) the main body of the spacecraft might be directed to go by the planet and place a small capsule in orbit about the planet; or (c) the main body of the spacecraft might be directed to fly by the planet and send a small capsule to enter the atmosphere of the planet and land upon its surface. Of these three alternatives, the last appears to be the most promising. The first alternative, the orbiter and lander, seems unattractive because simply placing a spacecraft in orbit about the planet appears to be sufficiently ambitious. The second alternative, the flyby plus orbiter, is unattractive because such an orbiter would obtain little or no information which could not be obtained from the fly-by vehicle. The third alternative, which will subsequently be referred to as the split capsule, appears attractive and will be discussed further.

UNCLASSIFIED

B. SCIENTIFIC CRITIQUE OF *MARINER B*

R. W. DAVIES

G. NEUGEBAUER

(This Section is UNCLASSIFIED)

Scientifically, the *Mariner B* program is almost purely exploratory, and this is reflected in the choice of experiments.

Earth-based observations of Mars have helped to orient the exploratory program and have made it possible to ask questions, the answers to which would greatly increase our understanding of the planet. The observations of the distinct surface features of Mars, and especially of seasonal changes in these surface features, have excited the popular and scientific imaginations for many years. The question of the existence of extraterrestrial life has become one of the cornerstones of the space program, to a large extent because of the observation of Mars.

The character of the Martian atmosphere is also important, and it is logical to learn more about it in conjunction with investigations of the surface, because the surface and atmosphere interact strongly. The uncertainties relating to the atmosphere are sufficiently small (in contrast to those concerning Venus) that engineering studies for a landing can be formulated. More precise upper limits on the amounts of constituents in the atmosphere would not materially influence the initial stages of the scientific program, although accurate density measurements would make the engineering planning of subsequent missions more secure.

The scientific portion of this study was initiated at the request of the National Aeronautics and Space Administration (NASA) Planetary and Interplanetary Subcommittee. It was their belief that a capsule–spacecraft mission would be of extreme interest. The present study of the scientific subsystem confirms that belief. The capsule–spacecraft system offers several exciting possibilities, and was studied in fairly great detail. Time limitations did not permit an adequate technical comparison with a flyby designed to take advantage of the additional 300 lb that the omission of a capsule might provide.

The flyby can be considered a step toward a Martian orbiter, whereas the capsule is a step toward a long-life soft lander. Scientifically, an ideal Martian mission would be a combination orbiter–lander that could operate intermittently for a Martian year. Nevertheless, as the subsequent discussion will demonstrate, an interesting and valuable set of scientific experiments can be performed within the constraints of time, orientation, and communication capabilities of the capsule–spacecraft system.

UNCLASSIFIED

C. MARS ORBITER

W. GIN

(This Section is CONFIDENTIAL)

1. Introduction

Although the scientific value of the planetary orbiter is great, the energy requirements for establishing a useful spacecraft in orbit are in excess of the capability that can reasonably be expected in 1964. However, an analysis of the weights that can be injected into orbit was made to ascertain this fact.

2. Problems and Assumptions

The problem is to place the *Mariner B* spacecraft into an elliptical orbit about Mars. The hyperbolic excess velocity with respect to the planet is taken to be 4.5 km/sec. The orbit selected for this discussion has a periapsis altitude of 800 km and an apoapsis altitude of 16,000 km. In general, the minimum altitude is constrained by the dispersion, and the maximum altitude is dictated by the feasibility of scientific investigation. Figure 1 shows that any increase in periapsis would require more retroenergy, whereas an increase in apoapsis would conserve relatively little retroenergy. (For altitude-biased ignition as described below, the impulse is not applied at the vertex of the approach hyperbola, and the impulse-velocity requirement is about 20% greater than shown in Fig. 1.)

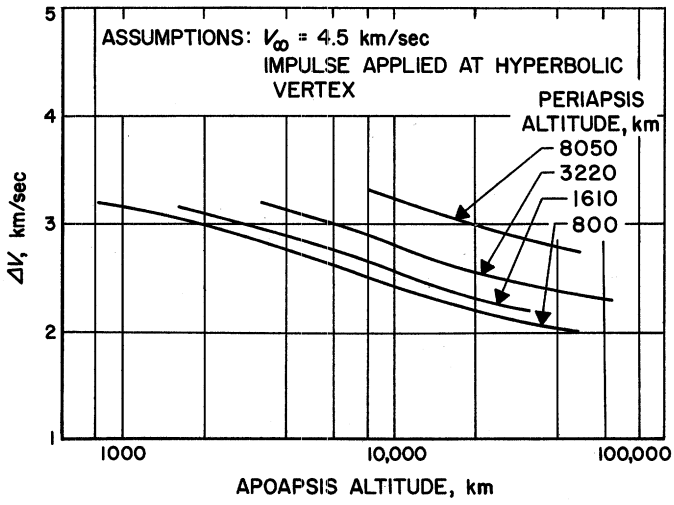

Figure 1. Impulse–velocity requirements for Mars orbit

In order to compare the orbiter with the split-capsule mission, the same spacecraft boost-injected weight of 2055 lb is assumed. A hydrazine monopropellant midcourse and approach propulsion system is used which provides one midcourse correction and two approach corrections. The propellant weight is 126 lb, and the propulsion-system inert weight is 82 lb. The midcourse and approach propulsion-system weights are quoted only for reference and are not used in the calculation of the retromaneuver. The weight before retroignition conservatively reflects the situation in which midcourse and approach propellant has not been spent, because the spacecraft is on the desired nominal trajectory. Therefore, the weight before retroignition is the injected weight.

The guidance-and-control and trajectory accuracies are assumed to be the same as those for the split-capsule mission: a 2-σ dispersion of $\pm$800 km, or a total possible 1600-km variation in the periapsis altitude of the approach hyperbola. The nominal approach hyperbola has a periapsis of 1600 km, and a single retroimpulse is triggered by an altimeter at a predetermined altitude of 2400 km, which assures ignition within the $\pm$800-km dispersion. In the most severe case, the periapsis of the approach hyperbola is 800 km above the surface. The motor is fired at a constant pitch angle of 53 deg counterclockwise to the local horizontal. No prior jettisoning or expenditure of midcourse- and approach-maneuver fuel is assumed.

The retrorocket is a solid-propellant motor with liquid injection to provide thrust-vector control. A propellant specific impulse of 300 sec and a motor mass fraction

UNCLASSIFIED

(ratio of loaded propellant to total initial motor weight) of 0.93 are used. This performance capability reflects the conservatively projected state of the art for the time period of the mission.

The results of the calculations are shown in Table 1. The case for an injected weight of 1750 lb, which is a possible (and perhaps more likely) *Atlas–Centaur* boosted weight, is also shown.

Table 1. Mars-orbiter data

Orbital parameters		
Hyperbolic excess velocity relative to Mars, km/sec	4.5	
Dispersion of entry altitude, km	±800	
Pitch angle, deg	53.2	
ΔV for retromaneuver, km/sec	2.72	
Periapsis, km (from center)	4,120	
Apoapsis, km (from center)	19,320	
Minimum altitude, km (from surface)	800	
Maximum altitude, km (from surface)	16,000	
Orbiting period, hr	22.6	
Weight summary	Gross weight prior to retro	
	2055 lb	1750 lb
Retrorocket-motor weight, lb	1333	1134
Gross weight in orbit, lb	815	695
Weight in orbit excluding propulsion hardware, lb	514	438

3. Conclusions

The inescapable conclusion from the weights shown in Table 1 is that the *Mariner B* Mars-orbiter mission is not feasible technically. The weight in orbit, excluding all propulsion hardware, of 400 to 500 lb is not enough to accommodate all the other essential subsystem requirements for power, communications, structure, scientific instrumentation, etc. It is estimated that the weight in orbit, excluding propulsion hardware, must be increased by a factor of about two to three over that shown in Table 1 before such a mission is practicable.

Various approaches may be adopted to increase the total performance capability. These include the relaxation of the dispersion tolerance on the approach trajectory, increasing the ellipticity of the orbit, using a two-stage retromaneuver, assuming a more risky but higher state-of-the-art performance for the retrorocket, and jettisoning useless weight prior to retroignition. All these approaches, except for dropping useless weight, will afford only small gains in payload in orbit. For example, if the midcourse- and approach-propulsion system with its full load of propellant were jettisoned before retroignition, the final payload in orbit, excluding remaining propulsion hardware, might be increased by only 25%. It appears, therefore, that Mars orbiters must be deferred until the *Voyager* series is operational.

UNCLASSIFIED

UNCLASSIFIED

D. MARS LANDER

J. DAVIS

(This Section is UNCLASSIFIED)

Consideration was given in this study to a landing vehicle as a candidate for the *Mariner B* mission to Mars. The following is a summary of the general requirements of such a mission, which strongly affect the desirability of a lander as a first mission:

(1) The spacecraft must incorporate those subsystems or functions required for the cruise mode.

(2) The spacecraft must incorporate designs in the areas of structure, heat shield, parachute- and landing-energy absorbers as dictated by the current and the best assumption of the atmospheric parameters, surface winds, and surface characteristics and their attendant uncertainties.

(3) The entry spacecraft must communicate directly with the Earth through utilization of an articulated high-gain antenna. Orientation of the antenna toward Earth during the motions of entry is impractical, and entry data must therefore be collected and stored for transmission after landing.

(4) The spacecraft must survive landing and provide for orientation, Earth-tracking, and instrument operation.

(5) The difficulties in deployment and general utilization of solar panels of the area required at Mars will most likely dictate the incorporation of more advanced or unique power sources such as fuel cells, nuclear devices, wind mills, etc.

As was pointed out in item (1) above, the lander must possess a cruise or midcourse mode of operation, which means that it must function as a spacecraft, with attitude, power, propulsion, communication, guidance, etc. Later in this Report it will be shown that these functions consume most of the weight which the *Centaur* can launch to Mars. In addition, however, the lander must be protected for atmospheric entry, must survive landing, and must operate on the surface for a reasonable time. When the weights associated with those functions are added to that of the cruise spacecraft, the weight exceeds the capability of the *Centaur* by many times.

UNCLASSIFIED

UNCLASSIFIED

PART III
THE SPLIT CAPSULE

UNCLASSIFIED

A. MISSION DESCRIPTION

C. R. GATES

(This Section is CONFIDENTIAL)

1. Introduction

In this Section the split-capsule mission will be described in general terms. In succeeding Sections the spacecraft and capsule subsystems will be discussed in detail.

Assuming that the *Mariner A* Venus spacecraft is a starting point for this study, certain different and fundamental requirements for a Mars spacecraft are immediately apparent. In particular, the flight times and communication distances are roughly doubled, and the solar-radiation intensity is cut in half. Furthermore, the imminent *Voyager* missions—planetary satellites and landings—demand the development of approach guidance.

The capsule represents an attempt to gain needed engineering and scientific knowledge which cannot be obtained from the spacecraft. The capsule should be in parallel, rather than in series, with the spacecraft, in the sense that the presence and behavior of the capsule should not jeopardize the spacecraft. Of course, this objective, like perfection, can only be sought after and is not fully attainable; for example, the weight allotted to the capsule could probably be used in increasing the reliability of the spacecraft.

2. Flight Sequence

For the split-capsule mission, launching will occur from the Atlantic Missile Range (AMR) in late November and early December, 1964. Some extension to the shroud of the *Centaur* vehicle may be needed. Conventional southeast azimuths are satisfactory, and injection occurs off the east coast of South Africa. The flight time is in excess of 200 days, and arrival at Mars occurs in July 1965.

The sequence from injection through midcourse maneuver(s) resembles that of *Mariner A*. The spacecraft is separated and the launch vehicle is retarded by retrorockets. Storage batteries supply power until Sun acquisition occurs, after which the principal axis of the spacecraft is pointed toward the Sun and a solar-energy collection and conversion system supplies power. The spacecraft needs 380 w of raw power, which requires, at the distance of Mars, 164 ft^2 of solar panels. A more efficient solar-thermionic system is also being considered (see Section IIIB-6).

Following solar acquisition a 4-ft antenna radiating 25 w at 2300 mc is pointed toward the Earth. While the *Mariner A* spacecraft uses a Sun–Earth attitude reference, the *Mariner B* will be capable of using a Sun–star reference.

Next, one or two midcourse maneuvers, based on radiotracking data, will be executed. The midcourse propulsion system will, as in *Mariner A*, use monopropellant hydrazine motors; however, the thrust level will be increased to 200 lb. Configurations using a single motor on the centerline and several motors off the centerline have been examined. One may recall that space on the spacecraft centerline is at a premium; also, several motors off the centerline can better accommodate variations in the center of gravity.

During the coasting flight various measurements of the behavior of the spacecraft and the nature of the interplanetary medium will be transmitted to the Earth.

As the spacecraft approaches Mars, the approach-guidance system begins to function. In this system the angles between Mars and other visible objects, such as the Sun, stars, planets, etc., are measured, and a corrective maneuver is computed. The magnitude of a typical approach maneuver would be several tens of meters per second, and it is thus comparable to, although somewhat greater than, a midcourse maneuver. The maneuver would be executed in a direction approximately perpendicular to the flight path. The computations required are not complex, and could be performed in the spacecraft, on the Earth, or in some combination of the two.

The approach-guidance system is such that maneuvers made remote from the planet require small velocity increments but yield high dispersions at the target, while the converse holds for maneuvers made close to the target. It is economical to make more than one maneuver, and for the *Mariner B* mission two maneuvers appear adequate. The first maneuver would be performed at a distance of one to two million kilometers from Mars, and

UNCLASSIFIED

the second at about one-half million kilometers. The resultant dispersion at the target would be several hundred kilometers.

It is proposed that the spacecraft–capsule combination be placed on a trajectory which, if continued, would impact the planet. The two approach maneuvers would, as required, correct the vehicle to such a trajectory. Following the second approach maneuver the capsule will be released and allowed to hit the planet; the spacecraft will be accelerated laterally by means of a "separation maneuver" so as to miss the planet by a distance of about 8000 km. Approximately 20 hr will elapse between separation and entry.

The capsule will be passive and will make an uncontrolled, aerodynamic entry into the atmosphere of Mars. The capsule will weigh approximately 300 lb and will be of a blunt, nose-cone-like configuration. It will consist of structure, ablation and heat-protection material, a parachute for final descent, a radio transmitter for establishing one-way communication from capsule to spacecraft, batteries, and scientific instruments.

As the capsule enters the atmosphere its angular orientation will be random, and atmospheric forces will act so as to point the protected side of the capsule toward the surface. An acceleration of 30 to 50 Earth g's will be experienced briefly, and measurements of this acceleration, together with pressure and temperature, will be relayed to the parent spacecraft. When the capsule has slowed sufficiently, a parachute will be deployed from the rear of the capsule in order to yield a final impact speed at the surface which may permit the capsule to survive. Some scientific measurements after impact appear feasible, although the random orientation of the capsule may present difficulties. In addition, it appears feasible to provide photographic coverage during the descent phase.

From separation to impact, the capsule is visible to the spacecraft. However, shortly after impact the spacecraft, as seen from the capsule, will go below the horizon and will appear to set. About 1 hr will pass before the spacecraft will appear to rise, and about 12 hr before the spacecraft sets again. The exact times of setting and rising are strong functions of the impact point of the capsule and of the trajectory of the spacecraft. The distance between capsule and spacecraft increases rapidly after the impact of the capsule, and since the communication link between spacecraft and capsule is not highly directive, it will not be possible to maintain communication for more than about one-half the period of rotation of the planet.

The parent spacecraft will receive, store, and retransmit to the Earth the data obtained from the capsule. In addition, the spacecraft will contain instruments for making independent and significant scientific measurements of the planet. A number of the planetary scientific instruments will be mounted on a platform which can be pointed toward the planet so as to observe radiation from the planet at a variety of frequencies.

3. Remarks

A number of technical problems attend the split-capsule idea and deserve further investigation. Not the least of these problems is the fact that the ability of the launch vehicle to carry the weight required by this mission appears marginal. Various solutions may be possible. For example, a capsule of reduced weight may be appropriate. Another alternative, in the event that it is desired to fire two spacecraft at the 1964 Mars opportunity, is to fire one spacecraft with the capsule in the middle of the firing period and a second spacecraft without the capsule at either the beginning or the end of the firing period. A third alternative, of course, is to remove the capsule entirely, and the split-capsule concept contains this convenient and ready-made backup position.

A number of challenging technical problems appear in the capsule itself. Two of the most pressing of these problems are (a) the stability of the capsule upon entry and (b) the communications link between capsule and spacecraft. These, as well as other problems, will be discussed in detail throughout the Report.

A final problem is that of reliability and sterilization. It is proposed that the spacecraft–capsule combination be placed on a trajectory which would, without the final separation maneuver, result in the spacecraft hitting the planet. Thus, a loss in the approach-guidance and propulsion system would cause complete loss of the mission, and the possibility of the spacecraft hitting the planet may require that it be sterilized. A possible solution to this problem, which is discussed in detail in Appendix A, is to place a propulsion system on the capsule. In this arrangement, the spacecraft–capsule combination would be placed on a trajectory which would miss the target planet. Then, in place of the separation maneuver, the capsule would be accelerated laterally by means of its own propulsion system so as to cause it to hit the planet. Since the capsule weighs far less than the spacecraft, less fuel is consumed in this maneuver, and a weight saving in fuel results. The disadvantage, of course, is the complexity involved in the additional propulsion system and the means by which it must be controlled.

UNCLASSIFIED

B. SPACECRAFT

1. Trajectories

W. E. BOLLMAN

(This Section is CONFIDENTIAL)

a. Introduction

In the analysis of trajectories to Mars in 1964, four major parameters were observed: payload capability, declination of outgoing asymptote, error sensitivity, and asymptotic approach speeds near Mars. The subsequent paragraphs include Martian trajectories in general, Martian trajectory selection, and typical trajectories.

b. Characteristics of Martian Trajectories in 1964

Several characteristics of Martian trajectories are shown in Figs. 2 to 8 as a function of launch date in 1964. The lowest C_3 (twice total geocentric energy) shown in the Figures is the minimum-energy trajectory to Mars in 1964. As shown in all seven Figures, two Martian trajectories of a constant geocentric energy, which is greater than the minimum energy, exist for a given launch date within a specific launch-time interval for heliocentric central angles* less than 180 deg. The earliest and latest possible firing dates to Mars for a constant geocentric energy may be found at the two extremes of the closed loop (points of vertical tangency). The curves are plotted such that the top part of one curve of a constant energy corresponds to the top part of any other curve of the same geocentric energy. Pertinent trajectory characteristics for a given launch date and arrival date can be found from the plots.

c. Planetary Trajectory Selection

Examination of the Martian trajectories (Fig. 2 to 8) for a planetary launch era reveals a wide range of possibilities. To limit this range, it is appropriate to seek trajectory constraints based on practical engineering considerations. Such constraints can come from the areas of attitude control, guidance, power communication, and scientific mission. More familiar constraints are those associated with tracking, range safety, error sensitivity, and payload capability.

(1) Preinjection Trajectory Selection

(a) Payload capability and declination of asymptote. The amount of injected weight for any vehicle is dependent on the preinjection trajectory. In selecting the preinjection trajectory to Mars, the declination of the outgoing asymptote is the major parameter to observe. As the launch date and required flight time vary, the declination of the outgoing asymptote will vary (see Fig. 3). This, in turn, causes the central angle between the launch pad and the asymptote to change. Variations of the central angle require the use of a parking orbit between the first and second *Centaur* burning periods in order that injection may occur near perigee of the near-Earth conic. This positioning of injection will tend to maximize the payload capability. It is found that asymptotes with increasingly positive declinations require longer parking orbits. Asymptotes with increasingly negative declinations require shorter parking orbits. If the absolute value of the declination of the asymptote is greater than the latitude of the launch pad (28.309° for AMR), then utilization of a band of launch azimuths symmetrically about 90° east of north will not allow the probe to reach the desired declination without additional variation in yaw during powered flight and subsequent payload losses. Launch azimuths are restricted by range-safety requirements to lie between 46 and 114° east of north. However, the southeast launchings (94 to 114°) are preferred in order to utilize the deep-space-net facilities. Payload calculations are made using the *Centaur* vehicle as defined in Section IIIA, a 100-nm circular parking

*Heliocentric central angle is defined as the angle between the Earth at launch, the Sun, and the planet at arrival, directed from the Earth–Sun line measured eastward.

orbit between the two *Centaur* burnings, and a launch azimuth of 114° east of north. Figure 9 shows a plot of allowable spacecraft weight vs. C_3.

Notice in Fig. 3 that for launch dates earlier than November 15, the declination of the asymptote varies several degrees per day for a given arrival date. For a few of the launch days in this period, the declination of the asymptote is greater than the latitude of the launch site. Such trajectories would not be utilized.

(b) Firing period. In order to allow flexibility in the mission, a several-day firing period is essential. The possibility of two shots to Mars in 1964 is dependent on several factors: (1) whether one or two launch pads are available, (2) the minimum interval between firings, and (3) the required geocentric energy or payload capability over the entire firing period.

(2) Postinjection Trajectory Selection

Trajectory-error sensitivity is a strong function of flight time. In other words, the higher the flight time, the greater the error sensitivity. However, high flight times are essential for minimum-energy-type trajectories and for maintaining low asymptotic approach speeds near Mars. Low asymptotic approach speeds are preferred to the higher speeds for several reasons: (1) Less impulse is needed for a miss maneuver near the planet, (2) longer communication time between bus and capsule is available, (3) survival of the capsule is more likely, (4) angular rates of the bus near Mars are less, and (5) there is more time for the power-cruising mode near the planet.

d. Typical Trajectories

(1) General Properties

With the logic of previous paragraphs in mind, it appears that probable arrival dates for the mission to Mars in 1964 will range from July 4 to July 19, 1965. Such arrival dates will allow the use of low energies and will also yield low asymptotic approach speeds at Mars encounter.

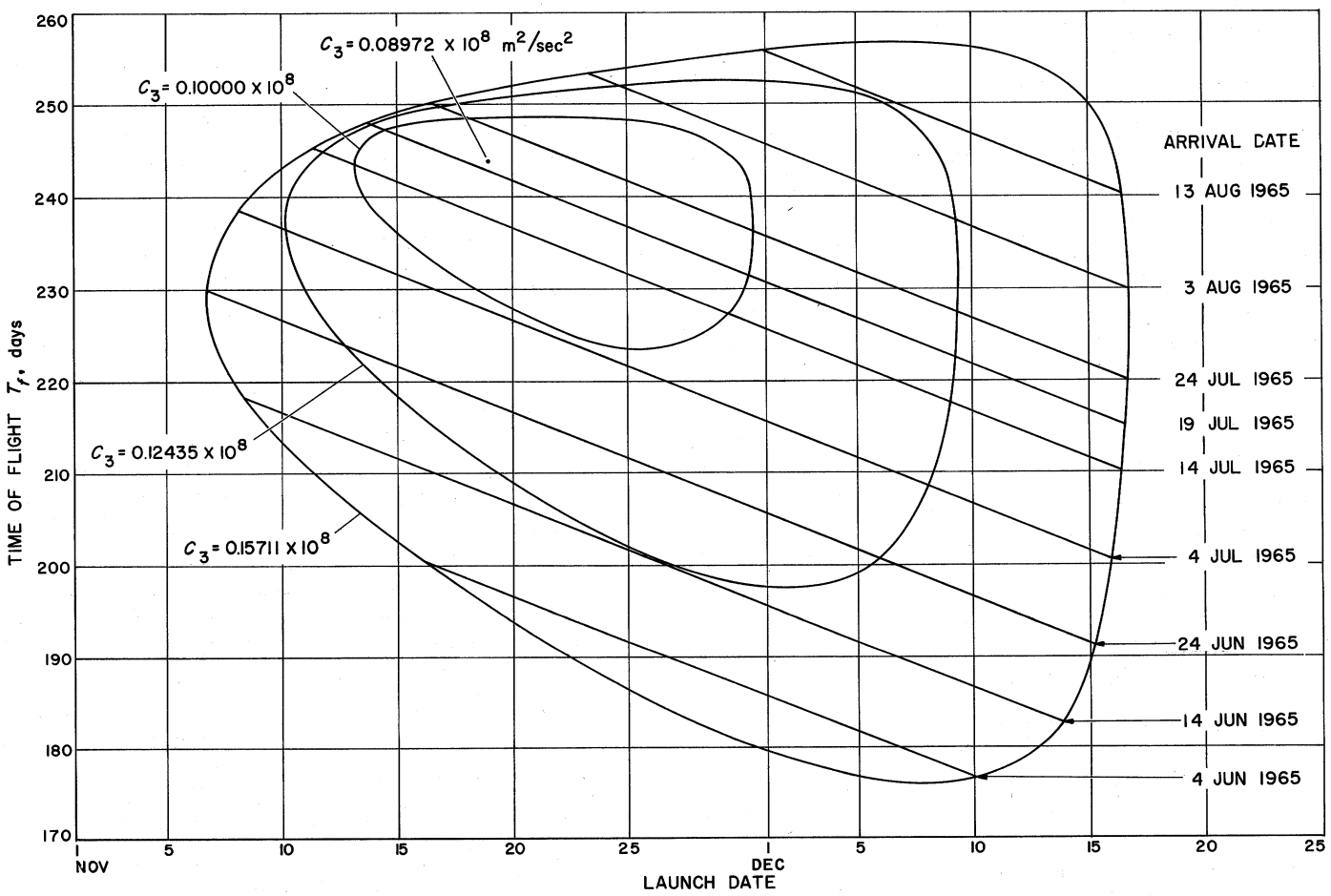

Figure 2. Mars 1964, time of flight vs launch date

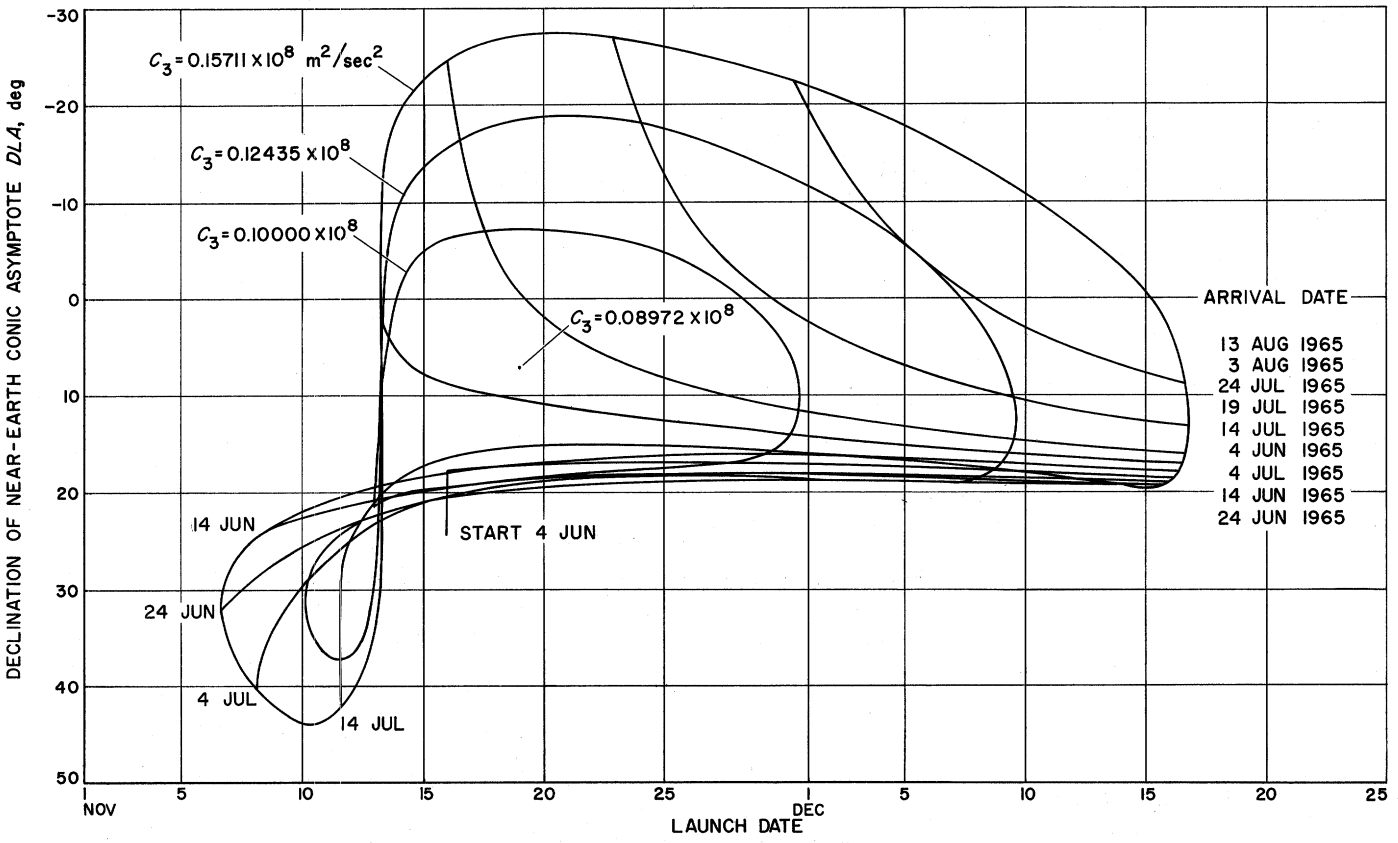

Figure 3. Mars 1964, declination of near-Earth conic asymptote vs launch date

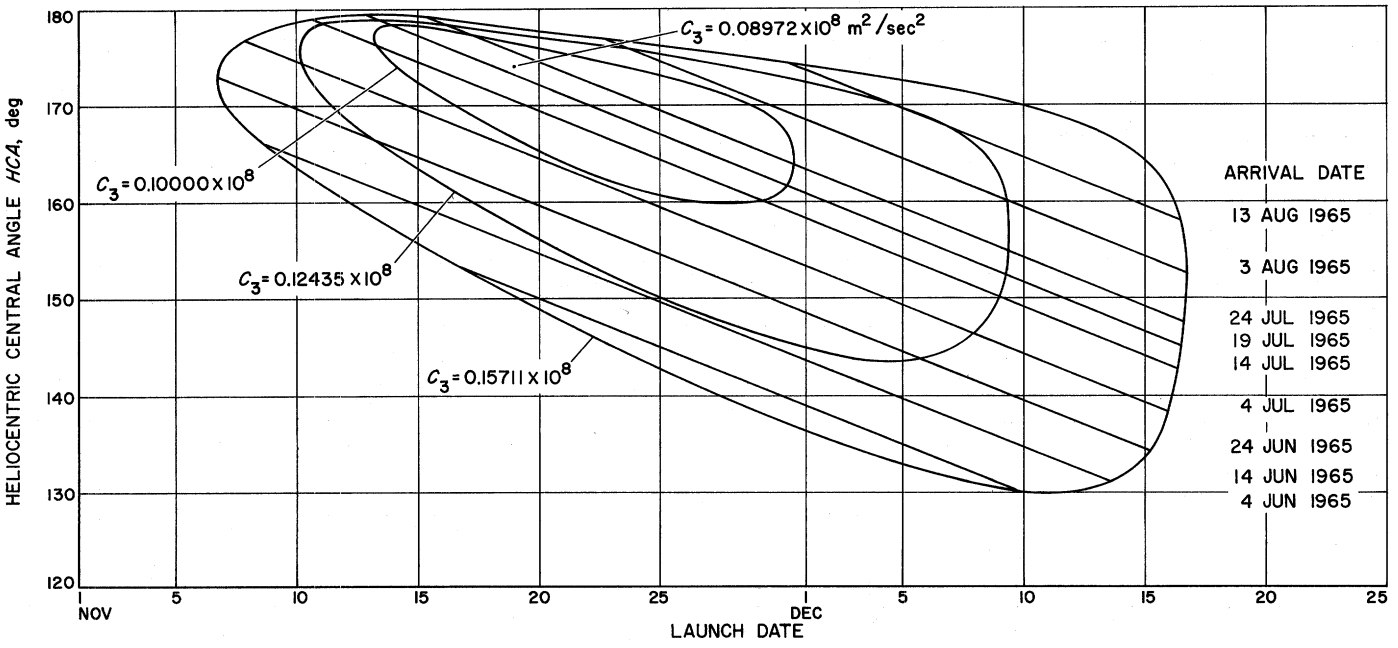

Figure 4. Mars 1964, heliocentric central angle vs launch date

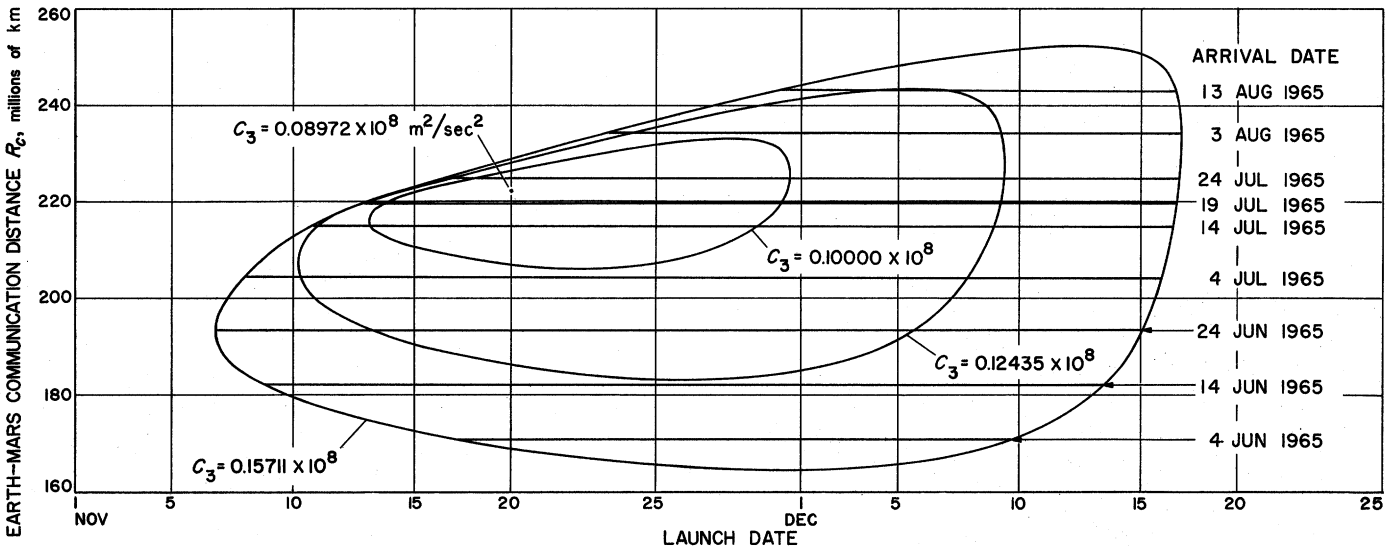

Figure 5. Mars 1964, Earth–Mars communication distance vs launch date

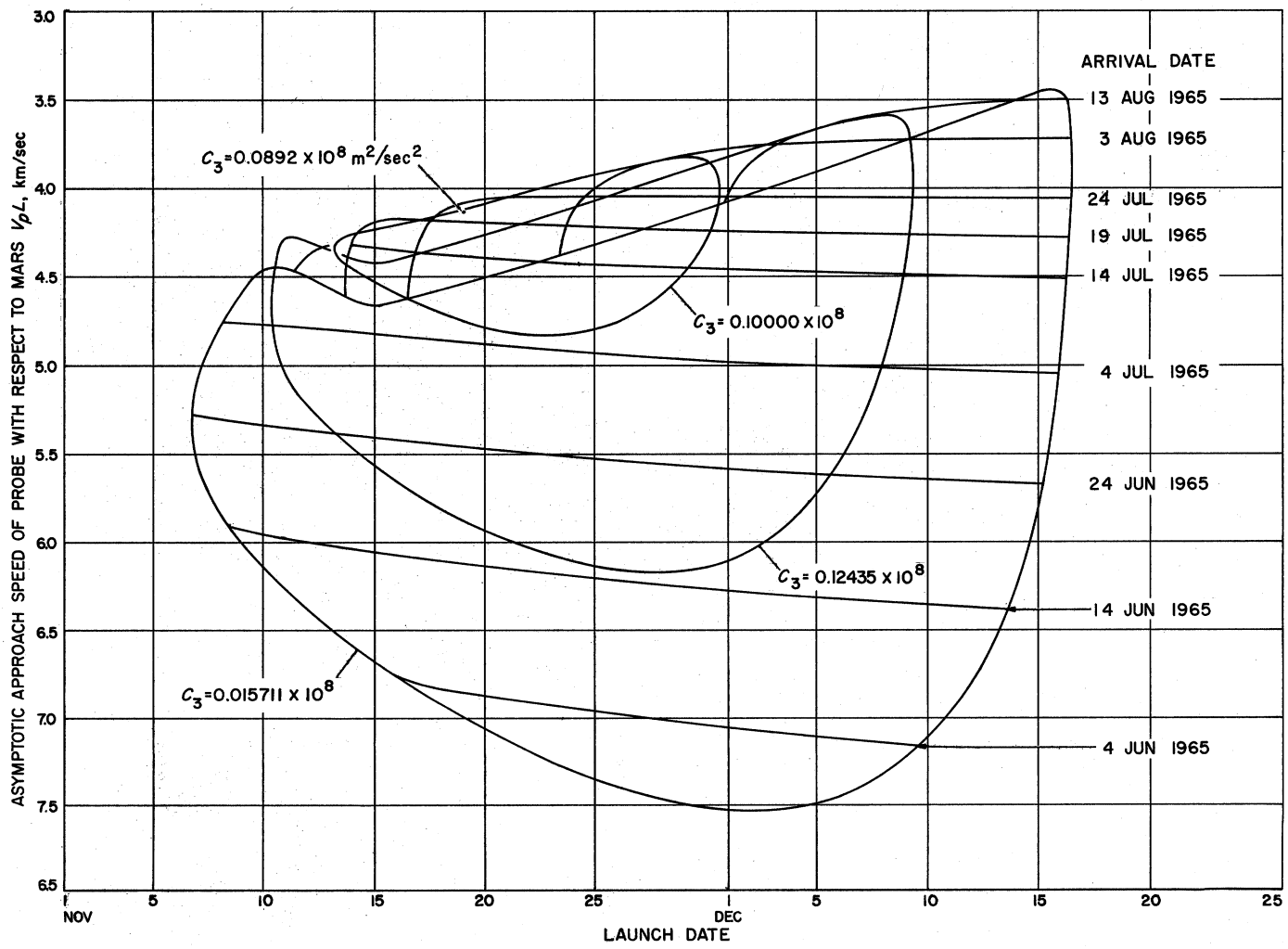

Figure 6. Mars 1964, asymptotic velocity of probe with respect to Mars vs launch date

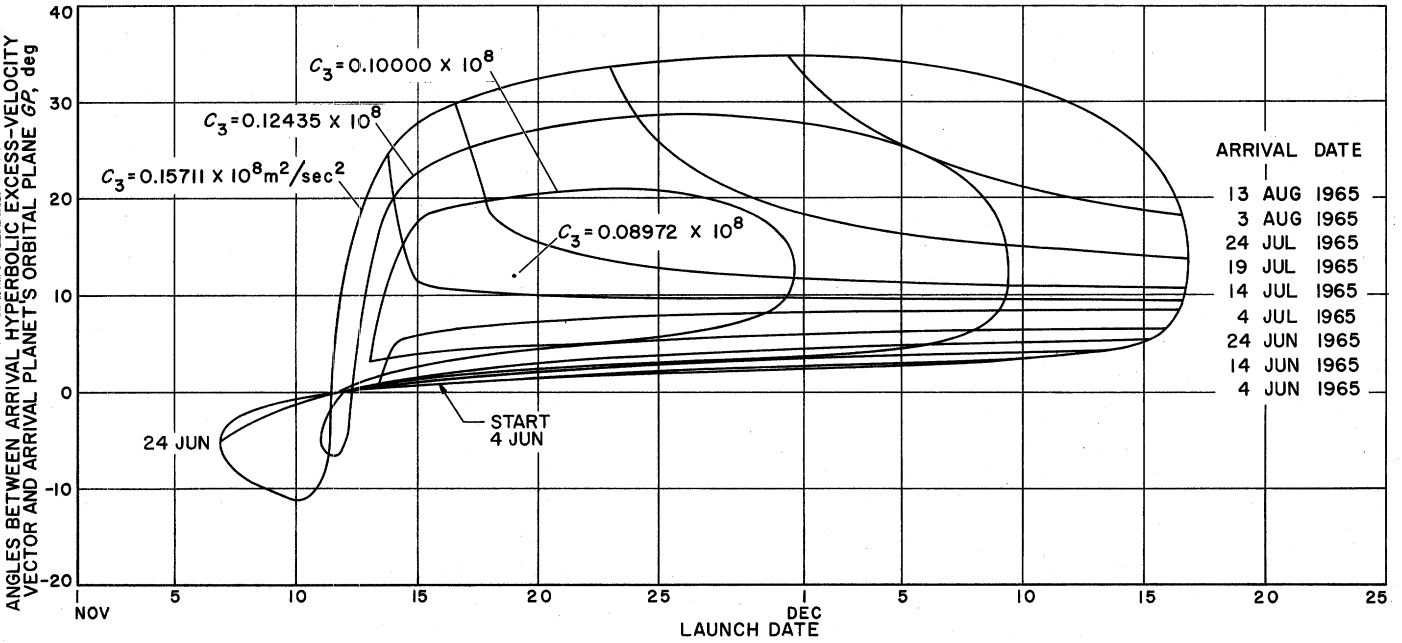

Figure 7. Mars 1964, angles between hyperbolic excess-velocity vector and arrival planet's orbital plane vs launch date

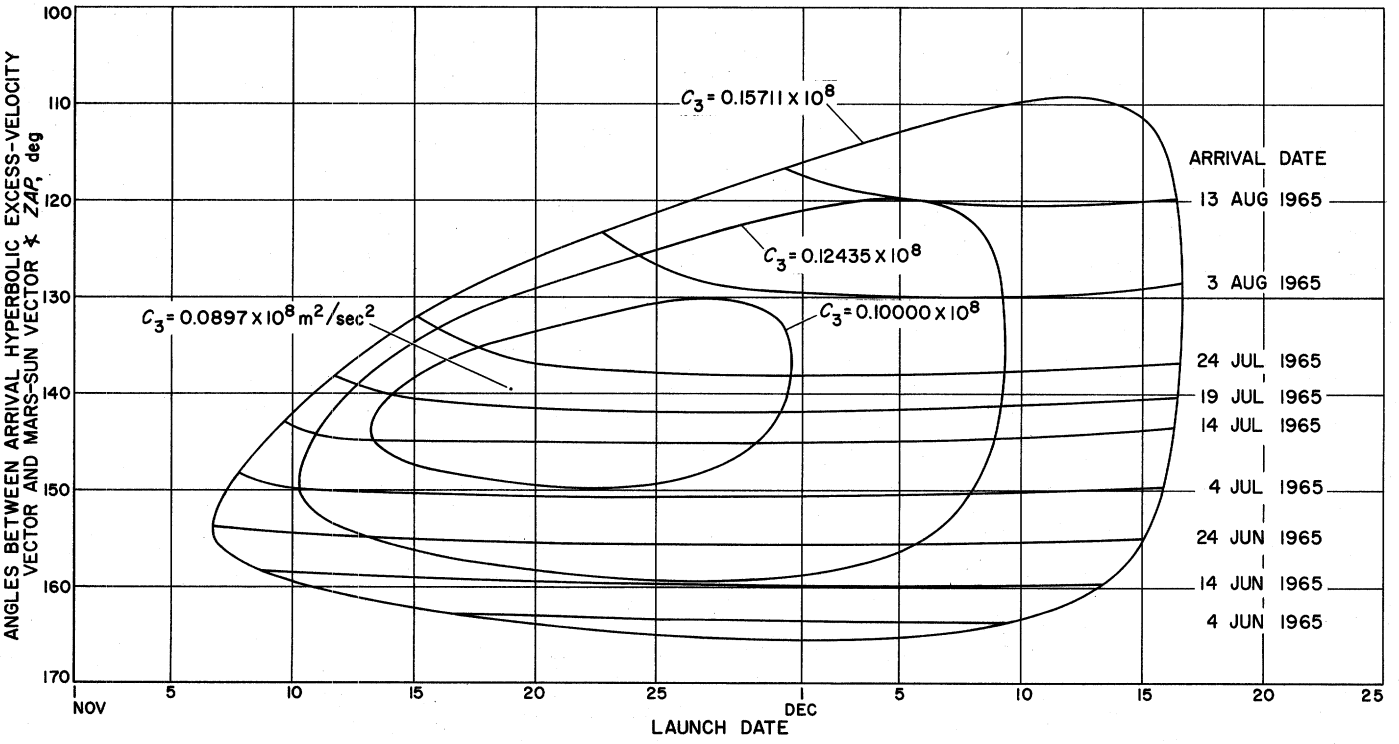

Figure 8. Mars 1964, angles between arrival hyperbolic excess-velocity vector and Mars–Sun vector vs launch date

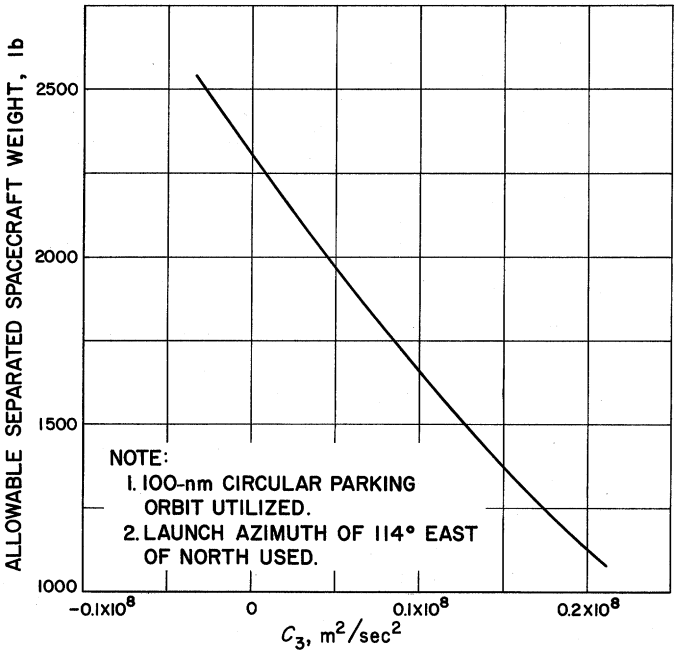

Figure 9. Allowable separated spacecraft weight vs C_3

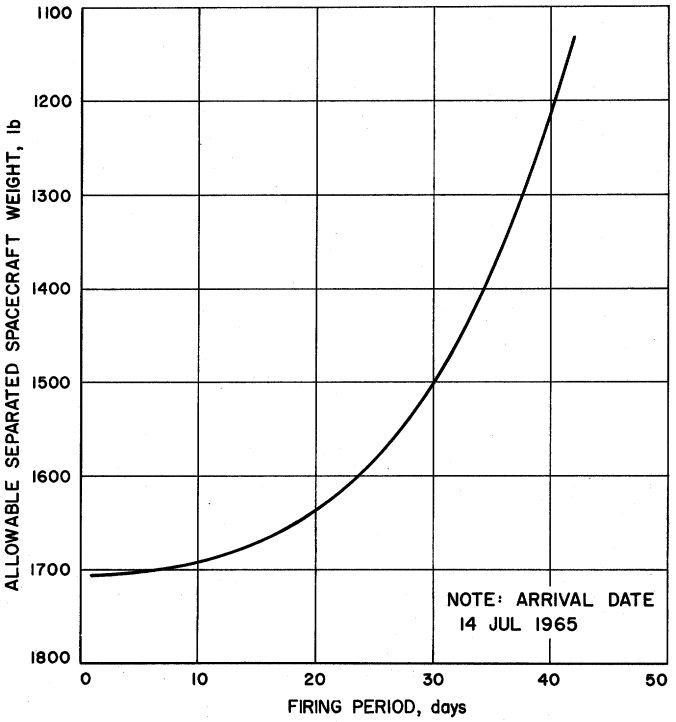

Figure 11. Allowable separated spacecraft weight vs firing period to Mars

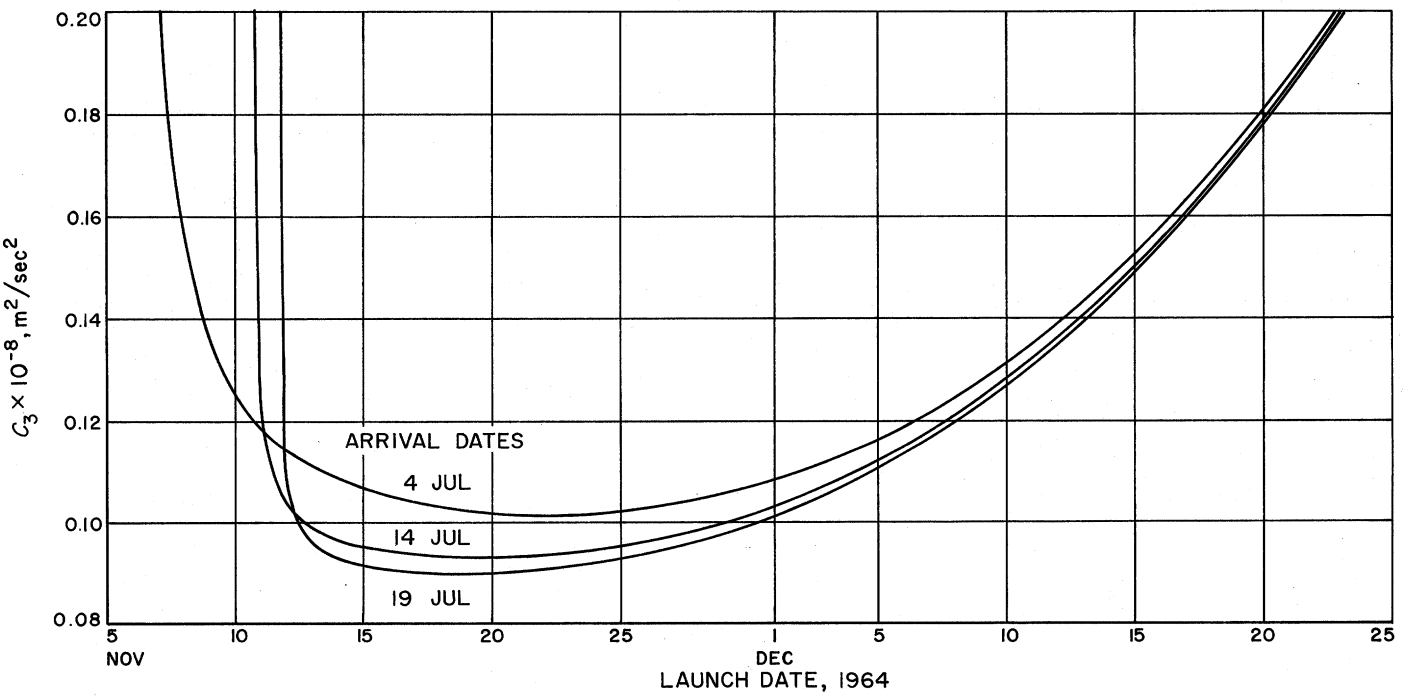

Figure 10. C_3 vs launch date (for Mars encounter)

(2) Firing Period

Figure 10 shows a plot of required C_3 vs launch date for three arrival dates: July 4, July 14, and July 19. Figure 11 shows a plot of payload capability vs firing period for an arrival date of July 14. Noting the variation of payload weight with firing period in Fig. 11, it is apparent that in order to have two split-capsule missions, the interval between firings must be reduced to a minimum. Such a minimization suggests the use of two launch pads.

(3) Earth Phase

From Fig. 3, note the variation of the declination of the asymptote for the range of arrival dates from July 4 to July 19. As mentioned earlier, the greatest variation occurs before November 15, 1964. After this date, however, the variation becomes smaller, and geocentric injection will occur in the same region for a given launch azimuth. For southeast launchings, the general location of geocentric injection is off the east coast of South Africa. Figure 12 shows a plot of parking-orbit coast time vs launch date for three launch azimuths, assuming an arrival date of July 14. Figure 13 is a plot of launch time from AMR vs launch date for the same three azimuths, assuming an arrival date of July 14. Figure 14 shows the Earth track for launching on November 15 and arriving on July 14, 1965, for two launch azimuths.

(4) Heliocentric Phase

For the arrival date of July 14, 1965 and launchings of November 15 and December 6, 1964, several heliocentric plots show the projection of the transfer orbit in the eclipter (Figs. 15 and 16), Earth–probe communication distance vs calendar date (Fig. 17), Earth–probe–Sun angle vs calendar date (Fig. 18), Earth–probe–Mars angle vs calendar date (Fig. 19), and Sun–probe–Mars angle vs calendar date (Fig. 20).

(5) Planetocentric Phase

A discussion of the Martian phase of the typical trajectories follows in Section IIIC.

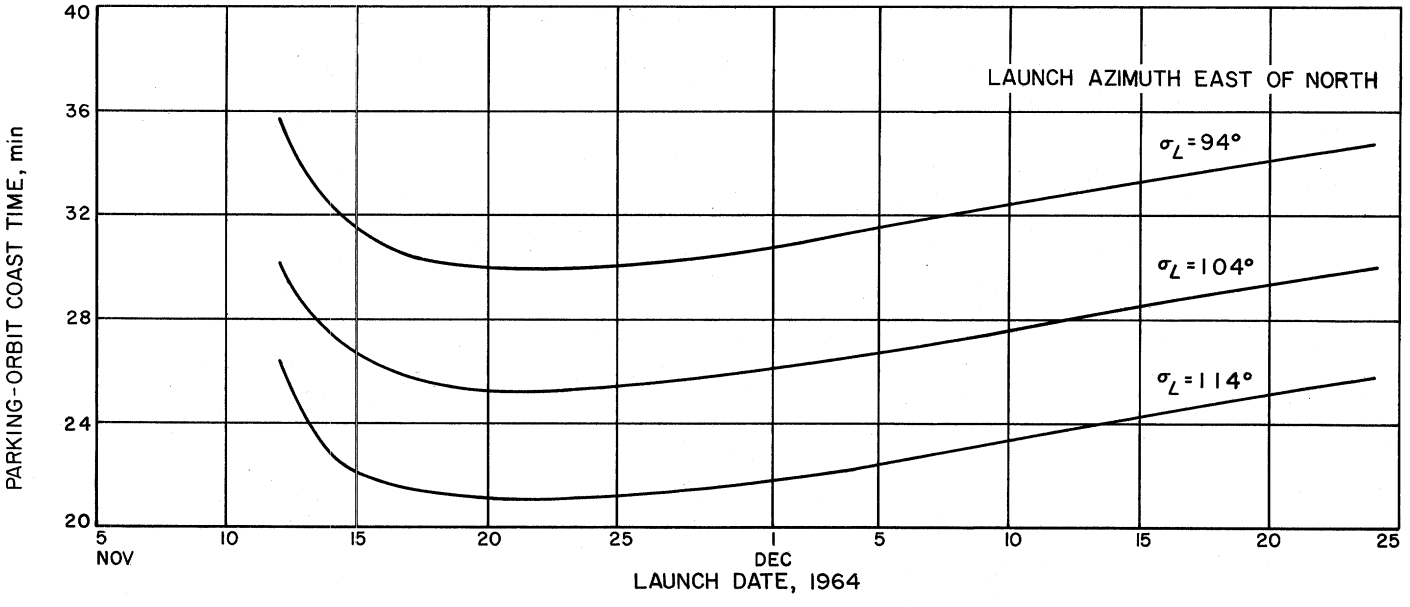

Figure 12. Parking-orbit coast time vs launch date (arrival date, 14 July 1965)

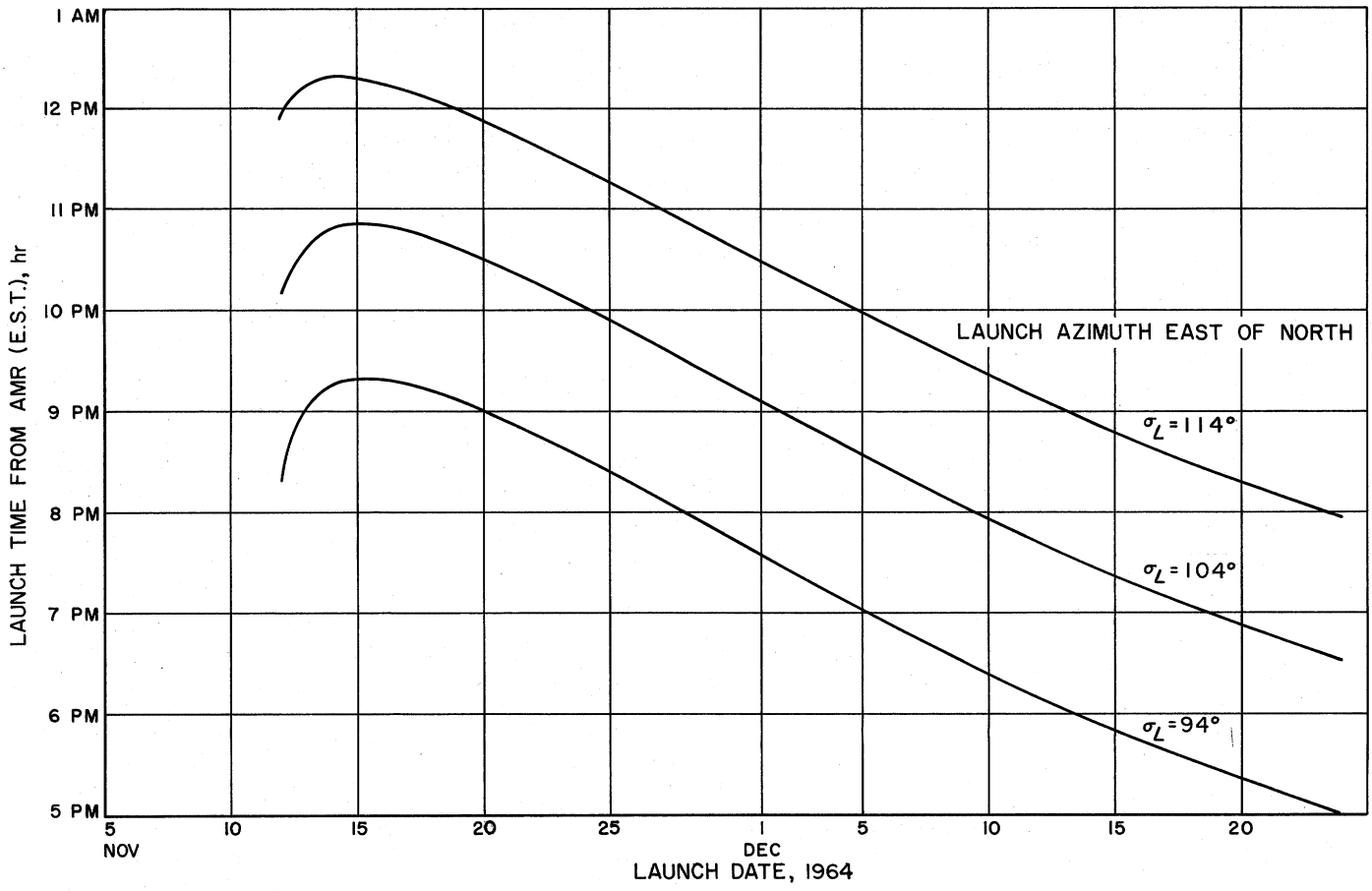

Figure 13. Launch time (E.S.T.) vs launch date (arrival date, 14 July 1965)

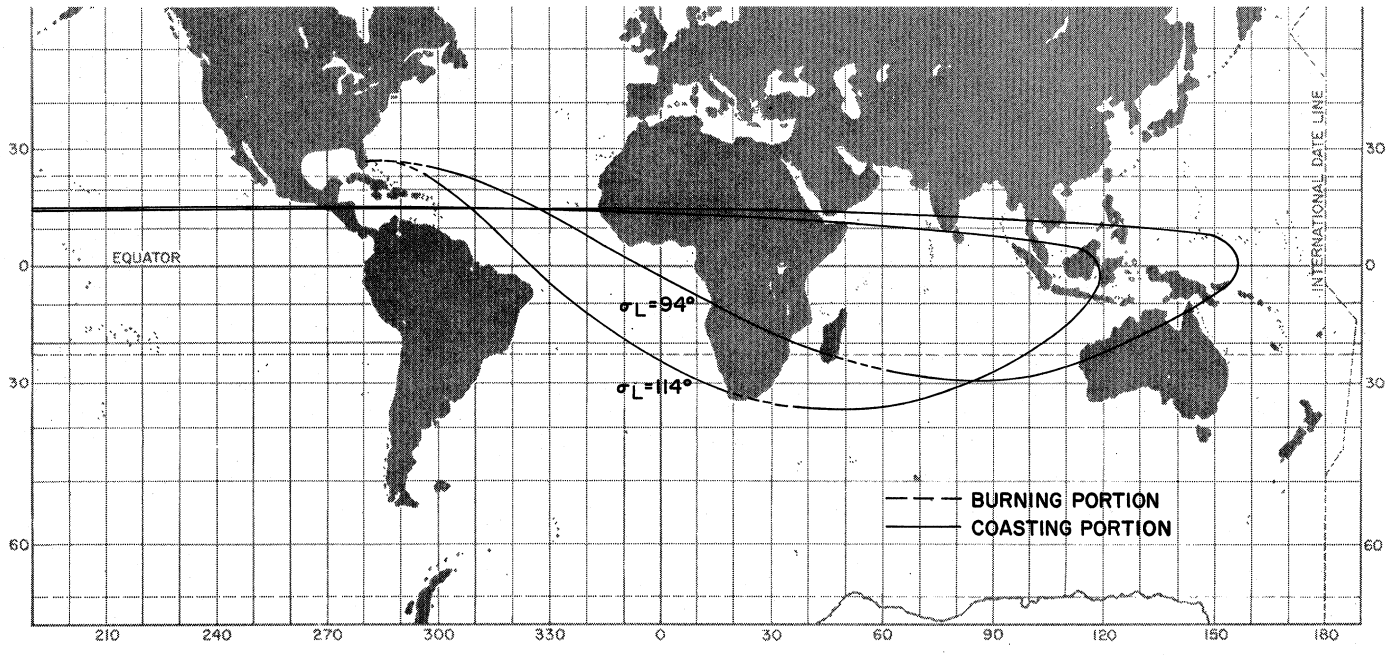

Figure 14. Mars 1964 Earth track (launch date, 15 November 1964; arrival date, 14 July 1965)

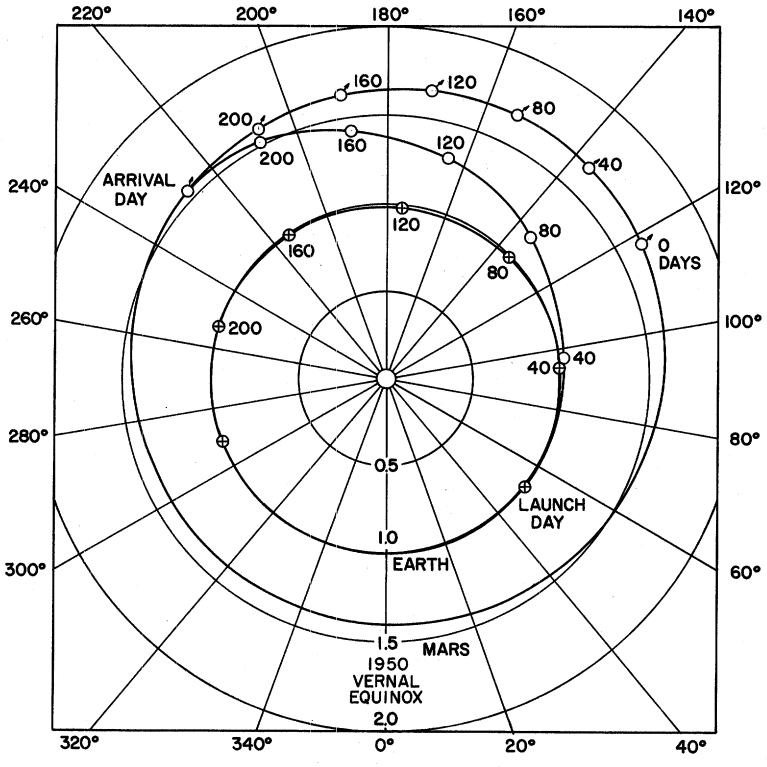

Figure 15. Heliocentric transfer orbit (launch date, 15 November 1964; arrival date, 14 July 1965)

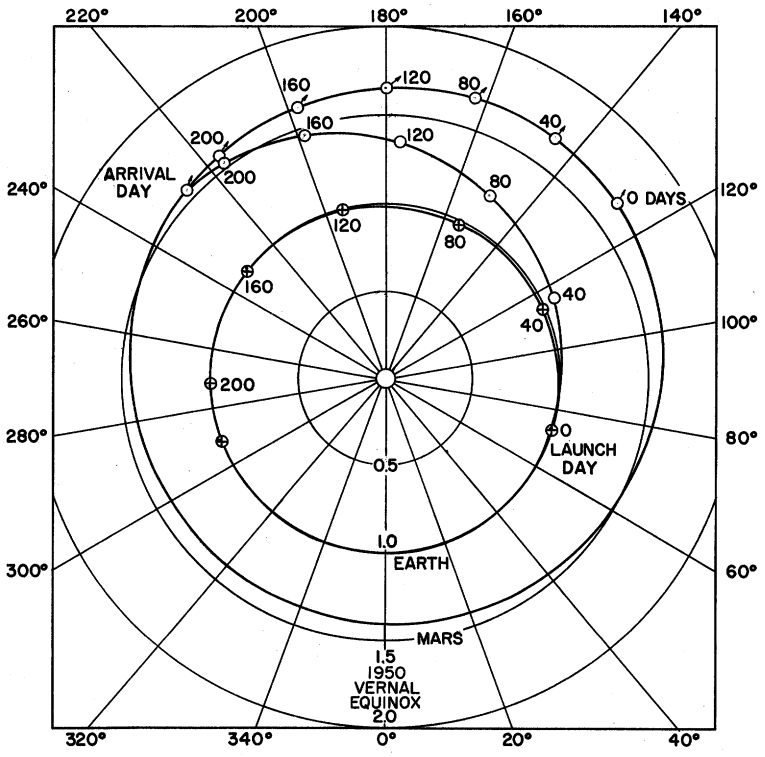

Figure 16. Heliocentric transfer orbit (launch date, 6 December 1964; arrival date, 14 July 1965)

UNCLASSIFIED

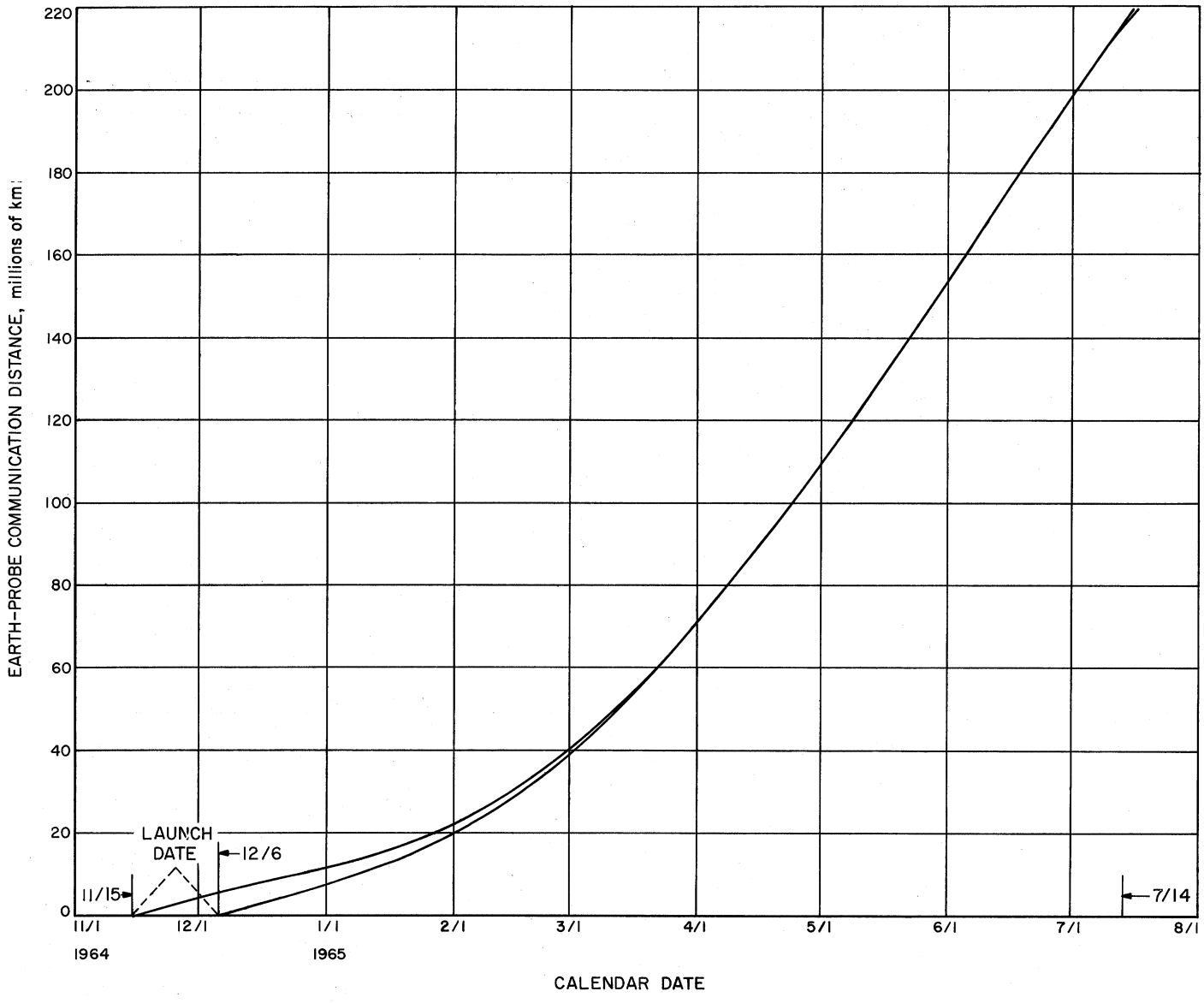

Figure 17. Earth–probe communication distance (arrival date, 14 July 1965)

UNCLASSIFIED

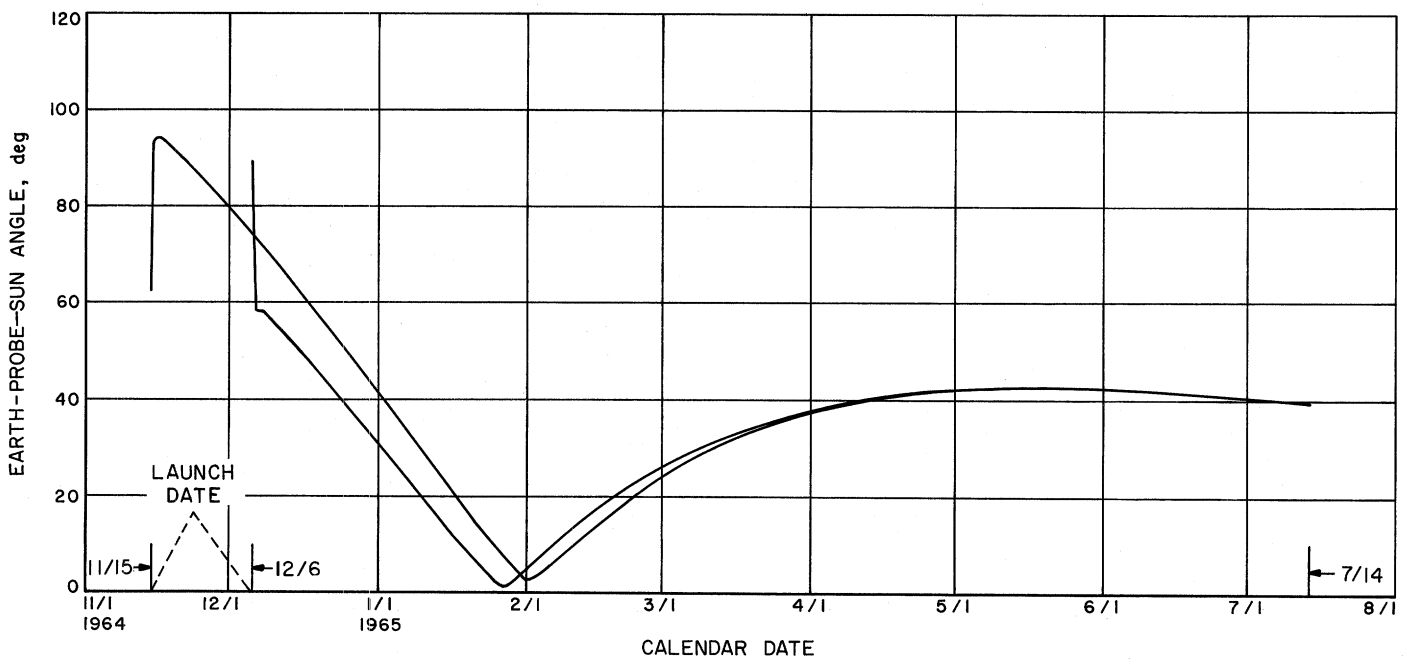

Figure 18. Earth–probe–Sun angle vs calendar date (arrival date, 14 July 1965)

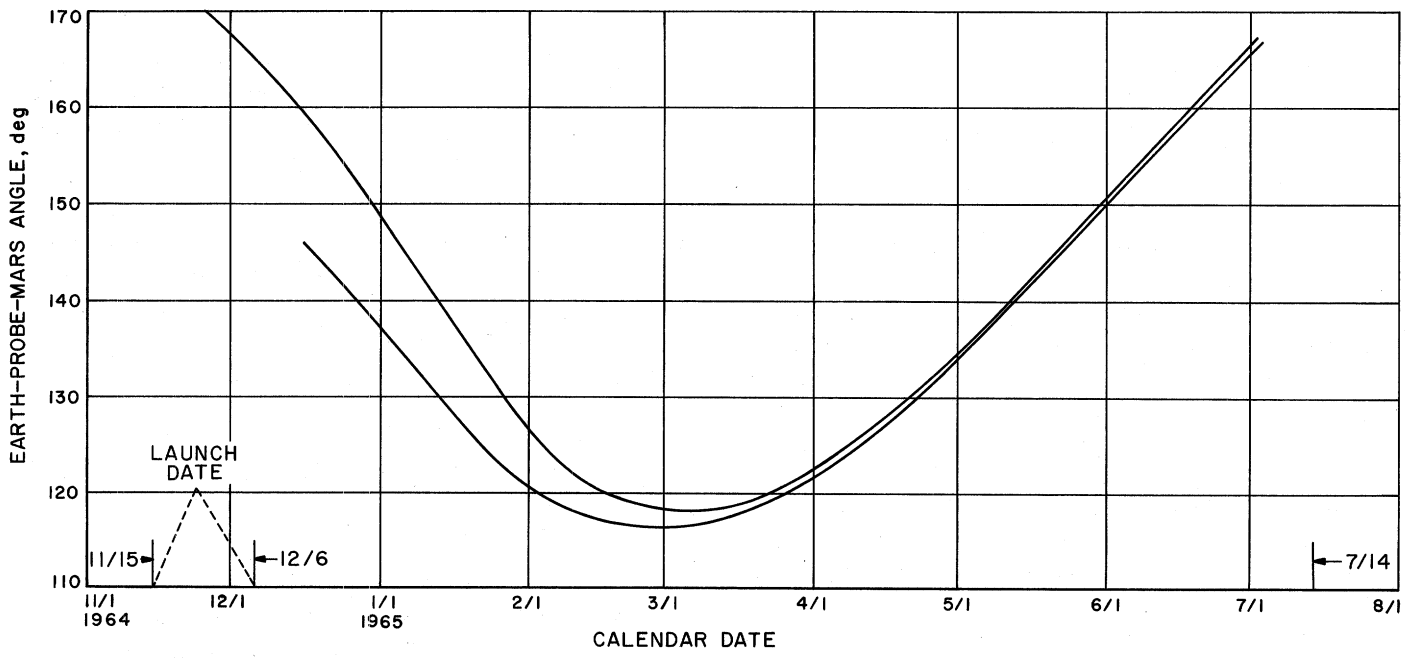

Figure 19. Earth–probe–Mars angle vs calendar date (arrival date, 14 July 1965)

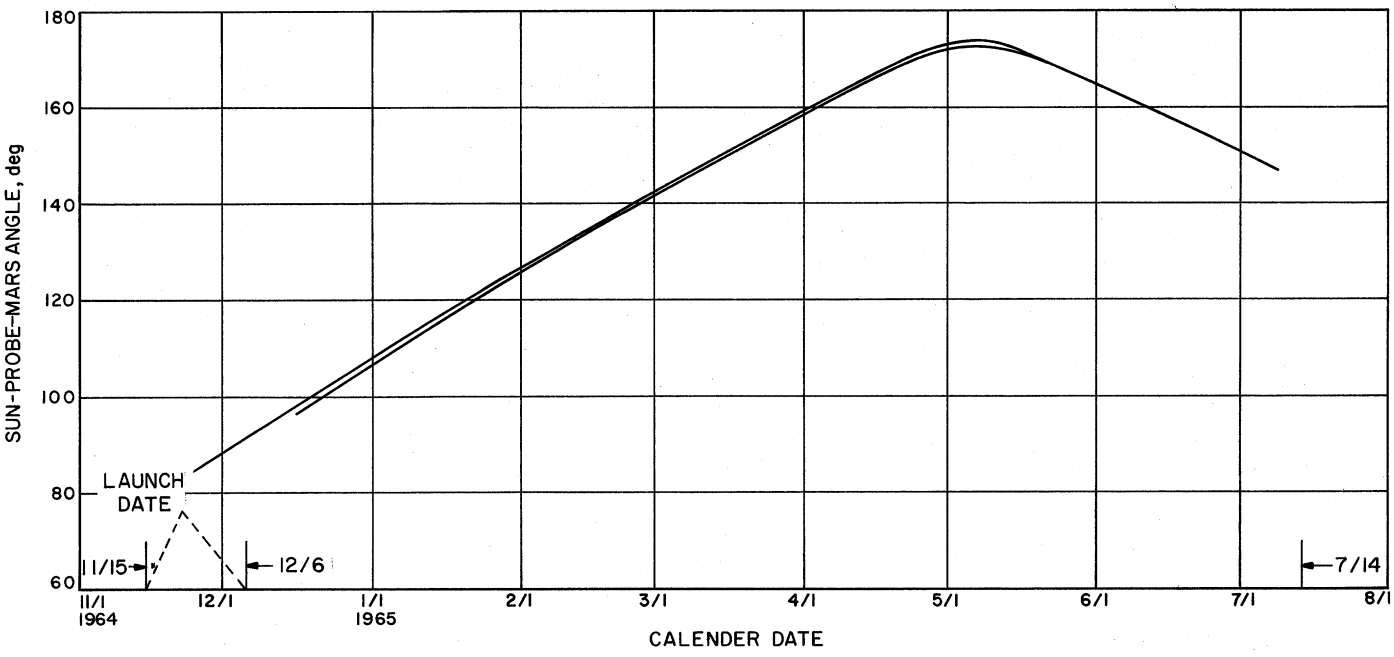

Figure 20. Sun–probe–Mars angle vs calendar date (arrival date, 14 July 1965)

2. Space Science

R. W. DAVIES

(This Section is UNCLASSIFIED)

a. Martian-Surface Investigations

The character of the Martian surface can be explored by two instruments aboard the spacecraft: an infrared spectrometer and a photographic system.

The use of infrared spectroscopy to study the surface features of Mars is suggested as the logical extension of work that has been performed from the Earth. Of specific relevance is the work of Sinton who, using the 200-in. telescope, looked through the Earth's infrared window between 3.4 and 3.7 μ and observed absorption bands in the reflection spectra near 3.5 μ. The bands were observed to come from that third of Mars which contains predominantly dark regions, and one explanation is that they are caused by organic molecules on the surface. It is proposed that advantage be taken of the proximity of the spacecraft to Mars to repeat these observations with a better spectral resolution, and with a geographical resolution about one hundred times better than that obtained from the Earth. It is also proposed to extend the search for the bands of organic molecules to the longer infrared wavelengths (between 5 and 8 μ); however, this is highly exploratory, and the water vapor in the Martian atmosphere will, in all likelihood, obscure the surface details.

Two spectrometers, an Ebert-type grating spectrometer and a Michelson interferometer, are being designed within the same weight, power, and volume constraints for *Mariner B*. Although the two spectrometers differ in detail, the main instrumental characteristics are:

(1) Weight: less than 20 lb

(2) Volume: smaller than 11 × 18 × 6 in.

(3) Power: less than 6 w

(4) Spectral range: 2 to 8 μ

(5) Spectral resolution: 330 Å

(6) Field of view: 2.5 × 0.25 deg (grating)
1 × 1 deg (interferometer)

(7) Shades of gray: 32

The sensitivity of the spectrometers can probably be increased by at least two orders of magnitude between 4 and 8 μ by the use of cryogenically cooled detectors. This would approximately double the values for items (1), (2), and (3). It is planned to have a two-dimensional scan with about 40 picture elements covering the entire planetary surface.

Most of the information we now possess about Mars was obtained by either visual or photographic observations, the clearest observations having been made when the Earth and Mars were closest. It is a natural suggestion to exploit this exploratory technique further from the spacecraft. It is feasible to construct a multiple-focal-length optical system with an 18-cm aperture and a maximum focal length of 150 cm within a weight of 15 lb. A 200 × 200-line vidicon system would be mated to these optics. The entire system can be conservatively estimated to weigh less than 30 lb. The optical system is designed to ensure sufficient illumination of the vidicon tube; the resolution is limited by the vidicon system.

The first pictures would be taken shortly after separation (approximately 360,000 km from Mars). If the 200 lines were completely filled by the disk of the planet, the resolution would be 33 km, comparable to the most optimistic estimates of what large telescopes flown on balloons can obtain. After a picture has been taken, the data (120,000 to 160,000 information bits) would be played back to the Earth in the subsequent 20-min period. In this manner it is possible to acquire 20 or more pictures of the entire planet without using up storage capacity. As the spacecraft approaches the planet, either the focal length could be shortened to enlarge the field of view to include the entire planet, or the picture could include a smaller area with higher resolution. The mode (one picture per ½ hr) could be used until planetary encounter (within 50,000 km of Mars), when the other planetary experiments commence their operation. After passing the planet and finishing the encounter period, this mode could be resumed, and pictures of Mars would be taken at large phase angles until the planet was about 600,000 km distant.

During the encounter period, high-resolution, narrow-field-of-view pictures would be obtained. It will be impossible to photograph the entire Martian surface in this way because the data system could not store all of the information. It is also doubtful if complete photographic coverage is important. One-kilometer-resolution photographs of the entire planet would be very interesting and exciting, but as in the case of the Moon, they would not settle any basic controversy on the nature of the surface. If the spacecraft were to photograph the visible half of Mars at one-kilometer resolution with eight shades of light intensity, it would require nine hundred 200 × 200-line non-overlapping photographs and storage of 10^8 bits of data. If all of these pictures were taken during the period of planetary encounter, the data system would have to read in 6×10^3 bits/sec. This would require developing an entirely new data-storage system.

b. Martian-Atmosphere Experiments

While the most direct means of measuring local atmosphere parameters is by using the capsule, considerable information about the atmosphere can be obtained from infrared and ultraviolet spectrometers aboard the spacecraft. Both CO_2 and water have bands in the infrared region which are sufficiently strong so that, if present estimates of the amounts on Mars are correct, quantitative estimates of the concentrations can be obtained. Also, if the concentrations of methane or carbon monoxide are within a factor of ten of the upper limits presently assigned to them, the existence of these gases can be ascertained.

In addition to this, information about the structure of the wings of the 4.3-μ carbon dioxide band should give a qualitative temperature profile of the Martian atmosphere. The details of the infrared spectrometer were described in Section IIIB-2a.

An ultraviolet-visible spectrometer aboard the spacecraft would attempt to identify qualitatively major constituents of the atmosphere, and those minor constituents which play an important role in the photochemistry of the upper atmosphere. The trajectory would permit spectroscopic measurements mainly of the lighted side and perhaps some on the dark side.

Two types of observations may be possible on the lighted side: aurora, and absorption and scattering experiments. Three types of dark-side observations are possible: airglow, aurora, and twilight glows.

Aurora. The Earth auroral emission is believed to come from electron bombardment of the upper atmosphere. The presence of an auroral emission of Mars would indicate that a similar mechanism was operating there. The geographic location of the aurora would indicate the position of the magnetic poles. On the night side, the aurora could be detected by analyzing ultraviolet and visual light and on the daylight side by ultraviolet light only. On Earth, the auroras occur more frequently on the night side. The most intense spectral feature is the atomic oxygen green line (5577 Å). This emission would not be expected to be strong on Mars, how-

UNCLASSIFIED

ever. If Mars has an appreciable magnetic field, an auroral emission will occur on the day side of the planet in the far-ultraviolet, where the Lyman-Beige-Hopfield bands of molecular nitrogen are found.

Airglow. The atomic and ionic recombination processes of certain terrestrial constituents often emit light. The intensity of the emission is proportional to the density of the reacting species. It is suspected that the atomic and ionic composition of the terrestrial planets differ primarily in their quantitative abundances of the light elements. The upper atmosphere of Mars probably has more nitrogen and less oxygen and hydrogen than that of either the Earth or Venus. The minor constituents can also prove to be important in the photochemistry of the upper atmosphere.

On the night side of the planet, a weak airglow could theoretically extend over the entire spectral region from 1250 to 6500 Å. On the daylight side, the airglow should be detected between 1300 and 1750 Å.

The ultraviolet-visual spectrometer for the *Mariner B* mission would probably be an improved and extended version of what is now planned for *Mariner A*. It would scan between 1100 and 6500 Å using two detectors, one sensitive to the ultraviolet and the other to the visual. The spectral resolution would be finer than the 10 Å planned for *Mariner A*. The *Mariner A* model will take some 180 spectra consuming 8×10^5 bits of information. Less than a third of that amount would suffice.

The angular field of view of the *Mariner A* model is 0.05×0.001 rad which, at 50,000 km from the planet, covers a region 2500×50 km. The monochromator is a grating Ebert f/4 system contained in a volume of $12 \times 7 \times 4$ in. The f/4 telescope has a 50-cm focal length and is folded into a cylinder of 6-in. diameter and 5-in. length. Reflecting optics with special coatings on the reflection surfaces are used throughout to permit the lower wavelength limit of 1100 Å.

The features of interest in the spectrum have intensities between 10^6 and 10^{12} photons/cm^2/sec. The optical system can deliver between 10^2 and 10^8 photon/cm^2/sec to the detector. The signal-to-noise ratio is improved by chopping the beam and employing a phase-sensitive electrometer. The detector is a photomultiplier tube with a sodium salicylate coating. It is contained in a 3-in. cube and weighs 2 lb. The electronics weigh 12 lb and require 2 w.

An estimate of the fraction of the atmosphere which is nonmolecular can possibly be derived by measuring the polarization of the light scattered by the Martian atmosphere. The measurements would have to be made at at least three wavelengths and about six orientations of the polarizers. Although no quantitative designs have been carried out on such instrumentation, the experiment has the feature that phase angles would be obtained by the probe which cannot be obtained from the Earth.

c. Interplanetary Experiments

In contrast to most of the experiments recommended in this study, interplanetary experiments are not new, and by 1964 particle and field experiments will have been flown some thirty or forty times. It would be foolish to suggest specific experiments until after the *Ranger* series has been flown, but it should be possible by 1964 to fly a few highly sophisticated experiments that would prove scientifically more significant than a large array of simple experiments.

It is certain that a low-energy (plasma) particle detector will be carried because it will be important to measure the energy spectra and number distribution in the region between the Earth and Mars. An ion chamber of the type being carried on *Ranger* and *Mariner A* will be carried as an absolutely calibrated monitor.

A magnetometer is essential; to eliminate it from the payload would destroy the major significance of the corpuscular experiments. Furthermore, during encounter, the magnetometer will measure the magnetic field of Mars as well as the interplanetary field.

Cosmic-dust experiments assume a high priority as the probe approaches the orbit of Mars and goes nearer the asteroidal belt, so that from the time of separation and afterwards, these measurements are especially significant.

The spacecraft design constraints imposed by the magnetometer, the plasma probe, and the ion chamber will be as stringent for *Mariner B* as they were for previous payloads. It is difficult to suggest any alternative to folding booms.

d. Compilation and Sequencing of the Scientific Subsystem

It is proposed to review here the sequence of operations of the scientific experiments presently planned for *Mariner B* and to discuss some constraints imposed by the spacecraft's capabilities. A compilation of the possible instrumentation is shown in Table 2.

From the time of launch until the spacecraft and capsule are separated, only the interplanetary particle and

UNCLASSIFIED

UNCLASSIFIED

fields experiments are active. Since the information rate of these is low, the data will be transmitted essentially in real time without seriously tying up the data-storage system. After spacecraft–capsule separation, photographs

Table 2. Compilation of spacecraft scientific experiments

Instrument	Weight, lb		Power, w	Stored information, bits
	Desired	Minimum		
Infrared spectrometer	35	20	10/6	$\lesssim 5 \times 10^5$
Ultraviolet visual spectrometer	25	25	5	$\lesssim 5 \times 10^5$
Photographic system	30	20	7	$\sim 10^7$
Magnetometer	10	10	3	~0
Cosmic-dust detector	10	10	1	~0
Radiation package	60	43	9	~0
Ion chamber	(3)	(3)	(~0)	
Plasma probe	(20)	(20)	(5)	
Other	(37)	(20)	(4)	
Polarization detector	15	0	5	?
Data-storage system	75	75	20	–

of Mars will be taken from the spacecraft approximately every ½ hr and will be transmitted to the Earth without permanently filling the data-storage system.

Limitations of the spacecraft system become important during the period of active encounter with Mars. These limitations are the Earth–probe information communication rate (100 to 200 bits/sec at Mars–Earth distance), the total time that stored data can be continuously transmitted (about 10 days), the total amount of scientific data that can be stored (proposed maximum of 2×10^7), and the time the probe is in the vicinity of the planet.

If planetary encounter is defined as that period of time during which the spacecraft is within 50,000 km of the planet, it lasts approximately 2×10^4 sec. A slightly modified *Mariner A* data system could be capable of reading 2.4×10^3 bits/sec into the storage unit, thus limiting the total amount of encounter information to 4.8×10^7 bits. This curtails the operation of only the photographic system, which was discussed earlier in this Section; it was emphasized that high-resolution photographic coverage of the entire planet was not necessary. The infrared and ultraviolet spectrometers require no more than 5×10^5 bits each, so that data-storage limitations do not pose problems for these experiments. A more advanced data system would not materially improve the infrared or the ultraviolet spectrometer experiments; in fact, it might indirectly impair them because they are already constrained by volume, weight, and power.

The ultraviolet spectrometer, the infrared spectrometer, and the photographic system must all scan the planetary disk; this will be accomplished by utilizing a common articulating platform. In general terms, the scan patterns of the infrared spectrometer and the photographic system concentrate on broad geographical coverage, while the ultraviolet spectrometer utilizes mainly latitudinal or longitudinal scans. Since all three instruments share the articulating platform, they must follow the same pattern, but it is not necessary for all of them to operate continuously. During early encounter, when the probe is between 50,000 and 43,000 km from the center of the planet, the scan will execute latitude or polar scans for the ultraviolet spectrometer, which does not require the fine geographical resolution available at close approach. Some photographs and infrared spectra of selected areas may also be included. Between about 27,000 and 17,000 km, or for about 2400 sec, the scan mode will probably consist of a 40-element square coverage of the planetary surface as required by the infrared and photographic system. The coupling between the infrared and ultraviolet systems can be realized since the infrared spectrometer scans one picture element in around 20 to 30 sec or a time comparable to the 50-sec time required to read one photograph into storage. This 40-element scan will be centered about the time when the Sun–Mars–probe phase angle is zero. Another similar 40-element scan should follow, the period being centered slightly earlier than the time of closest approach. During the latter portion of this scan, data from the capsule would take a major portion of the read-in time to the storage system. An effort will also be made to concentrate the scan on the probable landing area of the capsule. The scan mode described above ends just prior to the time when the probe is opposite the planet's terminator. A new mode will then commence, emphasizing the ultraviolet scan across the terminator. A final 40-element scan, or a modified 40-element scan, would then be employed in order that the photographic system and the infrared spectrometer could observe the daylight portion of Mars; the ultraviolet spectrometer would attempt to view the dark portion only. The final mode between about 25,000 and 50,000 km from the planetary center would primarily be dictated by the ultraviolet spectrometer, with some additional photographs being taken.

These numerical estimates are necessarily approximate, because they depend critically upon the choice of trajectory. A careful study will have to be made to optimize the trajectories and scan maneuvers.

UNCLASSIFIED

3. Midcourse-Guidance Analysis

P. K. ECKMAN

(This Section is CONFIDENTIAL)

The midcourse-guidance system for the *Mariner B* spacecraft is a direct extension of the *Mariner A* system, and operates in the following manner. At shutoff of the last stage the spacecraft is injected into a coasting orbit. Because of tolerances in the injection-guidance systems, the orbit will differ slightly from the standard trajectory. The spacecraft is tracked on this nonstandard trajectory by means of Earth-based radio-tracking stations of the Deep Space Instrumentation Facility (DSIF). Measurements of range rate, angular position, and range from the tracking stations are transmitted to a central ground-computing facility that determines the orbit which best fits the measured data according to a least-squares-error criterion. From the measured orbit, the central ground computer determines the midcourse-velocity increment required to correct quantities such as miss components and time of flight at the target. Appropriate attitude and speed commands are then transmitted to the spacecraft from one of the tracking sites. The attitude-control system orients the spacecraft, such that the midcourse rocket is pointed in the desired direction. The rocket is ignited and shuts off when the spacecraft accelerometer and integrator indicate that the commanded speed increment is attained.

a. Injection-Guidance Errors

A statistical description of the coordinate deviations at injection is necessary to determine the midcourse-correction capability needed to assure reaching the target. Such an analysis for the *Centaur* injection-guidance system has been performed previously in the *Centaur* Study Report.* Only a brief description of the analysis, along with updated numerical results, will be presented here.

The analysis was carried out as follows:

(1) An equivalent analytic model of the *Centaur* guidance system was defined to permit component errors to be simulated.

(2) Each error source was simulated to determine the resulting 1-σ injection coordinate deviations.

(3) This information was then used to form a noise moment matrix Λ, from which the variance and covariance of injection coordinates were obtained.

(4) The Λ-matrix was used to calculate the target miss components in the absence of midcourse guidance.

(5) The Λ-matrix was used to compute the rms midcourse correction capability needed for each mission.

The coordinates used in the analysis are defined in Fig. 21. The Earth is assumed to be spherical and the standard thrust vector to remain in the X–Y plane.

X–Y–Z = inertial Cartesian coordinates erected at launch; Y lies along the local vertical; Z is normal to the standard thrust plane

x = ground range, on sea-level sphere = $r_0\phi$

r = distance from Earth's center to missile

v = inertial speed of missile

γ = path angle above local horizontal

The noise moment matrix Λ is given by

$$\Lambda = \begin{bmatrix} \sigma_x^2 & \rho_{xr}\sigma_x\sigma_r & \rho_{xv}\sigma_x\sigma_v & \rho_{x\gamma}\sigma_x\sigma & 0 & 0 \\ — & \sigma_r^2 & \rho_{rv}\sigma_r\sigma_v & \rho_{r\gamma}\sigma_r\sigma_\gamma & 0 & 0 \\ — & — & \sigma_v^2 & \rho_{v\gamma}\sigma_v\sigma_\gamma & 0 & 0 \\ — & — & — & \sigma_\gamma^2 & 0 & 0 \\ — & — & — & — & \sigma_z^2 & \rho_{z\dot{z}}\sigma_z\sigma_{\dot{z}} \\ — & — & — & — & — & \sigma_{\dot{z}}^2 \end{bmatrix}$$

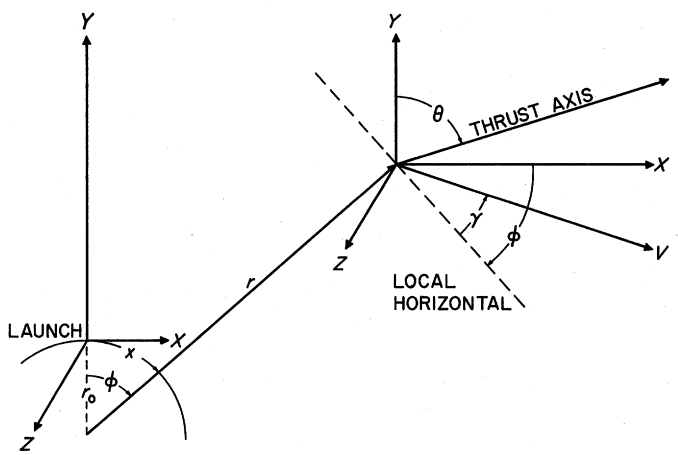

Figure 21. Guidance-analysis coordinate system

*"*Centaur* Study Report," Technical Memorandum No. 33-16, Jet Propulsion Laboratory, Pasadena, Calif., 5 June 1960 (SECRET).

A typical element of Λ has the form $\lambda_{ij} = \lambda_{ji}$. The diagonal elements give the variance of each of the six coordinate deviations, and the λ_{ij} $(i = j)$ elements constitute the covariances. If the elements of Λ are divided by their associated 1-σ values to make the diagonal terms equal to one, the resulting normalized matrix gives the correlation between pairs of injection-coordinate deviations.

The standard coordinate deviations and their correlations are given in Table 3 for four Mars trajectories. For each trajectory three sets of results are presented. The first set is based upon an analysis using Convair-Astronautics (CVA) Specification No. 55-05000, Revision C. The values given differ somewhat from those presented in the *Centaur* Study Report.* This is due in part to a change in trajectory, but primarily to revised computing techniques. A supplementary analysis was made to determine a pessimistic limit on the accuracy of *Centaur* guidance in case the specified component tolerances are not achieved. This was done by considering two sets of error sources. The first of these, referred to as "JPL current estimate," assumes functional errors which would result from using gyros and accelerometers representing the current state of the art, based on JPL's most recent evaluation. The other set assumes the 3-σ current-estimate errors to be a 1-σ errors and is consequently designated the "JPL pessimistic estimate."

Ibid.

The system used for expressing miss distance at the target resulting from injection coordinate deviations is one which defines two components of a miss vector normal to the asymptote of the standard approach hyperbola. Such a miss vector is independent of the transit-time variation which, in turn, is chosen as the third miss coordinate. By proper rotation of the miss coordinates, the miss components M_1 and M_2 represent the semimajor and semiminor axes of the 1-σ error ellipse at the target. The values of M_1 and M_2, as well as transit-time variation, are given for four trajectories in Table 4.

The miss components given represent miss distance at a massless target. For a Mars orbit, the actual miss distances will be somewhat less because of the focusing effect of the target's gravitational field, the amount of reduction depending on the standard miss distance.

b. Midcourse-Maneuver Requirements

The midcourse-speed increments required to correct for injection errors are given in Table 5. The method of

Table 3. Standard coordinate deviations and correlations for four Mars trajectories

Coordinate deviations and correlations	Transit time, days											
	216.1			220.9			230.3			235.3		
	Launch: 12/6/64 Arrival: 7/10/65			Launch: 11/29/64 Arrival: 7/8/65			Launch: 11/22/64 Arrival: 7/11/65			Launch: 11/15/64 Arrival: 7/9/65		
	CVA specs	JPL current	JPL pessimistic	CVA specs	JPL current	JPL pessimistic	CVA specs	JPL current	JPL pessimistic	CVA specs	JPL current	JPL pessimistic
σ_x, km	3.98	9.91	29.7	3.89	9.71	29.1	3.78	9.49	28.5	4.08	8.50	25.5
σ_r, km	1.79	3.78	11.3	1.76	3.75	11.2	1.74	3.72	11.2	1.82	3.71	11.1
σ_v, m/sec	1.57	3.59	10.8	1.57	3.62	10.9	1.57	3.66	11.0	1.56	3.12	9.35
σ_γ, millirad	0.169	0.546	1.64	0.169	0.537	1.61	0.169	0.532	1.60	0.168	0.523	1.57
σ_z, km	1.28	2.17	6.51	1.33	2.27	6.80	1.38	2.37	7.10	1.22	2.05	6.16
$\sigma_{\dot{z}}$, m/sec	3.27	9.51	28.5	3.23	9.18	27.5	3.21	8.91	26.7	3.24	9.70	29.1
ρ_{xr}	−0.645	−0.662	−0.662	−0.652	−0.676	−0.676	−0.664	−0.692	−0.692	−0.635	−0.446	−0.446
ρ_{xv}	0.848	0.876	0.876	0.857	0.886	0.886	0.867	0.897	0.897	0.834	0.780	0.780
$\rho_{x\gamma}$	−0.118	−0.358	−0.358	−0.135	−0.371	−0.371	−0.160	−0.391	−0.391	−0.083	−0.298	−0.298
ρ_{rv}	−0.935	−0.927	−0.927	−0.932	−0.927	−0.927	−0.929	−0.926	−0.926	−0.939	−0.889	−0.889
$\rho_{r\gamma}$	0.646	0.568	0.568	0.664	0.591	0.591	0.683	0.616	0.616	0.624	0.510	0.510
$\rho_{v\gamma}$	−0.484	−0.503	−0.503	−0.495	−0.520	−0.520	−0.507	−0.541	−0.541	−0.468	−0.487	−0.487
$\rho_{\dot{z}z}$	−0.389	−0.439	−0.439	−0.372	−0.426	−0.426	−0.345	−0.403	−0.403	−0.431	−0.415	−0.415

Table 4. Uncorrected 1-σ Mars miss

Miss parameter	Transit time, days											
	216.1			220.9			230.3			235.3		
	CVA specs	JPL current	JPL pessimistic	CVA specs	JPL current	JPL pessimistic	CVA specs	JPL current	JPL pessimistic	CVA specs	JPL current	JPL pessimistic
Semimajor axis, km	49,800	115,000	344,000	59,400	134,000	401,000	65,800	145,000	436,000	65,600	164,000	492,000
Semiminor axis, km	4,150	10,000	30,000	3,740	8,610	25,800	2,960	7,150	21,500	1,600	3,910	11,700
Flight-time error, hr	5.82	14.88	44.64	6.28	15.23	45.70	7.32	17.11	51.33	6.12	15.84	47.53

Table 5. Required 1-σ midcourse capability

Errors corrected	Transit time, days											
	216.1			220.9			230.3			235.3		
	CVA specs	JPL current	JPL pessimistic	CVA specs	JPL current	JPL pessimistic	CVA specs	JPL current	JPL pessimistic	CVA specs	JPL current	JPL pessimistic
Miss components only, m/sec	1.97	4.59	13.77	2.11	4.76	14.27	2.15	4.86	14.60	2.01	5.01	15.0
Miss and flight-time, m/sec	3.10	8.16	24.49	3.34	8.57	25.71	2.93	7.53	22.58	2.84	6.89	20.68

calculating the required magnitudes is explained in another JPL publication.*

It will be seen that two values of speed increments are given for each trajectory. If it is required to correct only the miss components and not time-of-flight errors, then there is one degree of freedom which may be used to minimize the magnitude of the correction. If it is desired that the spacecraft be visible from a particular tracking station at encounter, it may be necessary to correct for time-of-flight errors with the midcourse maneuver. The two increments shown for each trajectory correspond to these two cases.

It has been assumed that the midcourse correction is made during one of the first few passes over Goldstone. However, the required speed increments change very little if the maneuver is made from 1 to 10 days after injection.

c. *Error Analysis*

The midcourse maneuver corrects for the relatively larger errors due to the injection guidance. However, the correction is computed from noisy data, and the execution of the maneuver is controlled by imperfect instruments. Thus, there will be small errors at the target due to errors in the midcourse-guidance system. The error coefficients associated with these system errors are listed in Table 6. The corresponding miss and flight-time variations for each error source are given in Tables 7 and 8, respectively.

Pointing accuracy refers to the accuracy with which the attitude-control system orients the thrust vector of the midcourse rocket. The pointing-error coefficient is an average over all possible firing angles, assuming all orientations are equally likely. The miss and time-of-flight errors due to the pointing error are proportional to the pointing error and the magnitude of the velocity correction. The current JPL estimate of pointing error is 0.441 deg rms.

Shutoff accuracy is the accuracy with which the magnitude of the velocity increment applied by the rocket is controlled. The shutoff-error coefficient is also averaged over all possible angles. The rms cutoff accuracy is assumed to be 0.467% of the correction ΔV.

The velocity-resolution error is a measure of the smallest increment of ΔV which can be commanded. It is a fixed error, rather than a proportional error, and is assumed to be 0.03 m/sec.

Since the computation of the correcting impulse is based on radio-tracking estimates of the orbit, errors in

*A. R. M. Noton, "Interplanetary Post-Injection Guidance," External Publication No. 653, Jet Propulsion Laboratory, Pasadena, Calif., 4 June 1959.

Table 6. Midcourse-error coefficients

Error source	Transit time, days: 216.1 Miss distance	216.1 Time of flight	220.9 Miss distance	220.9 Time of flight	230.3 Miss distance	230.3 Time of flight	235.3 Miss distance	235.3 Time of flight
Pointing	256 km/(deg m/sec)	0.0394 hr/(deg m/sec)	287 km/(deg m/sec)	0.0397 hr/(deg m/sec)	309 km/(deg m/sec)	0.0451 hr/(deg m/sec)	325 km/(deg m/sec)	0.0453 hr/(deg m/sec)
Shutoff	14,700 km/(m/sec)	1.65 hr/(m/sec)	16,400 km/(m/sec)	1.68 hr/(m/sec)	17,700 km/(m/sec)	1.88 hr/(m/sec)	18,600 km/(m/sec)	1.90 hr/(m/sec)
Resolution	14,700 km/(m/sec)	1.65 hr/(m/sec)	16,400 km/(m/sec)	1.68 hr/(m/sec)	17,700 km/(m/sec)	1.88 hr/(m/sec)	18,600 km/(m/sec)	1.90 hr/(m/sec)

Table 7. Miss at Mars due to midcourse errors

Error source and assumed accuracy	Transit time, days: 216.1 CVA specs km	216.1 JPL current km	216.1 JPL pessimistic km	220.9 CVA specs km	220.9 JPL current km	220.9 JPL pessimistic km	230.3 CVA specs km	230.3 JPL current km	230.3 JPL pessimistic km	235.3 CVA specs km	235.3 JPL current km	235.3 JPL pessimistic km
Pointing: 0.441 deg	350	921	2,763	423	1,085	3,255	400	1,027	3,080	407	989	2,966
Shutoff: 0.447% of ΔV	212	559	1,678	255	655	1,965	242	621	1,862	246	597	1,792
Resolution: 0.03 m/sec	441	441	441	492	492	492	531	531	531	558	558	558
Rms value	602	1,088	3,263	697	1,278	3,833	707	1,213	3,638	733	1,170	3,509
Radio tracking: 0.15 m/sec	~2,000 km											
Uncertainty, AU: 1/2000	~25,000 km											

Table 8. Time-of-flight variation due to midcourse errors

Error source and assumed accuracy	Transit time, days: 216.1 CVA specs hr	216.1 JPL current hr	216.1 JPL pessimistic hr	220.9 CVA specs hr	220.9 JPL current hr	220.9 JPL pessimistic hr	230.3 CVA specs hr	230.3 JPL current hr	230.3 JPL pessimistic hr	235.3 CVA specs hr	235.3 JPL current hr	235.3 JPL pessimistic hr
Pointing: 0.441 deg	0.0539	0.145	0.435	0.0585	0.150	0.450	0.0583	0.150	0.449	0.0567	0.138	0.413
Shutoff: 0.447% of ΔV	0.0229	0.0615	0.184	0.0251	0.0644	0.193	0.0246	0.0633	0.190	0.0241	0.0587	0.176
Resolution: 0.03 m/sec	0.0495	0.0495	0.0495	0.0504	0.0504	0.0504	0.0504	0.0504	0.0564	0.0570	0.0570	0.0570
rms value	0.0767	0.165	0.475	0.0811	0.171	0.492	0.084	0.172	0.491	0.0839	0.160	0.453
Radio tracking: 0.15 m/sec	~0.25 hr											
Uncertainty, AU: 1/2000	~3 hr											

the radio-tracking measurements will affect the miss at the target. The deep-space-net stations currently measure tracking angles and two-way doppler, but the relative accuracy of the measurements is such that the orbit is almost entirely determined by the doppler data. The range-rate data are assumed to be contaminated by gaussian noise with an rms value of 0.15 m/sec. From Tables 7 and 8 it will be seen that the errors at the target due to radio tracking are quite significant when compared with those resulting from injection guidance and the midcourse maneuver. The addition of range data reduces these errors substantially. For example, ranging with an an accuracy of 400 m, which is a very modest figure, will reduce tracking errors by a factor of approximately five.

For planetary trajectories, an additional source of error is the uncertainty in the astronomical unit (AU). In the ephemeris, the positions of the planets are tabulated quite accurately in terms of the AU. However, at the present time there is an uncertainty of about one part in 2000 in the conversion factor from AU to ordinary length units such as meters. It is anticipated that the uncertainty in the AU will be reduced in the near future by tracking of space probes, radar-ranging to Venus, and spectral observations. It is believed that the uncertainty in the constants, at the time of the *Mariner B* missions, will contribute negligible error compared to the other errors in Tables 7 and 8.

d. Approach Guidance

The dispersions described in the preceding Section are too great to permit satisfactory entry of a capsule into the Martian atmosphere. Approach guidance will be employed to reduce the miss distance to less than 320 km (1 σ) from the nominal guidance point. This accuracy allows considerable choice of landing area on Mars and meets the requirement that the atmospheric-entry angle of the capsule lie within proper limits.

The measurements used to determine the required approach maneuver consist of position fixes which are obtained by measuring the apparent angular diameter of the target planet and the angles between the planet and two stars. The measured fixes are compared with values for a standard trajectory, and the required correction maneuver is then computed.

The magnitude of the required approach correction depends directly on

(1) the initial miss distance M, which results after the midcourse maneuver

(2) the approach velocity V_∞ relative to the target

(3) the equivalent angular instrument errors $\delta\theta$

(4) the accuracy required at the target δM

The geometry assumed is shown in Fig. 22. The 1-σ values of the significant quantities are assumed to be

$$M = 4800 \text{ km}$$
$$V_\infty = 5 \text{ km/sec}$$
$$\delta\theta = 0.8 \text{ mil}$$
$$\delta M = 320 \text{ km}$$

The approach-maneuver propellant requirement for a fixed reduction in target miss is affected by the location and sequence of the approach maneuver. The miss distance after an approach maneuver is primarily determined by the accuracy of the fixes used to compute the maneuver. Thus, for a given set of instruments, the final miss decreases as the measurement points approach the planet, since absolute distance accuracy improves. On the other hand, more propellant is required to correct a previously existing error as the maneuver point is moved nearer the planet. By making a first approach correction relatively far from the planet, when the measurements are relatively inaccurate but the effectiveness of a unit weight of propellant in removing midcourse errors is high, and then a second (and possibly third) correction nearer the planet, with more accurate fixes to reduce the residual inaccuracies of the first maneuver, a saving is effected in the total propellant requirement for approach guidance. Table 9 shows typical results of such an optimization. It is seen that making two maneuvers results in a significant saving in velocity requirement, while making a third saves very little over a second. In each case, the final maneuver is made at the same radius from the target, that radius being determined by the assumed instrument errors and required accuracy at the target.

e. Miss Maneuver

As soon as possible after the final approach correction is performed, the capsule will be separated from the spacecraft, and the spacecraft will then perform a final maneuver so that it misses the target planet. This miss maneuver will be performed at a distance of approxi-

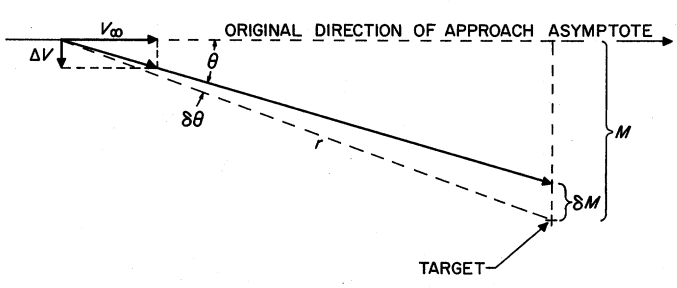

Figure 22. Approach-guidance geometry

Table 9. Approach-maneuver velocity requirements

Parameter	Number of corrections, n		
	1	2	3
2.5-σ velocity requirement, m/sec	150	77.5	74.0
First correction radius, km	0.40×10^6	1.55×10^6	2.43×10^6
Second correction radius, km	—	0.40×10^6	0.98×10^6
Third correction radius, km	—	—	0.40×10^6

Assumptions:
(a) Initial miss = 4800 km (1 σ)
(b) Velocity relative to target = 5 km/sec
(c) Equivalent angular instrument error = 0.8 mil (1 σ)
(d) Required accuracy at target = 320 km (1 σ)

mately 380,000 km from the target. If a maximum V_∞ of 5 km/sec is assumed and the focusing effect of Mars acting upon both capsule and spacecraft is taken into account, the transverse-velocity increment required to cause the spacecraft to pass 8000 km from the nominal capsule landing point is found to be 112 m/sec.

If one accepts the JPL pessimistic requirements for the midcourse maneuver in Table 5 and the approach correction requirements of Table 9, then one finds the following velocity requirements allocated for the entire mission:

2.5-σ midcourse (spacecraft plus capsule)..... 60 m/sec

2.5-σ approach (spacecraft plus capsule)..... 78 m/sec

8000-km minimum miss (spacecraft only).....112 m/sec

Since it is improbable that all the fuel allocated for midcourse and approach maneuvers would be used, there generally will be a capability of performing more than the minimum 8000-km miss maneuver. This is fortunate, since a miss greater than 8000 km will reduce (or eliminate) the eclipse time of the capsule-to-spacecraft link by the Mars horizon. It is useful to express the probability of miss-maneuver capability vs the miss maneuver. This is done in Fig. 23. It should be noted that the approach-maneuver and midcourse requirements are not independent, since the errors resulting at the target are largely a function of the magnitude of the midcourse maneuver. An exact analysis of the correlation has not been completed, but an upper and lower bound can be shown by assuming $\rho = 0$ and $\rho = 1$.

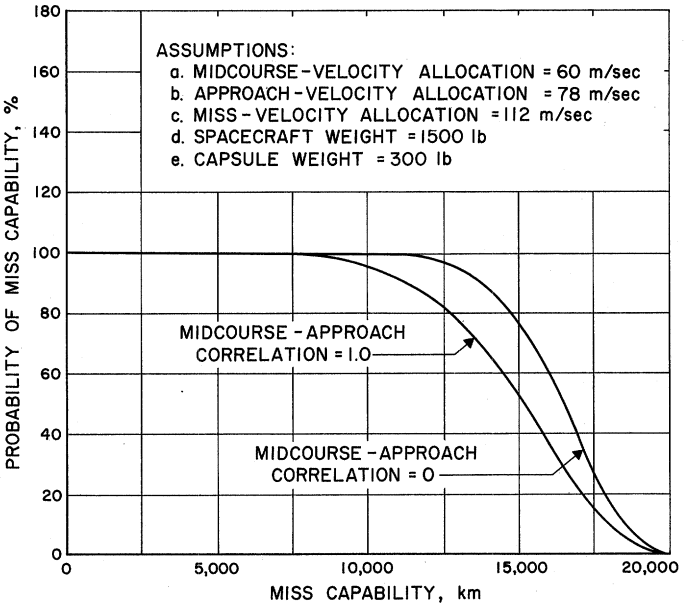

Figure 23. Probability of miss-maneuver capability

Finally, it should be pointed out that the dispersion of the spacecraft trajectory at closest approach to the planet will be approximately the same as that of the capsule trajectory; namely, 320 km (1 σ).

4. Guidance and Control

R. V. MORRIS, J. D. ACORD, W. G. BRECKENRIDGE, D. NEWELL, AND N. SIRRI

(This Section is UNCLASSIFIED)

a. Introduction

The guidance and control subsystems of the *Mariner B* spacecraft provide automatic control of the motion of the spacecraft and its movable-component assemblies, and automatic control of the interaction of certain spacecraft operations and processes. For convenience of discussion, the control of the translational motion of the spacecraft is called "guidance"; the control of the angular motion of

UNCLASSIFIED

movable assemblies and of the spacecraft about its own center of mass is termed "attitude control." The process-control functions consist mainly of initiating the actions of spacecraft subsystems or subsystem elements at the proper time or in the presence of certain sets of conditions.

The purpose of this Section is to present discussions of alternative methods of meeting some of the more difficult *Mariner B* guidance-and-control requirements, rather than to describe complete guidance and control subsystems. For certain cases, in which established techniques exist (from *Ranger* and *Mariner A* experience) that are well suited to meet *Mariner B* requirements, no alternative techniques will be discussed. Examples of such items are: (1) the use of the Sun to stabilize two axes of the spacecraft, (2) the use of an accelerometer to shut off the spacecraft-propulsion system, and (3) the use of an Earth-based radio-midcourse maneuver. It is assumed that the reader is familiar with the guidance and control subsystems utilized in the *Ranger* and *Mariner A* spacecrafts. Hence, when a concept or technique is discussed without a detailed explanation, or consideration of alternatives, use is generally being made of *Ranger* or *Mariner A* experience.

b. General Performance Requirements for the Mariner B Guidance and Control Subsystems

A set of requirements for guidance and control subsystem performance that appears sufficient to fulfill the *Mariner B* mission requirements follows. This set of requirements is the basis for the feasibility and tradeoff studies currently in progress.

(1) General

(a) The attainment of a high degree of reliability and an operational lifetime in excess of eight months, with minimal consumption of weight, space, and power.

(b) Growth potential toward a subsystem with expanding capabilities to match the increasing degree of ambitiousness that characterizes later spacecraft missions.

(c) Maximum use, in a manner consistent with the other parts of these requirements, of techniques developed in previous series of spacecraft.

(2) Guidance

(a) Capability of executing a radio-controlled midcourse-guidance maneuver during the first few days of flight that will enable the spacecraft to pass through a destination corridor not more than a few thousand kilometers in size.

(b) Capability of performing a series of approach maneuvers in the vicinity of the destination planet to accomplish the following objectives:

1. Establishment of an approach trajectory such that the capsule, when released from the spacecraft, will, without further propulsive maneuvers, have a probability greater than 0.997 of passing within 800 km of a specified point of entry into the atmosphere. The aiming point chosen leads to a nominal atmospheric-entry angle of 40 deg from the local horizontal, with dispersions in the range from 22 to 52 deg, and allows maximum communication between the capsule and the carrier.

2. Modification of the spacecraft trajectory following capsule release to cause the spacecraft to pass with a probability greater than 0.997 through a particular corridor between the surface of the destination planet and the Sun. This corridor has a minimum periapsis distance of 13,310 km and a maximum of 16,550 km (corresponding to an altitude above the surface at the point of closest approach from 8000 to 13,240 km). The additional constraints are imposed that the angular separation between the near limbs of the destination planet and the Sun always be greater than 6 deg, and that the angular separation between the near limbs of the destination planet and the Earth always be greater than 15 deg. The minimum periapsis distance is determined from the requirement of constant communication with the capsule. The maximum periapsis distance is limited to ensure significant observable doppler-frequency changes at the Earth, reasonable propellant requirements and observations of the planet, and the angular-separation requirements from limitations of the attitude-control sensors and the requirement of continuous communication with the Earth.

3. Capability of performing similar maneuvers when the Earth is the destination planet for an initial test flight.

UNCLASSIFIED

(3) **Attitude-Control**

(a) Capability of aligning the spacecraft reference axes with respect to celestial objects to an accuracy between 0.1 and 0.5 deg.

(b) Capability of pointing a directional antenna at the Earth to an accuracy of ±1.0 deg at ranges up to the maximum required for the performance of the spacecraft mission.

(c) Capability of orienting the spacecraft to any commanded orientation and maintaining that orientation for a period of 2 to 3 hr, with an accuracy compatible with that of (1).

(d) Capability of pointing a movable assembly at the destination planet to an accuracy of ±0.5 deg in the distance range from 11,310 to 153,310 km from the center of the destination planet (8000 to 150,000 km from the surface of the planet).

(e) Capability of re-establishing the spacecraft and antenna reference directions automatically following any noncatastrophic disturbance of the spacecraft attitude, programmed or otherwise.

(f) A lifetime at least 15 days in excess of the time to encounter with the destination planet to provide for transmission to the Earth of relayed or stored data using the directional antenna.

(4) **Computing, Control, and Sequencing**

(a) Performance of basic timing, sequencing, and process-control operations for the spacecraft.

(b) Performance of digital decision-making and computing operations for approach guidance, and for other subsystems as required.

(c) Capability of accepting from the communications or other subsystems, storing, and delivering in suitable form to the user, all quantitative command data transmitted to, or generated in, the spacecraft, for delayed execution.

c. Guidance

The task of the spacecraft guidance subsystem is to control the translational motion of the spacecraft with respect to the Sun and planets. The guidance loops required for performance of the mission being considered for the *Mariner B* spacecraft include a radio-controlled early midcourse-guidance loop to improve the accuracy in time and position of arrival in the vicinity of the destination planet and a planetary approach-guidance loop operating on vehicle-based observations (and, possibly, also ground-based radio data) of the vehicle motion to further improve the accuracy of delivering the capsule to its release point from the spacecraft, and subsequently to cause the spacecraft carrier motion to be modified in such a way that the spacecraft passes by the planet a few thousand kilometers above its surface.

The guidance-and-control aspects of the propulsion subsystem which serves as the common actuator for the midcourse- and approach-guidance loops are discussed first. The midcourse-loop operation, which is a direct extension of similar techniques on earlier *Mariner* and *Ranger* spacecraft, is reviewed. The major part of the Section is then devoted to the approach-guidance subsystem, which comprises the major addition to the overall guidance-and-control capability of the spacecraft.

(1) Thrust-Vector Control

In making both the midcourse and the approach-guidance corrections, a major concern is to control the incremental-velocity vector added to the existing spacecraft velocity vector in such a way that the magnitude and direction determined by the guidance computations are obtained.

The accuracy with which these velocity changes must be added is quite stringent. Directional accuracies of a few milliradians and magnitude accuracy to a small fraction of a meter per second are required. Consequently, subsidiary control loops are needed to insure that the velocity increments have the proper magnitudes (speed control) and directions (direction control).

(a) Speed control

The magnitude of the trajectory-correction velocity increment (the speed of the increment), is controlled in the *Mariner B* spacecraft in the same manner as is employed in *Mariner A*. There are four types of errors that enter into the speed-control system: accelerometer scale factor, accelerometer null offset, velocity resolution, and thrust tail-off variations. If $\dot{v}$ is the spacecraft acceleration (approximately constant because only a small percentage of the spacecraft weight is consumed for fuel) and v is

UNCLASSIFIED

the commanded spacecraft speed increment, then Δv, the speed error, is:

$$\Delta v = (K + \eta/\dot{v})\, v + \delta v_1 + \delta v_2 + \delta v_3$$

where

K = accelerometer scale-factor error (6×10^{-3}, 3 σ)
η = accelerometer null offset ($7.5 \times 10^{-4}\ g$, 3 σ)
$\dot{v}$ = spacecraft acceleration (0.1 g)
δv_1 = accelerometer velocity resolution ($\pm$0.015 m/sec)
δv_2 = command velocity resolution ($\pm$0.015 m/sec)
δv_3 = tail-off velocity variation (0.04 m/sec, 3 σ)

The numbers are typical of what may be achieved for the *Mariner B*. With the *Mariner B* acceleration, they give a proportional error of 0.96% (3 σ) and a resolution error of 0.054 m/sec (3 σ). Further improvements in the accelerometer might reduce the null-offset and scale-factor errors by a factor of about two, giving an error of approximately 0.5% (3 σ). It is also expected that the size of the accelerometer-rebalance pulses may be changed from 0.03 to 0.01 m/sec, which reduces the resolution errors to $\pm$0.005 m/sec each.

(b) Direction control

The rocket-motor nominal-thrust direction is essentially fixed with respect to the spacecraft. The direction of the velocity increment is controlled by initially turning the spacecraft before ignition so that the nominal-thrust line is pointed in the required direction. This is accomplished by using commanded turns, as is done in *Mariner A*; however, a study will be made to determine the optimum commanded-turn mode for *Mariner B*. The factors to be considered in such a study are indicated below.

Use of commanded turns to establish initial direction. Requirements as to the number of turns, the axes that are used, the limits on the turn size, and the accuracy of turning are discussed here. To point a single body-fixed line of the spacecraft in a specified direction requires not more than two single-axis turns (specific special orientations may require no turn or one turn). If the line to be pointed is parallel to a spacecraft control axis, then there are four possible choices of order and axes; if it is not parallel to any control axis, there are six choices. For a thrust line parallel to the roll axis, the turn choices are pitch–yaw, yaw–pitch, roll–pitch, and roll–yaw. Because pitch and yaw can be used interchangeably, only pitch–yaw and roll–pitch are discussed.

In either case, the maximum total angle turned is 270 deg; hence, neither has an advantage in this respect if there are no restrictions on the final direction. Such restrictions (e.g., that the direction be in a specified plane) may favor one order of turn over another, and reduce the maximum required turn. They are based mainly on the guidance-peformance requirements, but advantage can be taken of guidance-performance leniencies, such as a noncritical direction, to reduce the number, size, or complexity of the commanded turns.

One turn sequence may have an advantage over another by being inherently more accurate; e.g., the roll–pitch sequence, because it permits retaining Sun lock during the roll turn, eliminating any pitch and yaw gyro drift during this portion of the turn. In some cases, making expedient use of the previously mentioned direction restrictions may be even more advantageous.

The single-axis turns discussed are best adapted to an attitude-control system using a fixed rate of turn for a variable time. However, if the attitude-control system is capable of making accurate turns over a wide range of rates, then it is possible to orient the spacecraft using only a single turn of not more than 180 deg. This speeds up the total turning time, but is more difficult to mechanize, because it requires simultaneous turns about two axes, with turning rates calibrated accurately over a range from zero to a specified maximum rate. The orientation of a line parallel to a control axis can be accomplished in the minimum possible turning angle by means of simultaneous turns about the other two control axes.

The attitude-control system may also make turns based on position only, as would be the case if a stable platform were used. This can provide the most accurate turn, because it is independent of gyro calibration and integration errors. Accuracy is determined solely by the angle pickoff, tracking accuracy, and the platform-drift rate. The turns may be made one at a time or simultaneously, with no difference in accuracy other than that due to different lengths of the platform-drift time.

Any requirements placed on the commanded turns other than pointing the nominal-thrust line increases the number of turns required. It takes three turns to place the whole spacecraft in a specified orientation, as might be required to point the directional antenna toward the Earth during the motor firing. To insure that the final position of the antenna is not within the motor-exhaust stream might require control of five degrees of freedom (DF). Three of these can be provided by the spacecraft and two additional relative-motion DF are needed for the antenna (because the requirement of avoiding the exhaust cannot always be met if the antenna has only one DF). The more stringent requirement of pointing the antenna at the Earth continuously during, as well as after, the turn puts even harsher requirements on the commanded turns and absolutely requires simultaneous

UNCLASSIFIED

commanded-turn control of the spacecraft and antenna DF, unless the antenna is actively tracking the Earth.

The accuracy of the commanded turns depends on

(1) number, sequence, and axes of turns

(2) size of individual turns

(3) reference-sensor null offsets

(4) spacecraft reference-lock accuracy

(5) turn reference (e.g., gyros) alignment and drift

(6) accuracy in making the individual turns

(2) Autopilot Loops

The total task of the autopilot is the two-fold task of simultaneously controlling the location and direction of the thrust vector with respect to the spacecraft to maintain vehicle stability, and controlling the inertial direction of the spacecraft as a function of this vehicle-referenced thrust-vector position to obtain the correct inertial directions of the thrust vector and velocity increment.

Figure 24 shows the two autopilot loops used to complete this task. The inner stabilization loop measures the spacecraft inertial angular rate and position to control the direction and location of the thrust vector in such a way that it passes through the instantaneous spacecraft c.g. The outer path-guidance loop determines the direction of the thrust vector with respect to the spacecraft, computes the integrated effect of this direction, and uses this result as an input command to the inner loop to adjust the spacecraft inertial angular position to compensate for the change in direction of the thrust vector with respect to the spacecraft.

The methods of sensing the direction of the thrust vector vary with the basic method of controlling its direction and location; hence, these two topics are discussed together in the following paragraphs. A salient feature of all methods is that the measurement of direction is essentially a measurement in the feedback portion of a control system, which imposes definite requirements of accuracy in calibration and measurement. It is assumed that the thrust vector nominally lies along the roll axis. Steady-state deviations in direction between the direction of the

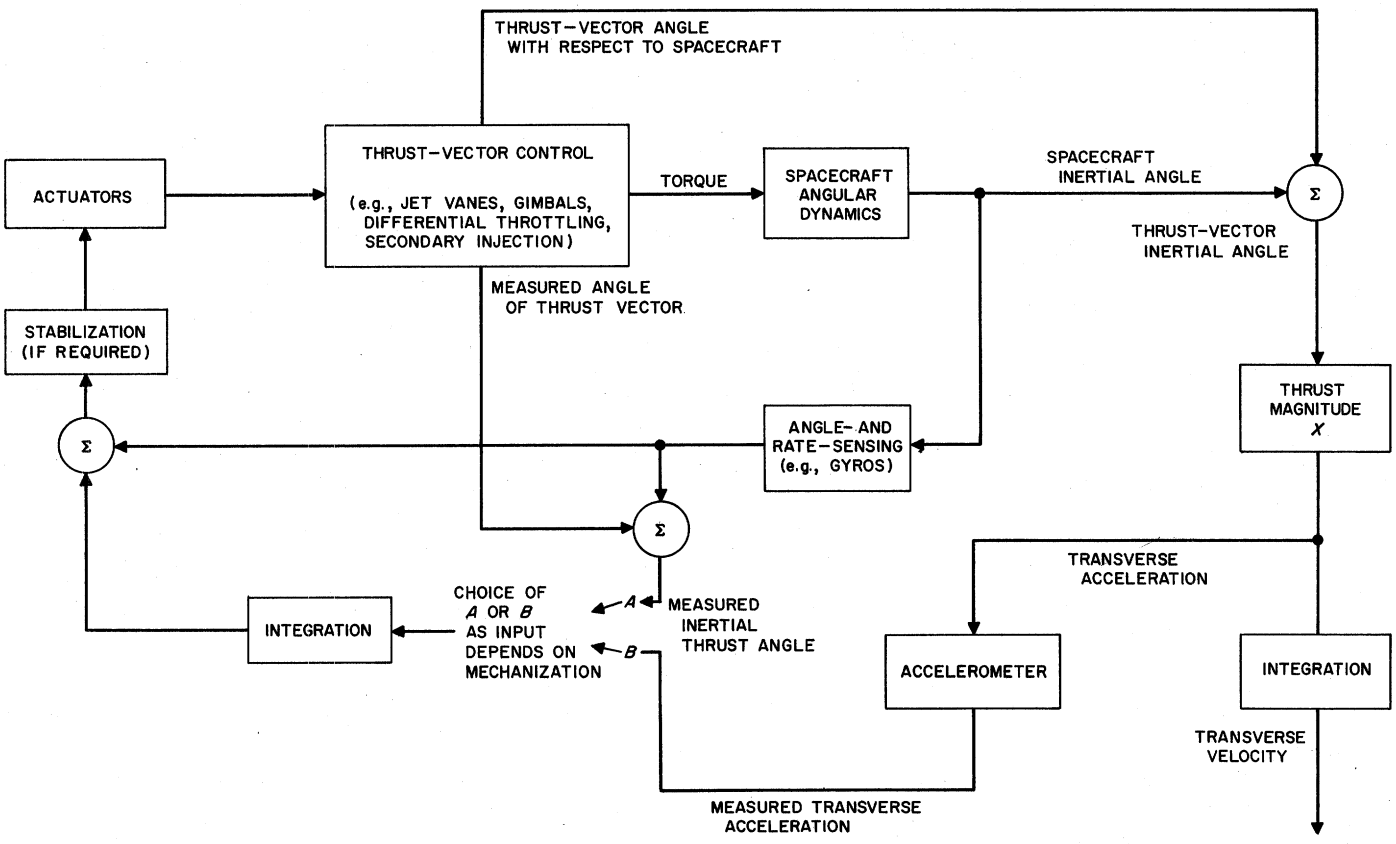

Figure 24. Autopilot diagram

UNCLASSIFIED

thrust vector and the roll axis occur as a result of nonparallelism between the real axis and the thrust line of zero torque (which passes from the point of application of the thrust vector to the instantaneous spacecraft c.g. and along which the thrust vector must lie such as to prevent continuous angular acceleration). Misalignment of the zero torque line results from transverse displacement of the c.g. or of the thrust point-of-application.

Control of the pitch and yaw torques on the spacecraft is effected by varying the direction or the transverse location of the resultant thrust line-of-action on the spacecraft. Control of the roll torque is effected by the generation of a resultant transverse force or couple acting on the spacecraft at some distance from the roll axis.

For single-motor propulsion systems, pitch and yaw torques are most often generated by controlling the direction of the thrust vector about a fixed point-of-application. Transverse motion of the thrust chamber will also be considered. The direction may be controlled by gimballing the thrust chamber to align it mechanically in the desired direction (requiring flexible propellant-feed lines); by secondary injection of a fluid into the rocket nozzle to disturb the normal flow pattern; or by jet vanes (as on *Ranger* and *Mariner A*) that project into the stream and produce side forces. The first two methods require that separate roll-control torques be generated, because the thrust-vector point-of-application lies along the roll axis. Torques about the roll axis are also obtainable directly from the forces of jet vanes, because they are at the sides of the nozzle.

For multiple-motor systems, either the location or direction of the thrust line-of-action may be controlled. Changes in the location of the resultant thrust line-of-action result from differentially controlling the relative thrust levels of two or more engines that have fixed directions with respect to the roll axis and are displaced from it. If these directions are not parallel to the roll axis (canted), changes in the direction of the resultant thrust may also occur. Torque couples, too, are generated by the differential throttling action. Changes in the resultant direction can also be obtained by changing the directions of the individual components about fixed points of application at constant thrust levels. The jet-vane system, at first glance, appears to possess a number of advantages. Pitch, yaw, and roll control can all be obtained with a single thrust chamber that is hard-mounted to the propellant tankage to avoid flexible feed lines. However, the vanes reduce the propulsion efficiency slightly as a result of the drag of the exhaust stream, operate in a high-temperature (and sometimes corrosive) atmosphere, and have the least capability for modifying the direction. The amount of deviation that can be produced is critically important, because the change in direction ρ required to counteract the effects of a transverse offset Δ in the position of the c.g., expressed in radians, is given by $\rho = \Delta/L$, where the amount Δ of transverse offset is divided by L, the distance (along the roll axis) between the point of application and the c.g. position. Because the spacecraft are relatively short, the denominator is small, resulting in large angular deviations to control a given c.g. offset. A larger angular range of the thrust direction can usually be obtained from a gimballed engine. The properties of secondary injection are still under investigation.

To obtain roll control directly from the rocket engine while maintaining the capability for a reasonable range of angular deviations, two gimballed engines displaced from the roll axis may be used. The couple resulting from differential gimballing at full thrust provides the desired roll torques.. A larger capability for c.g. offset control can be obtained by the differential throttling of a set of engines, fixed in location and direction, reducing the size of the actuators required. Roll control can be obtained by canting of the engines or by controlling individual thrust-vector directions (e. g., by jet vanes).

The ability to control in the presence of large movements of the spacecraft c.g. is desirable in order to eliminate stringent requirements on the accuracy and reliability of controlling the articulated elements. For example, motion of the planetary horizontal platform of the *Mariner A* by 1 deg near the stowed position results in a transverse c.g. motion of 0.03 in. *Mariner A* uses jet vanes, and $\pm$0.17-in. c.g. motion is the maximum allowable, with motion of 0.35 in. in either direction causing jet-vane saturation. With a gimballed motor, allowable c.g. motion might be increased by a factor of 3 to 5, and with differentially throttled engines, another similar improvement could be obtained.

Errors and disturbances enter the autopilot system from motion of the c.g., translational and angular misalignments of the thrust units, and null offsets within the control loops.

For direction-control systems, angular misalignments and control-system null offsets cause the direction of the thrust vector at zero input to be deflected from the nominal, requiring a steady-state signal to hold the thrust vector along the nominal direction for stability. An integrator can be introduced to provide this signal, preventing the error in thrust-vector direction that would result from changing the spacecraft direction to provide the offset signal. Translational offsets require that the thrust vector be turned from the nominal alignment to lie along the zero torque line for stability. If the vehicle attitude

UNCLASSIFIED

were such that the roll axis kept the desired direction, an error in the direction of the thrust vector would result. It is the task of the outer loop to detect this steady-state deviation in the direction of the thrust vector and cause the inner attitude control to turn the vehicle by an equal and opposite amount.

For location-control systems, control of c.g offsets does not change the resultant thrust direction for a set of axial motors but may change the direction for canted motors. Angular misalignments of the fixed-direction multiple motors cause a resultant direction error and require an outer loop. An integrator in the inner loop counteracts c.g. offsets and differences in the zero-control individual thrust levels.

Unfortunately, the actions of the inner- and outer-loop integral control tend to cancel one another, so that the complete elimination of the effects of one type of error leads to the full effect of the other type. However, statistically optimized gains can be selected that force the variance of the total error to be equal to, or smaller than, the variance of the smaller type of error.

The means for sensing the direction of the resultant thrust vector vary with the means of controlling its direction or location. For any system, an accelerometer may be used to detect the transverse acceleration. By nulling the integral of the transverse acceleration, the transverse velocity error is also eliminated, ensuring that the velocity increment will be added in the proper direction. For the jet-vane system, the relationship between the deflection of the vanes and the deflection of the thrust vector is reasonably linear before saturation occurs; hence, multiplication of the measured vane deflection by a gain provides a signal related to the direction of the thrust vector. Secondary injection systems can probably be calibrated in a manner similar to that used with the jet vanes. For intentionally canted multiple-motor systems, knowledge of the thrust levels of the individual engines can be used in much the same fashion as knowledge of the jet-vane deflections. An accelerometer appears to be required if the alignment accuracies of axial engines (expected to be in the neighborhood of 0.1 to 0.2 deg) require correction. For a gimballed system, the gimbal angles can be measured directly.

Although no choice of the *Mariner B* autopilot configuration will be made until the preliminary design period, leading contenders include a single-engine jet-vane system and a differentially throttled multiple-engine system. The latter still requires considerable analysis to determine its properties. It has been established, however, that control of pitch, roll, and yaw by the differential throttling of fixed, canted motors requires the use of at least four motors. If a three-motor system is desired, it is necessary to introduce a fourth control loop, such as jet vanes or gimballing of at least one motor.

(3) Midcourse Guidance

The midcourse-guidance loop and the approach-guidance loop successively act to increase the accuracy with which the spacecraft carrier delivers the capsule to its release point over the obtainable with injection guidance alone. With injection guidance only, errors in arrival of the spacecraft are many thousands of kilometers, and errors in the time of arrival range up to 12 hr or more. With midcourse guidance, the errors may be reduced to a few thousand kilometers and arrival-time errors to less than an hour. Approach guidance is then required to reduce the position errors to a few hundred kilometers.

Theoretically, either the midcourse- or approach-guidance systems alone could bring the spacecraft to the desired position and time with the accuracy required. However, for midcourse guidance, the accuracy of tracking and velocity control would require improvement considerably beyond present feasibility, and improved knowledge of the astronomical unit is required. For aproach guidance, the propellant requirements would be completely unreasonable if it were necessary to cope with the raw injection errors at the destination planet. Consequently, both systems are used, the midcourse making an early correction where the effectiveness of a unit weight of propellant is very high, reducing the arrival errors in time and position by as much as possible. Then, upon arrival near the destination planet, where more accurate determination of the final spacecraft path can be accomplished, approach maneuvers are made to remove the residual error left by the midcourse maneuver. The amount of error that can be removed by a unit weight of propellant is much smaller, and the approach maneuvers act as a "vernier" correction to the midcourse maneuver. The second use of the approach-guidance system is to change the trajectory of the carrier portion of the spacecraft following release of the capsule.

Usually, a single midcourse maneuver will be performed before the spacecraft has gone more than a million kilometers from the Earth. No further maneuvers are then performed until the spacecraft reaches its approach phase at about two million kilometers from the destination planet.

For a summary of the midcourse-guidance accuracy capabilities, the reader is referred to Section IIIB-3.

(4) Approach Guidance

The addition of the approach-guidance loop represents the major increase in the guidance-and-control capability of the *Mariner B* spacecraft over that of *Mariner A*. The basic guidance technique used for approach guidance is the same as that employed for midcourse guidance, in the sense that in both cases the guidance equations are based on the fact that the motion of the spacecraft along its actual trajectory is only slightly perturbed from a desired nominal trajectory. Because these perturbations are small, the equations of motion may be written as a set of first-order differential equations in the perturbation quantities, despite the fact that the total equations of motion are nonlinear. Once the linearized equations have been obtained, the problem of designing the midcourse- or approach-guidance subsystem reduces to that of designing a final-value control system with only impulsive forcing at particular times during the control interval. (The forcing may be considered impulsive because of the short duration of the maneuvers relative to the total flight time.) The difference between a conventional follow-up control system and a final-value control system is that the former continuously controls the present response, whereas the latter controls the response at a particular final time (i. e., the position of the spacecraft at the time the capsule is released). It is a result of final-value control theory as applied to approach guidance (or other systems described by linear differential equations) that the components of the velocity increment for each maneuver can be determined by simple matrix operations on the sensor outputs. For approach guidance, this type of determination of the velocity increments is probably adequate. For midcourse guidance, further increases in accuracy are obtained with an iterative process of improving the linear prediction of the velocity increment by comparison of the linear predictions with the results of integrated solutions of the total equations of motion that use the linearly predicted velocity increment as a forcing input. Although no alternate approach-guidance technique will be considered here, it should be pointed out that certain trajectory studies must be completed before all of the assertions made above can be verified. In the following portions of this Section, it is assumed that the above statements are valid, and various areas in which approach guidance differs from midcourse guidance are discussed.

A block diagram of the approach-guidance loops is shown in Fig. 25. A basic difference between midcourse- and approach-guidance loops is that midcourse uses Earth-based radio tracking stations for system-response measurement, whereas approach-guidance requires spacecraft-based measuring instruments which operate in the infrared or visible spectral regions. Features common to both loops are the use of a digital computer to perform the functions of the feedback, command-extraction, comparison, and part of the control elements, and use of the spacecraft propulsion system and its associated subsidiary loops as the actuator. The digital computer for approach guidance may be located in the spacecraft or on the ground. It is convenient for discussion of approach guidance to separate the determination of the current values of system response (i.e., the present position)—to be called "navigation"—from the determination and execution of the required maneuvers.

(a) Number and location of maneuvers

The number and location of the approach-guidance maneuvers are selected to meet the following design criteria:

(1) The error after the final maneuver is within the performance requirements.

(2) The minimum amount of fuel is required for the approach maneuvers.

(3) The smallest number of maneuvers compatible with (1) and (2) is chosen to minimize the guidance computation and maneuvering required and to maximize reliability.

The number and location of the maneuvers depend mainly on the required final accuracy, the dispersion before the maneuvers, and the navigation accuracy. Most other errors in the approach-guidance system have smaller effects. Figure 26 shows the simplified straight-line geometry of the measurements and corrections for approach guidance of the spacecraft in a single plane. The angles are shown expanded, but small angle approximations are assumed to hold. The variables shown in the Figure are defined as:

V_∞ = speed along the path

R_i = range for ith maneuver

A_{is} = standard star–spacecraft–planet angle for the standard trajectory

A_i = actual star–spacecraft–planet angle for a perturbed trajectory

A_{im} = measured star–spacecraft–planet angle

δ = error in path direction, unknown but constant

γ_i = error in measuring A_i

Y_0 = initial miss distance

Y_{01} = trajectory deviation at R_1

Y_i = miss after the ith maneuver

UNCLASSIFIED

The side velocity actually required to rotate the path to strike the target at any range is given by

$$\frac{\Delta Y_a}{V_\infty} = -\left(\frac{Y_a}{R_a} - \delta\right) \tag{1}$$

where a denotes actual quantities. Also,

$$\Delta A_a = A_a - A_{as} = \frac{Y_a}{R_a} \tag{2}$$

Hence,

$$\frac{\Delta Y_a}{V_\infty} = -\Delta A_a + \delta \tag{3}$$

and, in the absence of an error in path direction,

$$\frac{\Delta Y_a}{V_\infty} = -\Delta A_a \tag{4}$$

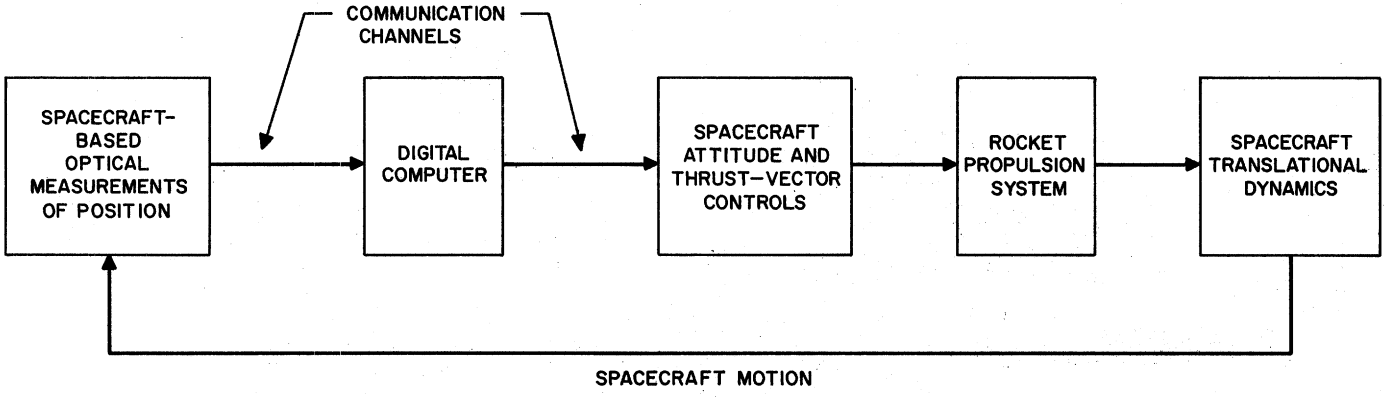

Figure 25. Approach-guidance loop

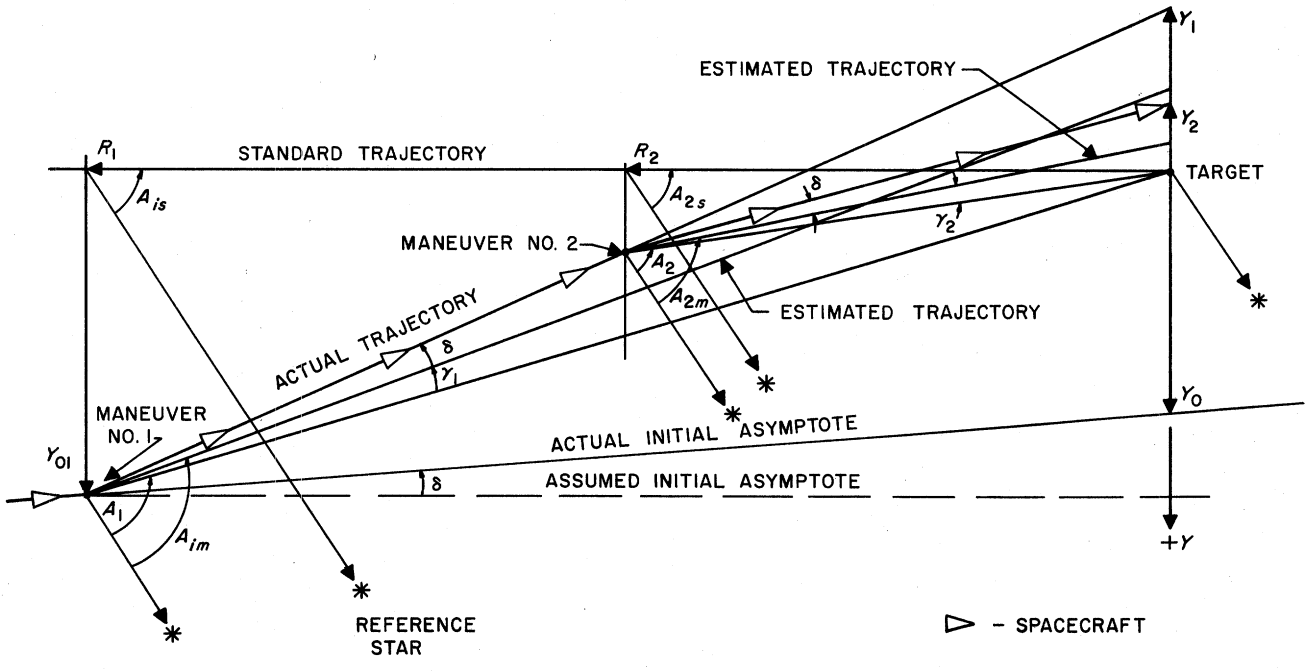

Figure 26. Single-plane approach guidance, two-correction manuever

UNCLASSIFIED

UNCLASSIFIED

For the first maneuver,

$$Y_{01} = Y_0 + R_1 \delta \tag{5}$$

$$A_1 = A_{1s} + \frac{Y_{01}}{R_1} = A_{1s} + \frac{Y_0}{R_1} + \delta \tag{6}$$

$$A_{1m} = A_1 + \gamma_1 = A_{1s} + \frac{Y_0}{R_1} + \delta + \gamma_1 \tag{7}$$

The measured angle error ΔA_1 is then,

$$\Delta A_1 = A_{1m} - A_{1s} = \frac{Y_0}{R_1} + \delta + \gamma_1 \tag{8}$$

Now, the side velocity ΔY_1 needed to rotate the path to hit the target can be estimated, on the assumption of no path-direction error, by substituting ΔA_1 for ΔA_a in Eq. (4):

$$\frac{\Delta Y_1}{V_\infty} = -\left(\frac{Y_0}{R_1} + \delta + \gamma_1\right) \tag{9}$$

The miss Y_1, resulting from this maneuver at R_1, is

$$Y_1 = Y_0 + R_1 \frac{\Delta Y_1}{V_\infty} = -R_1 (\delta + \gamma_1) \tag{10}$$

For a trajectory that strikes the target (collision course), the standard angle is independent of range. The maneuver at R_1, which, if free from errors in execution, changes the direction of the path by ΔA_1, is intended to put the spacecraft on a collision course. Hence, the standard angle A_{2s} at R_2 must be modified to get a corrected standard, A'_{2s}.

$$A'_{2s} = A_{2s} + (A_{1m} - A_{1s}) = A_{2s} + \frac{Y_0}{R_1} + \delta + \gamma_1 \tag{11}$$

The actual angle A_2 is

$$A_2 = A_{2s} + \frac{1}{R_2}\left[\frac{R_1 - R_2}{R_1} Y_1 + \frac{R_2}{R_1} Y_{01}\right]$$

$$= A'_{2s} + \left[\delta - \frac{R_1}{R_2}(\delta + \gamma_1)\right] \tag{12}$$

Also,

$$A_{2m} = A_2 + \gamma_2 = A'_{2s} + \delta + \gamma_2 - \frac{R_1}{R_2}(\delta + \gamma_1) \tag{13}$$

and

$$\frac{\Delta Y_2}{V_\infty} = -(A_{2m} - A'_{2s}) = -\left[(\delta + \gamma_2) - \frac{R_1}{R_2}(\delta + \gamma_1)\right] \tag{14}$$

Thus, by the same procedure,

$$Y_2 = Y_1 + R_2 \frac{\Delta Y_2}{V_\infty} \tag{15}$$

$$= -R_2 (\delta + \gamma_2) \tag{16}$$

Extending this analysis to the ith maneuver,

$$\frac{\Delta Y_i}{V_\infty} = -(\delta + \gamma_i) + \frac{R_{i-1}}{R_i}(\delta + \gamma_{i-1}) \tag{17}$$

and

$$Y_i = -R_i (\delta + \gamma_i) \tag{18}$$

The errors δ and γ_i are the uncorrected portions of errors in asymptotic-direction and angle measurements, which may be the residual errors after partial error reduction as discussed later in this Section. It is also assumed here that no correction of the knowledge of asymptote direction is made after the maneuvers have started.

The amount of fuel required for the total number N of maneuvers is determined by the sum of the individual velocity magnitudes. The propulsion-system performance is defined by

$$\Delta V = g_0 I_{sp} \ln\left(\frac{m_0}{m_0 - \Delta_m}\right) \tag{19}$$

where

m_0 = the initial spacecraft mass
Δm = the mass of propellant used
$g_0 I_{sp}$ = the motor equivalent exhaust velocity.

Let the fractional portion of the spacecraft mass used for fuel in a single maneuver be $\eta = \Delta m/m_0$. Then, if η is small,

$$\frac{\Delta Y}{V_\infty} \simeq \left(\frac{g_0 I_{sp}}{V_\infty}\right)\eta \tag{20}$$

and the total fraction μ of the spacecraft mass used to perform N approach maneuvers is

$$\mu = \left(\frac{V_\infty}{g_0 I_{sp}}\right) \sum_{i=1}^{N} \frac{|\Delta Y_i|}{V_\infty}$$

$$= \left(\frac{V_\infty}{g_0 I_{sp}}\right)\left\{\left|\frac{Y_0}{R_1} + \delta + \gamma_1\right| + \left|\delta + \gamma_2 - \frac{R_1}{R_2}\right.\right.$$

$$\left.\left. \times (\delta + \gamma_1)\right| + \cdots + \left|\delta + \gamma_N - \frac{R_{N-1}}{R_N}(\delta + \gamma_{N-1})\right|\right\} \tag{21}$$

The errors δ and γ_i always appear together, so that any bias in γ_i may be considered as part of δ, letting the error γ_i represent only the random portion of the uncorrected measurement error. Assume all γ_i have the same variance, σ_γ.

To find the optimum number and location of the maneuvers requires first that the standard deviations σ_{YN}

UNCLASSIFIED

and σ_{YR} of Y_N and the maximum allowable final miss Y_R must have the relationship that

$$\sigma_{YR} \geqq \sigma_{YN} = R_N (\sigma_\delta^2 + \sigma_\gamma^2)^{1/2} \tag{22}$$

Therefore,

$$R_N \leqq \frac{\sigma_{YR}}{(\sigma_\delta^2 + \sigma_\gamma^2)^{1/2}} \tag{23}$$

This sets the maximum range for the Nth maneuver. The final R_N will be slightly below this altitude as a result of other errors to be discussed later.

To optimize the number and location of maneuvers, the ranges for N approach must be found. This might be done by simultaneously setting $\partial\mu/\partial R_i$ equal to zero. However, this process is complicated by the presence of the magnitude symbols. Some insight may be gained from the upper limit for μ:

$$\mu \leqq \left(\frac{V_\infty}{g_0 I_{sp}}\right)\left\{\frac{|Y_0|}{R_1} + \left(2 - N + \frac{R_1}{R_2} + \cdots + \frac{R_{N-1}}{R_N}\right)|\delta| + \sum_1^{N-1}\left(1 + \frac{R_i}{R_{i+1}}\right)|\gamma_i| + |\gamma_N|\right\} \tag{24}$$

Taking the partial of the coefficient of $|\delta|$ with respect to R_i and setting it equal to zero yields $R_i^2 = R_{i-1} R_{i+1}$, indicating that the optimum ranges are terms in a geometric series. (The same result is obtained using the mean of the $|\gamma_i|$ terms.)

To find the ratio of the series, an assumed range R_0 is inserted, such that the variance of Y_0 is the variance of a maneuver made at R_0, with error variance $\sigma_\delta^2 + \sigma_\gamma^2$.

$$R_0 = \left(\frac{\sigma_{Y_0}^2}{\sigma_\delta^2 + \sigma_\gamma^2}\right)^{1/2} \tag{25}$$

Let

$$\rho = \frac{R_0}{R_N} = \frac{\sigma_{Y_0}}{\sigma_{Y_R}} \tag{26}$$

Then the ratio between successive ranges is

$$\rho^{1/N} \text{ and } R_i = R_N (\rho^{1/N})^{N+1-i}$$

Substituting these results into the equation for the upper limit of μ,

$$\mu \leqq \left(\frac{V_\infty}{g_0 I_{sp}}\right)\left\{\left(\frac{\sigma_\delta^2 + \sigma_\gamma^2}{\sigma_{Y_0}^2}\right)\rho^{1/N}|Y_0| + [2 - N + (N-1)\rho^{1/N}] \times |\delta| + (1 + \rho^{1/N})\sum_1^{N-1}|\gamma_i| + |\gamma_N|\right\} \tag{27}$$

If the ranges used are the optimum ranges, then the value of N that minimizes the upper limit of μ can be found by setting $\partial\mu/\partial N = 0$. The minimum may also be found by determining the cumulative distribution function of μ for a particular set of distributions for Y_0, γ_i, and δ and for various values of N. From this, the distribution is located whose desired confidence level (e.g., 99%) occurs at the lowest value of μ. The value of N corresponding to this distribution is then the optimum N.

More study is needed in the determination of the optimum number and location of maneuvers, both in the upper limit and in the actual value of μ. The optimum found, using only γ, δ, and Y_0, may require modification when errors in performing the maneuver are included. It appears that two maneuvers will be adequate, located at 1.5×10^6 and 0.4×10^6 km from Mars.

The errors discussed in the preceding paragraphs are those associated with determining what approach-guidance manuever is to be made. Errors in performing the maneuver will be considered next.

(b) Errors in performing maneuvers

An error in measuring range affects the accuracy as follows: If the measured range $R_{im} = R_i + \delta R_i$, and the maneuver is performed when R_{im} equals the standard maneuver range R_{is}, then the actual maneuver range is

$$R_i = R_{is} - \delta R_i \tag{28}$$

This leads to the following velocity and miss expressions:

$$\frac{\Delta Y_1}{V_\infty} = -\left[\frac{Y_0}{R_{1s}}\left(1 + \frac{\delta R_1}{R_{1s}}\right) + \delta + \gamma_1 - \frac{\partial A_{1s}}{\partial R}\delta R_1\right] \tag{29}$$

$$\left.\frac{\Delta Y_i}{V_\infty}\right|_{i>1} = -\left(\delta + \gamma_i - \frac{\partial A_{is}}{\partial R_i}\delta R_i\right) + \frac{R_{i-1s}}{R_{is}} \times \left(\delta + \gamma_{i-1} - \frac{\partial A_{i-1s}}{\partial R}\delta R_{i-1}\right)\left(1 + \frac{\delta R_i}{R_{is}} - \frac{\delta R_{i-1}}{\delta R_{i-1s}}\right) \tag{30}$$

$$Y_i = -R_i\left(\delta + \gamma_i - \frac{\partial A_{is}}{\partial R}\delta R_i\right) \tag{31}$$

where $-(\partial A_{is}/\partial R)\,\delta R_i$ is the error in A_{is} caused by making the maneuver at $R_i = R_{is} - \delta R_i$. Thus, a range error results in an error proportional to the miss existing before the maneuver, and an error in measurement from using A_{is}, the angle corresponding to R_{is}, at range R_i instead of R_{is}. Constant scale-factor errors in range contribute only to the error in the standard angle A_{1s} and to the removal of Y_0.

Other errors result from errors in adding the velocity increment. The latter are:

δV = velocity resolution error [in 4c(1a), this is $\delta V_1 + \delta V_2 + \delta V_3$]

and

ν = velocity scale factor error [$K + \eta/v$ in 4c(1a)].

If the maneuver of ΔY_i is commanded, the actual maneuver ΔY_{ia} performed is

$$\Delta Y_{ia} = \Delta Y_i (1 + \nu_i) \pm \delta V_i$$

The sign of δV is determined by the sign ΔY_i, because it is an error in the magnitude of the velocity. The general expressions for the velocity and resulting miss of the ith maneuver are quite involved, however.

Errors in the magnitude of the velocity increment propagate throughout all maneuvers and are not completely cancelled at the next maneuver, as was the case for the previously mentioned types of errors. This error propagation can be eliminated by measurements of the asymptote direction after each maneuver rather than estimation of the direction on the basis of the velocity command.

Another error in the performance of the approach maneuvers is the error in the velocity-vector direction. A simplified case that illustrates the effects of a pointing error considers maneuvers restricted to a plane perpendicular to the path. The pointing errors may be considered to have a yaw component $\delta\theta_y$ that rotates the velocity direction within the plane, and a pitch component $\delta\theta_p$ rotates the velocity-increment vector out of the plane and results in a component of the maneuver velocity perpendicular to the maneuver plane, i.e., parallel to the path, resulting in a change of the path velocity.

$$\Delta V_\infty = \delta\theta_{pi}\, \Delta Y_i \tag{32}$$

This error in path velocity then appears in the equation

$$\Delta Y_j = V_\infty (A_{jm} - A'_{js}) \tag{33}$$

where

$$V_\infty = V_{\infty s} + \Delta V_\infty \tag{34}$$

If the standard value of asymptotic velocity $V_{\infty s}$ is used in computing ΔY_j, then the computed value is

$$\begin{aligned}\Delta Y_j &= \dot{V}_{\infty s} (A_{jm} - A'_{js}) \\ &= V_\infty (A_{jm} - A'_{js}) \left(1 - \sum_{i=1}^{j-1} \frac{\delta\theta_{pi}\, \Delta Y_i}{V_{\infty s}} \right)\end{aligned} \tag{35}$$

Therefore, the $\delta\theta_p$ causes a proportional (scale-factor) error in all following maneuvers. It is assumed that $\delta\theta_p$ is not large enough to affect the in-plane component of the maneuver velocity.

The yaw pointing error has a more serious effect. The yaw error causes the direction of the maneuver to change, as shown in Fig. 27.

Neglecting other errors, the effect of the yaw pointing error is to rotate the position correction $(\Delta X_i, \Delta Y_i)_s$ by the angle $\delta\theta_y$, so that exact cancellation of the initial error is not obtained. The residual error is (X_i, Y_i).

$$(X_i, Y_i) = (Y_{i-1}\, \delta\theta_{yi}, - X_{i-1}\, \delta\theta_{yi}) \tag{36}$$

As a result of the yaw pointing error alone, the residual miss resulting from $\delta\theta_{yi}$ has a magnitude equal to the product of the initial miss and the yaw error, in a direction perpendicular to the initial miss on the plane perpendicular to the path.

The yaw pointing error results in correlation of the error in the X- and Y-directions, and can be investigated only in a three-dimensional analysis of the approach guidance. Such an analysis is also needed for the determination of impulse (fuel) requirements to combine the results of the actual guidance-measurement and maneuver-performance errors. The combination of two single-plane analyses would yield a conservative fuel requirement, because the total effects of some error sources (e.g., velocity-measurement scale-factor errors) are thus assumed to act in each plane. Correlation between planes also appears when the navigation-measurement planes are not orthogonal, as discussed below.

(c) Navigation errors

To determine the required approach-trajectory corrections, the capsule impact point or miss distance at the target planet must be estimated. This requires data equivalent to knowledge of the spacecraft position and the approach-velocity vector at some earlier time, and the forcing expected to be applied between that time and the time of impact or closest approach. The position information can be obtained by spacecraft-based celestial navigation, and the velocity data either by using position data taken at two separate times or by the assumption that the actual and standard velocities coincide. The process of determining the present spacecraft position and velocity is called navigation. The position of the spacecraft (observer) with respect to a selected reference body (the target planet) can be found by triangulation or by vector navigation. The triangulation is based on measured angles between celestial bodies having known positional or directional relationships to each other. Near a planet, the triangulation method does not give a suffi-

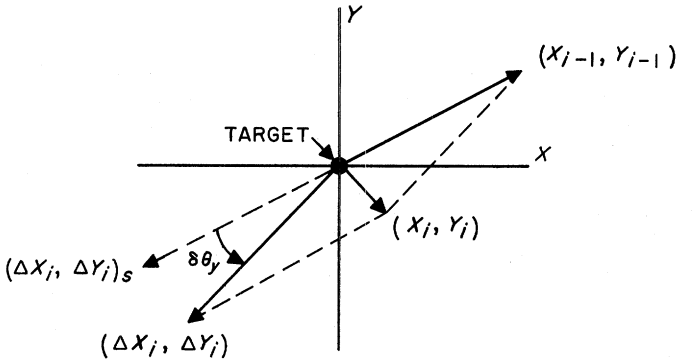

$$(\Delta X_i, \Delta Y_i)_s = -(X_{i-1}, Y_{i-1}) = \left(\frac{R_i}{V_\infty}\Delta \dot{X}_i, \frac{R_i}{V_\infty}\Delta \dot{Y}_i\right)$$

Figure 27. Effect of yaw pointing error

ciently accurate determination of position with respect to the planet because of the large distances involved in the celestial triangles. In vector navigation, only the direction from the target planet is determined by celestial-angle measurements, while the range is determined by other means to be discussed later in this Section. The reference objects that may be used to determine direction are: stars, the Sun, and planets. The order given is the order of increasing computational complexity if total position is to be obtained; however, in the *Mariner B* application only perturbations from the standard trajectory are needed, and all three reference types require the same computation processes.

The vectors from the spacecraft to the optimum set of reference objects (the target planet and two others) would form an orthogonal triad. Figure 28 shows the spacecraft-centered celestial triangles involving Mars,

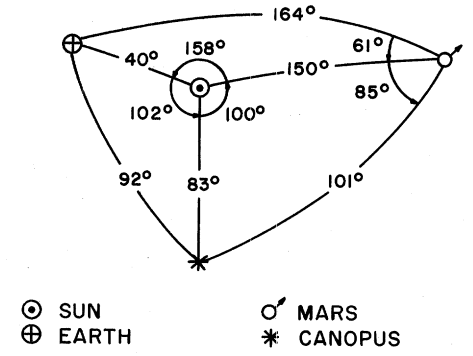

TYPICAL *MARINER B* TRAJECTORY AT TIME FOR APPROACH GUIDANCE

Figure 28. Spacecraft-centered celestial triangles

Earth, Sun, and Canopus (a star near the south ecliptic pole) for a typical *Mariner B* trajectory at the time of approach corrections. The angles of Mars are the angles between the Mars–spacecraft–reference planes. The choice of reference objects is not restricted to these, but they seem to be the ones most likely to be used. Mars and two of the others will be used for approach-guidance navigation. For convenience of measurement, the reference objects used for navigation should be the same as those used for attitude-control references.

Two star references will be used for an example of the type of computation necessary to find the position error. The Sun- and planet-reference computations are similar, but their derivation is complicated by the finite distances involved.

Define:

S_1 = unit vector from target planet to star No. 1
S_2 = unit vector from target planet to star No. 2
$\boldsymbol{\rho}$ = unit vector from target planet to spacecraft
θ_1 = spacecraft–target–star No. 1 angle
θ_2 = spacecraft–target–star No. 2 angle
ψ = angle between θ_1 and θ_2 planes

X-Y-Z coordinate system (see Fig. 29)

$\boldsymbol{Z} = \boldsymbol{\rho}$ unit vector = $\boldsymbol{k}$

$\boldsymbol{Y} = \dfrac{\boldsymbol{\rho} \times \boldsymbol{S}_1}{|\boldsymbol{\rho} \times \boldsymbol{S}_1|}$ unit vector = $\boldsymbol{j}$, perpendicular to the spacecraft–target–star No. 1 plane

$\boldsymbol{X} = \boldsymbol{Y} \times \boldsymbol{Z}$ unit vector = $\boldsymbol{i}$

The coordinate system is set up using the standard values of $\boldsymbol{\rho}$, $\boldsymbol{S}_1$, and $\boldsymbol{S}_2$.

It is desired to find an expression for the error $\delta\boldsymbol{P}$ in the position vector $\boldsymbol{P}$ as a function of the errors $\delta\theta_1$, $\delta\theta_2$, and δR in the spacecraft–target–star angles θ_1 and θ_2, and the range R. The standard position $\boldsymbol{P}(t)$ at a time t is defined by:

$$\boldsymbol{P}(t) = R(t)\,\boldsymbol{\rho}$$

where $R(t)$ = range at time t. Then, the error $\delta\boldsymbol{P}$ in $\boldsymbol{P}$ at t is

$$\delta\boldsymbol{P} = R\,\delta\boldsymbol{\rho} + \delta R\,\boldsymbol{\rho} \tag{37}$$

and, because

$$\delta\boldsymbol{\rho} = (\delta\theta_1)\,\boldsymbol{i} + (\csc\psi\,\delta\theta_2 - \cot\psi\,\delta\theta_1)\,\boldsymbol{j} \tag{38}$$

then,

$$\delta\boldsymbol{P} = R\left[(\delta\theta_1)\,\boldsymbol{i} + (\csc\psi\delta\theta_2 - \cot\psi\delta\theta_1)\,\boldsymbol{j} + \frac{\delta R}{R}\,\boldsymbol{k}\right] \tag{39}$$

UNCLASSIFIED

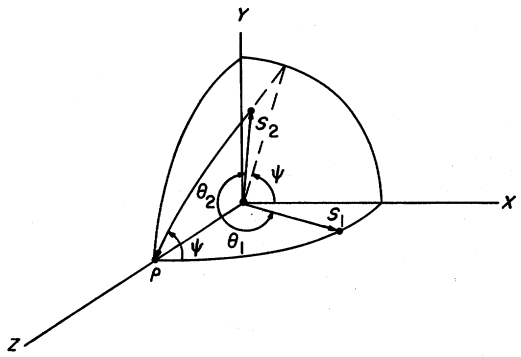

S_1, S_2 – UNIT VECTORS TO REFERENCE OBJECTS
ρ – STANDARD UNIT VECTOR TOWARD SPACECRAFT

Figure 29. Planet-centered coordinate system for approach guidance

Expressed in matrix form, the position error at time t is

$$\begin{bmatrix} \delta P_x \\ \delta P_y \\ \delta P_z \end{bmatrix} = \begin{bmatrix} R & 0 & 0 \\ -R\cot\psi & R\csc\psi & 0 \\ 0 & 0 & R \end{bmatrix} \begin{bmatrix} \delta\theta_1 \\ \delta\theta_2 \\ \dfrac{\delta R}{R} \end{bmatrix}$$

This error can be transformed (by a rotation matrix) into any coordinate system desired for guidance.

The quantities $\delta\theta_1$, $\delta\theta_2$, and δR can represent either deviations resulting from an actual $\delta \boldsymbol{P}$ or errors in measuring the quantities θ_1, θ_2, and R. In the latter case, the resulting $\delta \boldsymbol{P}$ is the error in determination of position due to measurement errors.

For some configurations of guidance instruments, it may not be possible to measure θ_1 and θ_2 directly. In such cases, errors in the angles that are measured can be related to errors in θ_1 and θ_2. Thus, for any point on the trajectory, with a selected set of references and measured angles, the measurement accuracies can be used to find the basic navigation accuracy.

As a pertinent example of indirect measurement of θ_1 and θ_2, let the second reference S_2 be the Sun, and assume that the guidance instruments are capable of reading cone (Sun–spacecraft–object) angles from the Sun β, and clock angles (angles between Sun–spacecraft–object planes) α. The situation in the Sun–spacecraft–planet plane is shown in Fig. 30.

$$\delta\theta_2 = \tan\varepsilon\left[\frac{\delta R}{R} - \frac{\delta|S_2|}{|S_2|}\right] - (1 + \tan\varepsilon\cot\beta_2)\,\delta\beta_2 \qquad (40)$$

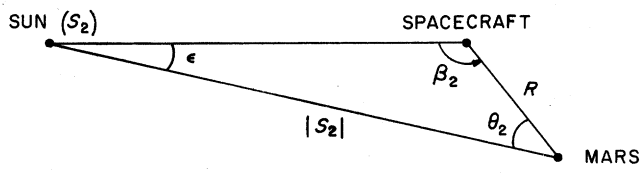

$$\theta_2 = \pi - \beta_2 - \epsilon$$
$$\text{SIN}\,\epsilon = \frac{R}{|S_2|}\,\text{SIN}\,\beta_2$$

Figure 30. Sun–spacecraft–planet plane

The spacecraft-centered celestial triangle is shown in Fig. 31, with the measured angles β_1, β_2, and α. The side opposite α is the Mars–spacecraft–star (S_1) angle and equals $\pi - \theta_1$. Hence,

$$\delta\theta_1 = \frac{1}{\sin\theta_1}[(\cos\beta_1\sin\beta_2\cos\alpha - \sin\beta_1\cos\beta_2)\,\delta\beta_1 + (\sin\beta_1\cos\beta_2\cos\alpha - \cos\beta_1\sin\beta_2)\,\delta\beta_2 - (\sin\beta_1\sin\beta_2\sin\alpha)\,\delta\alpha] \qquad (41)$$

Using the results with the previously obtained matrix expression for $\boldsymbol{P}$, the following substitution is made for the column matrix of errors:

$$\begin{bmatrix} \delta\theta_1 \\ \delta\theta_2 \\ \dfrac{\delta R}{R} \end{bmatrix} = \begin{bmatrix} \dfrac{\cos\beta_1\sin\beta_2\cos\alpha - \sin\beta_1\cos\beta_2}{\sin\theta_1} \\ 0 \\ 0 \end{bmatrix} \times \frac{\sin\beta_1\cos\beta_2\cos\alpha - \cos\beta_1\sin\beta_2}{\sin\theta_1} - (1 + \tan\varepsilon\cot\beta_2) \times 0$$

$$\times \begin{bmatrix} \dfrac{-\sin\beta_1\sin\beta_2\sin\alpha}{\sin\theta_1} & 0 & 0 \\ 0 & \tan\varepsilon & -\tan\varepsilon \\ 0 & 0 & 1 \end{bmatrix} \begin{bmatrix} \delta\beta_1 \\ \delta\beta_2 \\ \delta\alpha \\ \dfrac{\delta|S_2|}{|S_2|} \\ \dfrac{\delta R}{R} \end{bmatrix}$$

If the navigation observation is made at a specified measured range, then δR and $\delta|S_2|$ do not enter into the navigation equation but are used only to evaluate the navigation accuracy. The angle β_1 is the Sun–spacecraft–star angle, and *a priori* knowledge of the trajectory and time might give a more accurate determination of the angle than a measurement.

UNCLASSIFIED

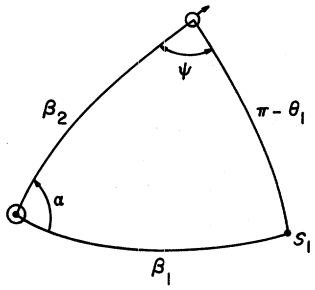

SUN, ⊙ IS S_2
ANGLES MEASURED BY GUIDANCE INSTRUMENTS FOR APPROACH–GUIDANCE EXAMPLE:
β_1 – CONE ANGLE OF S_1
β_2 – CONE ANGLE OF MARS, ♂
α – CLOCK ANGLE OF MARS

Figure 31. Spacecraft-centered celestial triangle

(d) Comparison of angular diameter and time for range determination

It has been stated previously that the range from the spacecraft to the destination planet is required as an input for the approach-guidance subsystem that will most probably be used in *Mariner B*. However, the choice of method for the measurement or estimation of this range has not been indicated.

The range can be measured by radar-ranging or by angular-diameter measurement, or estimated from knowledge of time of arrival at the target planet and the asymptotic approach velocity. Radar-ranging is presently not being considered for use in *Mariner B* approach guidance. The following paragraphs discuss the relative accuracies of the other two methods.

The relationship of the range R to angular diameter ϕ for a body of radius r is

$$R = \frac{r}{\sin\frac{\phi}{2}} \tag{42}$$

and for $R >> r$,

$$R \simeq \frac{2r}{\phi} \tag{43}$$

If

r_a = actual radius

$r_s = r_a + \Delta r$, measured radius used as the standard

Δr = error in radius

$R_e = \frac{2_{rs}}{\phi M}$ = estimated range

$R_a = \frac{2_{ra}}{\phi_a}$ = actual range

$\phi_M = \phi_a + \Delta\phi$ = measured angular diameter at R_a

ϕ_a = actual angular diameter at R_a

k = scale-factor error in ϕ measurement

$\delta\phi$ = uncertainty error in ϕ measurement

then,

$$R_e = \frac{2\,(r_a + \Delta_r)}{\phi_a + k\phi_a + \phi} = R_a\left(1 + \frac{\Delta r}{r_a} - k - \frac{\delta\phi}{\phi_a}\right) \tag{44}$$

and the error in measuring a range R_a is

$$\Delta R = R_e - R_a = R_a\left(\frac{\Delta r}{r_a} - k\right) - \frac{R_a^2}{2r_a}\,\delta\phi \tag{45}$$

As an example of the accuracy of this method of range determination, the following quantities and 3-σ error magnitudes are used:

$$\left.\begin{aligned} 2r_a &= 6620\text{ km} \\ \frac{\Delta r}{r_a} &= 1.5 \times 10^{-2} \\ k &= 4 \times 10^{-2} \end{aligned}\right\} \text{r.s.s.} = 4.3 \times 10^{-2}$$

$$\phi = 4 \times 10^{-4}\text{ rad}$$

$$\Delta R,\ 3\,\sigma = [(R_a \times 4.3 \times 10^{-2})^2 + (R_a^2 \times 6.05 \times 10^{-8})^2]^{1/2}$$

Then, at

$$R_a = 1.5 \times 10^6\text{ km}$$

$$\Delta R = [(6.45 \times 10^4)^2 + (13.61 \times 10^4)^2]^{1/2} = 151{,}000\text{ km}$$

and at

$$R_a = 0.4 \times 10^6\text{ km}$$

$$\Delta R = [(1.72 \times 10^4)^2 + (0.968 \times 10^4)^2]^{1/2} = 19{,}700\text{ km}$$

The values for R_a correspond to optimal maneuver points selected in Section IIIC-1.

The relationship between range, time, and velocity, $R = V_\infty\,(T_f - t)$, can be used when the spacecraft is sufficiently far from the planet that the range rate is the asymptotic velocity V_∞ with respect to the planet. The time of flight T_f is the time to closest approach to a massless planet at the same location; i.e., the gravitational acceleration and resultant trajectory focusing effects have been removed from the actual time of closest approach.

If

$T_{f_e} = T_f + \Delta T_f$ = estimated time of flight (as defined)

ΔT_f = error in T_f estimation

$t_c = t + \Delta t$ = spacecraft clock time

Δt = clock error

V_∞ = actual asymptotic velocity

UNCLASSIFIED

$V_e = V_\infty + \Delta V$ = estimated value of V_∞

ΔV = error in estimate of V_∞

then,

$$R_e = V_e (T_{f_e} - t_c) = (V_\infty + \Delta V)(T_f - t + \Delta T_f - \Delta t)$$
$$= R_a \left(1 + \frac{\Delta V}{V_\infty} \right) + V_\infty (\Delta T_f - \Delta t)$$

and the range error is

$$\Delta R = R_e - R_a = \frac{\Delta V}{V_\infty} R_a + V_\infty (\Delta T_f - \Delta t)$$

Because of the current uncertainties in the accuracies of orbit determination and the astronomical unit, it is difficult to evaluate this method at the present time. Further study is needed to determine how well the time-of-flight and asymptotic-velocity errors can be estimated. When this information becomes available, the evaluation of the velocity–time method of range determination will be completed and the choice of the range-determination method can be made.

(e) Combination of measurements

The purpose of the following paragraphs is to indicate the possibilities of reducing the effects of measurement errors upon the accuracy of the guidance subsystem. For *Mariner B* the errors associated with measuring the angles between Mars and other celestial bodies (most probably the Sun and Canopus) and with measuring the angular diameter of Mars are of prime interest. It is convenient to divide the measurement errors into four categories:

(1) Errors that are inherent in the way in which the reference body and sensor are used to measure spacecraft position (sometimes called systematic errors). An example is the case of a partially illuminated planet and a sensor which seeks the center of reflected light.

(2) Errors associated with comparing measurements made at different times, caused by changes in the transfer function of the measuring devices [sometimes called drift, as are certain errors in (4) below]. Also, an example is the change in gain of an optical sensor due to aging.

(3) Errors that are strictly a function of the value of the angle being determined (sometimes called linearity errors or input-related errors). An example is the quantization error in the readout of angular positions.

(4) Errors associated with an output that exists for zero input to the measuring device. This general category of errors will be called "random errors" in the present discussion. These errors are predominantly of two types, often called "bias" and "noise." An example is the voltage at the output of an optical sensor with zero incident illumination.

Errors in categories (1) through (3) are discussed later in this Section. The errors in category (3) are random in the sense that the values of the angles to be measured are not known exactly in relation to the quantization intervals. If there are no other disturbances to the measurement process, the effects of these errors cannot be reduced, for a given value of the observed quantity, by the use of multiple measurements of the same quantity at the same point. However, if the readout is influenced by the operation of a tracking-instrument control loop (either a positioning loop with respect to the spacecraft or one of the spacecraft attitude-control loops) operating in a limit-cycle mode, the effects of these errors begin to resemble the fourth category of randomly time-varying errors.

The effects of random errors can be reduced by obtaining additional measurements and performing operations on the measurements that determine statistically "best" estimates of the actual values measured or of quantities determined by these values. Simple averaging, least-squares fitting, and maximum-likelihood estimation processes are examples of methods that may be used, with the selection of the particular method being such as to strike a good compromise between the knowledge of the disturbance statistics, the added computations required, and the increase in accuracy so obtained.

The distinction between the bias and noise types of random error is conveniently made in terms of the autocorrelation function $\rho(\tau)$ of the output signal of the measuring device at zero input. If the normalized autocorrelation function is nearly zero for values of τ equal to and greater than the minimum time interval between measurements, then the random error at the time of one maneuver bears little predictable relationship to the random error at the time of the next maneuver. This type of random error is called "noise." Conversely, if the autocorrelation function is nearly unity for the total range of τ over which measurements are taken, then for a high percentage of the time, the random error during one measurement is nearly equal to the random error at the next measurement. This type of random error is called "bias." These same ideas can be expressed in terms of the spectral density of the output signal of the measuring device for zero input. For noise, this spectrum is more

UNCLASSIFIED

or less uniform over the bandwidth of the measuring device. For bias, this spectrum is nearly zero except for a narrow-frequency band about the origin.

Because the total length of the measurement period is short (5% or less of the total time from launch to the beginning of the measurements), although an error behaves like a bias error during the measurement period, it may not be possible to eliminate the effect before launch, because the value at the measurement period may be correlated very poorly, if at all, with the value at launch.

Experience in the *Ranger* program has indicated that for optical sensors bias errors are much more significant than noise errors. For example, in the *Ranger* Sun sensor the rms value of the noise error is about 1% of the bias error. (This is sometimes expressed by stating that the short-term null stability is 1% of the absolute null offset or long-term null stability.) In the *Ranger* Earth sensor, the rms value of the noise error is about 5% of the bias error. In determining these percentages, the test instrumentation errors are more significant in measuring noise than in measuring bias, which tends to make the above percentages larger than they should be.

A brief discussion of the estimation process in the presence of both bias-like (well correlated) and noise-like (poorly correlated) errors is warranted as a result of the experience with the *Ranger* sensors, because different types of operations are required to remove the two types of error. Bias-like errors can be removed by using a set of multiple measurements taken at separate locations, rather than a set taken at nearly the same location but separated in time. Here, use is made of differing geometrical configurations at the various measurement locations, a technique here called "space filtering" to indicate its relation to the statistical time- or frequency-filtering methods used to minimize noise errors. Examples of space filtering for the *Mariner B* optical sensors include: (1) observing the measured angles for two or more different locations of the spacecraft and relating these observations to the known change in geometry on the nominal trajectory and (2) plunging the sensor, i.e., rotating it 180 deg about its assumed optical axis during a short interval of time in which the external geometry remains nearly constant.

If both noise and bias errors are present, the estimation process must contain both statistical and geometrical operations, because statistical operations are not effective against bias errors. Describing the situation in terms of signal filtering, to which statistical estimation is related, the width of the frequency band around zero which contains the preponderance of the error power is, in a general way, inversely related to the characteristic value τ_c of time shift τ, at which the autocorrelation function becomes sufficiently small that errors separated by more than τ are effectively uncorrelated. Hence, because τ_c is small for noise errors, the noise power is distributed over a fairly wide band of frequencies.

The guidance information is mainly described by low-frequency signals, leading to reduction of the effects of noise by not accepting the high-frequency portions of the measurement power in the estimation process. Such components can be rejected by averaging processes. In contrast to noise, slowly varying signals have a long τ_c, and the majority of bias-error power is concentrated near zero frequency (a pure bias being equivalent to a DC signal), which makes it difficult to reduce error effects by rejecting a large part of the error power without also losing a large portion of guidance-signal power. Consequently, time filtering is not very effective against bias errors, and geometrical space filtering is required to reduce their effects.

Maximum-likelihood estimation (described immediately below) combines geometrical operations (described by the manipulations of the U-matrix in the following discussion) and statistical weighting operations (likewise described by the Λ_N matrix operations). Application of the maximum-likelihood technique of constructing estimation processes to the simple example of linear constant-speed motion of the spacecraft toward a massless destination planet results in specifying the same operations on the data that are called for if separate analyses of the methods of removing bias and noise errors are combined after individual investigation. Whether or not this property of describing a useful combination of time and space filtering is present in the more general case is yet to be studied.

One of the major tasks to be completed in the design of the approach-guidance loop is the determination of the need for additional measurements to improve guidance accuracy by using statistical techniques or space filtering, and the development and investigation of the characteristics and capabilities of various methods of obtaining and processing such additional measurements to improve the guidance accuracy.

Some of the considerations involved in using the maximum-likelihood technique to improve the accuracy of the *Mariner B* approach-guidance maneuvers will now be discussed. Maximum-likelihood estimation includes least-squares estimation as a special case when all of the error sources have normal distributions and are uncorrelated

with one another, both between sources and between values from the same error source at different measurement times.

In order to demonstrate the application of the maximum-likelihood estimation technique to the *Mariner B* approach-guidance subsystem, the following quantities are defined:

ϕ_i = a measured perturbation quantity; i.e., the deviation of a measured navigation angle from its standard value. Here $i = 1$ to N, where N = total number of individual measurements for each maneuver. The number of variables measured may be considerably less than N.

$q_i(T)$ = one of the three position coordinates or one of the three velocity coordinates of the spacecraft at the final instant T when the capsule is released. The variable may also be any other time t ($i = 1$ to 6).

In the theory of systems of linear differential equations, it is shown that, in the case of zero forcing, the variables at a final instant T are related to the values of these variables at any earlier instant t by a matrix equation of the form

$$\boldsymbol{q}(T) = F(T,t)\,\boldsymbol{q}(t) \tag{46}$$

where $F(T,t)$ is a square matrix, sometimes known as the matrizant, and $\boldsymbol{q}$ is the vector of the perturbations in the six spacecraft position and velocity coordinates. The perturbations in spacecraft position and velocity have been chosen as a specific example of the variables in a set of linear differential equations. If the $\boldsymbol{q}$ represented total quantities rather than perturbations in the position and velocity, the equations would not be linear.) Similarly, the value of $\boldsymbol{q}$ at any prior time t can be expressed in terms of $\boldsymbol{q}(T)$ by

$$\boldsymbol{q}(t) = F(t,T)\,\boldsymbol{q}(T) \tag{47}$$

It can also be shown that the position components of $\boldsymbol{q}(t)$ can be written as linear combinations of a set of perturbations from nominal optical measurements taken at time t. These perturbations in the measured angles are the ϕ_i defined above. As a result of these relationships, the vector $\boldsymbol{\phi}$ of all observable quantities ϕ_i used in determining an estimate of the vector $\boldsymbol{q}(T)$ is a function of $\boldsymbol{q}(T)$ that has the form

$$\boldsymbol{\phi} = U\boldsymbol{q}(T) \tag{48}$$

Now, let $\boldsymbol{\mu}$ be the vector of the actual set of measurements of the quantities $\boldsymbol{\phi}$ that is taken to determine the estimate of $\boldsymbol{q}(T)$ for a particular time and flight. If this set of measurements is additively corrupted by random errors, then

$$\boldsymbol{\mu} = \boldsymbol{\phi} + \boldsymbol{N} \tag{49}$$

where $\boldsymbol{N}$ is the vector of random errors. Equation (49), of course, can be solved for $\boldsymbol{N}$ in terms of the measurements $\boldsymbol{\mu}$ and the actual values of the observable quantities $\boldsymbol{\phi}$. The time-varying random properties of the errors are indicated by the matrix Λ_N obtained by taking the ensemble average of the product NN^T, where the subscript T denotes a transposed matrix or vector; hence,

$$\Lambda_N = \widetilde{\widetilde{NN^T}} \tag{50}$$

with the detailed form

$$\Lambda_N = \begin{bmatrix} \sigma_{N1}^2 & \sigma_{N1}\sigma_{N2}\rho_{12} & \sigma_{N1}\sigma_{N3}\rho_{13} & \cdots & \sigma_{N1}\sigma_{Nm}\rho_{1m} \\ \sigma_{N1}\sigma_{N2}\rho_{12} & \sigma_{N2}^2 & \sigma_{N2}\sigma_{N3}\rho_{23} & & \vdots \\ \sigma_{N1}\sigma_{N3}\rho_{13} & \sigma_{N2}\sigma_{N3}\rho_{23} & \sigma_{N3}^2 & & \vdots \\ \vdots & & & & \vdots \\ \vdots & & & & \vdots \\ \vdots & & & & \vdots \\ \sigma_{N1}\sigma_{Nm}\rho_{1m} & \cdots & \cdots & \cdots & \sigma_{Nm}^2 \end{bmatrix} \tag{51}$$

if there are m measurements, and hence, m components of $\boldsymbol{\phi}$ and $\boldsymbol{N}$. Transposition of the right-hand side of Eq. (50) shows that Λ_N is a symmetric matrix. This matrix is known as the noise-moment matrix of the vector $\boldsymbol{N}$ and, where $\boldsymbol{\phi}$ is not random and is additively corrupted by $\boldsymbol{N}$, also of ϕ.

The vector $\boldsymbol{\mu}$ is a function both of the components of the vector $\boldsymbol{q}(T)$ that is to be determined and of random vector $\boldsymbol{N}$. Consequently, the vector $\boldsymbol{\mu}$ itself and and also the components of μ_i are random variables. The method of maximum-likelihood estimation consists of postulating a joint distribution for all of the measurements (the vector $\boldsymbol{\mu}$), the distribution necessarily being a function of the components of the quantity $\boldsymbol{q}(T)$ that is to be determined, and of the random errors. The components $q_i(T)$ are then considered parameters to be selected for maximizing the joint probability that a set of measurements selected from the postulated joint distribution for the components of $\boldsymbol{\mu}$ will match the actually obtained measurements. Let this maximum-likelihood estimate of $\boldsymbol{q}(T)$ be denoted by $\boldsymbol{q}^*(T)$. It may be shown that, if all of the components of N have normal distributions, with standard deviations of σ_{Ni} for the components of N_i and correlations of $\sigma_{Ni}\sigma_{Nj}\rho_{ij}$ between the components N_i and N_j, then the maximum-likelihood estimate of $q^*(T)$ derived from the set of measurements is given by the equation

$$\boldsymbol{q}^*(T) = [U^T \Lambda_N^{-1} U]^{-1} U^T \Lambda_N^{-1} \boldsymbol{\mu} \tag{52}$$

UNCLASSIFIED

Some insight into the meaning of this matrix expression can be obtained by considering a special case, where the vector μ is partitioned into two component vectors, one component being a set ψ of measurements related to $q(T)$ by

$$\psi = Vq(T) + N \tag{53}$$

and the other component q' being an error-corrupted set of requirements or estimates of the components of $q(T)$. Thus,

$$\mu = \begin{bmatrix} \psi \\ \cdots \\ q' \end{bmatrix} \tag{54}$$

where ψ may be interpreted as a set of measurements taken near the present time and q' as an estimate of $q(T)$ obtained from a set of measurements taken at an earlier time. Then, U has the partitioned form

$$U = \begin{bmatrix} V \\ I \end{bmatrix} \tag{55}$$

where I is an identity matrix, and N has the form

$$N = \begin{bmatrix} N_\psi \\ \cdots \\ N_{q'} \end{bmatrix} \tag{56}$$

with the result that

$$\Lambda_N = \begin{bmatrix} \widetilde{N_\psi N_\psi^T} & \widetilde{N_\psi N_{q'}^T} \\ \widetilde{N_{q'} N_\psi^T} & \widetilde{N_{q'} N_{q'}^T} \end{bmatrix} \tag{57}$$

and, if the two parts of N are not correlated with one another, Λ_N is a diagonal matrix of the submatrices Λ_ψ and $\Lambda_{q'}$,

$$\Lambda_N = \begin{bmatrix} \Lambda_\psi & O \\ O & \Lambda_{q'} \end{bmatrix} \tag{58}$$

where O is a null matrix, with the result that

$$\Lambda_N^{-1} = \begin{bmatrix} \Lambda_\psi^{-1} & O \\ O & \Lambda_{q'}^{-1} \end{bmatrix} \tag{59}$$

Substitution of these results into the basic form of the estimation equation (Eq. 52) leads to the expression

$$q^*(T) = [V^T \Lambda_\psi^{-1} V + \Lambda_{q'}^{-1}]^{-1} [V^T \Lambda_\psi^{-1} \psi + \Lambda_{q'}^{-1} q'] \tag{60}$$

For the case in which the elements of N are all uncorrelated, the off-diagonal elements of Λ_N are zero, and the elements of the principal diagonal are of the form σ_{Ni}^2. As a result, the matrix Λ_N^{-1} is also a diagonal matrix, where the elements of the principal diagonal are of the form $1/\sigma_{Ni}^2$. Then, as the quality of the measurements decreases, the standard deviations increase, and the matrix Λ_N^{-1} approaches a null matrix. Similar results apply to the submatrices Λ_ψ^{-1} and $\Lambda_{q'}^{-1}$.

Now, having completed the preliminary definitions, consider the case where the standard deviations of the ψ measurements approach infinity, indicating a very poor knowledge of the ψ_i that approaches no knowledge at all. Then, the diagonal terms of Λ_ψ^{-1} approach zero, and Eq. (60) reduces to

$$q^*(T) = q' \tag{61}$$

Second, consider the case in which the standard deviations of the measurements q' approach infinity. Then, Eq. (60) reduces to

$$q^*(T) = [V^T \Lambda_\psi^{-1} V]^{-1} V^T \Lambda_\psi^{-1} \psi \tag{62}$$

Thus, it can be seen that the expressions of Eqs. (52) and (60) show the weighting factors to be placed upon the various measurements in determining the final estimate of $q^*(T)$, these weighting factors being determined by the quality of the measurements (which is indicated by the standard deviation and correlation information contained in the moment matrices). Inversion of the above conditions to the case in which one of the sets of measurements tends to perfection and the standard deviation tends to zero is another way of showing that the better measurements will receive the heavier weight.

The above example is useful for a further purpose, in that it can be used to determine the degree of accuracy required in the ψ measurements before they can profitably be used in conjunction with the q' measurements, or vice versa. For example, the ψ measurements might be optical measurements, and the q' might be estimates of $q(T)$ that are derived from radio-tracking and subsequent orbit-determination processes.

If the ψ measurements are optical measurements, and the q' are estimates of $q(T)$ obtained from other optical measurements taken at a different place earlier in the flight, then this maximum-likelihood method can yield position measurements which have no error due to bias errors in the measuring instruments. That is, if the geometrical relationships between measurements are appropriate, the maximum-likelihood method will effectively apply the space filtering mentioned earlier. This does not mean that the distinction between space filtering and time filtering made previously is invalid. The maximum-likelihood method applied to a given geometrical problem (say, the approach of a spacecraft toward a destination planet on a nonstandard trajectory) can also yield exactly the same estimate for the desired quantity (e.g., the miss distance at the destination planet) as a direct analysis

UNCLASSIFIED

UNCLASSIFIED

(say, the geometrical analysis required to determine the final position of the spacecraft by obtaining two separate position measurements of the spacecraft to determine velocity and then combining this result with one of the position measurements to obtain the desired results) where there are no errors present. This latter capability of the maximum-likelihood technique, like its ability to provide space filtering, is deterministic in character rather than statistical.

d. Attitude Control

The attitude-control loops of the *Mariner B* spacecraft may be classified as (1) pitch, yaw, and roll control of the spacecraft orientation, (2) the pointing of a directional antenna toward the Earth, (3) the pointing of a planetary horizontal platform toward Mars, (4) the autopilot loops associated with the midcourse and approach maneuvers, and (5) control loops for the guidance instruments.

Because two angular coordinates are required to specify completely the direction of a line in space, it follows that control of two angular degrees of freedom (DF) of a body are required to point an axis, or line, of the body in a specified direction. Thus, the minimum number of DF (and hence, of attitude-control loops) required to point objects in N directions simultaneously is $2N$. Three of these $2N$ DF are usually the spacecraft pitch, yaw, and roll DF, and the remaining $2N - 3$ are supplied through relative-motion joints between the objects and the spacecraft frame. The actual number of loops may be larger than this minimum to afford improvements in accuracy and alignment or to alleviate partial restrictions in fields of view caused by the geometrical configuration of the spacecraft.

(1) Pitch- and Yaw-Control Loops

It is required that the *Mariner B* pitch- and yaw-control loops be capable of

(a) eliminating tumbling rates acquired upon separation from the launch vehicle

(b) acquiring lock on the Sun (or other reference object for these axes)

(c) maintaining lock on the Sun with an accuracy of 0.1 to 0.5 deg

(d) automatically reacquiring the Sun at any time during the flight if a noncatastrophic disturbance causes loss of acquisition

(e) performing commanded turns with an accuracy of a few millirad

The techniques utilized to meet similar requirements in the *Mariner A* spacecraft are well suited for the *Mariner B* application.

(2) Roll- and Antenna-Control Loops

The roll- and antenna-control loops (the latter may include the roll loop) control the angular motion of the spacecraft about its roll axis and point a directional antenna at the Earth.

It is required that the roll-control loop be capable of

(a) eliminating the initial tumbling rate acquired at separation from the launch vehicle

(b) acquiring a specified reference object and maintaining lock with an accuracy of 0.1 to 0.5 deg

(c) automatically reacquiring the reference object at any time during the flight if a noncatastrophic disturbance causes loss of acquisition

(d) performing commanded turns about the roll axis with an accuracy of a few millirad

The antenna-control loop s must be capable of pointing the directional antenna toward the Earth with an accuracy of ± 1 deg.

The basic concepts associated with the roll- and antenna-control loops of the *Mariner A* spacecraft are applicable to *Mariner B*; however, some major changes are required, as indicated below.

The choice of reference for roll control is not so straightforward as that for pitch and yaw. The reference object could be a star or planet but should be in such a position that the Sun–spacecraft–reference object angle is near 90 deg, because the roll-alignment error is the sensor-roll error multiplied by the cosecant of that angle. Planets do not satisfy this constraint very well because of their large apparent motion with respect to the Sun; for example, roll control would be lost during one portion of the trajectory if the Earth were used. A star near a pole of the ecliptic satisfies the condition for trajectories near the ecliptic plane, such as those of *Mariner B*. Canopus is one of the brightest stars, and is located close to the south pole of the ecliptic; hence, it is a likely choice if a star reference is used.

The identification of the reference object should be simple, using the object light intensity in a specific spectral region and/or a unique geometrical relationship as

UNCLASSIFIED

seen from the spacecraft after the Sun has been acquired. For initial acquistion, the Earth is very bright, but there is the chance of not being able to distinguish between Earth and Moon on some days of the firing period. Also, the asymmetrical albedo of the Earth can cause a few milliradians of pointing error at the time of the mid-course maneuver. Furthermore, near the middle of the trajectory, the Earth passes near the Sun, becoming a narrow, faint crescent. In addition, an Earth sensor cannot be pointed along the Sun line without saturation by stray reflections of sunlight or, for very small angles, actual damage. Mars would not be a good reference because of low intensity for initial acquisition and large variations of spacecraft orientation resulting from near-Mars trajectory dispersions. Also, Mars passes near the Sun–spacecraft line at two points in the trajectory, once before and once after encounter.

A star has a constant, measurable light intensity, which is thus useful for identification; also, the sensor need not handle the large dynamic range of intensity required by a planet sensor.

The antenna can be pointed to the Earth either by tracking the Earth itself or by command positioning based on a known relative orientation between Earth and spacecraft. Pointing the antenna independent of the roll control requires two DF between the antenna and the spacecraft. If the Earth is used for roll control, then only one relative-motion DF is needed. This simplifies the antenna control but requires the inertial roll attitude of the spacecraft to change by about 180 deg during the flight. The roll-error degradation for small Sun–spacecraft–Earth angles does not affect the antenna pointing accuracy.

The antenna might optically track the Earth with two DF independent of the roll control but could lose the Earth as it passed near the Sun. Tracking the Earth by locking on the RF signal from the Earth eliminates this period of loss of reference but requires continuous RF transmission or control logic to hold the last known pointing direction until the signal is found again, and depends on the operation of the spacecraft receiver.

The antenna can be pointed toward the Earth using a known spacecraft orientation and the position of the Earth with respect to the spacecraft from the standard trajectory. With this method, the antenna pointing would be open-loop, using antenna-angle programs generated before launch. These programs could be corrected in flight by quantitative radio command from Earth or by intermittent optical or radio tracking of the Earth.

Considering all of the factors mentioned above and the fact that a star sensor is needed for approach guidance, a useful choice appears to be a star and a combination of tracking and programmed control of the antenna. This requires one additional DF in the antenna (or star-sensor) control and two angle programs, and provides excellent control of the spacecraft roll attitude. Further tradeoff investigations and reliability studies are required before a decision can be reached.

The requirements on an optical or RF Earth sensor are:

(a) The sensor should have outputs for errors in two orthogonal directions and an output indicating acquisition (Fig. 32).

(b) Dynamic range and sensitivity must be capable of sensing the Earth over a wide range of brightness to be defined by the trajectory.

(c) The sensor null offset must be low enough to provide 0.1- to 0.5-deg roll accuracy in the regions

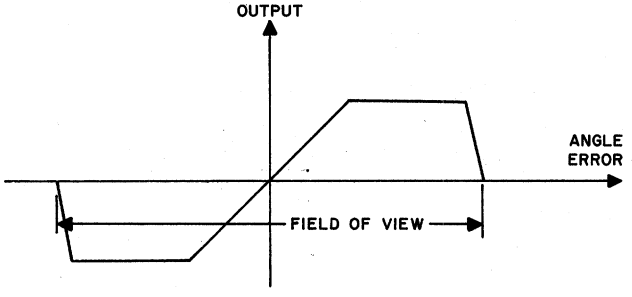

SINGLE-AXIS OUTPUT CHARACTERISTIC

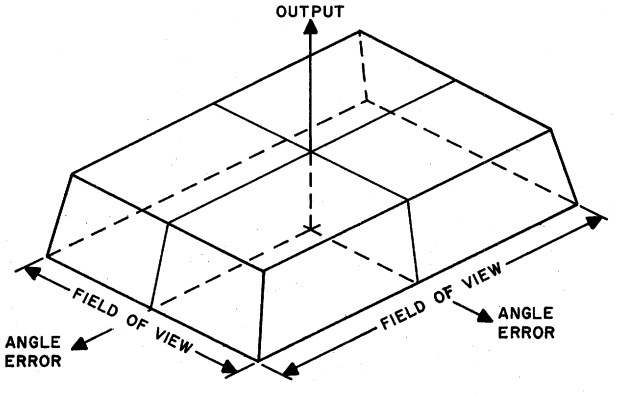

REFERENCE-ACQUIRED OUTPUT

Figure 32. Secondary-reference roll search and acquisition modes

UNCLASSIFIED

where accurate roll control is needed, despite degradation resulting from the size of the Sun–spacecraft–Earth angle.

(d) The sensor must have a linear range around zero and, if used with a rate signal for stabilization, saturate at a prescribed angle. The scale factor and saturation level must be independent of the widely varying incident-radiation intensity.

(e) The field of view in the roll direction must be large enough to allow the spacecraft to stop a roll-search turn without overshooting the field of view. In the direction perpendicular to the roll direction, the field of view should be large enough to accommodate the time variations in Sun–spacecraft–Earth angle over the time required to acquire the Earth. The field of view must be larger than the largest apparent size of the Earth at the time accurate control is required.

(f) If the sensor has multiple nulls, means must be provided for identifying the principal null.

The star-sensor requirements are:

(a) The star sensor should have outputs for errors in two orthogonal directions and an indication of star acquisition.

(b) The acquired signal should respond only to stars having the proper brightness in the specified spectral region.

(c) The sensor null offset must be low enough so that the roll-orientation accuracy is 0.1 to 0.5 deg, including degradation due to Sun–spacecraft–star angle.

(d) The sensor must be linear around the zero-error point over a specified angle-error range and must saturate at less than a specified angle error.

(e) The sensor field of view must be large enough to allow the spacecraft to stop a roll search without overshooting the field of view and to accommodate variations in acquisition time, but small enough to keep background starlight from triggering the acquired signal.

It may be necessary for a sensor to have two different fields of view as a result of the last requirement. Both mechanical and electronic configurations (the latter based on the image-dissector principle) for changing the field of view are possible.

Requirement (f) for the Earth sensor may be met by using an optical sensor for initial acquisition and the RF sensor for tracking.

If the Earth or star sensor is to be used for roll control, it must have the capability for uniquely identifying the Earth or the desired reference (e.g., by intensity, wavelength, or spectral distribution [color] of the incident radiation).

The actuation in the antenna-control loops can be produced by either stepping or continuous-rotation electric motors. The step size can be no larger than the portion of the ± 1-deg pointing accuracy allotted to the actuator. The maximum speed of rotation about a control axis must be at least as large as the maximum expected tracking rate due to the Earth's apparent motion, either in the normal attitude or, if continuous pointing during a turn is required, as the spacecraft performs commanded turns.

When the reference object for the roll-control loop is other than the Earth, then the antenna must be pointed independently of the roll orientation. This requires two DF, and possibly three if the spacecraft configuration does not allow two-DF pointing of the antenna without mechanical or RF interference by the spacecraft. For this discussion, two DF are assumed.

These two DF may be controlled by tracking loops or by programmed instrument-positioning loops, as shown in Fig. 33. If the antenna is pointed by tracking, then the optical or RF tracking sensor must supply three signals, two for controlling two tracking servos (one for each DF) and one to indicate that the Earth is acquired. The control criterion in each DF is the pointing error in that direction, and the servo must contain compensation for control-loop stability. The Earth-acquired signal switches out the pointing-error signals if the Earth is lost. These error signals should also be switched out when either the Sun or secondary reference is lost. When any of these loss-of-acquisition signals appear, the antenna should be locked in its current position until all are reacquired. For initial acquisition, for acquisition after an extended period of no tracking, or after the antenna is intentionally moved from its proper position, there must be a reference angle for each control loop to bring the antenna into position for acquiring and tracking the Earth. During spacecraft maneuvers, it is desirable to hold the antenna angles at their premaneuver values until the spacecraft is returned to its reference position, unless it is necessary to change these angles to remove the antenna from the rocket-motor exhaust, place it in a standard position for control of the center of gravity, or to track the Earth during the maneuver.

UNCLASSIFIED

UNCLASSIFIED

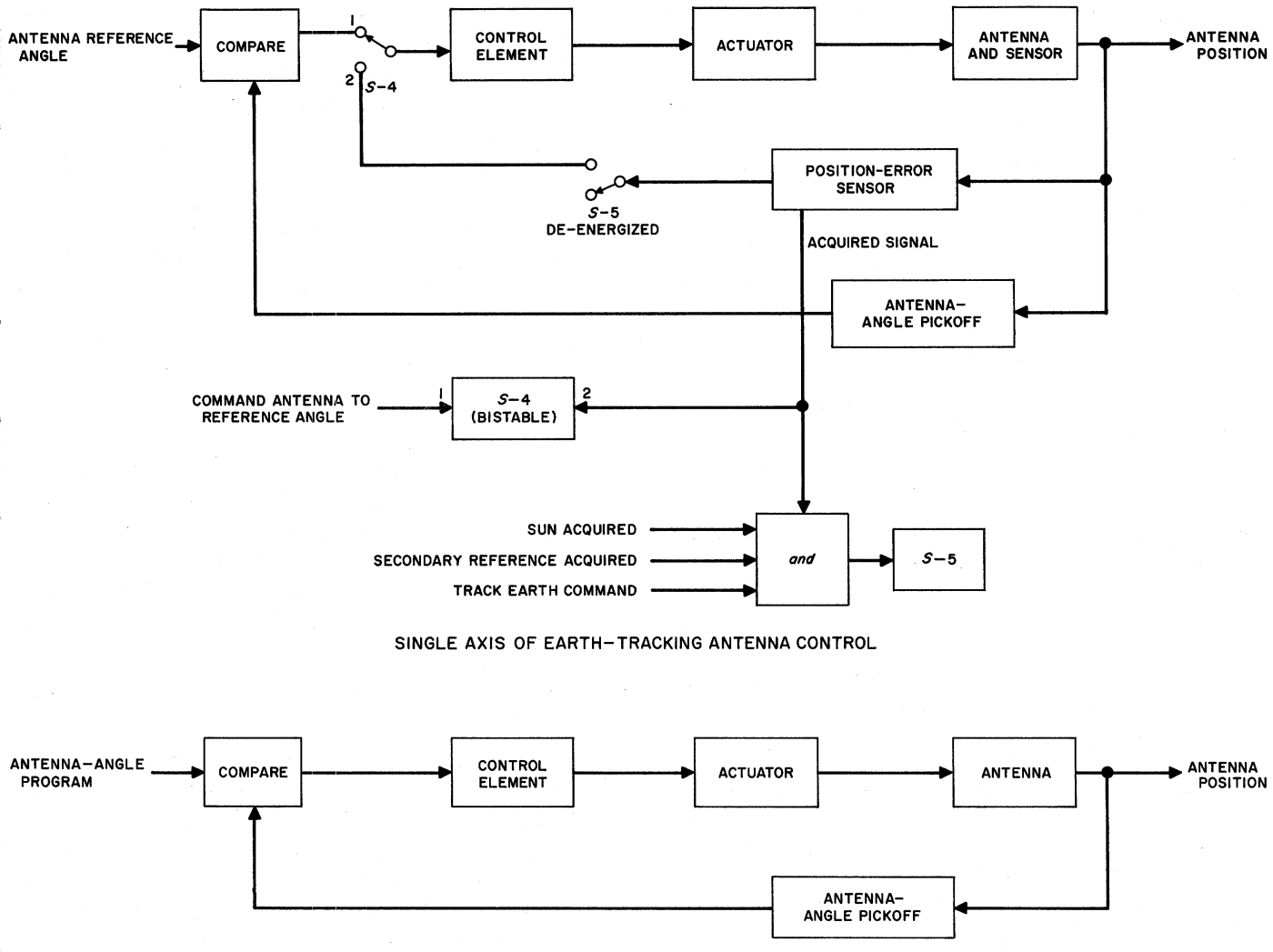

Figure 33. Directional-antenna control

Care must be exercised in the choice of the antenna gimbal axes to avoid a gimbal-lock condition.

It is not necessary that both degrees of freedom be on the antenna. The secondary reference sensor may have two relative DF, one relative DF and the spacecraft roll DF being used to maintain lock on the reference object, while the other relative DF and a single antenna DF are used to track the Earth. This complicates the determination of the spacecraft orientation in preparation for a maneuver and couples the motion of the antenna to the spacecraft-roll control.

Antenna-pointing by program is open-loop as far as pointing accuracy is concerned. From the preflight standard trajectory, the standard values of the two antenna angles are determined, and these angles, as functions of time, are stored in the spacecraft. The stored angles are compared to the antenna angles and the difference kept to zero. Deviations from the standard trajectory may require that these programs be changed in flight, but the changes would be small in the case of normally expected deviations. Partial mission failures may require large corrections.

The antenna program may be generated in several ways; e.g., analog, such as diode function generators, or digital, such as fitting the angle curves with polynomials in time and computing the angle at any required time. The digital methods can employ either a digital-analog converter with an analog antenna-control loop, or they can operate directly into a digital antenna-control loop.

UNCLASSIFIED

UNCLASSIFIED

Program correction can be accomplished by intermittent tracking of the Earth or by radio command based on the measured trajectory as compared to the standard. For an analog program, the correction could be inserted as a bias in angle or time, while for a digital program, the stored values or coefficients could be changed.

The time base for the program can be either the spacecraft sequencer clock or a separate clock (to eliminate dependence on the CC&S if the program source is separate).

(3) Planetary Horizontal Platform

The purpose of the planetary horizontal platform is to point scientific instruments toward the destination planet during the time the spacecraft is in the vicinity of the planet.

(a) The planetary horizontal platform (PHP) must be capable of acquiring and locking on the center of the planet with an accuracy of ± 0.5 deg and tracking the planet over the altitude range of from 153,300 km above the center down to 11,300 km and back out to 153,300 km. The tracking accuracy must be maintained in the presence of asymmetrical lighting or reflection.

(b) The reference source for the PHP sensor is the destination planet. The PHP could be pointed by programmed angles, but the dispersion of the trajectory might cause errors larger than 0.5 deg.

The planet sensor must be capable of searching for and locking on the planet when pointed in the general direction of the planet (within ± 70 deg). It must then track the center of the planet with less than 0.5-deg error, because some portion of the error must be allowed for the alignment between the sensor axes and the PHP. The requirement of tracking the center of the planet implies a sensor that does not track the centroid of light (except for uniform lighting in the sensor spectral region of sensitivity). The center can be found with a horizon-scanning sensor that tracks the center of the horizon circle or a sensor that geometrically locates the center from a portion of the horizon circle.

The sensor must have outputs giving the pointing errors in two orthogonal directions and a third output indicating that the planet has been acquired.

(c) The PHP probably must be pointed to the planet without loss of acquisition of the spacecraft reference objects or disturbing the directional-antenna tracking of the Earth. This implies at least two DF for the PHP attitude control. These degrees of freedom must be carefully selected to minimize complexity while allowing tracking of the planet during the total time in which the spacecraft is at less than 150,000-km altitude without the field of view of the planet sensor being obstructed by the spacecraft, or without mechanical interference between the spacecraft and the PHP. To meet this constraint, it may be necessary to use a third DF to move the PHP away from the spacecraft in order to provide wider angle coverage without interference. The choice of control-axis orientation is strongly dependent on the trajectory near the planet.

Another constraint in the permissible tracking range of the PHP is the reduction of control-loop gain due to degeneration of the PHP sensor and gimbal coordinate-axis relationships for a two-DF gimbal. Three gimbal axes and coordinate resolution of the pointing-error signal ease this constraint.

The actuation methods and control loops for the PHP can be similar to those for the two-DF directional antenna described earlier.

The tasks of the PHP are to find, lock on, and track the target planet. The first task is accomplished by pointing the sensor in the general direction of the planet from data based on the preflight trajectory or guidance planet-sensor angles, and starting the planet-sensor search routine. When the planet is acquired by the planet sensor, the mode of operation is automatically shifted from search to track. If the planet acquisition is accidentally lost, the PHP should lock in its current position and resume search. The PHP control loop is shown in Fig. 34.

The control criterion for the first mode of PHP control-loop operation is the standard angle for finding the planet. For the search mode, the control criterion is the search pattern, and for the track mode it is the pointing error. In all modes, the control loop is stabilized by suitable compensation.

(4) Attitude-Control Actuators

There are several methods for supplying attitude-control torques for a spacecraft, including mass expulsion, reaction torques from changing the magnitude or direction of the angular-momentum vector of a body rotating within the spacecraft, and solar-radiation pressure effects.

UNCLASSIFIED

UNCLASSIFIED

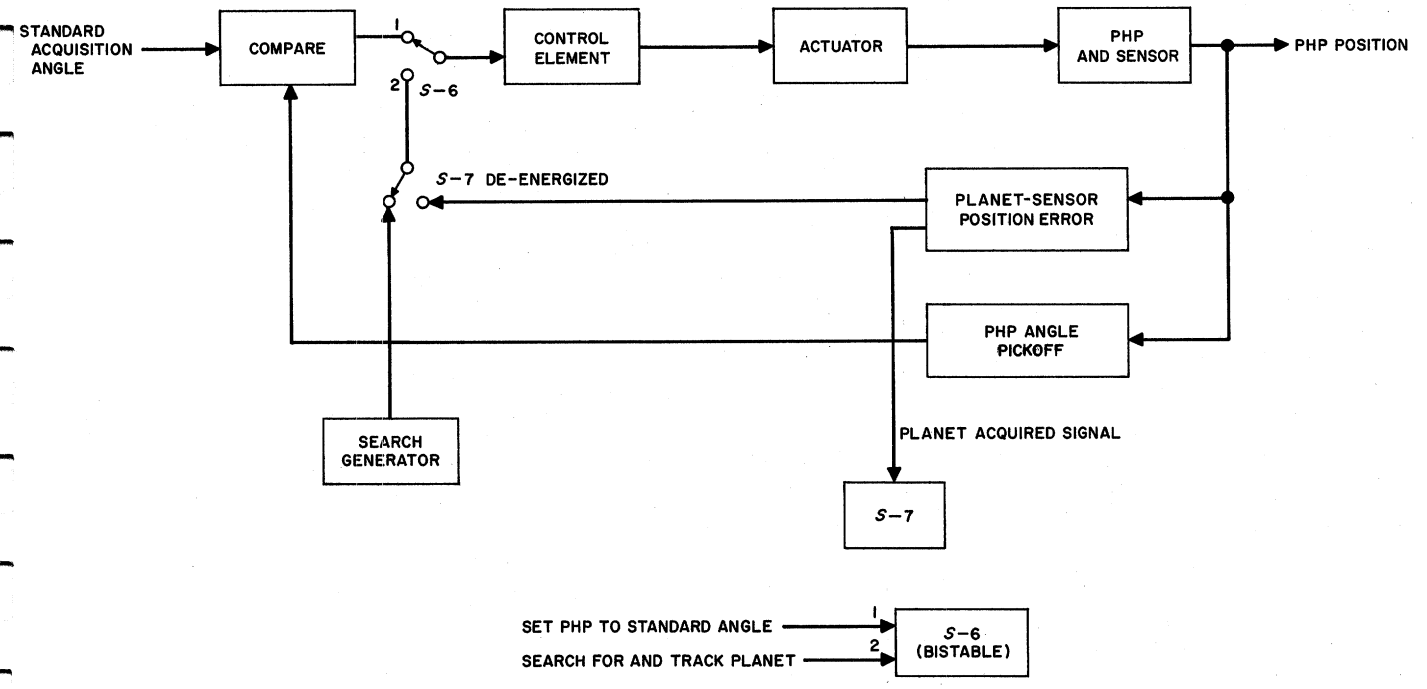

Figure 34. Planetary horizontal-platform control loop

Tradeoff studies of these methods are in process to determine the optimum combination of torquing methods for the *Mariner B*. The characteristics of each method are discussed below.

(a) Mass expulsion

A cold-gas mass-expulsion system similar to those used on *Ranger* and *Mariner A* can also be used on *Mariner B*. This type of system will not be described here, since extensive reference material exists from its previous applications. Hot-gas mass-expulsion systems will also be studied, but no work has yet been completed in this area.

(b) Reaction torques

The use of reaction torques for attitude control is based on the conservation of angular momentum. Changes in the rates of the spacecraft frame are achieved by shifting a suitable portion of the total angular momentum from the spacecraft frame to an internal body that is free to move in at least one DF with respect to the frame, rather than shifting it out of the boundaries of the spacecraft as is the case with mass expulsion. Reaction torques on the frame result from either process. The angular momentum is still present within the spacecraft storage-body system but is not externally apparent. Changes in the magnitude, the direction, or both, of the angular-momentum vector of the storage body produce equal and opposite changes in the angular momentum, and hence, the rates of the spacecraft.

A reaction-wheel storage system consists of a wheel free to rotate about a single axis with respect to the spacecraft. Reaction torque is generated by changing its rate of rotation, and hence, the magnitude of its angular momentum. A wheel for each of the three control axes would be needed for a complete spacecraft attitude-control system. Reaction wheels have the disadvantage that there is only one DF with respect to the spacecraft, resulting in gyroscopic crosscoupling torques when there is motion about either of the other two axes. These gyroscopic torques, which are dependent on wheel speed, can either be accepted, if it can be shown that they cause no serious effects, or compensated and possibly put to use with complicated control-loop logic.

Troublesome gyroscopic crosscoupling may be eliminated by removing the constraints in the other two DF, which requires a floated reaction sphere in place of the set of wheels. The flotation may be accomplished by a closed-cycle gas bearing, an electromagnetic field, or an electrostatic field. The reaction sphere provides torques on the spacecraft in the same manner as the wheel, but without causing gyroscopic crosscoupling torques. Electrostatic suspension is the only method of the three that does not produce retarding torques on the sphere.

UNCLASSIFIED

UNCLASSIFIED

A third reaction-torquer system involves the use of a pair of matched, initially counter-rotating, constant-speed wheels, with zero resultant initial angular momentum. If these wheels are gimballed in such a way that they can be rotated independently to point the spin axes in different directions, then an angular momentum in any direction less than or equal to the sum of the wheel momenta can be added to (or removed from) the spacecraft. Three-axis control by this method is quite complicated. It is much simpler to control only two axes, the third being controlled by a third wheel or by differential speed control on the two wheels.

Because all of the reaction systems are conservative systems, they suffer the common disadvantage that the results of all external-torque disturbances to the spacecraft accumulate in the reaction-device torques with a DC component, driving the device to larger and larger speeds or separations of gyro wheels. A method of removing this angular momentum from the spacecraft reaction-device system is needed to keep angular velocities or separations to an acceptable level. This resetting system must be nonconservative, using such methods as mass expulsion or solar-radiation torques.

A reaction-device system using mass-expulsion resetting needs less propellant than a system using only mass expulsion, because only the momentum from disturbances must be removed. The wheel momentum can be removed when the reaction device reaches a preset speed, so that a fixed-impulse resetting device, such as fixed-size slugs of solid propellant fired as needed, could be used with a possible total-system weight reduction.

To consider reaction-sphere system weight in more detail, let

H = angular-momentum capacity, lb_m ft^2/sec

Ω = speed limit per axis, rad/sec

a_0 = w/ft lb for 1-ft-radius sphere

T_0 = maximum torque capacity, ft lb

$$\frac{H}{\Omega} = \frac{2}{3} M_s r^2$$

$$M_s = \left(\frac{1.5H}{\Omega}\right) r^{-2} = \text{weight of sphere}$$

Let M_{ss_0} be the support-structure weight for the unit sphere, and assume that this weight varies exponentially between the second and third power of the radius. Then, the support-structure weight is

$$M_{ss} = M_{ss_0} r^i \qquad 2 \leq i \leq 3$$

The torquer area varies as the square of the radius, while the moment arm and gap S vary as the radius. The torque for fixed power is

$$T \propto \frac{\text{area} \times \text{moment arm}}{\text{gap}} \propto r^2$$

Therefore, the power is

$$a = a_0 r^{-2} \text{ w/ft lb}$$

The torquer peak power for each axis is

$$P_{pk} = aT_0 = a_0 T_0 r^{-2}$$

Let P_0 = power required by support system, torque-control electronics, etc. (assumed constant) and M_0 = weight of auxiliary equipment. The total peak power is

$$3P_{pk} + P_0$$

If the sphere-system power inverter weighs ρ_I lb/w, then the total weight, exclusive of the power or energy source, is

$$\Sigma m = M_s + M_{ss} + \rho_I (3P_{pk} + P_0) + M_0$$

$$= \left(\frac{1.5H}{\Omega} + 3\rho_I a_0 T_0\right) r^{-2} + M_{ss_0} r^i + (\rho_I P_0 + M_0)$$

For minimum weight, with r as the parameter,

$$\frac{\partial \Sigma m}{\partial r} = -2\left(\frac{1.5H}{\Omega} + 3\rho_I a_0 T_0\right) r^{-3} + iM_{ss_0} r^{i-1} = 0$$

$$r_{\text{opt}} = \left[\frac{2}{iM_{ss_0}}\left(\frac{1.5H}{\Omega} + 3\rho_I a_0 T_0\right)\right]^{1/(2+i)}$$

The minimum total weight (Figs. 35 and 36) is

$$M_{\min} = \left(\frac{2+i}{i}\right)\left(\frac{i}{2} M_{ss_0}\right)^{2/(2+i)}$$

$$\times \left(\frac{1.5H}{\Omega} + 3\rho_I a_0 T_0\right)^{i/(2+i)} + (\rho_I P_0 + M_0)$$

This optimization does not consider volume. If M_{ss_0} is low, then the optimum size would be large, and any volume constraint would force the size to be smaller than optimum. In addition to this weight, the weight of the resettling system must be considered. A sphere capable of holding all of the accumulated angular momentum without dumping would probably be much too large.

(c) Solar-radiation pressure

Solar-radiation pressure on movable vanes or on surfaces of controlled reflectivity can be used to supply attitude-control torques. Vanes would have to be differentially tilted to provide roll torques, while pitch and yaw torques could be provided by changing the spacecraft area presented to the Sun. Fixed vanes or proper

UNCLASSIFIED

choice of total configuration can provide passive "weathercock" stability toward the Sun, but the stabilization torques are obtained by rotating the whole spacecraft.

The solar-force vector acting on a surface of the spacecraft is a function of the flux density of incident radiation and particles, the angle of incidence of the solar radiation, and the area and reflectivity of the surface. The solar-torque vector acting on the spacecraft is the vector sum of torques caused by the force vectors on individual spacecraft surfaces.

Compared with control of the area moment, control of the reflectivity requires twice the controlled area, because the control is only half as efficient.

An advantage of solar-radiation control torques is the automatic gain control inherent in the system for the wide range of solar-radiation pressures that may be encountered. Once the movable elements are set to compensate for solar torques in a particular spacecraft configuration, they need not be moved unless the center of force shifts as a result of changes in the location or reflectivity of surface elements. Solar torques for reasonable surface areas are quite small and probably not useful for acquisition. They are useful, however, for a slow resetting of a reaction-torque system. Controlled vanes on the spacecraft may also complicate field-of-view problems.

(5) Attitude-Control Logic

The control logic used in the *Mariner B* attitude-control loops will depend on the type of actuation used and the mode of operation. During the first part of the acquisition mode, the attitude-control task is mainly to reduce tumbling, and the control criterion is essentially the spacecraft turning rate. When the rate has been reduce tumbling, and the control criterion is essentially allowable acquisition time, then the control criterion

PLOTTED FOR $i = 2$

$1 \le m_{SS_0} \le 100$

$1 \le \left(\frac{1.5H}{\Omega} + 3\rho_I\, a_0\, T_0\right) \le 100$

$$r = \left[\frac{\frac{1.5H}{\Omega} + 3\rho_I\, a_0\, T_0}{m_{SS_0}}\right]^{\frac{1}{4}}$$

$$m = 2\left[m_{SS_0}\left(\frac{1.5H}{\Omega} + 3\rho_I\, a_0\, T_0\right)\right]^{\frac{1}{2}}$$

PLOTTED FOR $i = 3$

$1 \le m_{SS_0} \le 100$

$1 \le \left(\frac{1.5H}{\Omega} + 3\rho_I\, a_0\, T_0\right) \le 100$

$$r = \left[\frac{\frac{1.5H}{\Omega} + 3\rho_I\, a_0\, T_0}{1.5\, m_{SS_0}}\right]^{\frac{1}{5}}$$

$$m = 1.96\left[m_{SS_0}^2\left(\frac{1.5H}{\Omega} + 3\rho_I\, a_0\, T_0\right)^3\right]^{\frac{1}{5}}$$

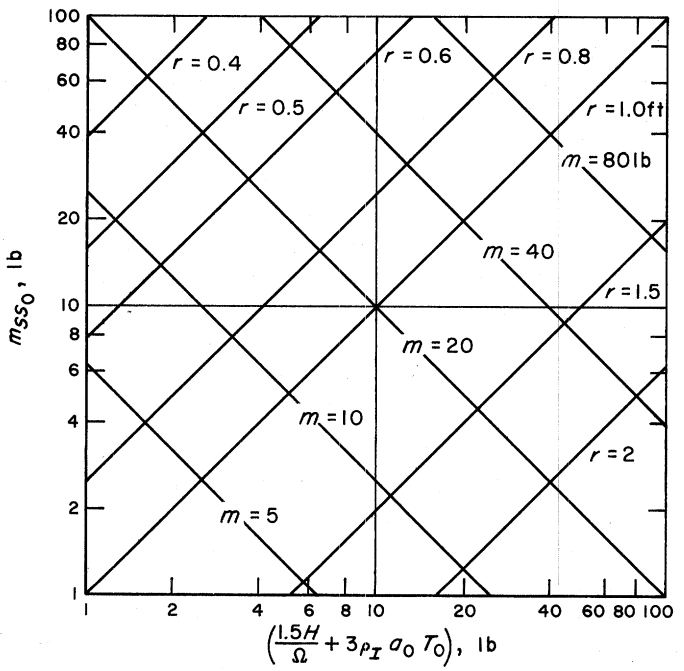

Figure 35. Optimum reaction-sphere weight and radius for $i = 2$

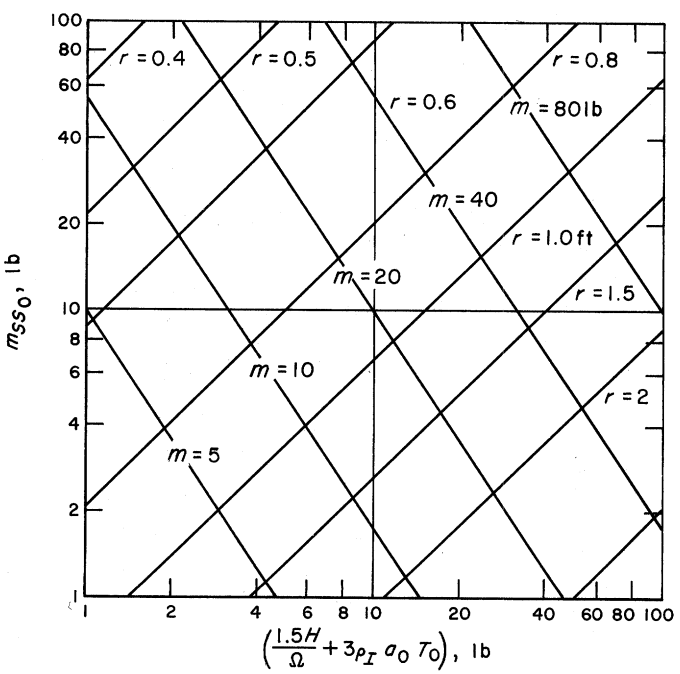

Figure 36. Optimum reaction-sphere weight and radius for $i = 3$

UNCLASSIFIED

involves both rate and position. It is desirable to maintain this rate of moving toward the desired position until that position has nearly been reached, followed by convergence on the desired position and zero rate. The position sensor must saturate; otherwise, acquisition is not by the desired path unless the spacecraft acceleration is high. This constraint is an advantage, because the sensor is not required to have a large dynamic range of output signal. A response worse than that for an unsaturated position sensor results when the rate sensor saturates before the position sensor.

The control element of the system may be either proportional or on–off. This changes the shape of the acquisition-phase trajectory but not its general form. The control element may also have a dead zone, with the line of zero torque becoming a band of zero torque about the initial line, again without changing the general form of the phase trajectory.

The attitude-control system must also perform the task of maintaining lock on the reference object. This task can be performed with the same control criterion. For systems with proportional control or on–off control with dead zone, the control criterion is $\Delta\theta + \tau\Delta\dot{\theta}$, but contrasting uses are made of the actuating difference. For proportional control,

$$\ddot{\theta} = -K_1(\Delta\theta + \tau\Delta\dot{\theta})$$

while for the on–off system

$$\ddot{\theta} = \begin{cases} +K_2, & \Delta\theta + \tau\Delta\dot{\theta} < -\theta_L \\ 0, & -\theta_L \leqq \Delta\theta + \tau\Delta\dot{\theta} \leqq \theta_L \\ -K_2, & \theta_L < \Delta\theta + \tau\Delta\dot{\theta} \end{cases}$$

With ideal components and no disturbance, each would reach a zero-rate condition. However, actual components have time delays, sensor-output rise times, hysteresis, etc., so that the actual operation results in steady-state offsets or a limit cycle. In this mode, the rate error may be taken from a rate sensor or derived from other signals available in the system, either by differentiation of the position signal or an integration of the forcing acceleration to obtain a signal proportional to rate. Practical devices to accomplish these tasks also cause some changes in the system response. The effects are more noticeable if a passive network is used. Even so, passive compensation is often preferable in view of smaller size and lower power requirements.

The control element controls the torquing device (reaction torquer, gas-jet valves, or solar-vane position control). Loss of lock on the reference object must cause the control system to revert back to the acquisition mode. Block diagrams of the control loops are shown in Fig. 37.

The attitude-control loops are also required to cause the spacecraft to make turns of commanded magnitude about the control axes. These commanded turns place the spacecraft in a desired orientation other than normal (where all reference objects are acquired). If the desired orientation involves pointing a single line fixed in the spacecraft, then any combination (there are six) of two single-axis turns could accomplish this goal. If, however, two lines fixed to the spacecraft are to be controlled, then three turns (12 possible combinations) are necessary. The number of turns is therefore determined by the simultaneous pointing requirements, while the order of turns (pitch, yaw, or roll) is set by such considerations as accuracy, simplicity of control logic, etc., and by possible constraints, such as continuous rather than final-value pointing control.

The turns might be performed in three ways: acceleration control, rate control, or position control. The first of these would require control of the spacecraft acceleration as a function of time. With a proportional actuation system and angular-acceleration measurement, this could be a closed loop, with less accurate calibration of the torquing device required. First and second integrals of the acceleration error can be used to improve the turning accuracy. Rate control would use a rate-measuring device with a calibrated rate command such that the integral of the command is the desired change in angle. Such a system is used on *Ranger* and *Mariner A*, where the command is equivalent to a fixed spacecraft angular rate inserted for a time equal to the desired turn angle divided by the fixed rate. The angle turned would have an error due to errors in calibration of the device and unequal start-and-stop transients of the control system. The error due to unequal start-and-stop transients can be eliminated by using the integrated rate error. The rate-commanded turn might also use a variable rate for a fixed duration, which requires rate-measurement-device calibration over a wide range of rates and a larger output dynamic range to handle the integral of the rate error.

Position control of commanded turns requires continuous knowledge of the orientation of the spacecraft, which can be obtained either by measuring the positions of reference objects relative to the spacecraft with sensors tracking the individual reference objects, or by reference to a platform stabilized either inertially or by sensors locked to celestial references. Pointing a given spacecraft-fixed line in any desired direction using tracking sensors requires two reference objects, wide coverage with the tracking sensors, and careful orientation of the centers

UNCLASSIFIED

UNCLASSIFIED

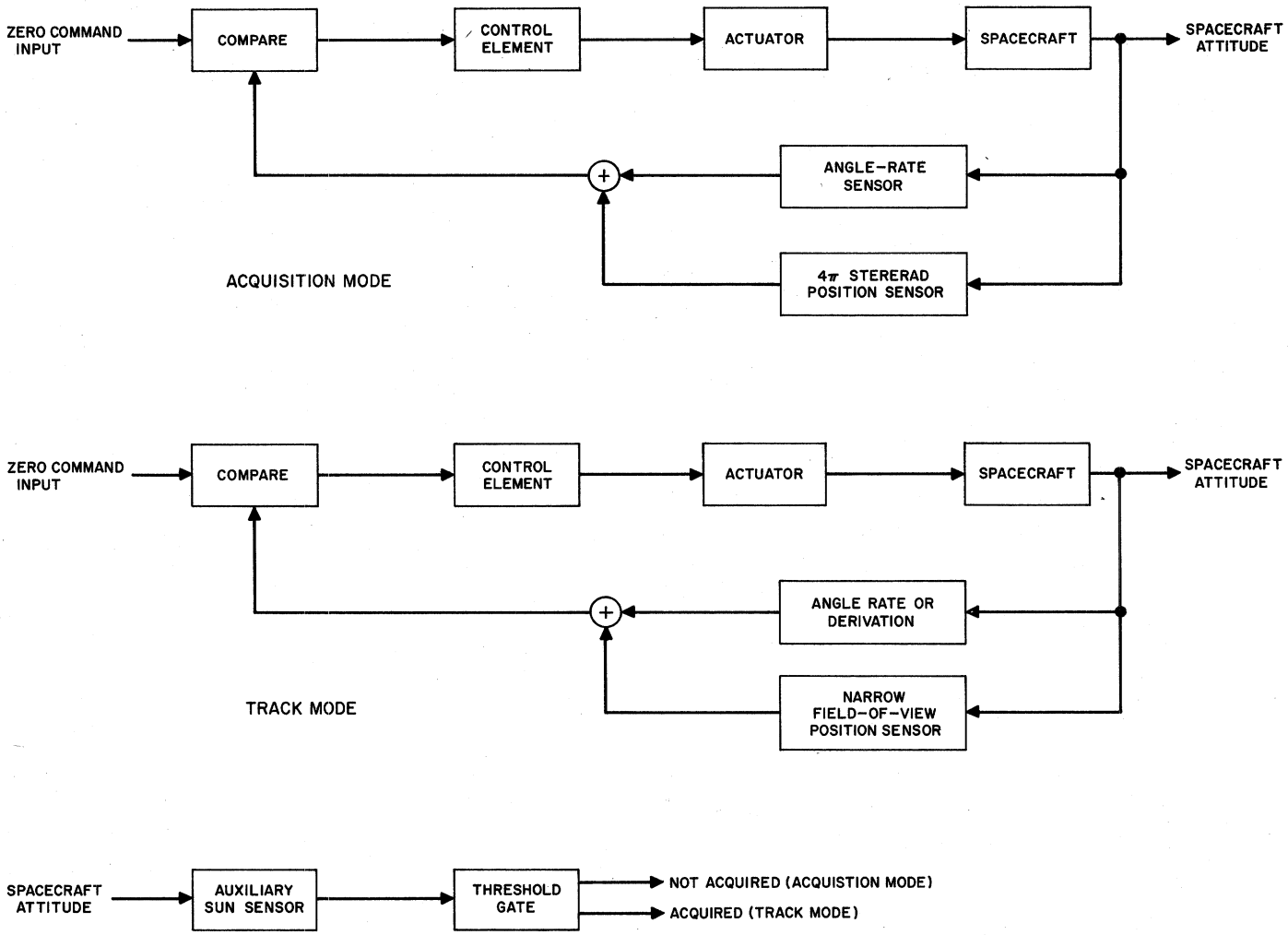

Figure 37. Pitch- and yaw-control loop

of sensor-tracking coverage with respect to the line to be pointed. Using more reference objects and switching from one reference to another as each reaches the tracking limit could reduce the severity of the restrictions but complicates the control logic. Pointing two spacecraft-fixed lines becomes an impossible task if only two reference objects are used. A constraint on the permissible pointing directions may reduce the tracking-range problem, if the geometry of possible references and sensor locations permits it. A stable platform could initially be set into a known orientation and then left while the spacecraft maneuvers around it to the desired position, as determined by the platform gimbal angles. Here, there are possible pointing-direction restrictions because of gimbal lock, unless a four-axis platform is used. The use of one- or two-DF gyros in lieu of a platform is possible in certain cases. In all types of position control, the actuating difference would be the difference between desired and actual values of the radiation sensor, platform, or gyro position signal, with some angle rate for system stability.

e. *Instrument Configurations*

It is desirable to use the same instruments for both guidance- and attitude-control functions. Alternative instrument configurations will be discussed here which meet both guidance and attitude-control requirements of the *Mariner B*.

(1) Relative Merits of Different Configurations

The basic instrumentation problem for approach guidance is the measurement of angles between the destination planet and at least two other celestial bodies. These angles are then compared with values based on the standard trajectory and time of observation to obtain perturba-

UNCLASSIFIED

tions that are used to compute the corrective maneuver. Several methods exist for extracting the necessary information from the instruments. The most straightforward is to mount sensors (one for each celestial object observed) to the same reference frame with movable linkages. (One sensor may be hard-mounted if the reference frame is movable.) Each sensor is driven to its null by instrument-positioning servos (or the spacecraft attitude-control system), and the desired angles are read from the mechanical linkage readouts at the standard measurement times. The advantages of this method are that the sensors are all working at their nulls, where calibrations are most accurate, and the angle measurements are continuously available for readout.

Another method using the same general mechanical setup is to command-position the sensor mechanical linkages to positions representing standard angles for some preset (future) time. At that time, the deviations from standard angles may be read directly from the sensors. Although this method may present some advantages in computation, it suffers from the disadvantage with respect to the sensor-nulling system that sensor linearity and scale-factor errors must be considered in addition to the other errors.

A different technique, which needs considerable further investigation but potentially offers greater accuracy than either of those previously mentioned, uses angles which are preset for a future time as in the second method above, but in this case, instead of observing the sensor error at a preset time, the time at which the sensor error crosses a preset zero value is noted. The time deviation from standard rather than an angle deviation is then used as a measure of trajectory error. This basic technique opens the door on possibilities for achieving higher accuracy. Consider a space "sextant," wherein the light from one celestial body is deviated through a preset angle, and a detector is arranged to signal the computer when the deviated beam coincides with a beam from a second object. A comparison of the deviation angle and the time of conicidence with stored standard values yields the desired guidance information. For extreme accuracy, the deviation angles might be ground on prisms which are indexed in the instrument for different times in flight. This sextant technique, while offering great potential accuracy, presents some formidable difficulties in its practical application. First, the plane of the angle deviation may not coincide exactly with the plane containing the two celestial objects and the spacecraft. Thus, the plane of deviation must be made controllable, or the coincidence detector must be made insensitive to noncoincidence along the cross axis. Second, the times of coincidence for different angles may differ, so that the computer must handle a different time for each angle measured. The third (and probably most severe) difficulty is the coincidence detector itself, which must be insensitive to the actual location of the images within its field of view while accurately recognizing coincidence of centers of images that are not points and may not even be uniformly lighted disks. Because such a detector appears beyond the state of the art at this time, the remaining configuration discussions consider only measuring instruments using one-body-at-a-time sensors.

Because the considerations that govern the choice of references (other than the destination planet) for attitude control are similar to those for approach guidance, it is assumed that the two stars used for approach-guidance observations (probably the Sun and Canopus) are also the references for attitude control. An argument in favor of such an approach is that the same sensors can be used for both guidance and attitude control. Accordingly, a combination approach-guidance/attitude-control instrument assembly containing sensors for two stars and the destination planet plus suitable mechanical linkages, instrument servos, and readout devices will be discussed.

Before investigating the possibilities of a multiple-sensor instrument assembly, it is appropriate to consider the technique whereby angles are measured by turning a single sensor (or possibly the whole spacecraft) to look at the reference objects sequentially. This method for obtaining navigation data has some strong theoretical advantages. It requires only one optical system and at most two DF (excluding attitude-control requirements). Some types of bias errors are automatically eliminated by measuring a turned angle on one sensor rather than an included angle between two sensors. However, two principal difficulties are apparent at once. First, the celestial objects being observed require different types of detectors for best accuracy, i.e., chopper–photomultiplier devices for stars, occulting disk and photocell detectors for the Sun, and accurate image-center-finding detectors for partially lighted planets. Inclusion of all three types in a single sensor presents formidable problems. The second difficulty is that of spacecraft-attitude stability while turning through the included angles. For residual angular rates of about 1 deg/hr (5×10^{-6} rad/sec), the complete measurement of a celestial angle (two detector nulls plus the instrument turn) must take place in less than one minute if the angle error is to be held below one minute of arc. Turning the spacecraft itself to measure angles with a fixed sensor also appears impractical at present for the following reasons. Making spacecraft turns to better than one-minute accuracy currently requires a

three-axis stable platform, which has undesirable weight, power, and reliability features. Also, because of dependence on solar power, it is not desirable to disturb the basic Sun-pointing orientation of the spacecraft more than absolutely necessary.

It should be borne in mind that each choice of data-extraction method and instrument configuration implies particular requirements for, and constraints upon, the attitude-control system and the guidance computer. In general, the simpler instrument configurations result in greater complexity in the attitude control, the computer, or both. In examining several possibilities for the instrument assembly, the following basic requirements are assumed:

(a) The attitude-control system and guidance loops use the same Sun–star reference system. Approach guidance also uses a destination-planet sensor.

(b) The instrument contains only one sensor for each body being observed.

(c) The guidance scheme uses the "measure-angle-at-a-preset-time" data-extraction method, and all angles required for one fix are measured simultaneously.

The simplest instrument configuration that meets these requirements consists of a body-fixed two-axis Sun sensor for pitch and yaw control, a single-DF star sensor for roll control, and a two-DF planet sensor. Thus, the six DF necessary to point three lines in space simultaneously are divided equally between the spacecraft (pitch, yaw, and roll) and the instrument (star cone angle and planet cone and clock angles). The instrument servos can easily drive their respective degrees of freedom to obtain sensor nulls, but nulling of the spacecraft-controlled sensor axes is a more difficult matter. The simplest type of attitude control uses an on–off mass-expulsion technique with a dead band centered on its detector null. The angles read from the instrument gimbals are therefore in error by a combination of the attitude-control instantaneous errors. Two principal methods are available for handling this problem. One involves additions to the attitude-control system that eliminate the dead band or reduce it to a value less than the allowable observation error. The other method requires the computer to make allowance for the known attitude errors in processing the data from the gimbal readouts. Also, the computer must process three angles, instead of two, to get a fix with this configuration, because instead of measuring Sun–planet–probe and star–planet–probe angles directly, the instruments measure the Sun–probe–planet (planet cone) and Sun–probe–star (star cone) angles and the dihedral angle between the planes defined by the other two measurements (planet clock angle).

An instrument configuration which, at first glance, makes minimum demands on the spacecraft attitude control and the computer and measures the desired navigation angles directly is a six-DF setup wherein a planet-tracking sensor is mounted by two wide-angle DF to the spacecraft. The star and Sun sensors are then connected to the planet tracker with two DF each. The elevation angles are desired navigation angles, and azimuth motions are required only for locating and tracking the references. A disadvantage (other than mechanical complexity) of this configuration is the difficulty of extracting attitude-control information from the Sun and star sensors through such a complex gimbal setup, particularly during the measurement period.

A third possible instrument configuration strikes a compromise between the first two. The simple instrument assembly discussed above, consisting of a fixed Sun sensor, a single-DF star sensor, and a two-DF planet sensor, can be mounted to a sub-base that is then connected to the spacecraft through three limited-action (say, $\pm 1/4$ deg) DF, allowing motion about the spacecraft pitch-, yaw-, and roll-control axes. The latter motions permit the sub-base to be operated as a Sun–star stabilized platform, while the spacecraft operates in a limit-cycle mode, controlled by relatively crude position readouts on the limited-action joints. This configuration, while technically having six DF, differs from the other six-DF system mentioned above, because the limited motions involved do not present field-of-view problems other than those present in the simplest configuration considered; because the limited-action gimbals can be made very rigid; and because attitude-control information is readily derived from the gimbal-position readouts or from the Sun and star sensors directly if the three limited-action gimbals are locked. A disadvantage of this configuration, when compared to the planet-tracking six-DF configuration is that the computer must handle an extra angle per fix. Table 10 summarizes the configurations discussed here.

(2) Instrument Servos and Readouts

The approach-guidance/attitude-control instrument assembly will, in general, require a servo and readout for each degree of freedom. Most of the servos will have to operate in at least two different modes: (1) positioning in response to an external command and (2) tracking a reference source in response to sensor-error signals. If the instrument gimbals are held fixed in commanded positions while guidance angles are derived from that com-

UNCLASSIFIED

Table 10. Summary of guidance-control instrument-configuration discussion with accuracy estimates

Basic instrument configuration	Attitude-control constraints	Computer constraints	Random-error estimate			
			For approach-guidance angles @ 400,000 km[a]			
				Bias millirad	Related millirad	Noise millirad
I						
A. Three DF Sun sensor; hard mounted to spacecraft Star sensor; roll axis hard mounted to spacecraft Star sensor; cone axis gimballed to spacecraft Planet sensor; both axes gimballed to spacecraft	Dead band reduced by trim control or tighter jet control to about ±0.15 millirad or less on all three axes during approach-guidance observations	Approach-guidance problem involves three angles (star cone angle plus planet clock and cone angles)	Star cone angle Planet cone angle Planet clock angle	0.4 0.40 0.45	0.1 0.51[b] 0.51[b] plus orthogonality error	0.18 0.21 0.22
B. Same as above	Requires Sun-sensor and star-sensor roll-axis linearity and scale-factor errors to be less than about 0.15 millirad from initial calibration over attitude-control dead band	Same as IA plus: attitude-control sensor errors, suitably combined, must be added to the three angles read from the instrument gimbals. Analog to digital conversion probably required on errors	Star cone angle Planet cone angle Planet clock angle	0.37 0.37 0.44	0.1 0.51[b] 0.51[b] plus orthogonality error	0.2 0.23 0.24
II						
Six DF; limited action on 3 Sensors same as in I but mounted to three-axis limited-motion platform. Platform motion of about ±0.25 deg about spacecraft pitch, yaw, and roll axes. Platform Sun–star stabilized	Attitude-control information may be required from crude position sensors on limited-motion gimbals during approach observations to prevent reaching gimbal limits of travel	Same as IA	Star cone angle Planet cone angle Planet clock angle	0.37 0.37 0.45	0.1 0.51[b] 0.51[b] plus orthogonality error	0.18 0.18 0.18
III						
Six DF; wide angle Planet sensor; both axes gimballed to spacecraft Star sensor; both axes gimballed to planet sensor Sun sensor; both axes gimballed to planet sensor	Attitude-control information from Sun and star sensors must be resolved through gimbal structure	None; Sun–probe–planet and star–probe–planet angles are measured directly	Star–probe–planet angle Sun–probe–planet angle	0.37 0.45	0.51[b] 0.51[b]	0.18 0.18

[a] Angles to planet will be more accurate at longer ranges.

[b] Further study of Mars as an optical reference should lead to reasonably good knowledge of the relations.

mand position plus the sensor error signals, then positioning must be quite accurate, because any error in the positioning of the sensor is a direct error in the guidance measurement. If, however, the command positioning is used only for reference acquisition and the tracking mode is used during observations, the positioning accuracy required is only that necessary to assure that the reference will be in the sensor field of view. (A search program superimposed on the command position may be required if the reference-object position is not predictable to sufficient accuracy.) The accuracy of the servos in the tracking mode must always be commensurate with the guidance-observation accuracy (see error discussion to follow) because any residual tracking error is included in the final guidance-angle measurements. Required tracking rates are very low, being set primarily by the residual attitude-control angular rates, although somewhat higher rates will probably be required for slewing to a commanded position. Readout of the instrument gimbal angles to guidance accuracy will probably require digital

UNCLASSIFIED

UNCLASSIFIED

systems, especially because a digital computer is used. Digital readout can be obtained either by direct angle encoding or by counting pulses to an incremental-type actuator. The latter method would probably require an extra register in the computer to store the actual angle, while in the former method the encoder itself could serve as the register. Indirect-encoder drive through an intermediate analog system (inductosyn, multipole resolver, etc.) could be used but would probably add complexity, with little gain in accuracy.

Actuators for the instrument servos may be electric motors of either continuous or incremental (stepping) types. If incremental actuators (which are attractive from a power-saving standpoint) are used, their threshold and granularity must not be greater than the uncertainty of the readout device.

Considerations similar to those discussed above for guidance-instrument positioning and tracking apply to the loops required for control of large movable assemblies such as the directional antenna and planetary horizontal platform. The antenna servo, however, will probably contain a dead band to eliminate the need for responding to attitude-control rates (because the limit cycle is probably smaller than the required tracking accuracy), and PHP tracking rates are somewhat higher as a result of the requirement to track the planet as the carrier passes a few thousand kilometers from it.

(3) Error Sources, Types of Error Expected, and Magnitude Estimates

In measuring the angle between two celestial objects, the following error sources must be considered:

(a) Sensor null offsets—the angular difference between the sensor electrical-null direction and the mechanical axis of the sensor

(b) Sensor linearity and scale-factor errors (These need to be considered only if the sensor is operated off null.)

(c) Sensor-mounting and alignment errors—the angular difference between the sensor mechanical axis and the readout connection (includes gear errors, if used)

(d) Servo-tracking errors

(e) Angle-readout granularity errors—error due to quantizing the angle (maximum equals ½ the least significant bit size)

(f) Gimbal-orthogonality errors—error in the guidance measurement introduced by nonorthogonality of the gimbal axes when the star–probe–planet angle is represented by a combination of star cone angle and planet clock and cone angles

The errors to be expected from the above sources can be roughly separated into four categories (as defined earlier in this section):

(a) Bias errors

(b) Noise errors

(c) Input-related errors

(d) Drift errors

Not all of the above error categories will apply to all of the error sources, nor will all of the error sources appear in every measurement or configuration. Table 11 shows preliminary estimates of the occurrence and magnitude of the various error sources. Consider, for example, the measurement of the Sun–probe–planet angle at 10^6-km distance, with the Sun and planet sensors operating at null, and the Sun sensor hard-mounted to the reference frame (spacecraft or sub-base). The applicable rms errors are given in Table 12, with the resulting total errors.

f. Computing, Control, and Sequencing

The sequencing function and some or all of the control functions required in the *Mariner B* spacecraft may be performed by a device separate from the guidance computer; or all three functions may be performed by a single device. A study is in progress to determine the more desirable configuration. General requirements for all three areas are discussed here.

(1) Approach-Guidance Computer

If it is assumed that all of the approach-guidance computations are performed by a computer contained within the spacecraft, then the *Mariner B* CC&S equipment must have considerably more capability than the *Mariner A* CC&S. It can be shown, provided that linear perturbation equations describe the spacecraft dynamic characteristics sufficiently well over the control interval, that the components of each trajectory-correction velocity impulse can be computed by performing simple matrix operations upon the measured values of the perturbations. It is possible to coalesce all of the separate operations for determining the velocity-increment components into a very compact matrix equation. Once the components of the increment vector have been determined, the speed and turn commands to the speed control and spacecraft attitude control can be derived by additional multiplication and

UNCLASSIFIED

UNCLASSIFIED

Table 11. Estimated approach-guidance measurement errors vs error sources and types

Error sources and types	Bias 1-σ value	Drift 1-σ value	Related 1-σ value	Noise, 1-σ value (except as noted)
Sources				
Sensor null offsets				
Sun sensor				
Near Mars	0.15 millirad	0.005 millirad/2 days	NA	0.005 millirad
Near Earth	0.6 millirad	0.005 millirad/2 days	NA	0.01 millirad
Star sensor	0.3 millirad	0.01 millirad/2 days	NA	0.03 millirad
Planet sensor	0.3 millirad	0.01 millirad/2 days	About 3% of planet angular diameter; some correlation with planet lighting	0.03 millirad
Types				
Sensor linearity and scale-factor errors (apply if sensors are used off null)				
Sun sensor				
Near Mars	NA	NA	NA	0.15 millirad over ± 1 millirad range
Near Earth	NA	NA	NA	0.25 millirad over ± 1 millirad range
Star sensor				
Roll axis	NA	NA	NA	0.15 millirad over ± 1 millirad range
Cone axis (operates at null)	NA	NA	NA	NA
Planet sensor (operates at null)	NA	NA	NA	NA
Sensor-mounting and alignment errors (referenced to readout)	0.1 millirad	0	0.1 millirad Correlated with gear positions; NA for hard-mounted sensors	0.1 millirad NA for hard-mounted sensors
Servo-tracking errors	0.05 millirad	0.01 millirad/day	NA	0.1 millirad
Angle-readout granularity errors (assume 0.1-m bit size)	NA	NA	NA	0.05 millirad (max.) 0.03 millirad (1 σ approx.)
Gimbal-orthogonality errors	NA	NA	Not estimated; correlated with sensor cone angle; can be calibrated	NA

division by scalars, and by the extraction of square roots and of direct and inverse trigonometric functions.

For each maneuver, the computer inputs, or "measured values of the perturbations" consist of at least one set of perturbations in two angles and the range as discussed earlier in this Section.

The range measurement may be replaced by an estimate of range based on time of flight, as described in Section 4c (4d). The computer may be required to perform statistical operations on several measurements of the same quantity in order to obtain greater accuracy, as discussed in Section 4c (4e).

The use of the simple computer inputs mentioned above is based on the fact that it can be shown that two measurements of spacecraft position taken at sufficiently separated time instants, combined with a knowledge of the forcing applied during the interval between measurements, provide information that is equivalent to simultaneous measurements of both position and velocity at a particular instant. This amount of information is required for the purpose of making an estimate of the final values of the spacecraft position and velocity.

Although a detailed study of the requirements of the approach-guidance computer is just beginning, a good estimate of these requirements can be obtained from Sections 4c and 4e. An important item that has not yet been considered here (except by implication in Eq. 60) is an investigation of what improvement in accuracy can be obtained by including ground-based radio data or esti-

UNCLASSIFIED

UNCLASSIFIED

Table 12. Example of Sun–probe–planet angle measurement errors

	Bias millirad	Drift millirad	Related millirad	Random millirad
Sun sensor	±0.15	—	—	0.005
Planet sensor	±0.3	—	0.21	0.03
Sensor mounting (Sun)	±0.1	—	—	—
Sensor mounting (planet)	±0.1	—	0.1	0.1
Servo tracking (Sun)	±0.05	—	—	0.1
Servo tracking (planet)	±0.05	—	—	0.1
Angle readout	—	—	—	0.03
Maximum	0.85		0.36	0.365
R.S.S.	0.37		0.23	0.18

mates based on such data as inputs to the approach-guidance computer.

At the present time, it appears that the approach guidance of the *Mariner B* spacecraft can be accomplished with only position measurements operated upon by a relatively simple digital computer capable of addition, subtraction, multiplication, division, and the extraction of square roots and of direct and inverse trigonometric functions.

(2) Approach-Guidance Computer Location and Information Flow

The need for a (digital) computer to perform approach-guidance functions has been indicated. However, it is not clear whether that computer need be carried into space by the spacecraft, or whether it may remain on the Earth, receiving measurement inputs and issuing commands through the spacecraft–to–Earth and Earth–to–spacecraft radio links of the DSIF and the associated terrestrial communications channels and input–output equipment. Similar questions apply to the other process-control functions. The factors affecting the *Mariner B* approach-guidance computer location and the concomitant communication-channel requirements are listed here. (In this Section, the "communication channels" are defined as all of those elements not specifically a part of the guidance measurement instruments or the approach-guidance computation device, thus including spacecraft command-decoding equipment, ground telephone lines, etc.)

The factors affecting the computer location have been divided into technical, operational, future-growth, and (for completeness) program-planning factors. A quantitative evaluation of the various factors is currently in progress.

(a) Technical factors

1. What are the gains or losses in accuracy and in reliability associated with various levels of approach-guidance refinement? Examples of these "levels of refinement" include:
   - *a.* Basic guidance computations for final-value control of the translational motion of the spacecraft.
   - *b.* Additional computations for improving the accuracy of the guidance-loop operation; e.g., statistical weighting of several measurements of spacecraft motion.
   - *c.* Ancillary computations; e.g., correlation of several messages of the same data to improve the reliability of message transmission and utilization.
2. What minimum level of refinement is required for each location of the computer? (For example, the location of the computer on the Earth coupled with noisy communication channels might require certain ancillary computations, although this does not currently appear to be the case.)
3. What computing operations, subroutines, and memory are required for each level of refinement of the guidance computations?
4. How much time is available for the processing of information between performing guidance measurements and executing a forcing maneuver?
5. How much input and command data, from what sources, must be handled for each maneuver; and how many maneuvers are to be made?
6. What are the capabilities of the communication channels from spacecraft to Earth and Earth to spacecraft, in terms of
   - *a.* electrical and nonelectrical transit time between the spacecraft and a computer located on the earth?
   - *b.* the rate of transmitting information?
   - *c.* the accuracy of transmitting messages, either singly or multiply, to be processed at the receiving location for improvement in the

UNCLASSIFIED

UNCLASSIFIED

reliability of transmission? Two types of messages should be considered: those that transmit quantitative data and those that initiate time references at one location based on information from the other.

7. What are the weight, volume, and power requirements of spacecraft-contained computing equipment?

(b) Operational factors

1. With what other data must the approach-guidance computing and control operations share the communication channels; and are sufficient time and bandwidth available for the competing requirements?
2. What are the probabilities that communication-channel outages, either short-term (less than 1 to 2 hr) or long-term (2 hr or more), will affect the ability of the approach-guidance loop to perform its tasks; and how are these probabilities affected by the location either at DSIF sites or centrally, of Earth-based guidance computers?
3. What is the estimated reliability of the computer in each Earth or spacecraft location considered; and how do the various types of transient errors and outages affect the ability of the approach-guidance loop to perform its task?
4. What are the requirements for modifying either the form or the parameters of the guidance equations after launch as a result of post-launch information on the trajectory and performance of the spacecraft subsystems; and how easily may changes be accomplished for each computer location?
5. What are the effects of guidance-computer location upon the spacecraft process-control elements?

(c) Future-growth factors

1. What are the future needs of the spacecraft for self-contained guidance and computation?
2. What are the long-term effects upon spacecraft guidance and spacecraft computer technology of expending the time and effort needed to deliver a spacecraft-contained approach-guidance computer on the *Mariner B* schedule as balanced against a longer-term advance-development program before operational flight is required?
3. Could the computer, or the basic computer design, be easily adapted to other of the self-contained computation requirements either for guidance or for other purposes?

(d) Program-planning factors

1. What degree of approach-guidance accuracy and reliability is required for the *Mariner B* missions? What degree is desired?
2. How would these factors be affected by the deletion of the split capsule from the mission?
3. What is the relative importance of the split capsule and of long-term spacecraft engineering development?
4. How much time, money, and manpower are required, and how much is available, for the approach-guidance analysis, computer design and programming, computer development, training of ground operators, developments and changes in the space and terrestrial portions of the communications channels and in the DSIF?

(3) Control and Sequencing

The CC&S is a subsystem that provides services to many portions of the spacecraft, and its design cannot proceed without relatively detailed and firm inputs from all the subsystems expecting to use the CC&S services. This requirement sometimes leads to a duplicative trend of constructing several similar CC&S-like units internal to the various subsystems, on the grounds that the individual designers feel that they cannot define their requirements sufficiently early to meet the CC&S design schedule. The degree of centralization most conducive to the success of the over-all spacecraft system is a separate, serious question that requires considerable thought and study of both philosophical and detailed practical factors. It should be pointed out that, although the concern here is primarily with control and sequencing functions, the question of the degree of centralization of the CC&S also involves many computer-like items, such as (1) the processing of scientific data and (2) the use of digital techniques within various servo-control loops for making logical decisions and for stabilization, although these latter items are not discussed here. The following discussion is based on the presumption that some degree of centralization has been deemed beneficial to the space-

UNCLASSIFIED

UNCLASSIFIED

craft system design. For the design of the spacecraft to proceed smoothly, the degree of centralization of the computing and process-control services that will most enhance the chances of success for the *Mariner B* program must be chosen early in the preliminary design.

(a) Relative degrees of dependence upon Earth-based and spacecraft-contained process control

The entire family of computing and process-control operations can either be based upon the Earth or in the spacecraft. The concepts of completely Earth-commanded or self-contained spacecraft, and several combinations of them, have been proposed and investigated for different types of missions. The technical factors affecting the location of the approach-guidance computer have been discussed in Section 4f (2). This discussion indicates a basis for the generalization of the question to the remainder of the process-control field.

For the *Mariner A*, the course of action adopted included both a realization that significant improvements in performance could be obtained by providing some degree of Earth-based control, and a desire to make the spacecraft as independent of requirements for Earth-based control as possible in the performance of its mission under nominal conditions. Usually, for process control requiring decisions, the decision-making process should be located at the source (i.e., on the ground or in the spacecraft) of the major portion of the decision information in order to yield the least complex system. The entire question of Earth-based vs spacecraft-contained process control will be re-examined for the *Mariner B*.

(b) Process-control requirements and capabilities

A comprehensive investigation of the process-control requirements for the *Mariner B* spacecraft has not yet been initiated, but preliminary indications are that the capabilities developed for *Mariner A* will meet most of the needs, although larger numbers of operations are probably required. The capabilities include:

1. Phased cyclic timing signals and pulse trains for the control of (interrelated) repetitive operations
2. Timed and other quantitative commands that can be specified and preset before launch, such as the times of actuation for pyrotechnic devices to unfold assemblies stowed in a position compatible with shroud constraints and incompatible with flight operations (e.g., solar-cell panels)
3. Timed and other quantitative commands that must be set, reset, or corrected after launch through the RF communication links, such as the speed of the midcourse-velocity increment
4. Computation of velocity increments added by rocket thrust to determine the time for motor shutoff

A capability not developed for the *Mariner A*, which has been shown to be desirable by later *Mariner A* design experience, is the ability to issue commands to certain subsystems based upon the state of conditions external to the spacecraft or existing in other subsystems. Two examples are provided by the switching of power to subsystems that need not operate until normal attitude acquisition has been established, and by the switching of communications RF power between a nearly omnidirectional antenna prior to acquisition and the directional antenna after acquisition. In the former case, the spacecraft must operate on batteries until lock on the Sun is established for the collection of solar power. The batteries can be made lighter, or alternatively, more reserve can be provided with the same weight, if the subsystems that need not operate until solar acquisition has been established are energized by a command generated when the attitude-control subsystem indicates that such a state exists. For the communications example, it is desirable, before lock on the Earth is established, to radiate through the omnidirectional system to provide telemetry of the acquisition operations and to ensure the collection of tracking data, during the early hours of flight, that are crucial to orbit-determination accuracy. The best indication of antenna tracking, however, is the reception of a signal transmitted through the directional antenna; hence, a useful command is one automatically transferring RF output radiation from the omnidirectional antenna to the directional antenna (for at least a nominal period) upon receipt of a signal from the attitude control that indicates Earth lock.

In the design of the CC&S for the *Mariner A*, the timed commands for performing certain related operations, such as the sequence of operations at planetary encounter, are arranged in special subsequences that can be initiated either by the master timing sequence of the CC&S that is started at launch and contains the correct time for initiation under nominal conditions, or by a radio command from the Earth. Furthermore, if it is necessary that an action occur at a particular time that is most easily recognizable on the Earth, some way of establishing a time reference in the spacecraft is necessary. Past experience with the RF command-system design has indicated that it is undesirable to depend on a single opportunity for the transmission of an irrevocable start command at the precise instant when the time reference is to be estab-

UNCLASSIFIED

lished. Consequently, the capability has been developed to initiate a count-down to the starting of the subsequence at the critical reference time. By making the length of the count-down adjustable by radio command, several opportunities for attempts to transmit the subsequence start command may be obtained if the length of the count-down transmitted at each attempt is made equal to the time remaining between the particular command-transmission attempt and the desired reference time of initiating the subsequence.

g. Performance-Evaluation Problems and the Use of the 1963 Test Flight

Evaluation of the performance of the approach-guidance loop presents some problems that have not been previously encountered in the design of lunar and planetary spacecraft. Proper evaluation of guidance-loop performance usually requires that there be an independent evaluation of the trajectory with instruments that are not used in the guidance and are sufficiently accurate to detect any guidance errors. This consideration usually acts, together with cost and weight, to rule out instruments carried aboard the spacecraft. With spacecraft operating as satellites or in the near vicinity of the Earth, such as lunar probes, radio tracking can be used to evaluate the trajectory performance, and hence the guidance-subsystem performance, independently.

Such techniques are not fruitful in evaluating the performance of the approach-guidance loop in the vicinity of the destination planet, because the accuracies that would be required of the Earth-based radio-tracking instruments are considerably beyond current estimates of feasibility. Indeed, if more accurate radio-tracking instruments were available, they would probably be used to improve the accuracy of the approach maneuvers.

Another method of trajectory evaluation that may be considered is the use of angle and angular-diameter data derived from the PHP to assist in determining the orbit. Even if this is feasible (and there are doubts concerning accuracy), only half the story is told, because no indication of the trajectory which would have resulted if there had been no maneuver is available. Consequently, the only indication that the correct guidance computations have been performed is the passage of the spacecraft through a region predicted by the guidance computations. If there are errors, the sources are unidentifiable among the sensing instruments, computing equipment, the equations used, and the parameters supplied to the computer.

A technique that will provide an indication of the location of the error sources is the use of the scheduled 1963 test flight with trajectories that permit the performance of guidance experiments related to the Earth as a destination planet. Then, the trajectory may be independently evaluated by the radio-tracking facilities of the DSIF, and the telemetered measurements and the results of guidance computations may be compared with values derived from Earth-based radio-tracking data.

Furthermore, the radio-tracking facilities of the DSIF can be used for a preliminary evaluation of the proper functioning of the guidance instruments on the flight that is directed toward the destination planet. This may be done by performing sets of observations on the Earth as the spacecraft is outward-bound for the destination planet, and making dry-run calculations on these observations to determine the velocity vector required for "correction" of trajectory errors. Such an evaluation experiment requires that the configuration of the spacecraft permit the necessary guidance observations, either in the normal spacecraft attitude or in a commanded-turn attitude. Likewise, the computer may require an extra set of coefficients, although computation with an already existing set of coefficients and the Earth-directed observations may possibly be used.

If a stellar reference object is used for the attitude-control system, and if the attitude-control and guidance measurement instruments are integrated, accurate telemetry of the Sun–star angle can be compared against the values that should prevail for the actual trajectory as determined by Earth-based radio tracking and orbit determination. It is also conceivable, though less likely, that if a sufficiently bright object is present in the proper geometric location, the planet sensor could be periodically exercised.

Finally, if the geometric conditions permit, post-maneuver observations by the guidance instruments themselves, as the spacecraft is outward-bound from the destination planet after encounter, can be used to gain a partial evaluation of the system performance. These measurements will be particularly useful if the measurements of star- (and, if possible, planet-) sensor angles can be made during the long cruising phase of flight and combined with the near-Earth measurements to permit determination of sensor errors and error shifts that occur as time passes.

Considerable further analysis of the flight performance-evaluation problems associated with the approach-guidance loop is required to make the best use of the

information that can be obtained during the test and the planet-bound flights of the *Mariner B* spacecraft in evaluating the performance of the approach-guidance loop, which is the major addition to the guidance-and-control capability of planetary spacecraft resulting from the *Mariner B* spacecraft program.

5. Communications

D. O. MUHLEMAN

(This Section is UNCLASSIFIED)

a. Introduction

Because of the nature of the *Mariner B* split-capsule mission, a unique communication system is required. One of the primary purposes of the split-capsule concept is to transmit scientific and engineering data concerning the atmosphere and surface of a planet, with a package of minimal weight and complexity. Thus, high-power transmitting equipment, large high-gain antennas, attitude-control mechanisms, etc., are left on the parent spacecraft which serves as a relay station for the data. Such a procedure appears feasible, whereas it does not appear possible for the entire spacecraft to enter into the planetary atmosphere. The successful development of the communication relay system, however, requires several new developments, particularly in the area of reliable automatic signal acquisition.

The basic concept of the relay communication system presented in this study involves the use of a phase-coherent one-way narrowband communication link from the capsule to the spacecraft, where an automatic phase-tracking loop is utilized to remove the doppler shift caused by the relative motion of the capsule and the spacecraft. This communication link will be "locked" before the capsule has been separated from the spacecraft and is so designed that it will remain in lock for the major portion of the mission. A procedure for reacquisition of phase lock is discussed in Section IIIC-4, but the problem should be recognized as a serious one. The relay link is completed with a two-way communication system between the spacecraft and the JPL Deep Space Instrumentation Facility (DSIF).

The communication system presented here is a strong function of the schedule for the *Mariner B*. It has been assumed that flight-equipment development must be complete by late 1962 and that the DSIF will have the capability planned for 1964. In particular, it has been assumed that the three primary 85-ft antenna systems will be operational at 2295 mc.

b. System Characteristics

(1) Spacecraft-to-Earth Link

A binary-phase-coherent pulse code-modulation system has been assumed for this portion of the communication link. The performance characteristics of such a system have been demonstrated and found to be highly satisfactory for purposes of data transmission. Better systems may be possible but have not yet been experimentally demonstrated, and will not be considered here. The system functions by phase-modulating a subcarrier $\pm\pi/2$ rad with binary-coded information.* The detailed characteristics for the spacecraft-to-Earth link are presented in Table 13.

It can be seen from the Table that the resulting data rate available is 86 bits/sec, with the probability of 10^{-3} of an error in any one bit. The portion of the power required to track the carrier was computed by requiring that the phase error in the tracking loop not exceed 1 rad more than 4 σ of the time. This is a stringent requirement but seems consistent with the required data accuracy. (No data are transmitted when this loop is out of lock.) The 10-cps bandwidth in the tracking loop is required to track the 2-m/sec^2 final maneuver of the spacecraft at Mars, where the system is near threshold. The synchronization-loop power was computed by also requiring a 4-σ lock. It was assumed that the polarization of the transmitted and received signals was matched, and no loss was assumed for polarization mismatch. An additional 2-db loss was assumed for the modulation process over and above the 1.1-db loss for transmitting the carrier and synchronizing subcarriers. If the modulation loss could not be handled in the system pad, the data rate would be reduced to 86 bits/sec, with an error rate of 10^{-3}.

*The detailed analytical aspects of the system, along with the other analytical procedures used here, are presented in "The Communication Problem Associated With a Space Vehicle Split Into Two Vehicles in the Vicinity of Mars," by D. O. Muhleman, Jet Propulsion Laboratory, Pasadena, Calif. (to be published).

UNCLASSIFIED

Table 13. Spacecraft-to-Earth link (at Mars)

Operating frequency	2295 mc ($\lambda = 0.13$ m)
Communication distance (maximum)	222×10^6 km (−267 db)
Total power radiated	25 w (44 dbm)
Over-all system temperature	80°K
Antenna gain, 4-ft parabola	26 db (assumes a 1-deg pointing error)
Antenna gain, 85-ft ground antenna	53.2 db
System pad	7 db
Tracking loop	
Power	5 watts (37 dbm)
$2B_{L_0}$ (bandwidth)	10 cps
Synchronization loop	
Power	0.5 w (27 dbm)
$2B_{L_0}$ (bandwidth)	1 cps
Data communication	
Power	19.5 w (42.9 dbm)
Modulation loss	2 db
Bit error probability	1 part in 10^3
Bit rate	86 bits/sec
Time to dump 2×10^7 bits	2.73 days

The data rates reported above are those available in the vicinity of Mars, and consequently much higher rates will be available during transit and at midcourse correction. Thus, it will be possible to transmit a considerable amount of engineering information during transit, but the system of necessity will be able to handle capsule data and other scientific information only after the final approach maneuver. It has been assumed that the power reported in Table 13 will be available continuously from injection to 10 days after encounter.

(2) Earth-to-Spacecraft Link (Command System)

It is reasonable to consider two fundamentally different Earth-to-spacecraft command links, one utilizing the high-gain antenna on the spacecraft and the other the omnidirectional antenna. The omnidirectional antenna has the virtue of being able to receive a signal in the event of a loss of attitude control and might possibly be helpful in regaining control and re-direction of the high-gain-antenna system. However, in the vicinity of Mars the signal-to-noise ratio in the bandwidth of the receiver is extremely low with the omnidirectional antenna. Therefore, it seems reasonable to assume that the high-gain-antenna system would be utilized for the primary command functions and that a backup omni system would be available for emergencies.

The system characteristics for the Earth-to-spacecraft link are presented in Table 14. A phase-shift keyed pulse code-modulation system similar to that used in the spacecraft-to-Earth link was assumed for these calculations. It should be noted that figures are presented for both the omni and the high-gain system. The computations for the high-gain system assumed an error probability per bit of 10^{-7} and a corresponding figure for the tracking and synchronization loops, whereas the computations for the omni system assume an error rate of 10^{-4} per bit with corresponding figures for the tracking and synchronization loops. Both systems yield a sufficient bit rate, but an error rate for "commands" of 10^{-4} is poor. The high-gain system has a tremendous bit rate (2.2×10^4 bits/sec) with a low error rate. In practice, such a high bit rate could probably not be utilized because of decoding problems. Therefore, the bit rate would be reduced to well under 10^3 bits/sec and the error probability correspondingly improved.

Table 14. Earth-to-spacecraft link (at Mars)

Operating frequency	2115 mc ($\lambda = 0.14$ m)
Communication distance	222×10^6 km (−267 db)
Total power radiated	100 kw (80 dbm)
Over-all receiver temperature	2000°K
Antenna gain, 4-ft parabola	26 db
Antenna gain, 85-ft antennas (3)	53 db
System pad	7 db
Tracking loop	
Power	1.6 kw (60 dbm)
$2B_{L_0}$ (bandwidth)	20 cps
Synchronization loop	
Power	6 w (37.8 dbm)
$2B_{L_0}$ (bandwidth)	2 cps
Data communication	
Power	60.4 kw (77.7 dbm)
Bit error rate	1 part in 10^7
Bit rate	1.1×10^4 bits/sec
Modulation loss	38 kw (75.8 dbm)
Tracking loop (omnidirectional system)	
Power	89.5 kw (79.5 dbm)
$2B_{L_0}$ (bandwidth)	20 cps
Synchronization loop (omnidirectional system)	
Power	9.0 kw (62.4 dbm)
$2B_{L_0}$ (bandwidth)	2 cps
Data communication (omnidirectional system)	
Power	1.5 kw (61.8 dbm)
Bit error probability	1 part in 10^4
Bit rate	1 bit/sec

UNCLASSIFIED

It can be seen that very accurate commands can be processed for the *Mariner B*. For purposes of illustration, a typical "message" is defined:

3 angles with 5 decimal digits =	15 characters
1 velocity with 6 decimal digits =	6 characters
1 "distance," 6 decimal digits =	6 characters
4 spaces =	4 characters
Total	31 characters

Such a message requires N bits:

$$N = 4 + \log_2 10^{27}$$

$$N = 94 \text{ bits}$$

If the probability of one bit being wrong is denoted by P_e, then the probability of one of these messages being detected without error is given by

$$P_s = \text{success probability} = (1 - P_e)^{94}$$

$$P_s = (1 - 10^{-7})^{94} = (1 - 94 \times 10^{-7})$$

$$P_s = 0.99999$$

and the probability of a message failure is one part in 10^5. Therefore, highly accurate commands can be reliably transmitted to the *Mariner B* spacecraft. This is a significant factor in considering the question of whether guidance-and-control computations should be done primarily on the Earth or with a special-purpose digital computer in the vehicle. This problem is discussed in more detail in Section III B-4.

Finally, Table 15 gives a weight summary for the spacecraft portion of the communication system.

Table 15. Spacecraft communication-system weights

Spacecraft components	Weight, lb
4-ft antenna	12
2300-mc transponder and ranging equipment	51
Telemetry encoder	29
Omnicommand antenna	2
Command decoder	14
Capsule RF receiver and demodulator	5
Backup low-power 2300-mc transmitter, antenna, and 1-w power supply	4
Total	117

6. Power

T. W. KOERNER

(This Section is UNCLASSIFIED)

a. Introduction

The function of the power system is to supply secondary power to the spacecraft and capsule for a period extending from shortly before launch to a maximum of about 10 days after closest approach to the planet. The duration of this mission is expected to be approximately 240 days. The flight sequence will include a launch and acquisition phase, a cruise period, a midcourse maneuver, a second and much longer cruise period, two approach maneuvers separated by a cruise period, a miss maneuver followed by a cruise period, and a planet-encounter phase followed by a final cruise period. Since the power system for *Mariner B* will probably be operated with solar energy, the duration and spacing of the various maneuvers during which solar energy is assumed to be unavailable, as well as the power levels required during all phases of flight, are significant to the definition of the power system. (See Fig. 38 for a schedule of operations.)

b. Power Requirements

A tabulation of the estimated regulated and raw-power requirements of each of the loads during each of the major phases of the spacecraft flight is given in Table 16. The few raw-power requirements indicated in the Table are shown following the slash marks. In several instances there are loads which have a peak raw-power demand of several watts and an average power consumption of a small fraction of a watt; these have been deleted from the Table. Included in the Table are several loads requiring regulated power on a low-duty cycle; these loads are

UNCLASSIFIED

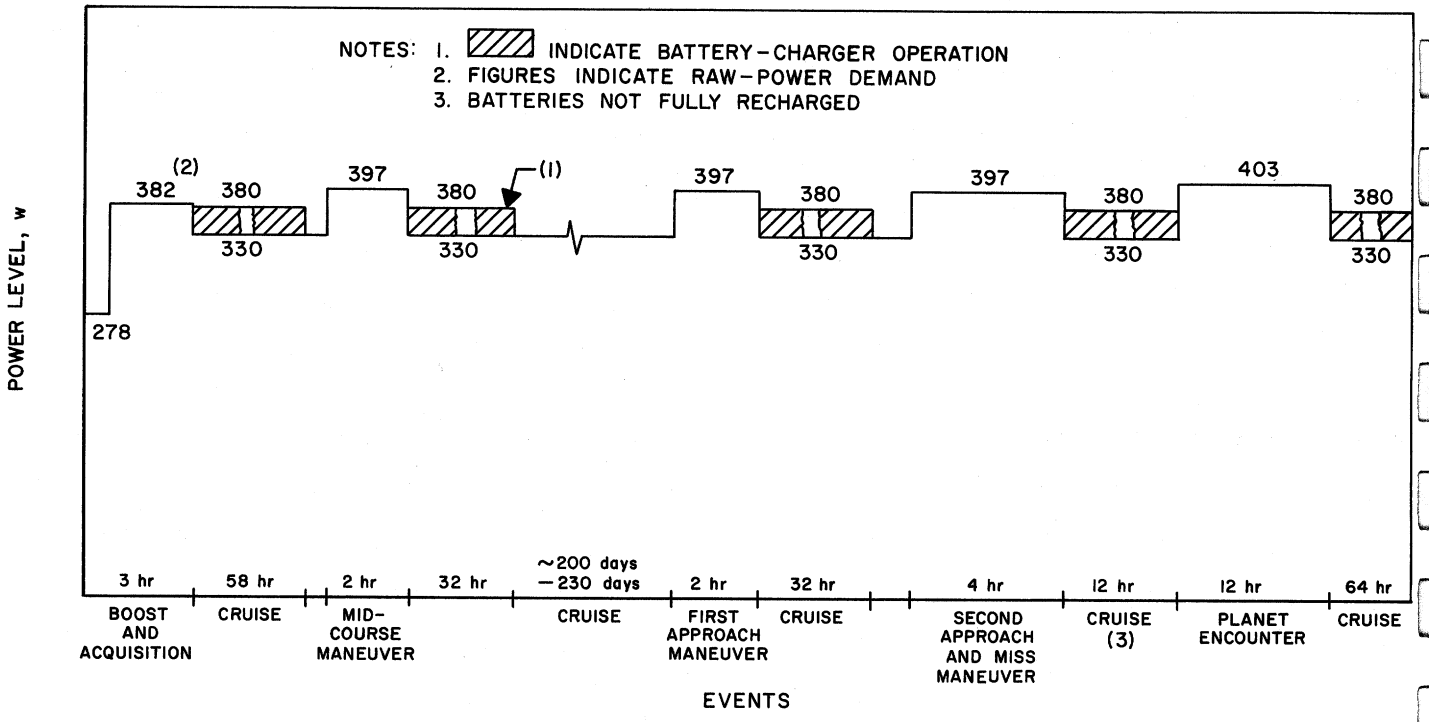

Figure 38. Schedule of operations, spacecraft power system

indicated by an asterisk. Energy consumption of these loads is considered negligible; however, the peak power consumption is important from the standpoint of inverter and transformer–rectifier sizing.

Assuming an over-all conversion efficiency of 60% from raw electric power to regulated power, the raw-power requirements for the launch and acquisition phases of the trajectory are 278 and 370 w, respectively. The com-

Table 16. Regulated and raw-power requirements

Spacecraft parts	Load, w					
	Launch	Acquisition	Maneuver	Cruise	Planet encounter	Transformer–rectifier sizing
Command system	5	5	5	5	5	5
Data encoder	15	15	15	15	15	15
Transmitter	100	100	100	100	100	100
Sequencer	25	25	25	25	25	25
Computer[a]				100[a]		100
Planet scanner[a]				8[a]		8
Antenna drives		3	3	3	3	3
Attitude control	22	36/12	50/4	15	15/5	50
Star tracker		10	10	10	10	10
Inertial sphere		10	10	10	10	10
Momentum dump[a]				20[a]	20[a]	20
Horizon scanner					10	10
Horizontal platform		3	3		3/5	3
Science experiments		15	15	15	25	25
Data-automation system					15	15
Total	167	222/12	236/4	198	236/10	379

[a]Intermittent loads.

UNCLASSIFIED

UNCLASSIFIED

bined duration of these modes of operation is estimated to be a maximum of about 3 hr. During this period the spacecraft will not be oriented to the Sun, and the electrical loads must be supplied from energy-storage equipment within the spacecraft.

Upon completion of the acquisition maneuver, the spacecraft is properly oriented and the power system may supply the needs of the spacecraft from solar-energy conversion. The raw-power demand for the operation of the spacecraft in this mode of flight is estimated to be 330 w. An additional 50 w of raw power has been allocated to recharging the energy-storage system, bringing the total raw power required during cruise to 380 w. Assuming a charge–discharge cycle efficiency of 50% for the energy-storage system, the maximum energy drain of about 1450 whr during this phase would require a maximum recharge time of approximately 58 hr. It is not necessary that the energy-storage system be fully recharged prior to beginning the midcourse maneuver; however, sufficient energy must be replaced so that this phase of operation does not completely discharge the storage system.

The midcourse maneuver is designed to remove the majority of the trajectory errors which have accumulated from the time of launching. During most of this period, the spacecraft will be rotating, causing the solar-energy-conversion system to cease functioning and requiring the energy-storage system to supply the needs of the spacecraft. Raw-power requirements are estimated to be 397 w during this phase of operation, which is expected to have a maximum duration of 2 hr. Energy consumption during this period will be 794 whr, based upon the preceding estimates.

The cruise period following the midcourse maneuver will be by far the longest phase of the flight; it is estimated that the maximum duration of this phase will be about 230 days. Power level during this period is estimated to be 380 w until the energy-storage system has been recharged, after which the power required will drop to 330 w. Recharge time is expected to be about 32 hr, provided that the midcourse maneuver is initiated with a fully charged storage system. If the midcourse maneuver occurs prior to the time required for complete recharge, more than 32 hr will be needed after the maneuver in order to restore full charge to the storage system.

Two approach maneuvers are contemplated for the *Mariner B* in order to reduce flight-path errors with a minimum of propulsive effort. It is expected that the first of these maneuvers will be initiated 83.5 hr prior to closest approach to Mars. The maximum duration of this maneuver is estimated to be 2 hr; the power level will be 397 w. The drain upon the energy-storage system will be 794 whr.

The cruise period following the first approach maneuver will permit complete recharging of the energy-storage system. Power required during this period will be about 380 w until the energy-storage system has been recharged; this will occur about 32 hr after the completion of the maneuver.

The second approach maneuver will begin about 22 hr before the closest approach to Mars. Duration of the maneuver and power requirements during the maneuver are assumed to be the same as those of the previous approach maneuver, namely, 2 hr and 397 w, respectively; energy drain is therefore 794 whr, as before.

Immediately following the second approach maneuver, the capsule is released and the spacecraft performs a final maneuver intended to cause it to avoid impact upon Mars. This maneuver is also assumed to be 2 hr in duration and to require 397 w of power, resulting in an additional 794 whr drain upon the energy-storage system. These two 2-hr consecutive maneuvers and their total energy consumption of 1588 whr of energy determine the minimum capacity of the energy-storage system for the spacecraft.

The completion of the miss maneuver approximately 18 hr prior to closest approach permits the spacecraft to resume its solar orientation and re-establishes the cruise mode of operation. The power requirement is once again 380 w, including 50 w for recharging the energy-storage system. This mode of operation continues until about 6 hr before closest approach, by which time approximately 300 whr of energy have been restored to the energy-storage system.

At this time, the power requirements are expected to increase to 403 w in order to supply the additional equipment being operated in the vicinity of Mars. The recharger is turned off, and the full 380-w capability of the power source is then available to supply the loads. The energy-storage system is required to supply the difference between the 403-w demand and the 380-w power-source capability, which it can do for about 12 hr. About 6 hr after closest approach, the energy-storage system once more has reached the limit of its capability, and the cruise mode is resumed.

A modified cruise mode could be used at this point if it were desirable to have somewhat greater power than 330 w to operate the system. This could be accomplished

UNCLASSIFIED

UNCLASSIFIED

by reducing, or possibly eliminating, the recharge power, making available up to 50 additional watts. Operation in this mode could continue for 10 days or more, if necessary, in order to permit transmission of data back to Earth.

c. Power Sources

(1) Solar Panels

Several power-system configurations have been investigated for possible application to the *Mariner B* spacecraft. The first and most conservative approach is the use of silicon photovoltaic cells, a silver–zinc battery, and a set of inverters, transformer–rectifiers, and regulators. This system is essentially an extension of the *Mariner A* power system, scaled to meet the additional power requirements and the lower solar-flux levels for *Mariner B*.

The solar panels are designed for a power level at the maximum-power point of 410 w, 30 w greater than the expected cruise demand. The 30-w pad is used to avoid operation at the maximum-power point. The 410-w design is based upon the solar-flux level at the Mars aphelion, a design which is somewhat pessimistic in view of the fact that the planetary encounter most distant from the Sun is expected to have a solar-flux level approximately 7% greater than that at the aphelion. In addition, a 20% increase has been included in the sizing of the panels in order to account for degradation of the solar cells due to ultraviolet radiation and micrometeorite and proton bombardment.

The solar-panel area required to supply the above power level is estimated to be 164 ft^2. Assuming that a modest development program can maintain the present solar-panel "density" at 2 lb/ft^2, the weight of these solar panels would be 328 lb. It is estimated that approximately six months would be required to develop a lightweight structure which could match the *Mariner A* solar-panel "density" in spite of a fourfold increase in area.

The power capability of the solar panels is a function of the solar-flux level and the temperature of the panels, which, in turn, is related to the incident solar flux. As the spacecraft proceeds along its trajectory from Earth to Mars, the changing solar flux will cause the power capability of the panels to decrease from an initial value of about 1160 w, assuming zero initial degradation, to the 410-w level indicated previously. The increasing percentage load on the solar panels as the flight progresses causes the panel voltage to decrease slowly with time; this effect is partially offset by the decreasing temperature of the panels, which tends to cause a rise in voltage. It is expected that the total variation of solar-panel voltage during the flight will not exceed 20%, which will aid in minimizing the losses in the regulators.

The excess power available during the first portion of the flight could be used to increase the charging rate of the battery, shortening the charging time. This would require additional capacity of the battery charger, which would increase its size and weight. A small loss of efficiency would then occur near the end of the flight because of the operation of the charger at a fraction of its capacity.

A silver–zinc battery appears to be most suitable for use in the *Mariner B* because of its relatively high capacity per unit weight. The number and depth of discharges are such that it does not appear necessary to use a relatively heavy nickel–cadmium battery, which has considerably better life under repeated cycling. The estimated battery-charge status vs time is indicated in Fig. 39. Battery capacity is estimated to be 1588 whr, based upon four consecutive hours of maneuvering at a 397-w power level. The battery performance characteristic has been conservatively assumed to be 27 whr of usable energy per pound, resulting in a battery weight of 59 lb. Typical performance figures for a silver–zinc battery in a single discharge are 60 to 80 whr/lb. The derating accounts for loss of battery capacity with repeated charging and discharging. The efficiency of the charge–discharge cycle has been assumed to be 50%, including both battery and charger losses.

The electrical-conversion system will be composed of a battery charger, boost regulator, static inverters, and transformer–rectifiers. Over-all conversion efficiency of the boost regulator, inverters, and transformer–rectifiers is assumed to be 60%.

The inverter capacity is determined by the peak regulated power drawn from the system at any time. The maximum occurs just prior to the approach maneuvers,

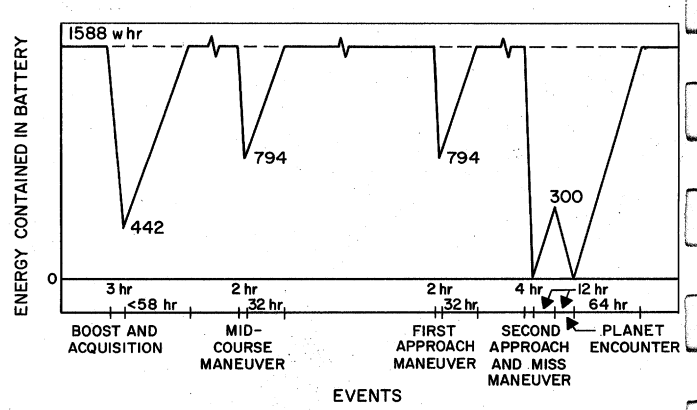

Figure 39. Battery-charge status

UNCLASSIFIED

at which time the computer is operating, drawing 100 w regulated power. It is assumed that momentum-dumping from the inertial sphere, which requires an additional 20 w regulated power, is coincident with the computer operation, bringing the peak regulated power to 318 w. Total weight of inverters, based upon a performance figure of 10 w regulated power per pound, is 32 lb.

The transformer–rectifier capacities are determined by their individual loads. The two large (100-w) units which power the computer and the transmitter are estimated to weigh 5 lb each. The remainder of the units, totaling 179 w of regulated output, are assumed to have an average performance figure of 10 w/lb of regulated output, resulting in a weight of 18 lb. Total weight of all transformer–rectifier units, which are assumed to be located within the package containing the load, is 28 lb.

The boost regulator, which must be capable of handling an input power of about 530 w, is estimated to weigh 13 lb. The battery charger, which accepts 50 w of power from the solar panels, is estimated to weigh 5 lb, bringing the total weight of the electrical-conversion system to 78 lb.

The total weight of solar panels, battery, and electrical-conversion system for the configuration described above is 465 lb. (See Table 17 for a tabulation of characteristics for this system.) A tentative solar-panel arrangement investigated is composed of eight panels, approximately 4×5 ft each. The eight panels are placed end to end in two groups of four panels each, the two groups being located on opposite sides of the spacecraft in a manner similar to an aircraft wing. The "wing span" of this arrangement is about 46 ft. Stowage of the panels within the *Centaur* shroud is accomplished by folding at the panel junctions. This arrangement has three serious disadvantages: the weights are excessive, a large number of joints and actuators are involved in extending and retracting the panels, and the extension of the panels approximately triples the spacecraft inertia in some axes and poses a severe attitude-control problem as a result of the low resonant frequency of the extended panels. Alternate configurations which distribute the panels about the periphery of the spacecraft and thus reduce angular inertias and "springiness" effects also interfere with the viewing angles of the transmitting antenna and the planetary horizontal platform.

(2) Solar Panels with Concentrators

In an attempt to reduce solar-panel weights, consideration was given to the use of lightweight reflectors for concentrating solar energy upon a reduced area of solar cells. Unfortunately, such a procedure also increases the projected area of the array because of reflection losses and operation of the solar cells at a higher temperature and, therefore, somewhat lower efficiency. It is estimated that the 410 w produced by 164 ft² of nonreflector solar panels could also be produced by 197 ft² of solar array using integral reflectors. Probably the lowest "density" that can be obtained with this technique is about 1 lb/ft², resulting in a solar array weighing 197 lb, or a saving of 131 lb over the nonreflector panels. A considerable development effort would be required to obtain a flight-worthy array of this weight; it is estimated that 12 to 18 months might be required. This arrangement would probably reduce the spacecraft inertias somewhat because of its lighter weight; however, the stowage and flexing problems would probably increase in severity.

Table 17. Spacecraft power-system characteristics

System	
Cruise power at Mars	330 w raw
	190 w regulated
Weight	465 lb
Maximum maneuver time	4 hr
Battery-recharge power	50 w raw
Charge–discharge efficiency	50%
Solar panels	
Area	164 ft²
Weight	328 lb
Maximum power capability at Mars	410 w
Maximum power at Earth	1160 w
Silver-zinc battery	
Capacity	1588 whr
Weight	59 lb
Performance coefficient	27 whr/lb
Electrical-conversion system	
Peak power input	530 w
Weight	78 lb
Efficiency	60%

(3) Solar-Thermionic System

Alternate configurations using solar concentrators in conjunction with thermionic diodes have also been investigated, with somewhat more promising results. The most attractive arrangement is a single 9.5-ft-diameter concentrator permanently affixed to the aft end of the spacecraft. The only deploying action required for this power system is the erection of the converter unit at the focal point. The total weight of the collector, converter, and erecting mechanism is estimated to lie between 75

UNCLASSIFIED

and 125 lb, compared to 197 and 328 lb for the solar arrays discussed previously. The frontal area of the concentrator is approximately 71 ft². The solar-thermionic systems require much closer control of the vehicle attitude relative to the Sun than do solar cells; it is estimated that the 9.5-ft concentrator would require an orientation accuracy of approximately 0.1 deg. The large concentrator would also require that multiple rocket motors be used for maneuvering because of the location of the converter unit on the roll axis of the spacecraft. This could be avoided by the use of several smaller collectors and converters.

A second solar-thermionic system investigated makes use of four fixed, 5-ft-diameter collectors sectioned in a manner similar to a four-leaf clover (see Fig. 40). Each segment has its own deployable converter unit. The weight of this system would probably be slightly higher than that using the single large concentrator because of the requirement for multiple converters and actuators. Also, the power output of this system would probably be slightly lower as a result of the somewhat poorer utilization of the available area. The absence of a converter unit on the spacecraft roll axis would permit a small segment to be removed from each of the central corners of the concentrators in order to accommodate a single rocket motor.

One of the greatest causes for concern regarding the use of a solar-thermionic system for *Mariner B* is the uncertainty in the time required to develop a flightworthy system. At the present time the plasma diode is just beginning to demonstrate useful lifetimes. The erection and stabilization of the converter unit at the focal point, the control of the vapor pressure in the plasma diode, and the inclusion of multiple diodes within the converter in order to obtain adequate voltage output are some of the problems which require additional development effort. Concentrator development is in a somewhat more advanced state. A 5-ft-diameter electroformed nickel concentrator of the requisite accuracy has already been demonstrated, although its weight was slightly excessive and the use of nickel might be incompatible with some of the scientific instruments because of its ferromagnetic properties. Development of larger concentrators will require considerably greater effort because of the necessity of fabricating a large master.

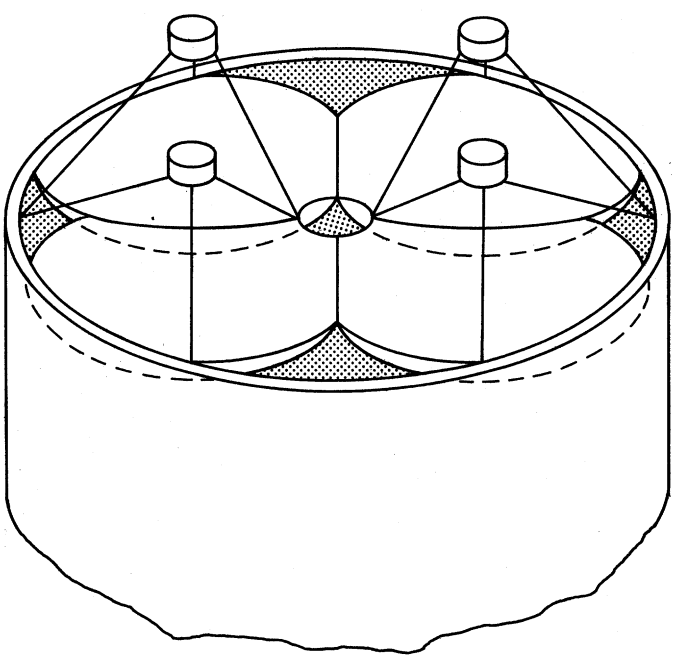

Figure 40. Segmented concentrator

At the present time a contract for the development of a solar-thermionic power source using 5-ft concentrators is being opened for bid. The schedule calls for delivery of a prototype unit with a power capability of about 130 w in 6 months and a second unit in 10 months. The results of this contract may be available in time to permit serious consideration of a solar-thermionic system for *Mariner B*.

(4) Nuclear Power Sources

Nuclear power sources offer several advantages over solar power sources for use in spacecraft. These are primarily the elimination of large solar-energy collectors and their associated attitude-control problems, the ability to operate independently of solar illumination, and the reduction in size, or elimination, of energy-storage equipment.

Consideration has been given to the use of a nuclear reactor as a power source for *Mariner B*. An extension of the *SNAP 10* configuration, which is a reactor-powered thermoelectric generator estimated to deliver 300 w and to weigh about 310 lb, appears to be most suitable. Linear scaling of this unit to a power level of 380 w would result in a power source weighing 393 lb without shielding. This weight is about equal to the combined weights of solar panels and battery in the first configuration considered; however, the shielding required would probably increase the weight of the reactor power system by at least 20%, making the reactor system considerably heavier than the heaviest solar-powered configuration considered.

A brief examination has been made of the feasibility of using a radioisotope thermoelectric-generator (RTG)

UNCLASSIFIED

power source for *Mariner B*. The analysis of a Curium 242-fueled, 100-w thermoelectric generator by the Martin Company has been used as a basis for estimating characteristics of a configuration for *Mariner B*. The Martin analysis indicated that a 100-w unit whose useful life was six months would weigh about 77 lb and contain about 62 g of isotope. This unit was at least partially optimized for power-to-weight ratio.

The power required is estimated to be about 380 electrical watts 280 days after encapsulation of the radioisotope. The 280-day period includes an allowance of 40 days from encapsulation to launching. Scaling the 100-w units in order to account for changes in power level and lifetime results in a system whose initial thermal power level is 33,800 w and which contains 277 g of isotope. This is about 4.5 times the level of the 100-w unit. Assuming that four generators slightly larger than the 100-w units are used, linear scaling of weight should not be greatly in error. The combined weight of the four units is estimated to be 345 lb.

One of the more difficult quantities to establish in estimating characteristics of nuclear systems is the amount of shielding required. It is assumed here that requirements are similar to those for the *Surveyor* spacecraft, in which shielding estimates were fairly consistent at about 1 lb of shield per gram of isotope. On this basis, shielding for *Mariner B* would weigh 277 lb.

The battery weights for the RTG system are considerably smaller than for the solar-powered systems discussed because of the capability of the RTG to operate independently of spacecraft attitude. For the 380-w RTG system, the battery capacity is estimated to be 276 whr, determined by the 403-w demand for 12 hr at planet encounter. Battery weight is approximately 11 lb.

The total weight of the RTG system, including the RTG source, shielding, battery, and electrical converters, is estimated to be 711 lb. Even if shielding estimates are too high by a factor of five, the RTG system cannot compare favorably on a weight basis with any of the solar-powered systems discussed previously.

7. Propulsion

R. R. BRESHEARS

(This Section is UNCLASSIFIED)

The midcourse-propulsion system will be utilized to provide trajectory-correcting impulses to the spacecraft for midcourse and terminal (approach) corrections and to separate the spacecraft from the landing capsule. After separation, the capsule will enter the Martian atmosphere. The spacecraft will fly by the planet at a distance of about 7500 km.

The *Mariner B* mission is unique because it is the first attempt at making a planetary-approach correction. Some experience in executing this maneuver will be gained in the 1962 *Mariner A* Venus mission. An advanced-development experiment will be performed by restarting this propulsion system shortly after planetary encounter. (No approach-correction guidance equipment will be aboard the spacecraft.) Most of the components to be used in this experiment have been designed for use in the *Mariner B* as well as the *Mariner A* midcourse-propulsion systems. Experience gained in the *Ranger* and *Mariner A* flight programs, combined with extensive environmental testing, should yield a nitrogen-pressurized monopropellant hydrazine propulsion system which is highly reliable and well suited for this mission.

The *Mariner B* system will be constructed in much the same way as its predecessors. It will use catalytic decomposition of hydrazine monopropellant, a single propellant tank, and one or more high-pressure nitrogen-storage spheres. The nitrogen-gas spheres will be isolated from the pressurization system with explosive valves during ground handling, launch, and through the long coast period between the midcourse and the approach corrections. The nitrogen supply has been sized assuming that all the gas has leaked from the propellant tank during the long coast period.

Figure 41 shows schematically two versions of the propulsion system which are being considered. The simpler

UNCLASSIFIED

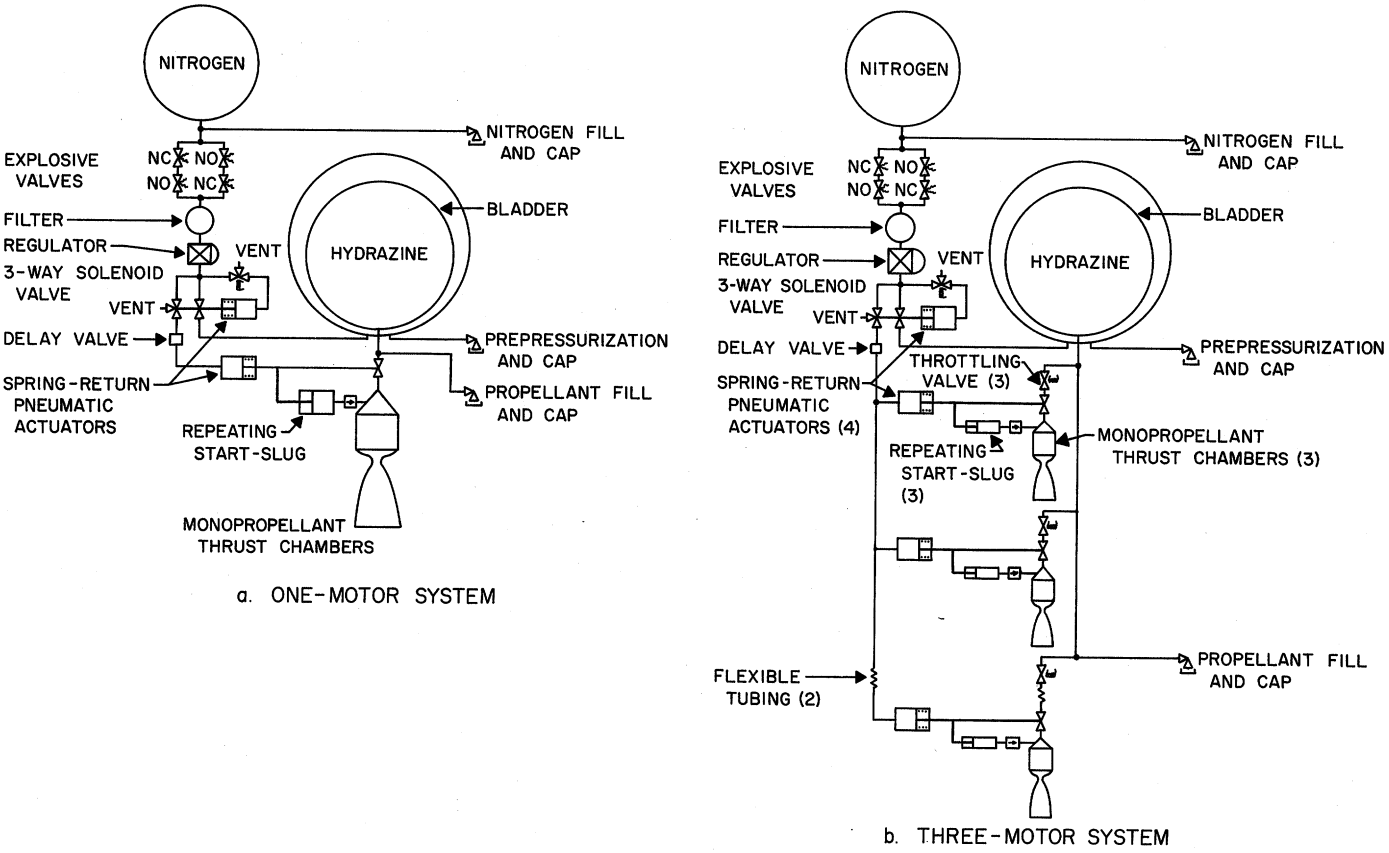

Figure 41. Midcourse and approach-correction propulsion system

of the two employs a single 200-lb-thrust monopropellant rocket motor mounted on the roll axis of the spacecraft. Using this configuration, the landing capsule must be mounted on the thrust axis. When the capsule is released, the spacecraft center of gravity will remain within the thrust-vector control capabilities of the midcourse-motor jet vanes. The alternate system uses three monopropellant rocket motors which are operated simultaneously and are differentially throttleable. This system can permit large center-of-gravity excursions and relieve the crowded centerline of the *Mariner B* spacecraft. However, this system is about 21 lb heavier and has a reliability estimated to be 2 to 7% lower than the one-motor configuration. Each motor would have its own propellant valve, throttling valve, and starting system. Roll control could be accomplished by using a jet vane or hinging one of the motors. This version would use essentially the same propellant-feed system as the one-motor system. The monopropellant thrust chambers presently being developed for *Mariner A* could be used for each of the throttleable motors in the three-motor system. These motors would be operated between their lowest operating chamber pressure (150 psia) consistent with good performance and an upper value of 245 psia, corresponding to 120 to 195 lb total thrust. This throttling range would permit approximately a $\pm$5-in. spacecraft center-of-gravity excursion as compared to the one-motor capability of approximately $\pm$0.5 in. using jet vanes. This value of $\pm$0.5 in. is comparable to that of the *Mariner A* spacecraft. The thrust would be controlled using a throttling valve placed upstream of the propellant valve and the injector. The fixed-area injector would have a minimum pressure drop of 100 psi (at minimum thrust) to insure good propellant atomization at all thrust levels.

Both of the systems will require temperature control within the limits of 35 to 165°F. This requirement is more severe for the three-motor version because of the relatively exposed propellant-feed lines connecting the tankage with the rocket motors.

Table 18 lists the assumptions upon which the requirements of the propulsion system are based. Of special note is the approach velocity, which is conservatively assumed to be 5.0 km/sec. For some of the possible trajectories the approach velocity is as low as 4.2 km/sec, which would result in a 16% propellant-mass saving for the

UNCLASSIFIED

UNCLASSIFIED

Table 18. Assumed mission parameters

Approach velocity	5.0 km/sec
Mass of spacecraft at injection	2100 lb
Mass of capsule	315 lb
Spacecraft fly-by periapsis	11,300 km
Angle between approach-velocity vector and miss-maneuver velocity-impulse vector	110 deg
Approach-guidance-system instrument accuracy (effective)	±2 millirad
Motor location	
One-motor system	Roll axis
Three-motor system	120 deg apart, 36 in. from roll axis

Table 19. Maneuver requirements

Maneuver	Required velocity impulse (2.5 σ) m/sec	Required propellant (monopropellant N_2H_4), lb	Approximate time after injection, days	Approximate distance from Mars km
Midcourse correction	60	55	4	
First approach correction	38.7	35	230	1,500,000
Second approach correction	38.7	35	233[a]	400,000
Miss maneuver	115	81	233[a]	382,000
		Total 206		

[a]Minimum time between restarts, 1 hr.

Table 20. Propulsion-system description

Propulsion-system characteristics	One-motor system	Three-motor system
Propellant	Monopropellant N_2H_4	Monopropellant N_2H_4
Pressurization gas	N_2	N_2
Specific impulse	232[a] lb sec/lb	236 lb sec/lb
Thrust	200 lb	120 to 195 lb (total)
Chamber pressure	200 psia	150 to 245 psia
Expansion ratio	75:1	75:1
Maximum number of starts	6 (only 4 are required)	6 (only 4 are required)
Minimum time between starts[b]	1 hr	1 hr
Chamber temperature	1800 to 1900°F	1800 to 1900°F
Minimum propulsion-system temperature	35°F	35°F
Maximum propulsion-system temperature	165°F	165°F
Propellant-tank outside diameter (sphere; not including flanges or brackets)	24 in.	24 in.
Nitrogen-tank outside diameter (sphere; not including flanges or brackets)	15 in.	16.5 in.
Motor length	17 in.	10.3 in.
Maximum motor diameter (nozzle exit)	8 in.	2.9 in.
Propulsion-system masses		
Propellant	206 lb	202 lb
Reserve and holdup propellant	5 lb	5 lb
Nitrogen gas	14 lb	19 lb
Propulsion-system hardware	80 lb	100 lb
Total propulsion system	305 lb	326 lb

Propulsion-system characteristics	One-motor system	Three-motor system
Power requirements[c]		
Midcourse	start ①, ② shutoff ①, ②	start ①, ② shutoff ①, ②
First approach correction	start ①, ② shutoff ①	start ①, ② shutoff ①
Second approach correction	start ① shutoff ①	start ① shutoff ①
Spacecraft deviation maneuver	start ① shutoff ①, ②	start ① shutoff ①, ②
Telemetering requirements, either system		
During coast periods		
Propellant-tank pressure		
Propellant temperature		
Propellant-tank temperature		
Nitrogen-tank pressure		
Nitrogen temperature		
During firings		
Propellant-tank pressure		
Nitrogen-tank pressure		
Thrust-chamber temperature		
Acceleration history		
Blip records for solenoid-valve and propellant-valve actuation		
Jet-vane deflection angles or throttling-valve positions		

[a]This performance assumes fully deflected jet vanes.
[b]Estimated time needed for motor to cool before it can be restarted.
[c]One start signal and one shutoff signal will be required from the central computer and sequencer.
① 0.5 to 2.5 amp at 18 to 28 v for 0.030 sec.
② 1.5 to 2.5 amp at 18 to 28 v for 0.005 sec.
These requirements do not include those for jet-vane or throttling-valve actuation or telemetering transducers.

UNCLASSIFIED

UNCLASSIFIED

approach corrections and the miss maneuver. Also contained in Table 18 is the optimum miss-maneuver angle of 110 deg with the approach-velocity vector. This angle optimizes the time for data-communication between the opening of the capsule's parachute and the eclipse of the spacecraft. By making the miss maneuver in the optimum direction and using a fly-by periapsis of 10,800 km, the nominal communication time is 3300 sec, with a minimum of 2300 sec (2.5 σ) and a maximum of infinity (no eclipse).

Table 19 shows the velocity-impulse and propellant requirements for each of the maneuvers to be performed by the midcourse-propulsion systems. These numbers are based upon the data contained in Table 18 and data taken from Section IIIB-3 of this study. Note that the propellant requirements for each trajectory correction and the miss maneuver are added arithmetically, which is somewhat conservative since the corrections are not completely interdependent.

Table 20 contains a description of the midcourse-propulsion systems which will fulfill the requirements of the *Mariner B* spacecraft. Data for the two systems are shown in this Table.

Table 21 compares the *Mariner B* with *Mariner A* and *Ranger* propulsion systems to indicate the similarity between the three propulsion units.

Figure 42 shows the estimated masses of the two midcourse-propulsion systems as a function of injected gross vehicle mass.

Several possible variations of the propulsion system should be considered. Four rigidly mounted motors, slightly canted with respect to the roll axis and differentially throttleable, are offered as an alternate to the three-motor system. This combination can provide pitch, yaw, and roll control as required by the spacecraft. This system does not require the development of the hinge joint or jet vane and actuator which provide roll control for the three-motor system. Two disadvantages of this system are a weight penalty, estimated to be 8 lb, and decreased reliability because of the additional motor unit as compared with the roll-control system required by the three-motor unit. It may be possible to increase the reliability of the fly-by mission and reduce the propulsion-system weight by using a propulsion system on the landing capsule to perform the miss maneuver. (See Appendix A for a discussion of this possibility.)

Table 21. Comparison of midcourse-propulsion systems

Propulsion-system characteristics	*Mariner B* (one-motor system)	*Mariner A*	*Ranger*
Propellant	Anhydrous hydrazine	Anhydrous hydrazine	Anhydrous hydrazine
Pressurizing gas	Nitrogen	Nitrogen	Helium
Thrust, lb	200	50	50
Thrust-vector control	Jet vanes	Jet vanes	Jet vanes
Specific impulse,[a] lb sec/lb	232	222	222
Propellant mass, lb	211	32.1	13.7
Propulsion-system-hardware mass, lb	80	34.4	21.2
Pressurizing-gas mass, lb	14	3.4	0.1

[a]This performance assumes fully deflected jet vanes.

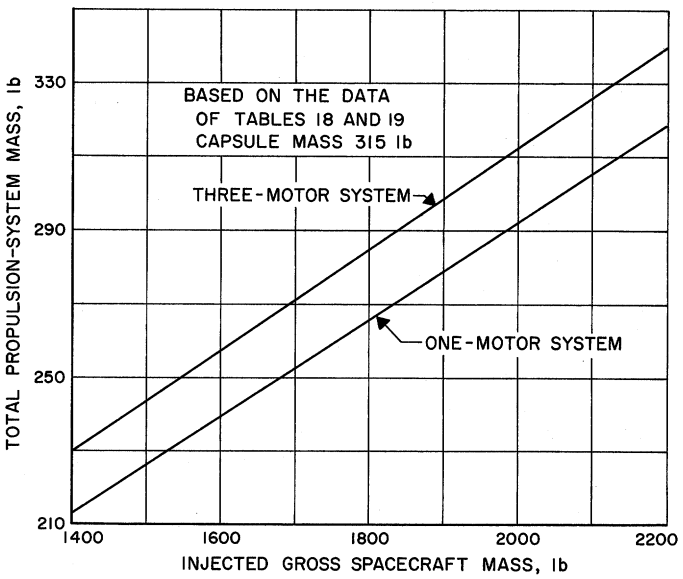

Figure 42. Total propulsion-system mass as a function of injected gross spacecraft mass

UNCLASSIFIED

8. Configuration

J. DAVIS

(This Section is CONFIDENTIAL)

a. Introduction

The configuration of a spacecraft for the proposed *Mariner B* mission poses some problems that have been met on preceding spacecraft designs and others that are new. This configuration study attempts to utilize the technology developed in both the *Ranger* and *Mariner A* programs.

The primary purpose of this portion of the study is to clarify the tradeoffs necessary to achieve an optimum spacecraft and to determine feasibility, rather than to develop one specific solution and configuration.

Presented here are the major design goals, the design constraints, the design approaches, weight breakdowns, configurations, general criteria used for evaluation of those configurations, and a discussion of work to be done before, or early in the preliminary design phase.

b. Design Goals

The major goal of the study was to develop a spacecraft configuration which incorporates the following:

(1) The largest probability of mission success.

(2) The largest probability of contributing to planetary-program success.

(3) Adaptability to a variety of mission requirements.

(4) Minimum obstruction by various spacecraft components to the viewing capability of subsystems such as the Earth antenna, navigation sensors, articulated booms, scientific instruments, etc.

(5) Minimization of temperature-control problems in the basic design.

(6) Minimum structural weight.

(7) Minimum critical alignments.

Planetary-program success, mission success, and growth potential are interrelated. Configurations which optimize mission success without regard to growth potential or over-all planetary-program goals are only superficially satisfactory. On the other hand, configurations which optimize growth potential or development without regard to mission objectives may result in a marginal expectation of mission success. The growth potential of a spacecraft, as used here, is measured in its adaptability, in total or in part, to more than one mission. A fly-by spacecraft, for example, that minimizes the major constraints which would limit the later adaption of a retromotor, capsule, or its usability on a different trajectory would be more desirable than one which holds no consideration for such possibilities.

The alignments between the attitude-control system, the navigation sensors, the servoed booms, and the spacecraft structure are critical. Close tolerances and small expectations of relative motion must be obtained. A configuration which minimizes the number and size of these alignments is desired.

c. Design Constraints

The spacecraft configuration must satisfy the following:

(1) Accommodation of the *Centaur* R&D nose fairing with a 4-ft cylindrical extension.

(2) A total weight within the *Centaur* booster capability with a reasonable firing window (see Section IIIB-1).

(3) Compatibility with the constraints of the trajectory with respect to articulation of members, attitude control, communication distance, etc.

(4) The boost environment as defined in the *Mariner A* specification (JPL30218 & 30221).

(5) Maintenance of a maximum allowable lateral offset of the center of gravity.

(6) Accommodation of the capsule, high-gain antenna, midcourse-propulsion system, power source, guidance-and-control system, Earth and capsule communications system, instruments, and associated electronics.

(7) Maintenance of a heat balance in accordance with the temperature-sensitive components and subsystems.

d. Configuration and Integration

A spacecraft is an assembly of subsystem elements tied together and supported by structure. The elements which have exerted major effects on the configuration are presented in Table 22, along with the variations for each which were considered in this study. There are at least

UNCLASSIFIED

Table 22. Elements of configuration

Subsystems	Possible variations
Power	Flat solar panel Flat panel with reflectors Parabolic solar concentrators with thermionic converter
Communications	Parabolic dishes 4 to 7 ft in diameter with fixed and folded feeds
Propulsion	One, three, and four motors
Planet boom	
Electronics	
Capsule (see Sect. IIIC-6)	

two ways to accomplish a configuration study. One is to start with a basic structure and arrange the required elements thereon to optimize weight, performance, etc. Another approach is to start with the elements, arranging them within the nose fairing in the most logical and optimum manner. The structure is then added to tie the elements together and support them on the booster. Various configurations can thus be compared on the basis of mission goals and structural weight and complexity.

This configuration study has covered many possible combinations, integrating the subsystems and variations on subsystems required for *Mariner B*. Although some of the configurations are of value only in determining what approaches are impractical, all are included in Appendix B for reference purposes.

Two of the designs were selected for detailed presentation. They represent the two approaches to configuration design mentioned above. Figure 43 represents a minimum step from the *Mariner A* design; Fig. 44 assumes and utilizes whatever is necessary to approach spacecraft optimization within the confines of the design goals and constraints.

The configuration shown in Fig. 43 has a 4-ft-diameter high-gain antenna (largest possible with assumed nose-fairing constraint), a single midcourse motor; 160 ft² of solar cells on foldable panels, and the *Mariner A* electronics boxes.

The configuration shown in Fig. 44 has a 7-ft-diameter high-gain antenna with a foldable feed, three midcourse motors, a 9.5-ft-diameter parabolic solar concentrator with a thermionic converter at its focus, and three temperature-integrated volumes for electronics packaging.

Both spacecraft accommodate the same instrument complement as listed in Section IIIB-2. The most striking

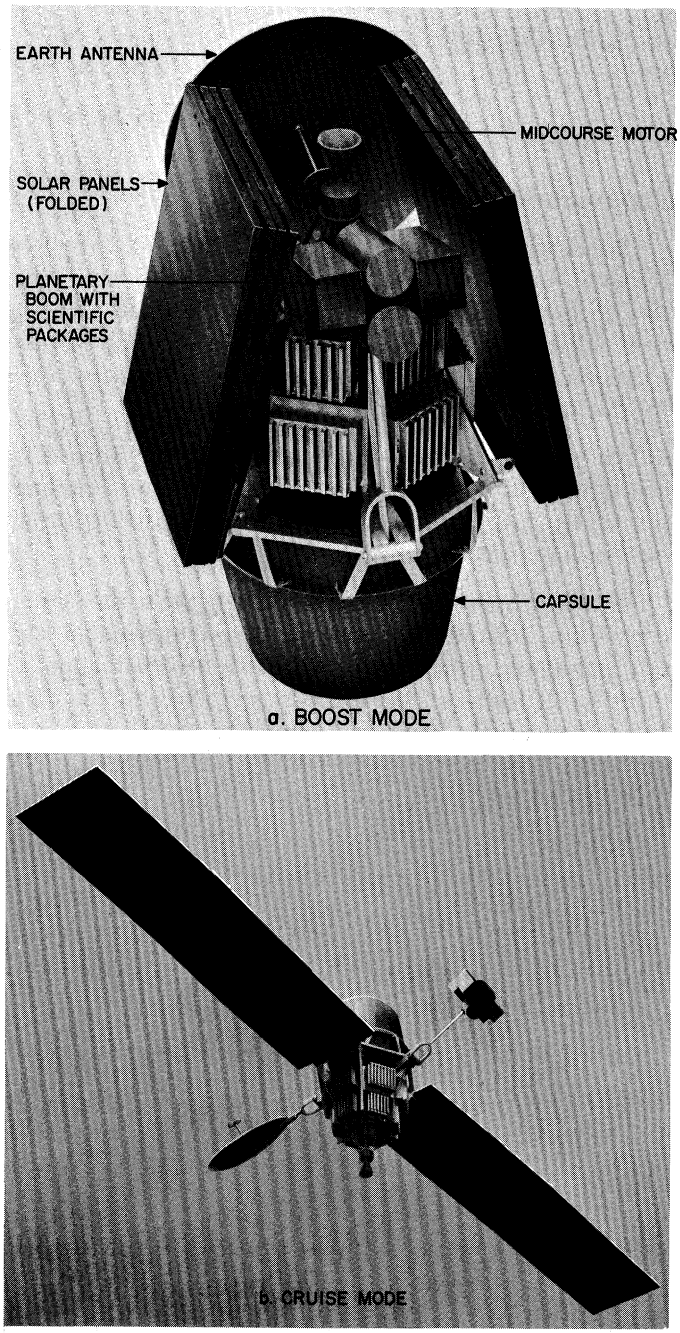

Figure 43. *Mariner B* spacecraft, incorporating solar panels

difference between the two configurations is in the power system. Neither configuration must have the specific system shown; either could be redesigned to accommodate other systems. However, they do represent the range of types of solar-power systems.

In the case of the solar panels, the nose-fairing envelope limits the flexibility of arranging the length, width, and

UNCLASSIFIED

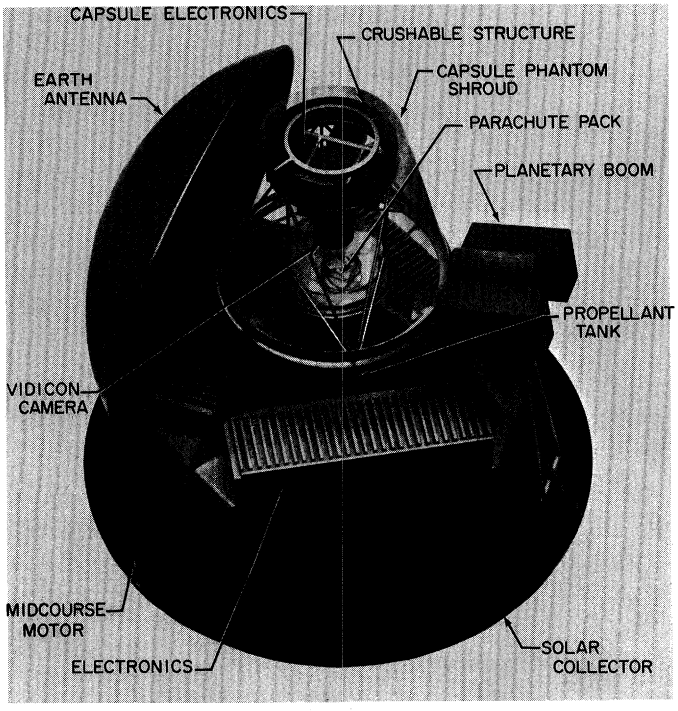

Figure 44. *Mariner B* spacecraft, incorporating a solar collector

number of panels to achieve the area required. The solar panels greatly reduce the look-angle capability of the antenna, sensors, and planetary boom. These combined constraints demand a foldable array which consistently culminates in a 40- to 50-ft tip-to-tip span of the spacecraft. Such mechanization of solar panels requires either severe weight penalties in structure to withstand the midcourse-correction accelerations or the refolding of the array during the maneuver. (For arrays, see Appendix B.)

The configuration in Fig. 44 offers considerable relief in accommodating the equipment for converting solar energy to electrical energy—a parabolic solar concentrator with a thermionic converter at the focus. For the same amount of power as that produced by solar panels, the frontal area of the collector is reduced by a factor of two and the weight by a factor of three to four. In addition, having the power system concentrated at the center of the vehicle reduces the look-angle problem.

Another major difference between the two configurations is in the electronics-packaging technique. In the converted *Mariner A*, the electronics are housed in 12 separate boxes. In the configuration shown in Fig. 44, the number of separate volumes is reduced to three, offering possible advantages with respect to total weight of the combined spacecraft structure and electronic housings. This configuration provides for a more uniform distribution of heat by conduction and greater flexibility in positioning sources of heat. Every effort should be made to achieve an acceptable passive temperature-control system; however, fewer boxes would also simplify the employment of an active system. This approach, in addition, reduces inter-box-cabling complexity.

A third and important difference to be noted is in the treatment of the midcourse-motor system. A number of the spacecraft elements have their most favorable positions along the axis of symmetry. Generally, more than two of these elements require placement at the extremities of the spacecraft. One solution to this configuration dilemma involves the use of multiple midcourse motors in parallel, located off the centerline. The justification for a multiple midcourse-propulsion system rests more strongly, however, on the capability of such a system to handle larger lateral c.g. offsets than a single-motor system. If vehicles are to incorporate movable booms and antennas, and if these must be deployed before all midcourse maneuvers are completed, then there must be adequate capacity in the thrust-vector-alignment system to allow for any random position of these members. Lack of this capacity makes mission success dependent on the successful operation of a series of otherwise independent components.

e. *Weights*

Weight breakdowns for the two configurations shown are given in Table 23. The first column lists recent *Mariner A* weights for comparison. The second and third

UNCLASSIFIED

Table 23. Weight summary, lb

	Mariner A	Figure 43		Figure 44	
		high	low	high	low
Attitude control and guidance	155	220	220	220	220
Attitude-control system	93	113	113	113	113
Servos	35	40	40	40	40
CC&S	27	67	67	67	67
Communications	144	115	115	137	115
High-gain antenna	12	12	12	34	12
Transponder	89	53	53	53	53
Encoder	29	29	29	29	29
Decoder	14	14	14	14	14
Backup omni system	—	2	2	2	2
Capsule RF receiver and demodulator	—	5	5	5	5
Power	199	437	306	234	184
Panels or collector	100	328	197	125	75
Battery	60	59	59	59	59
Converters, etc.	39	50	50	50	50
Propulsion	71	292	255	286	250
Dry system	36	78	71	92	86
Propellant	32	201	173	178	150
Nitrogen	3	13	11	16	14
Science	200	260	203	260	203
Magnetometer	8	10	10	10	10
Ultraviolet spectrometer	20	25	25	25	25
Infrared spectrometer	—	35	20	35	20
Vidicon	—	30	20	30	20
Cosmic dust	10	10	10	10	10
Radiation	102	60	43	60	43
Polarization	—	15	—	15	—
Data automation	60	75	75	75	75
Structure	216	275	260	265	215
Basic frame	86	120	120	90	80
Electronics boxes	38	40	40	90	50
Supports	18	20	20	15	15
Miscellaneous	7	10	10	10	10
Articulating head	17	20	20	20	20
Thermal control	50	50	40	40	40
Capsule support	—	15	10	—	10
Miscellaneous	65	105	75	105	75
Wiring	60	100	70	100	70
Pyrotechnics	5	5	5	5	5
Total without capsule	1050	1704	1434	1507	1262
Full capsule		300	300	300	300
Total with full capsule		2004	1734	1807	1562
Reduced capsule		80	80	80	80
Total with reduced capsule		1784	1514	1587	1342

columns give the upper and lower estimates, respectively, for the configuration of Fig. 43, and the fourth and fifth columns for the configuration of Fig 44. In general, the higher figure represents the "worst expectation of weights," while the lower represents a more optimistic value. Note that opposite the item "panels or collector," four weights are listed, which strongly affect the final spacecraft total. Flat solar panels weigh 328 lb; panels with reflectors weigh 197 lb. The solar concentrator with thermionic converter was estimated to weigh between 125 and 75 lb.

The propulsion weights are a function of the velocity increment required in all maneuvers and the total non-propulsive weight.

A comparison of the total weights with booster capability and firing period is of extreme interest in determining mission feasibility. Figure 45 lists the eight total weights given in Table 23 with the corresponding firing windows.

f. Special Problems

As mentioned in the introduction, there are unresolved problem areas in the spacecraft design which need to be

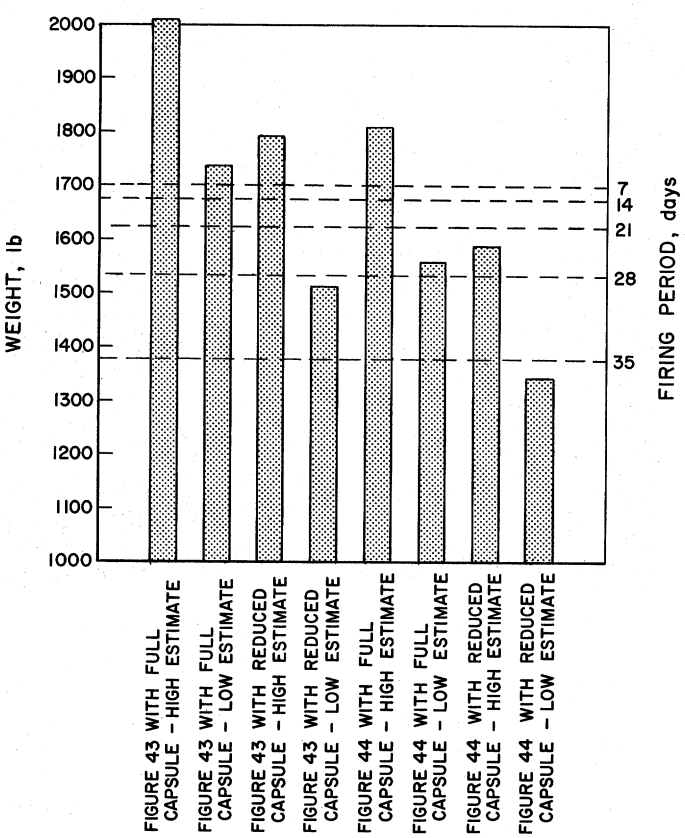

Figure 45. Estimated weights of Table 23 compared with firing period

UNCLASSIFIED

explored before, or very early in, the preliminary design phase.

(1) It will be necessary to study methods of overcoming the dependence of mission success on the successful deployment of any or all of the various movable elements. This dependence is reflected in the ability to point the midcourse motor through the center of gravity, wherever it may be. The number of degrees of freedom necessary for each of the movable elements of the spacecraft is dependent on the relative motion between the spacecraft and the bodies being tracked, and on the choice of the attitude-reference system. Freedom of movement must be given to the Earth antenna, the target-planet sensor, the secondary body sensor, and the spacecraft. A study of the relative freedom of each item for particular trajectories is necessary.

(2) Potential weight advantages may be gained by positioning a single midcourse motor on the capsule, flying a miss trajectory with the spacecraft, and maneuvering the capsule to intercept. An investigation of the system implications of such a configuration must be made. A further treatment of this subject is given in Appendixes A and B.

g. Conclusions

The power requirements of the *Mariner B* mission approach and may exceed limits in utilization of solar panels with respect to weight, integration, and deployment. As shown in the weight-breakdown tables, configurations utilizing solar panels and a 300-lb capsule leave very little or, in some cases, no margin for increasing the firing period and allowing for growth. This condition could be improved (ameliorated) by the incorporation of a smaller 80-lb capsule; however, the total weight for the high estimate of Fig. 43 is still marginal.

A thermionic power system offers considerable advantage in both weight reduction and configuration simplification. Use of this power source would permit incorporation of a heavier capsule with more margin for growth and firing period.

The geometric incorporation of the remaining subsystems within the nose-fairing envelope appears to be a reasonable task, and is a normal extension of the techniques developed on *Ranger* and *Mariner A*.

C. CAPSULE

1. Approach Trajectory and Accuracy Analysis

P. K. ECKMAN

(This Section is CONFIDENTIAL)

a. Approach Geometry

For a better visualization of the trajectory geometry in the vicinity of the target, some of the orbital characteristics of the Earth and Mars are depicted in Fig. 46. The Earth has an orbital period of some 365 solar days, and its equator is inclined about 23 deg to its orbital plane (i.e., the ecliptic plane). The Sun's position as viewed from the Earth on March 21st, the first day of spring, defines a reference direction called the vernal equinox, from which the heliocentric longitude of a body is measured. The orbital period of Mars is 688 "Earth days," and its orbital plane is inclined about 2 deg to the ecliptic, the ascending node occurring at a heliocentric longitude of 48 deg. Mars rotates about its polar axis every 24 hr 37 min, and its equator is inclined some 25 deg to its orbital plane. Note that the winter solstice (i.e., the first day of winter for the northern hemisphere) occurs at a longitude of about 347 deg for Mars and at 90 deg for the Earth.

Figure 47 shows a typical 1964 *Mariner B* trajectory. The probe is launched on November 15, 1964 and encounters Mars on July 14, 1965, resulting in a flight time of 240 days. The heliocentric latitude of Mars at encounter is only +0.067 deg, since Mars crosses the line of descending nodes four days later on July 18, 1965. Note that the probe passes "behind" Mars in the sense that it reaches the intersection of its flight path and Mars' orbit after Mars has crossed this point.

The target encounter geometry will now be examined in detail. Shortly after the final approach correction is made (at a distance of 400,000 km from Mars) the capsule is separated from the parent spacecraft and continues its flight toward the designated landing area. Approximately one hour after capsule separation occurs, the spacecraft is given a transverse velocity increment to cause it to miss the planet by some specified distance. Because the approach guidance and miss maneuvers are performed at such great distances from the planet, the approach asymptotes for both capsule and spacecraft are essentially parallel (and fixed in direction) for a given arrival date. This is quite fortunate as it allows the trajectory designer to move the position of these lines about rather freely to satisfy the constraints which various spacecraft subsystems place upon the trajectory.

It is desirable that the approach geometry meet the following conditions:

(1) The nominal entry angle of the capsule into the atmosphere is 40 deg above the local horizontal.

(2) The capsule lands in the hemisphere which is experiencing summer at the time of arrival.

(3) The capsule lands in an area which can be scanned or viewed from the spacecraft as it "flies by."

(4) After the capsule lands and the spacecraft disappears from view (i.e., sets below the horizon), the time until the spacecraft is visible again from the capsule is minimized. This can be accomplished both by landing the capsule on that side of the planet which rotates with the direction of the spacecraft and by keeping periapsis as large as possible without placing excessive requirements on the propulsion system.

(5) The spacecraft maintains line of sight with the Earth during, and for at least 10 days following, encounter to allow transmission of stored data.

(6) The spacecraft attitude-control secondary reference (probably Canopus) is never occulted by Mars.

(7) The spacecraft remains in the sunlight for the entire mission.

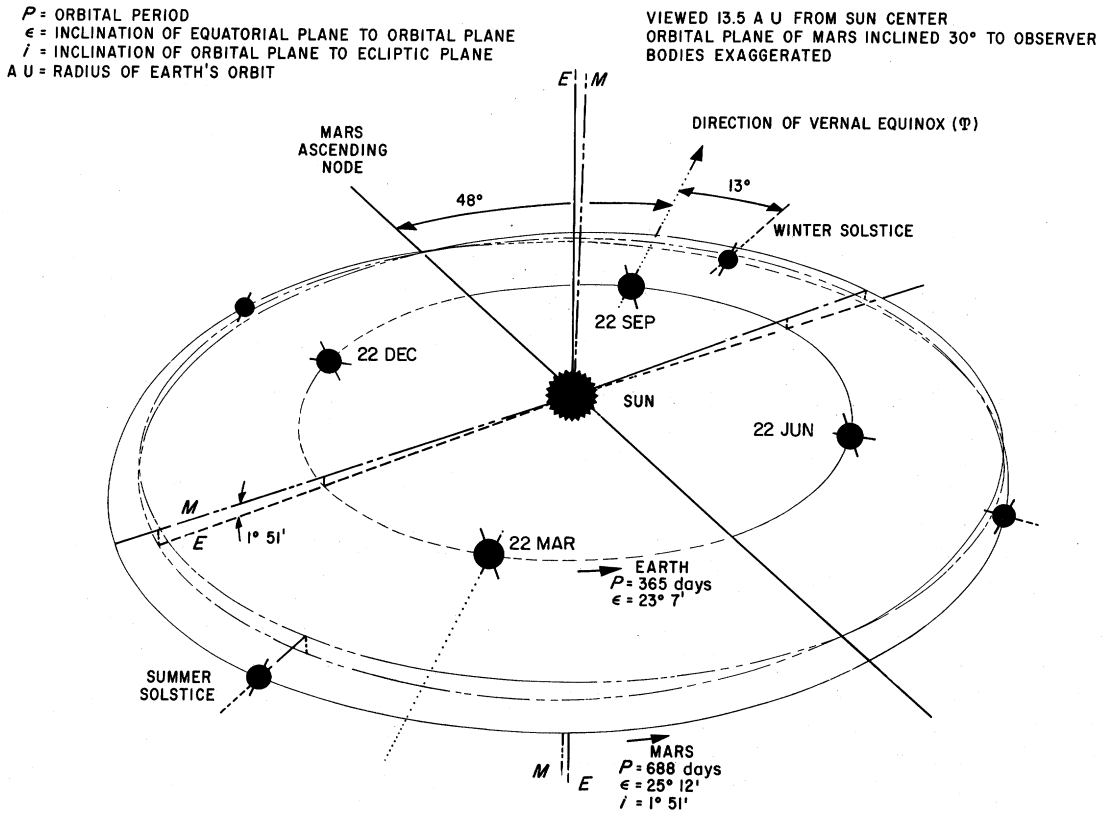

Figure 46. Earth–Mars solar geometry

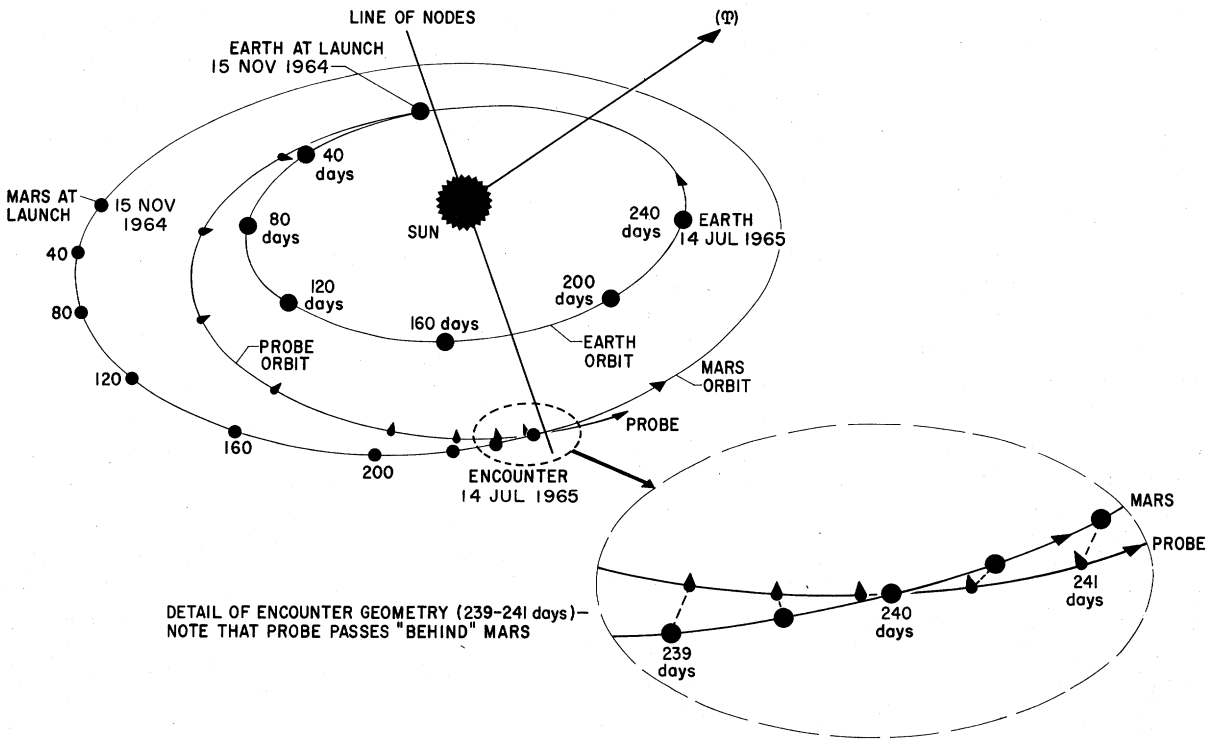

Figure 47. Typical Mars 1964 trajectory

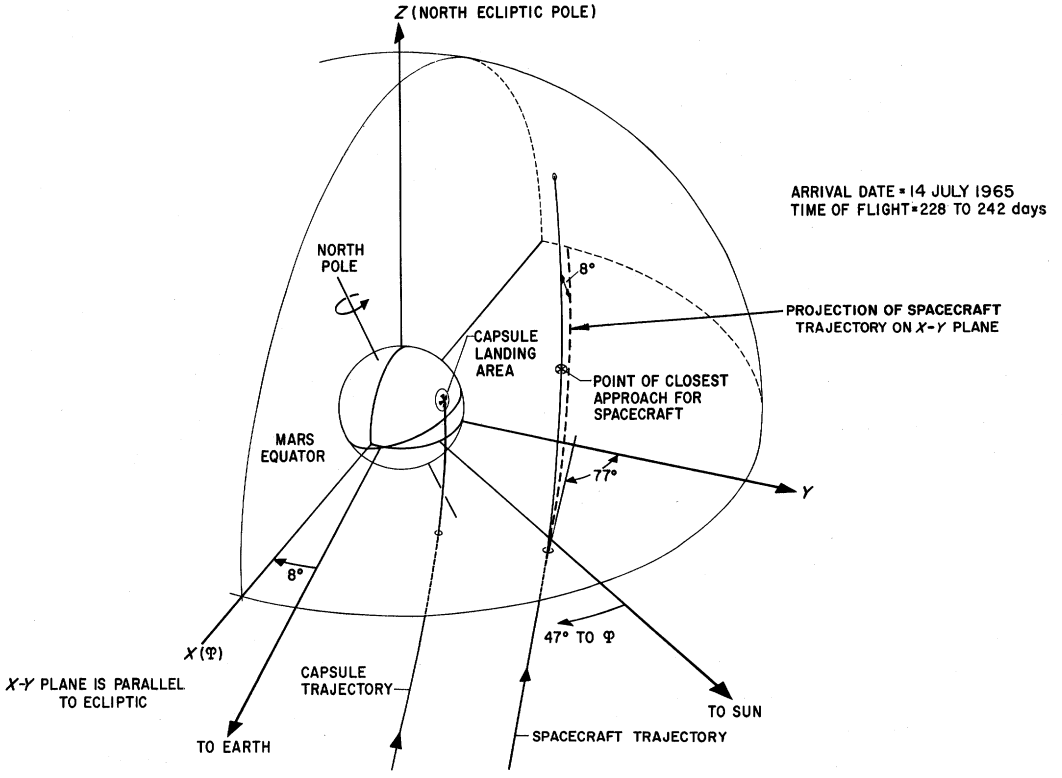

Figure 48. Approach geometry for split-capsule Mars trajectory

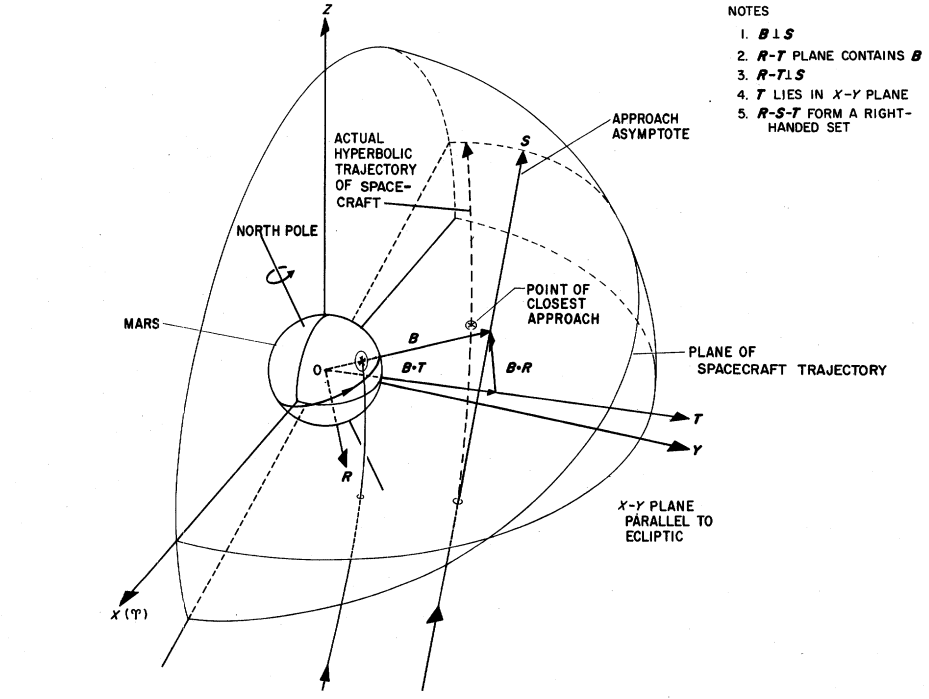

Figure 49. Description of miss-distance coordinates

UNCLASSIFIED

Trajectories which arrive during the period July 4 to July 19, 1965 satisfy most, if not all, of these constraints. Figure 48 depicts an arrival on July 14 for purposes of illustration. A rectangular coordinate system is shown, centered at Mars, with the *X-Y* plane chosen parallel to the ecliptic and the *X*-axis defined in the direction of the vernal equinox (Υ). Directions to the Earth and Sun are shown essentially in the *X-Y* plane, lying 8 and 47 deg, respectively, from the vernal equinox. The polar axis, the equator, and the direction of rotation of Mars are also shown.

The approach asymptotes of the capsule and spacecraft are inclined to the ecliptic by about 8 deg, passing upward through the *X-Y* plane. In Fig. 48 they have been positioned so that the capsule lands on the northern hemisphere near the equator and toward that side on which the spacecraft will pass, and that the point of closest approach by the spacecraft lies about 4200 km above the *X-Y* plane and 6900 km from the surface of the planet.

It is useful to designate explicitly the position of the spacecraft trajectory as the spacecraft passes by the target planet. In Fig. 49 approach asymptote ***S*** can be seen passing within a distance ***B*** of the target center. A plane (***R-T***) is established which is perpendicular to ***S*** and contains ***B***. The intersection of this plane with the *X-Y* plane (parallel to the ecliptic) is designated as the ***T*** direction. A third direction ***R*** completes a right-handed set of coordinates ***R-S-T***. The trajectory is now specified if the following are defined: V_∞, the hyperbolic excess velocity of the probe with respect to the target; ***S***, the direction of the approach asymptote; and the miss components, $\boldsymbol{B}\cdot\boldsymbol{T}$ and $\boldsymbol{B}\cdot\boldsymbol{R}$.

The target approach geometry is essentially independent of the launch date for the firing windows being considered; it does, however, depend markedly upon arrival date. The changes of reference directions with arrival time can be visualized easily by placing a celestial sphere around Mars and observing the traces made on this imaginary sphere by vectors to the reference bodies of interest. Figure 50 depicts such a sphere, showing the changing directions to the Sun and Earth. The variation of the approach asymptote with encounter date is also shown. Relative to the target-centered *X-Y* plane the approach-asymptote inclination increases with later arrivals. To assure line-of-sight communication between the spacecraft and Earth, it may be desirable to choose a late encounter date.

The near-encounter geometry and look angles will be described next. Figure 51 shows Mars for an encounter on July 14, 1965, as it will appear to the spacecraft following the final approach maneuver. Relative to the target,

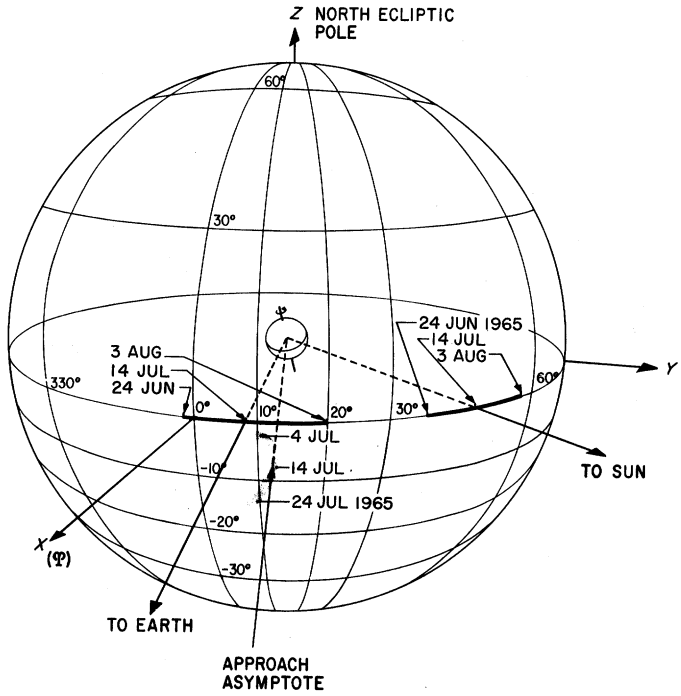

Figure 50. Reference-vector traces on a Mars-centered celestial sphere

the probe passes "upward" through the target-centered *X-Y* plane. The asymptotic miss components $\boldsymbol{B}\cdot\boldsymbol{T}$ and $\boldsymbol{B}\cdot\boldsymbol{R}$ are shown, as is the actual point of closest approach. Mars appears nearly fully illuminated (i.e., gibbous) and will remain so until the spacecraft has nearly reached the point of closest approach to the planet.

b. Miss Maneuver

Because the *Mariner B* spacecraft will have approach-guidance capability, it is possible (and probably desirable) to vary the location of the spacecraft's periapsis (i.e., the point of closest approach to Mars) after capsule separation has occurred. For example, suppose that the mid-course and approach maneuvers have been successfully performed and that enough propellant remains to impart a velocity ΔV to the spacecraft when the target miss maneuver is performed. In what direction should the increment ΔV be applied to best satisfy the geometrical constraints of the spacecraft systems? An answer to this question should be sought both by the engineer who performs a preliminary design of the spacecraft and its trajectory, based on a statistical estimate of ΔV, and by the terminal-guidance computer (regardless of whether it is ground-based or on-board), based on a knowledge of what miss capability actually exists following the final approach correction. To illustrate this point, a set of seven spacecraft

UNCLASSIFIED

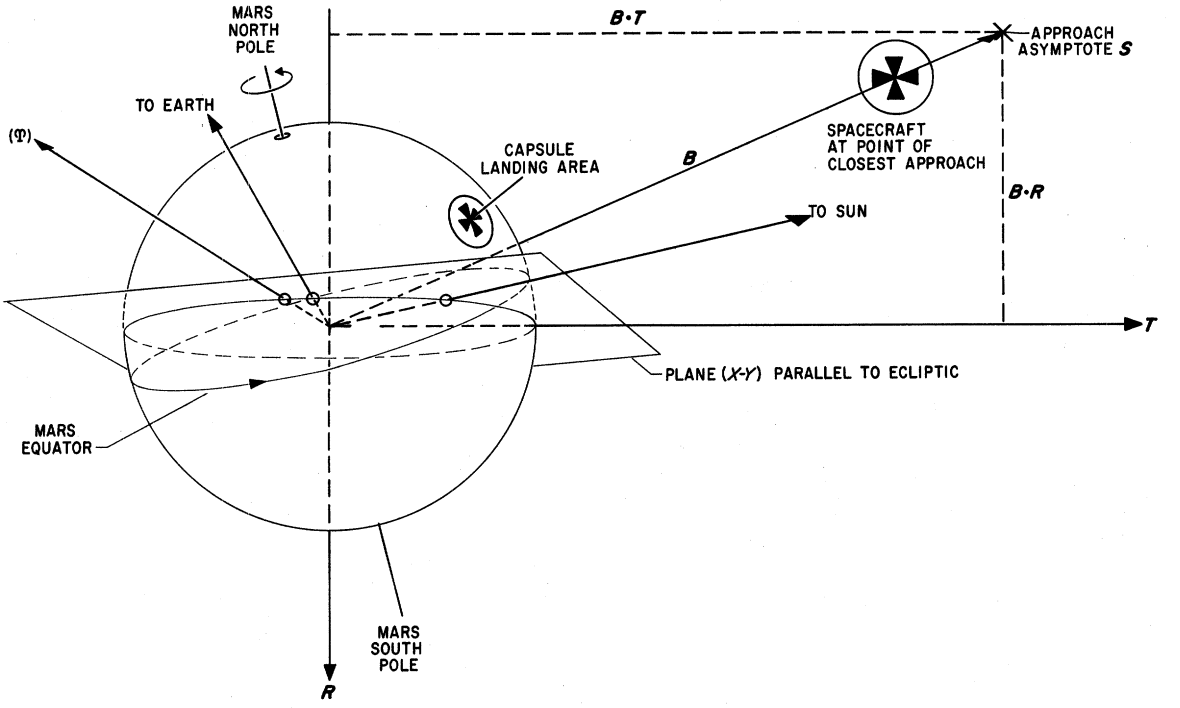

Figure 51. Mars seen from spacecraft as it will appear for a 14 July 1965 arrival

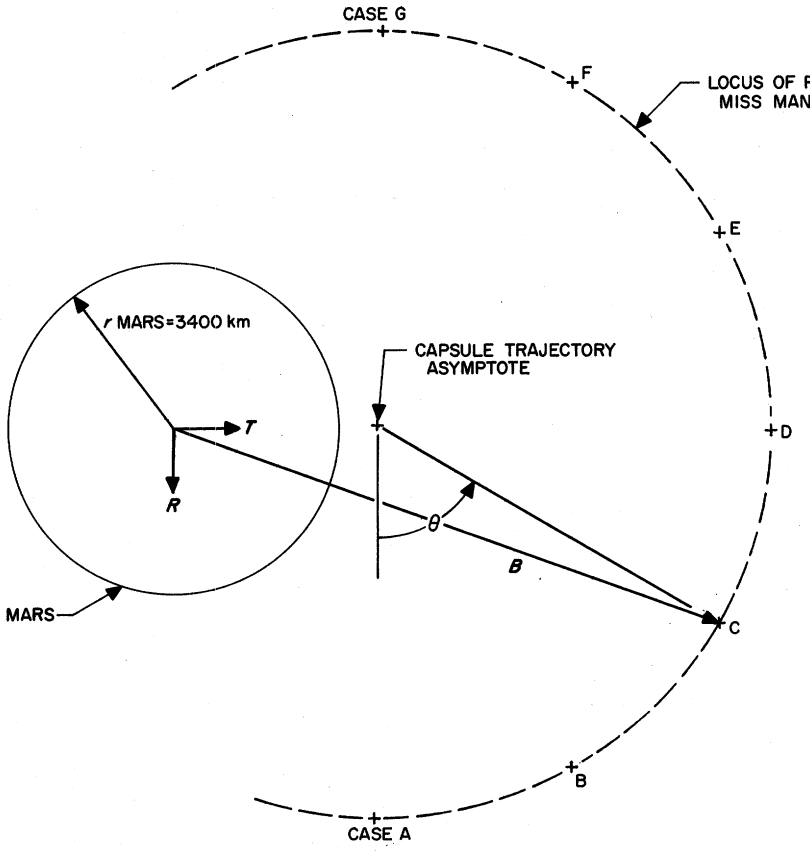

CASE	θ, deg
A	0
B	30
C	60
D	90
E	120
F	150
G	180

Figure 52. Spacecraft aiming points

UNCLASSIFIED

trajectories has been generated whose approach asymptotes pass a fixed distance from the aiming point for the capsule's asymptote, but whose periapsis locations vary from one trajectory to the next. All of these trajectories encounter Mars on July 14, 1965. Figure 52 shows the aiming points for the seven cases. For this example, it is assumed that a miss capability of 8000 km exists and that the ΔV is applied normal to the approach asymptote so that this miss is fully realized. As pointed out in Section IIIB-3e, this capability will be available at least 99% of the time and is thus quite conservative. It has also been assumed that the nominal capsule landing point lies in the X-Y plane of Fig. 48. Although the final choice of the landing area will probably be at a Mars latitude of 0 to 30° North, depending on scientific and eclipse requirements, the example considered here typifies the kinds of analysis and results which are to be expected. Figures 53, 54, 55, and 56 are self-explanatory. In each Figure various angular relationships are plotted for each of seven periapsis locations. The period of interest is of about 20-hr duration, centered about the time of closest approach.

To describe the look angles from the spacecraft to certain bodies, an attitude-reference system has been adopted, as shown in Fig. 57. A primary and secondary body define a reference direction and reference plane, respectively. Two angles, called cone angle (β) and clock angle (α), serve to define the direction to any other desired body at a given time. For the set of trajectories considered here, the Sun was chosen as the primary reference and the

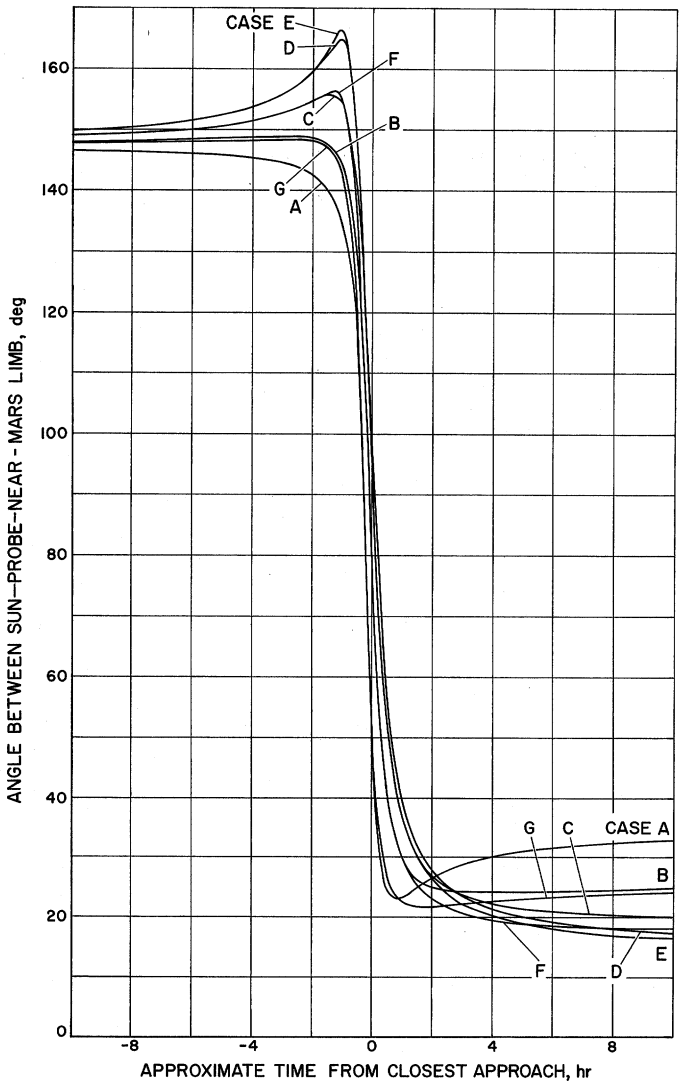

Figure 53. Sun–probe–near-Mars-limb angle vs time

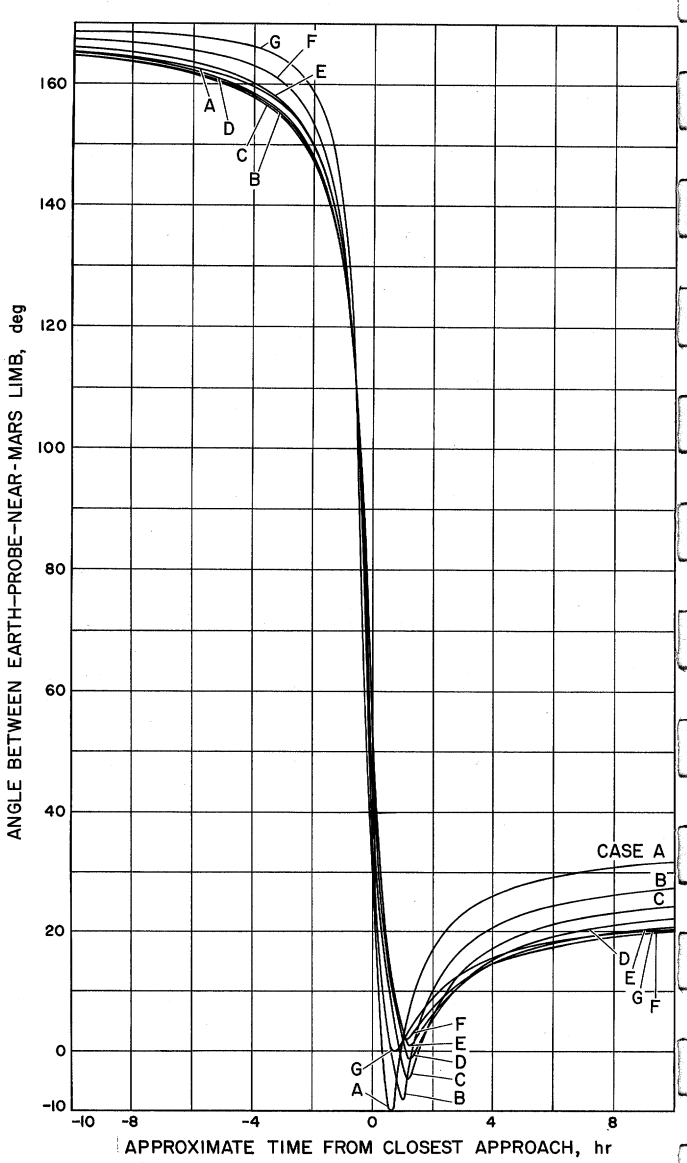

Figure 54. Earth–probe–near-Mars-limb angle vs time

UNCLASSIFIED

star Canopus as the secondary reference. The cone and clock angles of Mars are of particular interest, since these angles determine the articulation required by certain spacecraft subsystems as the probe encounters the target. Figures 58 and 59 show these angles for each trajectory.

Another relationship of interest is the Earth–probe–Sun angle throughout the flight. A typical trajectory for 1964 Mars missions is shown in Fig. 60. Note that this angle reaches a minimum value of less than 3 deg about 170 days after launch.

Another study has been initiated to determine the effects of varying the magnitude of the miss-velocity increment ΔV, and of applying this impulse in a direction other than normal to the approach asymptote S. By optimizing this direction, a significant reduction (or elimination) of eclipse time between capsule and spacecraft may be realized. The results of this analysis are presented next.

The approach trajectory, which results after the final approach correction, will place the spacecraft (with capsule) on a path to impact the planet in the northern hemisphere (0 to 30° north latitude) on the lighted side. The nominal entry angle will be 40 deg within a range from 24 to 52 deg (2.5 σ) because of the dispersion in the capsule impact point. This landing area places the capsule in the best possible position in relation to the bus from a communications viewpoint while still avoiding any appreciable chance of missing the planet.

The capsule is separated from the spacecraft at about 400,000 km from the planet and then follows the impact trajectory. For this particular study, the spacecraft is maneuvered into the fly-by trajectory by a velocity increment applied in the plane of the impact trajectory, so that the capsule sees the spacecraft pass "overhead" during the data-transmission period.*

*A separate study, not included here, has shown that, for a given ΔV, the period before spacecraft setting can, in general, be maximized by flying the spacecraft directly over the capsule, providing the capsule landing area is within 30° latitude of the Mars equator.

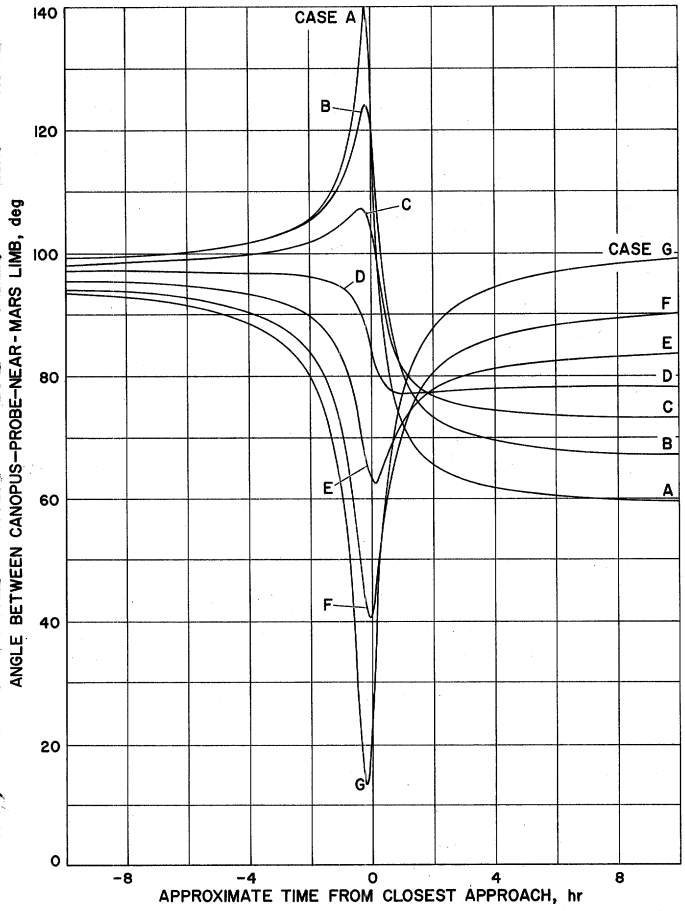

Figure 55. Canopus–probe–near-Mars-limb angle vs time

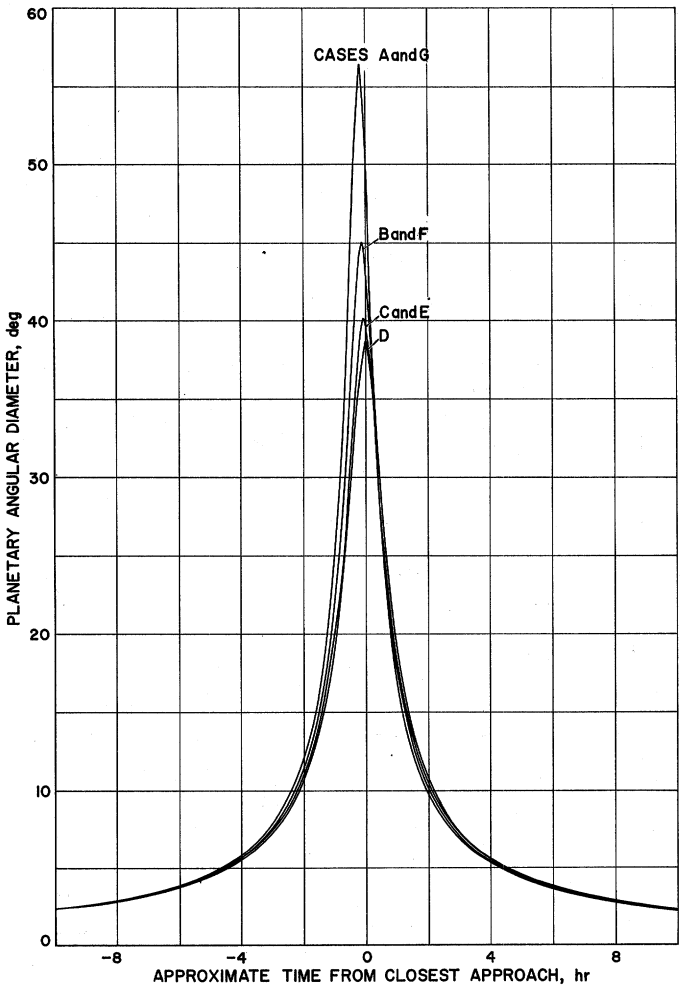

Figure 56. Mars angular diameter vs time

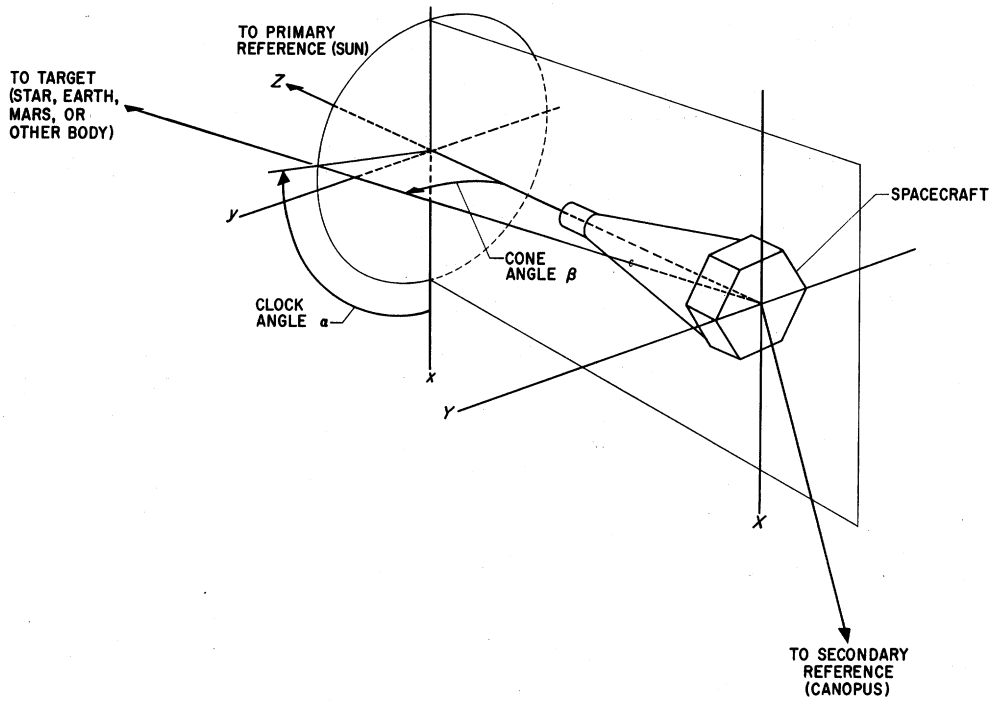

Figure 57. Spacecraft altitude-reference system

To analyze the trajectory geometry and communication situation described, a series of fly-by trajectories have been computed, all lying in the same plane. The following parameters were assumed:

(1) V_∞, hyperbolic excess velocity, 4.5 km/sec

(2) r_S, distance from Mars at time of capsule separation, 320,000 km

(3) θ_E, capsule entry angle above local horizontal, 40 deg

(4) 2.5-σ dispersion in θ_E, 24 to 52 deg

(5) $|\phi|$, angle between miss-velocity increment ΔV, and V_∞, 90 to 165 deg

(6) α, communication horizon angle above capsule's local horizontal, 0 to 40 deg

Figure 61 shows the effect of several miss-velocity increments fired at 90 deg to the approach trajectory, and Fig. 62 illustrates the corresponding times available before the spacecraft sets below the capsule's horizon. With the propulsion-weight allocations previously stated, the spacecraft will be capable of a minimum closest-approach altitude of about 8000 km. For this "worst" case, Fig. 62 shows that the spacecraft will probably set below the capsule's horizon about an hour after entry and will then rise again after another hour has elapsed. This situation is undesirable but can be tolerated for the mission now proposed. Even for the most unfavorable capsule dispersion ($\theta_E = 52$ deg), a closest-approach altitude of 12,000 km would completely eliminate this period. As has been stated in Section IIIB-3e, such a capability will exist for at least 85% of successful missions. After the first eclipse period, the rising and setting events become essentially diurnal as the spacecraft moves away from the planet. Data-transmission from capsule to spacecraft is planned through the first 12-hr period of visibility.

The effect of miss impulse direction, $|\phi|$, upon the first eclipse period is demonstrated in Figs. 63 through 66. Figure 63 shows the geometry of the problem and emphasizes lines of constant time for a miss maneuver applied at an angle of 90 to 165 deg from the approach-asymptote direction. Figures 64 through 66 show the times to spacecraft setting and rising for entry angles of 20, 40, and 52 deg, respectively. It is seen that a value of $|\phi|$ from about 105 to 115 deg results in minimum eclipse time. Table 24 lists the important results of Figs. 63 through 66.

It should be mentioned that the velocity increments ΔV which are shown in the above Figures are for one particular value of r_S, namely, 320,000 km. The ΔV required at other r_S is inversely proportional to the value of r_S. For example, the ΔV of 134 m/sec shown for r_S of 320,000 km is reduced to a requirement of only 112 m/sec when the

miss maneuver is performed at the nominal miss-maneuver distance of 380,000 km.

c. Sequence of Events

Table 25 lists a possible sequence of events as they might occur for a 1965 Mars encounter. The Table is intended only as an example of the general order of significant phenomena and is subject to change. For example, if the approach-guidance-instrument accuracies were to improve markedly, the two approach corrections and the miss maneuver might be made at greater distances from the target. The early photographs referred to in the Table would probably be taken only at occasional intervals during the period designated. As soon as the miss maneuver has been completed and the bus regains its correct orientation, transmission of scientific data will commence. Data-transmission is shown to continue until approximately nine days after closest approach. There appears to be nothing critical about the final transmission date; a longer playback period could readily be realized if necessary.

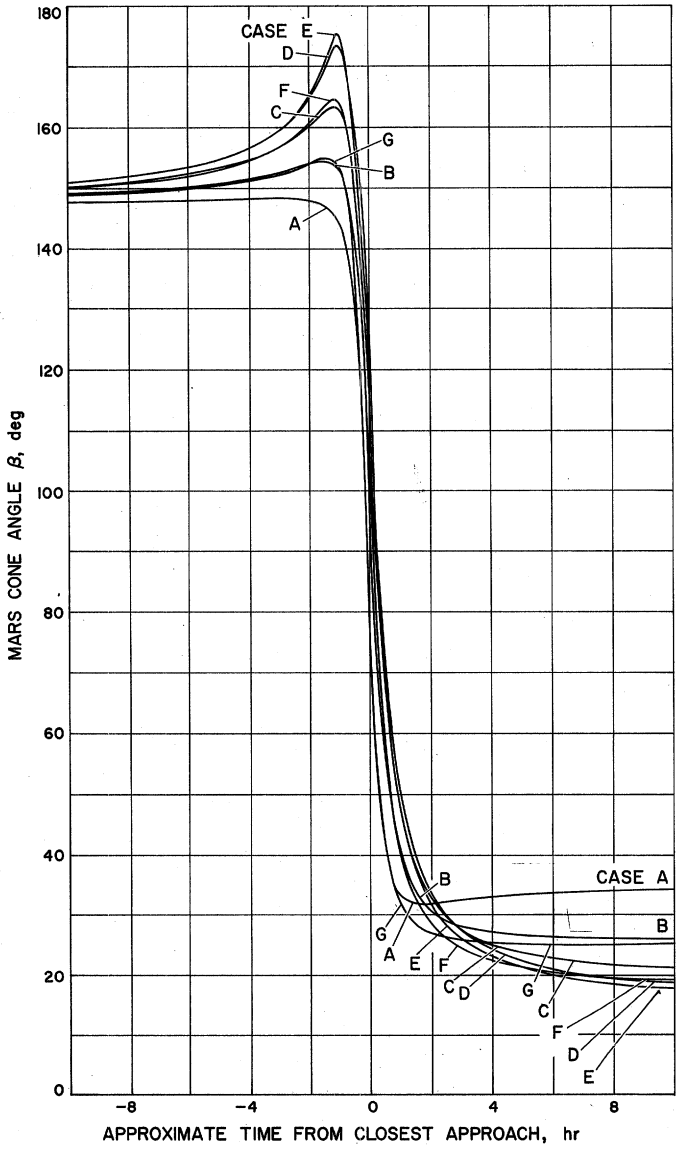

Figure 58. Mars cone angle β vs time

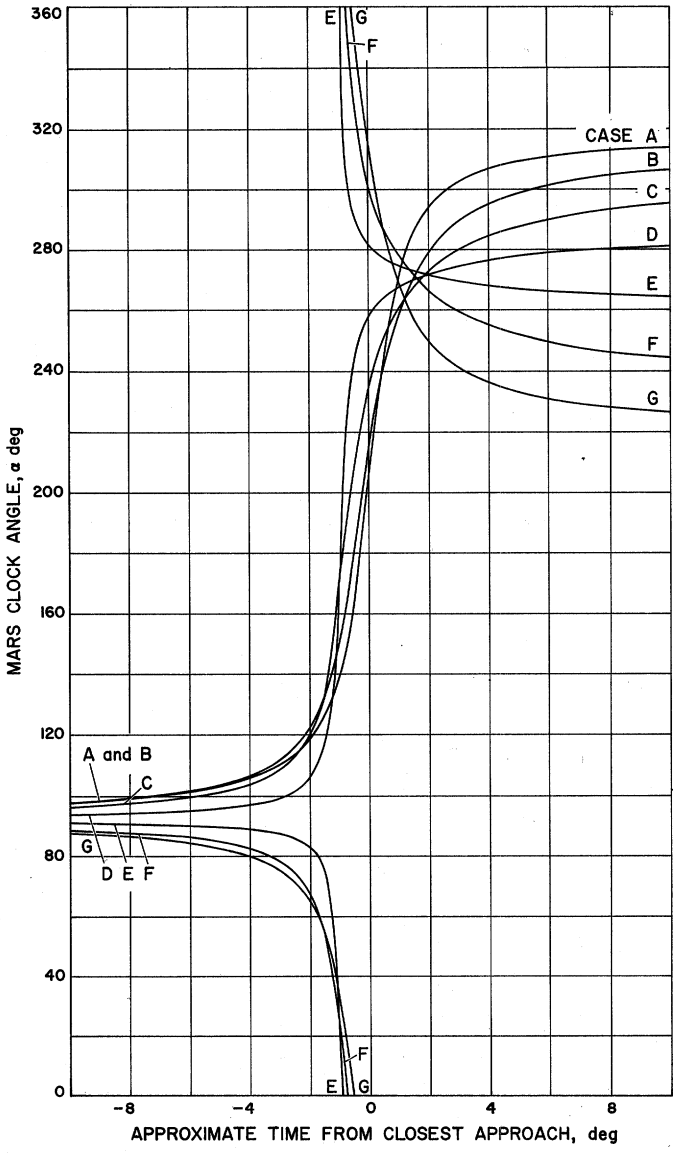

Figure 59. Mars clock angle α vs time

UNCLASSIFIED

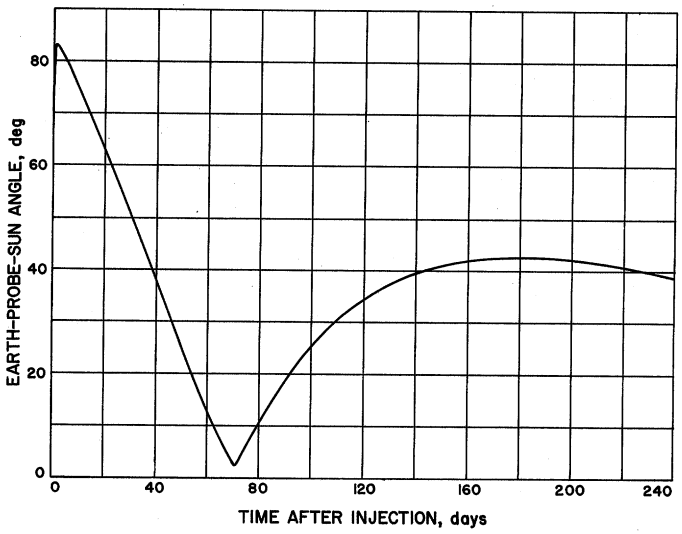

Figure 60. Earth–probe–Sun angle during transit

Table 24. Capsule–spacecraft communication optimization

Capsule entry angle, deg	Time interval, sec (min)		Spacecraft-to-capsule distance, km		
	Capsule entry to spacecraft setting	Spacecraft setting to spacecraft rising	Capsule entry	Spacecraft setting	Spacecraft rising
20	no eclipse	no eclipse	10,200	—	—
40	4800 (80)	2800 (47)	10,200	19,200	31,200
52	3100 (52)	8900 (148)	10,200	13,000	50,200

Assumptions:

(a) Angle between miss impulse and approach asymptote $\Phi = 110$ deg.

(b) Communication horizon angle $\alpha = 0$ deg.

(c) Altitude of closest approach = 8000 km.

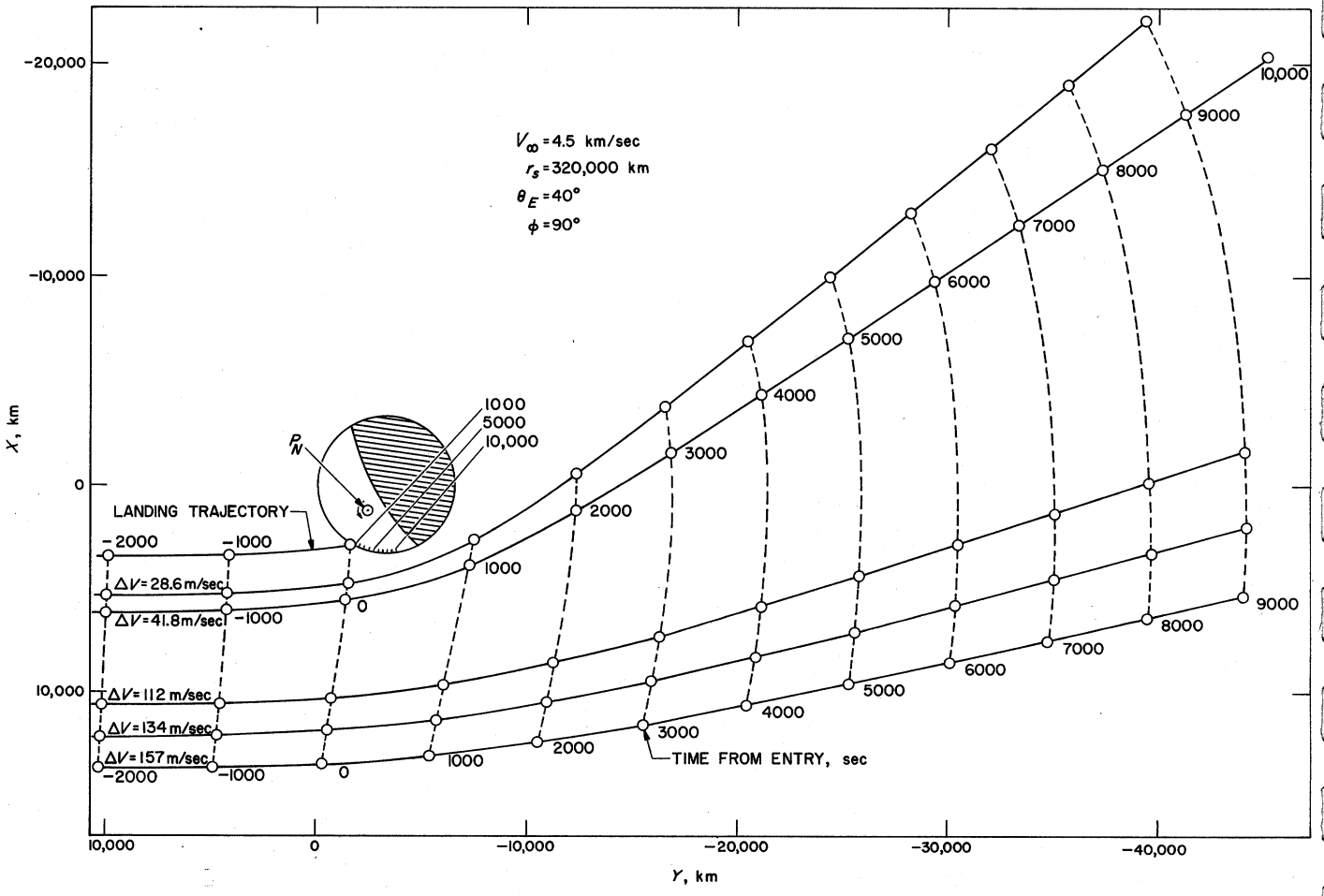

Figure 61. Mars split-capsule trajectories—effect of miss-maneuver magnitude ΔV

UNCLASSIFIED

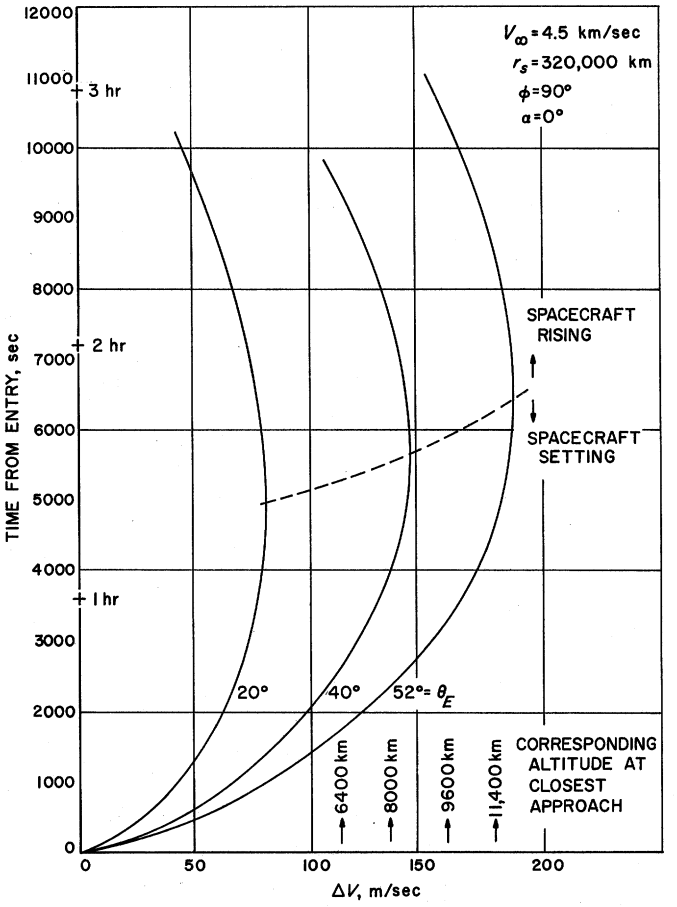

Figure 62. Mars split-capsule trajectories — communication time for 90-deg flyby impulse

Table 25. Typical *Mariner B* encounter sequence

Event	Distance from Mars, km	Time from closest approach	
		sec	hr
Approach correction No. 1	-1.5×10^6	-0.3×10^6	−83
Approach correction No. 2	-0.40×10^6	$-0\,08 \times 10^6$	−22
Miss maneuver	-0.38×10^6	-0.076×10^6	−21
Early photographs	-0.36 to -0.06×10^6	-0.072 to -0.012×10^6	−20 to −3.3
Encounter experiments	−60,000 to 60,000	−12,000 to 12,000	−3.3 to 3.3
Late photographs	0.6×10^6	0.12×10^6	33
Final data-transmission	4.0×10^6	0.8×10^6	220

UNCLASSIFIED

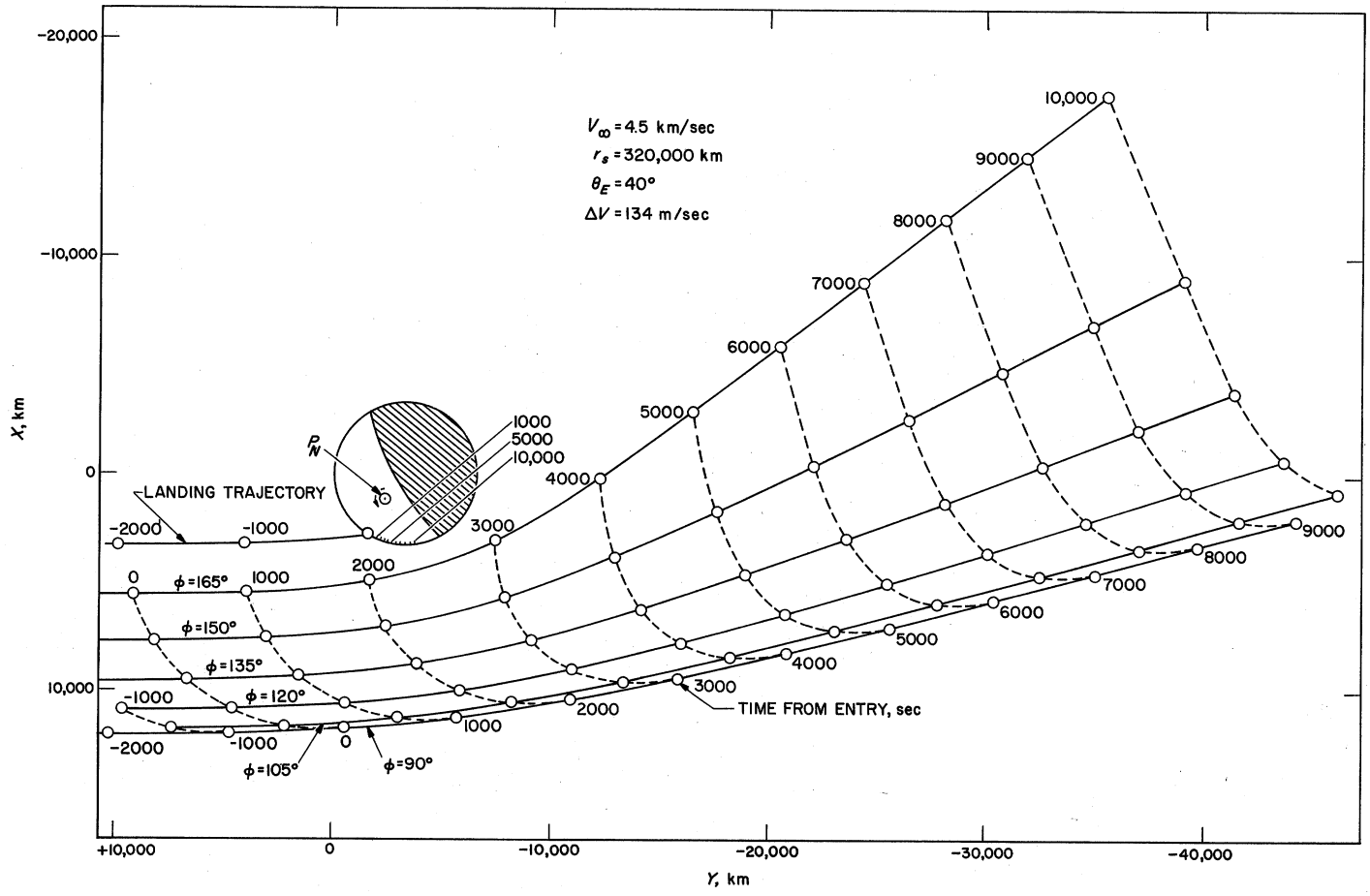

Figure 63. Mars split-capsule trajectories—effect of flyby impulse direction θ

UNCLASSIFIED

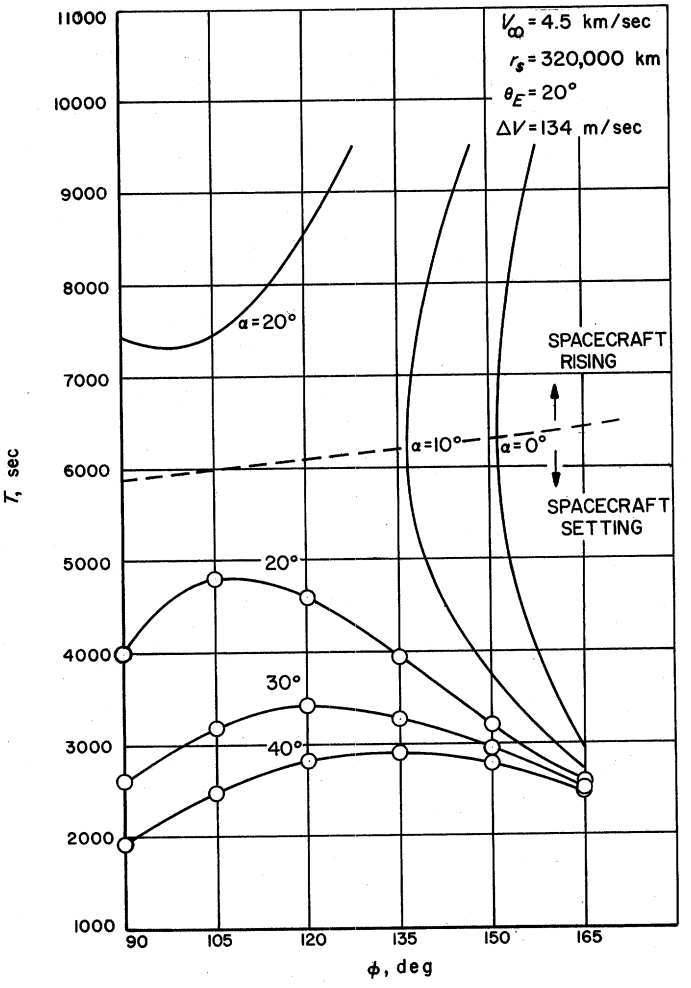

Figure 64. Mars split-capsule trajectories—effect of impulse direction on "eclipse" time for a 20-deg entry angle

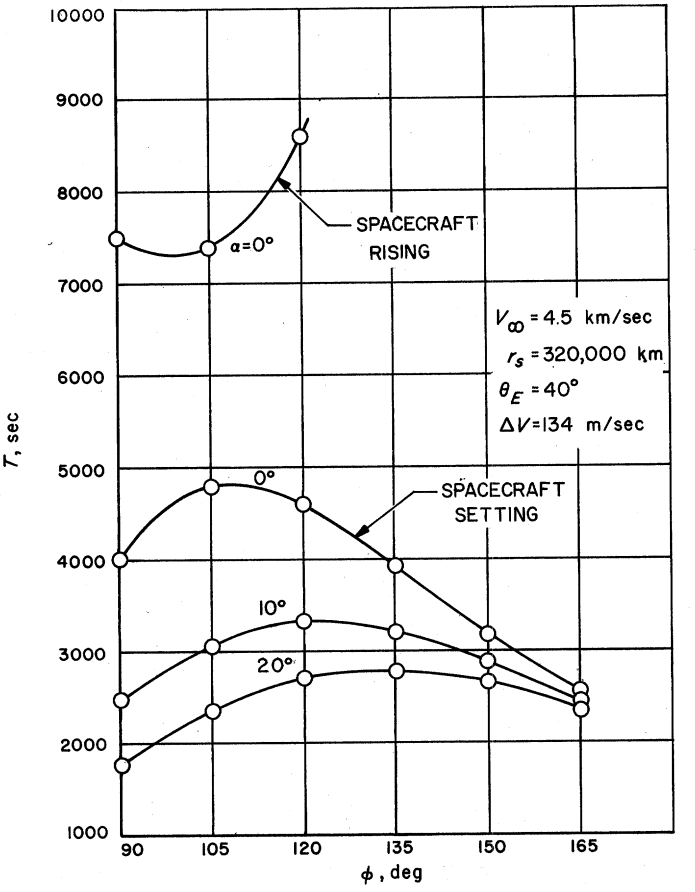

Figure 65. Mars split-capsule trajectories—effect of impulse direction on "eclipse" time for a 40-deg entry angle

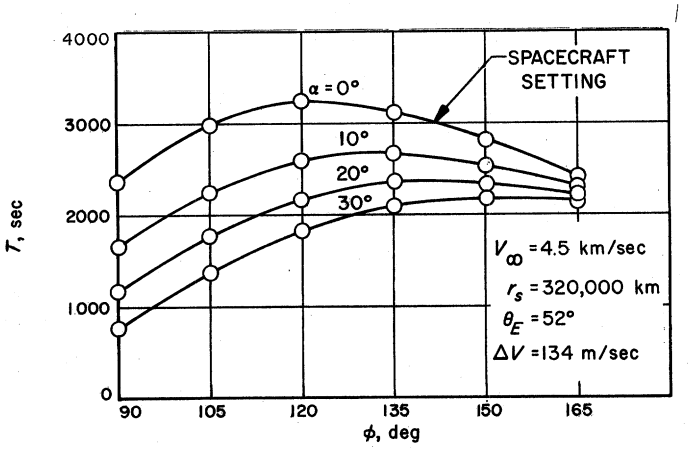

Figure 66. Mars split-capsule trajectories—effect of impulse direction on "eclipse" time for a 52-deg entry angle

UNCLASSIFIED

2. Entry Dynamics and Heating

E. POUNDER

(This Section is UNCLASSIFIED)

a. Entry-Maneuver Description and Philosophy

(1) Guidelines

The role of the entry capsule in the over-all *Mariner B* mission has two basic aspects. First, the capsule carries a major fraction of the Mars-oriented scientific experiments; and second, it provides an opportunity to obtain engineering information on the Martian atmosphere which will materially upgrade the designs of the *Voyager* landers to follow.

To make this role a practical one, several guidelines must be followed. These are:

(a) The interface between capsule and spacecraft must be a very simple one and cannot compromise the spacecraft performance in any basic way.

(b) The basic philosophy of the entry design should be simple and passive, should be based on existing technology, and should contain no advanced-development elements.

(c) The design must be carefully and realistically correlated with the rather sketchy information available on the Mars atmosphere. Every attempt to improve the atmosphere model should be made, but dependence on such improvements for mission success would be unwise.

(d) The possible abort modes in the atmosphere should be evaluated, and the system should provide data-recovery under abort conditions.

At the time of this Report, it is believed that technical compatibility with guidelines (1), (2), and (3) has been reasonably demonstrated. The abort situation has not been considered to date but must be clearly understood before final decisions regarding the mission are made.

(2) Entry and Landing Description

The entry and landing plan can be described briefly as follows: The capsule separates from the spacecraft at about 400,000 km from the planet on a trajectory designed to hit the atmosphere as indicated in Section IIIC-1. Thereafter, it proceeds toward the planet in a passive manner for about 24 hr. A communication link will probably be maintained with the spacecraft, but no experiments will be conducted and no data transmitted. It appears probable that no attitude control will be required.

The capsule will contact the planet with an entry angle of about 40 deg and a velocity of about 22,000 ft/sec. (This is the full orbital velocity at the planet, since no retromaneuver external to the atmosphere is contemplated.) The capsule attitude will be controlled primarily, if not completely, by aerodynamic forces so that the heat shield is oriented properly to the flight path. Thereafter, a nonlifting ballistic type entry will be experienced. A heat pulse and a deceleration pulse of about 10-sec duration will occur, dissipating essentially all the kinetic energy of the capsule with respect to the planet. During this period, the body will move in an almost straight line and will exhibit a moderately damped pitching motion. Accelerometer data and, hopefully, pressure and temperature data will be taken to obtain specific knowledge of the upper atmosphere. At the very end of this phase, the capsule will reach transonic velocities (about 1000 ft/sec), and the pitching motion may become divergent, depending critically on the final design. In such a case a drogue parachute or some other stabilizing device will have to be deployed. The time interval for the entire entry phase will be about 70 sec.

The capsule will decelerate to a velocity of 750 ft/sec at an altitude of about 60,000 ft. At this velocity, the current concept calls for the deployment of a large parachute which will decelerate the package further to 75 ft/sec. At the same time, the heat shield—or a major portion of it—will be jettisoned to expose the vidicon and other equipment. The parachute descent will require 15 to 20 min, and during this period the experiments requiring large information-transmission rates will be performed. The package will contact the surface vertically at about 50 ft/sec, unless significant surface winds are encountered.

The capsule will land on some final energy-absorbing structure, and the parachute system will be detached. No attempt will be made to orient the package on the ground except as required to accommodate the transmitting antenna. The remainder of the high-rate data will be sent to the spacecraft and some low-data-rate nonoriented experiments will be performed. Data transmission will continue for 16 hr through one Martian night. Within the dispersion of the selected landing point, the spacecraft may set below the capsule's horizon for a period of several hours, but this will not occur before the high-data-rate transmission is complete.

UNCLASSIFIED

(3) Feasibility

As mentioned above, the technical feasibility of the capsule seems to be on firm ground, and the following discussion documents this in some detail. It is interesting here to compare the mission with other similar cases; Table 26 shows several projects prominent in the United States programs.*

Entry velocity V_E, entry *angle* θ_E, and ballistic coefficient m/C_DA, or the definitive vehicle parameters and reciprocal scale height β and reference density ρ_0' characterize the atmosphere. Table 26 indicates that, in terms of these quantities, the *Mariner B* case is close to those of both *Mercury* and *Discoverer*, so that much of the R&D effort for these projects is applicable. Maximum deceleration is higher but still well within design capability, and heating rate is comparable. The heating problem is further simplified by the steeper entry angle which reduces exposure time and, thus, total heat-shield weight.

Also tabulated are the Venus-entry and lunar-return cases, which share the entry spotlight with *Mariner B* in the JPL program. Note that both of these missions require higher values of V_E, which increases deceleration and heating markedly. Also the radiative "gas-cap" heating becomes important, complicating the heat-shield design. Thus, these cases, along with the *Apollo* program, embody increased performance requirements and should be considered second-generation designs.

*H. M. Schurmeier, "Summary of Activities of Interest to the NASA Committee on Missile and Space Vehicle Aerodynamics," Jet Propulsion Laboratory, Pasadena, Calif.; unpublished memo, January 30, 1961.

Table 26. Comparison of typical entry situations

	JPL			Mercury	Apollo	Discoverer XIII
	Mars hyperbolic (Mariner B)	Venus hyperbolic (C-2)	Lunar return hyperbolic			
V_E, ft/sec	22,000	40,000	36,000	26,000	36,000	26,000
θ_E, deg	40 to 90	15 to 90	90			4
W, lb	300	1000	30	2200	6000	350
m/C_DA, slugs/ft^2	1	3.5	3 to 4	2		2
β, 1/ft	2.4×10^{-5}	4.8×10^{-5}	4.3×10^{-5}	4.3×10^{-5}	4.3×10^{-5}	4.3×10^{-5}
ρ, slugs/ft^2	4×10^{-4}	6×10^{-2}	2.7×10^{-3}	2.7×10^{-3}	2.7×10^{-3}	2.7×10^{-3}
$(v/g_E)_{max}$	43 to 67	100 to 435	320	10	10	11
$(q_s)_{max}$, Btu/ft^2/sec	202 to 280	3×10^4 to 8×10^4	like Venus	200		250
Ablation weight/ total weight	0.035 to 0.043	0.20 to 0.30				
Convective heat transfer	probably laminar	turbulent	turbulent			
Radiative heat transfer	no	yes	yes	no	yes	no
Corridor or approach accuracy, mi	+500	200 to 300	?	a few	a few	a few
Range control (lift)	no	no	no	no	yes	no
Landing scheme	parachute	parachute	parachute or balloon	parachute	parachute or glider	parachute
Heat shield weight/ total weight, lb[a]	0.085 to 0.075	0.30 to 0.55				

[a]Including structure.

UNCLASSIFIED

b. Criteria for the Entry Maneuver

(1) Guidelines

In discussing the mission described above the major constraints on the capsule entry maneuver must be considered. Guidelines may be listed as follows:

(a) Major objectives

1. The spacecraft to pass the planet on the lighted side at a reasonably close miss distance (say, less than 10,000 mi).
2. The capsule to enter the atmosphere and land without on-board guidance or propulsion after separation from the spacecraft.
3. Communication to be maintained between capsule and spacecraft for a significant period of time after atmospheric entry—specifically, line of sight through the first half of the planetary day.
4. Communication to be undisturbed by capsule deceleration and atmospheric ionization.
5. The capsule attitude to be controlled at entry in some manner.
6. The spacecraft not to be eclipsed by Mars as seen from Earth.

(b) Major initial constraints

1. Dispersion of the approach trajectory after approach corrections (1-σ value about 200 mi).
2. Amount of impulse which can realistically be applied to the fly-by maneuver ($\Delta V \simeq 100$ ft/sec).
3. Distance from the planet at which the maneuver can be made (about 250,000 mi).

(2) Dispersion in Entry Parameters

In order to select a landing point for design purposes, the dispersions in the approach trajectory must be converted into dispersions in the entry parameters. Specifically, the functions $V_E(V_\infty)$, $\theta_E(V_\infty, S)$, and $\Phi(V_\infty, S)$ are needed. The first is simply

$$V_{E_I}^2 = \frac{2K}{r_E} + V_\infty^2$$

from which

$$\Delta V_{E_I} = \frac{\Delta V_\infty}{\left(\frac{2K}{V_\infty r_E^2} + 1\right)^{1/2}}$$

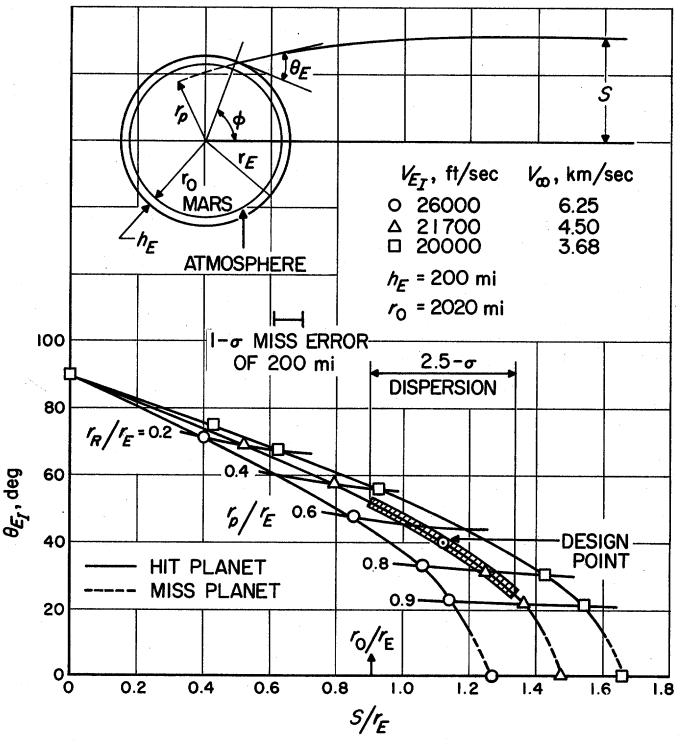

Figure 67. Entry angle vs miss distance, Mars

Figures 67 and 68 show θ_{E_I} and Φ plotted vs S/r_E for various approach velocities.

The current approach-parameter dispersions are (2.5-σ values) ± 500 mi for error in S and ± 250 ft/sec for error in V_∞. The corresponding error in V_E is ± 170 ft/sec for $V_\infty = 4.5$ km/sec and $V_E = 21{,}700$ ft/sec for $V_\infty = 6.6$ km/sec. This is a very small error and plays no significant role in the entry study.

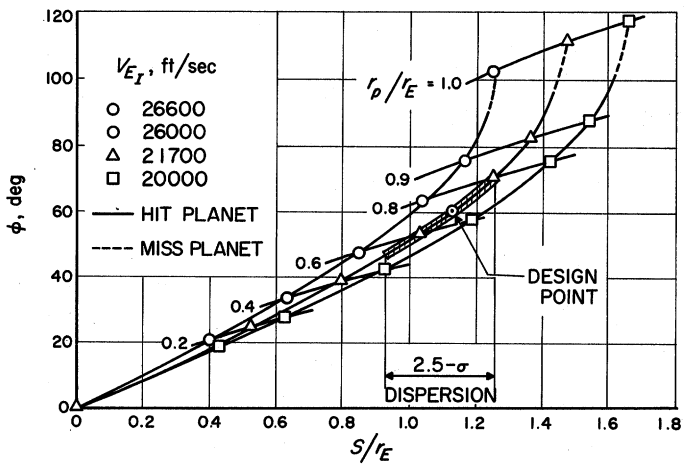

Figure 68. Central angle vs miss distance, Mars

UNCLASSIFIED

UNCLASSIFIED

From the Figures, it is clear that the dispersions in θ_{E_I} and Φ are functions of the landing point selected and are quite significant. In fact, the design entry angle was picked from these charts to provide a landing point as far around the planet on the fly-by side as possible, without appreciable chance of missing the planet. The values selected for the study and corresponding 2.5-σ dispersions are shown in Table 27.

At $h = 200$ mi, the planetary rotational velocity is about 1300 ft/sec; therefore, the quoted values must be changed by a small but significant amount when making any detailed studies of the atmospheric trajectories.

Table 27. Approach- and entry-parameter summary

Parameter	Nominal value	Dispersion 2.5 σ
V_∞, km/sec	4.5	$\pm 3.1 \times 10^{-2}$
S/r_E	1.12	± 0.225
V_{E_I}, ft/sec[a]	21,700	± 170
θ_{E_I}, deg[a]	40	24 to 52
Φ, deg	60	79 to 45

[a]Given in inertial coordinates.

c. Martian Environment

The purpose of the mission under consideration is the study of the physical makeup of the Martian atmosphere and surface. An unfortunate corollary is that the first entry-vehicle design will be based on estimates of physical properties from astronomical observations only and from analyses of these data aided by terrestrial experience. The success of the mission depends heavily on the interpretation of the information, however meager; thus, every effort must be made to understand it correctly.

(1) The Atmosphere

An initial attempt has been made to formulate an atmosphere model for design purposes, based on published information. The model in its current form is included in the first Addendum to this Section. It represents a good first approach, but can and should be significantly upgraded by further study.

A model of this kind must present nominal values and error estimates. Some of the important parts of both will be summarized here for quick reference.

Composition. 97% N_2 with small amounts of CO_2, water, and argon.

Temperature. 240°K on the surface, with significant variations due to diurnal, seasonal, and latitude effects; 175°K in the stratosphere, with small variations due to uncertainties in the radiation balance. The distribution with altitude assumes an adiabatic lapse rate to the stratosphere temperature. There is probably an excursion to lower temperatures at the tropopause which has been ignored here, but should be considered in refining the model further.

Pressure. 90 millibars at the surface, with a 5 to 10% dispersion.

Density. 2.48×10^{-4} slugs/ft^3, with altitude distribution based on the temperature assumptions. The isothermal upper atmosphere allows the use of an exponential density relationship for entry design analysis, as defined in Addendum 1. Within the limitations of the isothermal approximation, the density dispersion can be expressed in terms of β, the reciprocal-scale height.

For the entry analysis, the parameters which appear explicitly are

$$\beta = \frac{gM}{RT}$$

and

$$\frac{\rho_0'}{\beta} = \frac{p_0}{g}$$

Since g and M are relatively well known, the errors in β and ρ_0'/β are due to errors in T and ρ_0, respectively. For purposes of the present study, the following is assumed:

$$\frac{\Delta\beta}{\beta} = \pm 0.15$$

$$\frac{\frac{\Delta\rho_0'}{\beta}}{\frac{\rho_0'}{\beta}} = \pm 0.09$$

The realism of these values is hard to assess here and should be studied further. The value for β contains a 10% pad to account for errors in the isothermal assumption.

(2) Surface

The information available on Martian surface conditions falls almost completely in the realm of speculation, and any landing design must be based on the most general assumptions at this time. Desirable information from the engineering point of view includes:

(a) Winds near the surface; magnitudes and variation with time, latitude, and altitude

(b) Texture and density of the surface and microscopic terrain features

(c) Amount of dust in the atmosphere

UNCLASSIFIED

UNCLASSIFIED

It must be assumed that design constraints in relation to these features will have to be based on theory, comparison with experience on Earth, and common sense, and that no significant data can be obtained prior to landing, or until a close flyby can be made with suitable experiments on board. This situation is a prime factor in the decision to orient the capsule experiments to the parachute-descent period.

d. Entry Performance

(1) Trajectories

To aid in the study of the Martian entry, a series of trajectories have been computed and are presented in plotted form in Figs. 69 through 76. The computations are based on the following assumptions:

(a) The planet rotates with a period of 24 hr 37 min, and the atmosphere rotates with it like a solid body.

(b) Mars physical values are taken from *Space Technology.**

(c) The capsule enters the equatorial plane in the direction of rotation.

(d) The stratosphere part of the atmosphere model is used so that

$$\rho = 4.09 \times 10^{-4}\, e^{-2.37 \times 10^{-5} h}$$

The lapse rate near the surface is not included.

(e) A point source body under drag only is considered; no lift or angular motion is included.

(f) No variation of $m/C_D A$ is included, and the parachute effects are ignored.

Three variables are considered; θ_{E_I}, V_{E_I} and $m/C_D A$. Figures 69 through 72 show the effect of θ_{E_I} in the range of the design dispersion. Figures 73 through 76 illustrate V_{E_I} effects.

The nominal value of $m/C_D A = 1$ slug/ft² used here has been selected to meet several prime constraints. First, a sufficiently low value must be picked to assure subsonic speeds at a reasonable altitude for the deployment of the parachute. Second, the value must be compatible with weight and size numbers that are practical. Third, the

*H. S. Seifert, Editor, *Space Technology*, John Wiley & Sons, New York, 1959, pp. 8–10.

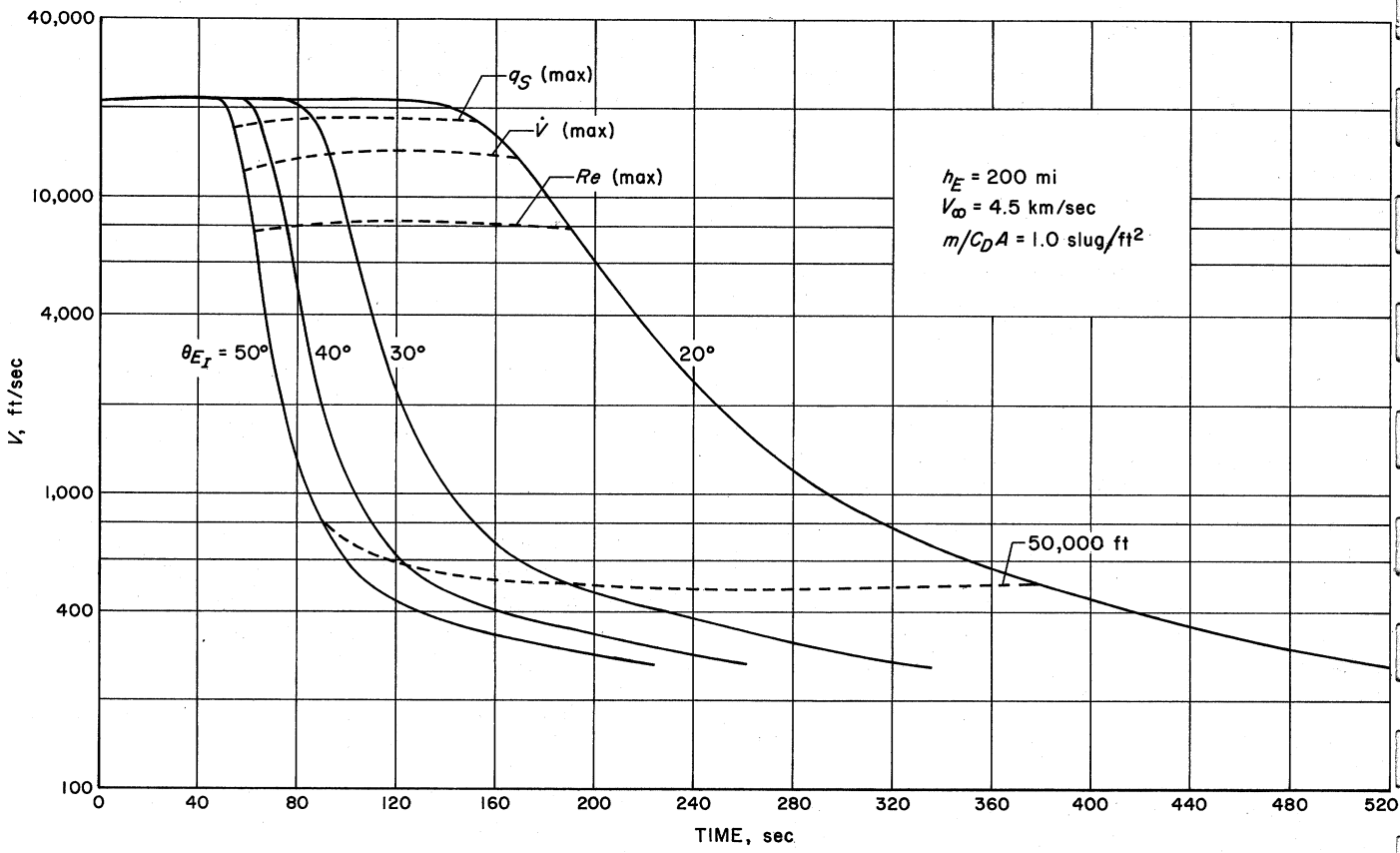

Figure 69. Mars entry, velocity history—effect of entry angle

UNCLASSIFIED

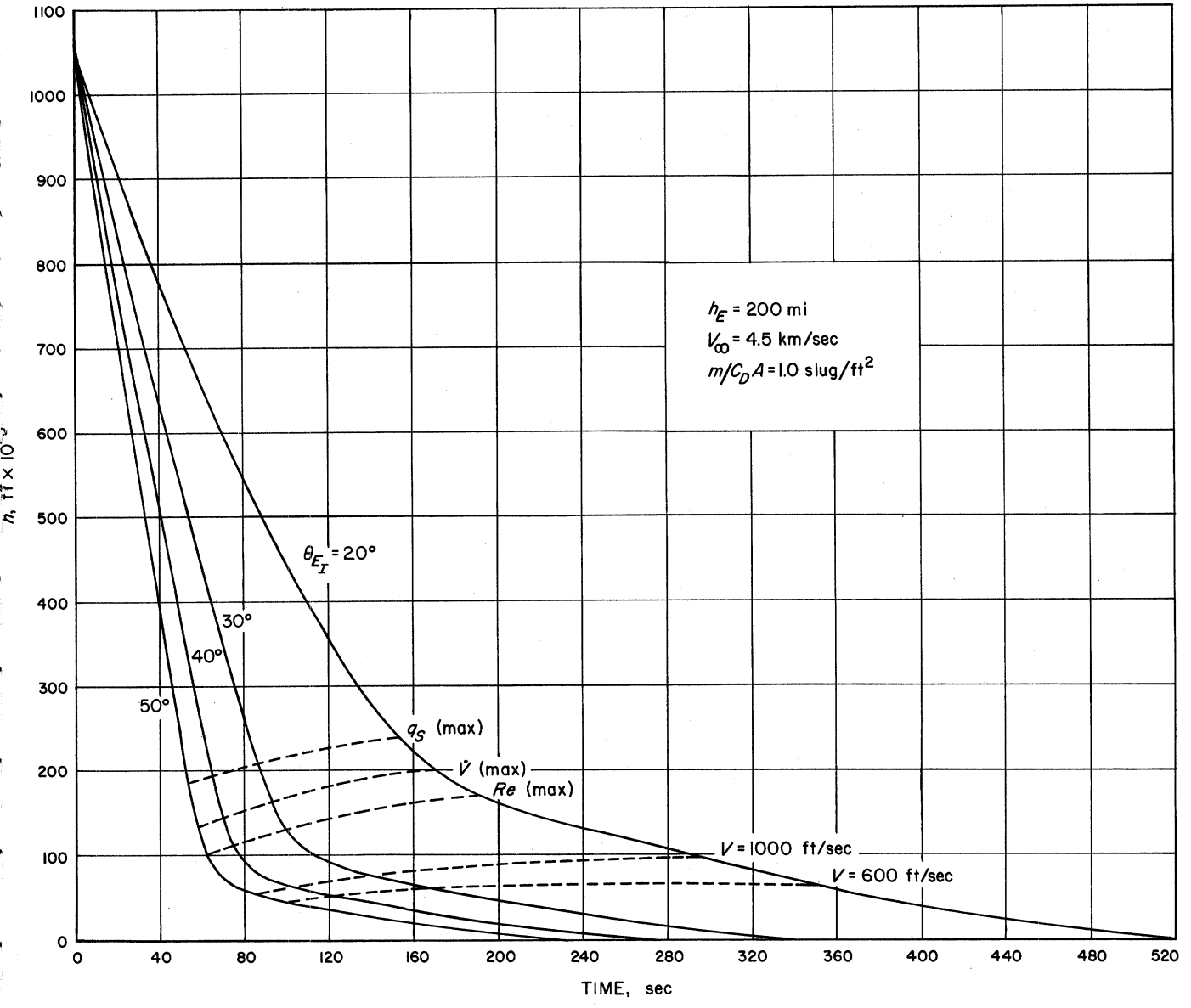

Figure 70. Mars entry, altitude history—effect of entry angle

value of C_D must be suitable for the shape of body desirable from an aerodynamic-stability point of view. And finally, the value must not be so low that buckling modes design the structure, since such a situation increases structural weight considerably. Suitable values for these quantities are:

$$\left.\begin{array}{r}\text{Earth weight} = 300 \text{ lb} \\ \text{diameter} = 4 \text{ ft} \\ C_D = 0.8\end{array}\right\} \text{giving } \frac{m}{C_D A} = 0.93$$

A variation of ±20% about the nominal ballistic-coefficient value does not affect the results of Figs. 69 through 76 to any significant extent. Dispersions due to atmospheric errors will be considered later at appropriate points. The interested reader can quickly evaluate them for himself from the analysis of the paper by Allen and Eggen.*

A quick look at the Figures reveals several important facts:

(a) The atmosphere begins to affect the motion at about 500,000 ft.

*H. J. Allen and A. J. Eggen, "A Study of the Motion and Aerodynamic Heating of Missiles Entering the Earth's Atmosphere at High Supersonic Speeds," NACA TN 4047, 1957.

UNCLASSIFIED

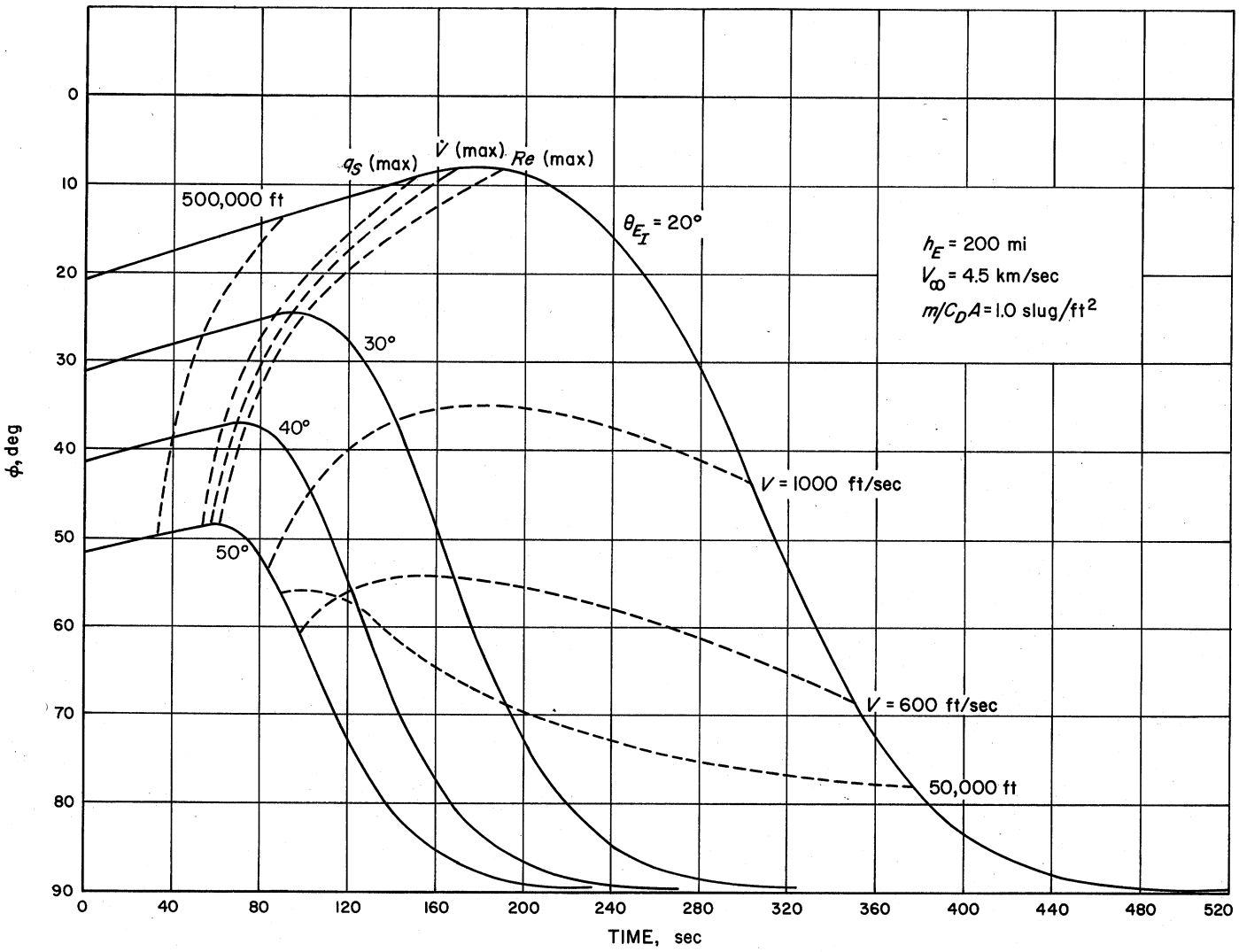

Figure 71. Mars entry, path-angle history—effect of entry angle

(b) The effects at θ_{E_I} are quite important over the dispersion range considered, whereas velocity and ballistic coefficient influences are very small.

(c) The parachute deployment, which should occur between 1000 and 600 ft/sec, is in a band of altitudes between 50,000 and 100,000 ft (above the model tropopause), so that the isothermal assumptions should give reasonable results to the deployment point. Parachute deployment at these altitudes should satisfy the mission requirement.

(d) The path angle at the time of deployment is about 50 deg and has a weak dependence on θ_{E_I}.

(e) The time from 500,000 ft to parachute deployment varies from 1 to 4 min with θ_{E_I}.

Remember that the velocities shown at the surfaces are incorrect because of the assumptions listed above. A typical value can be derived as follows:

$$V_0 = \sqrt{\frac{2g}{\rho_0}} \sqrt{\frac{m}{C_D A}}$$

Assume $C_D = 0.5$ (subsonic value), such that $m/C_DA = 2$ slugs/ft².

$$g = 13.16 \text{ ft/sec}^2$$

$$\rho_0 = 2.48 \times 10^{-4} \text{ slugs/ft}^3$$

Therefore,

$$V_0 = \sqrt{\frac{4\,(13.16)}{2.48 \times 10^{-4}}} = 460 \text{ ft/sec}$$

UNCLASSIFIED

UNCLASSIFIED

(2) Loading (Heating and Decelerations)

Aerodynamic loading on the capsule can be described in terms of the following quantities as functions of time:

(a) Laminar-stagnation-point convective-heat-transfer rate Q_s

(b) Total heat transferred—the integral of (1)

(c) Reynolds number

(d) Deceleration along the flight path

(a), (b) and (c) are inputs for the heat-shield design and (d) for the structural design. (Pressure distributions can easily be related to the acceleration.) Figures 77 through 85 are plots of these quantities for the same variables used for the trajectory results and for a 20% variation in m/C_DA.

Significant conclusions are:

(a) A maximum laminar-heating rate of about 240 Btu/ft²/sec is shown. This maximum is close to the nominal value for $\theta_{E_I} = 40$ deg.

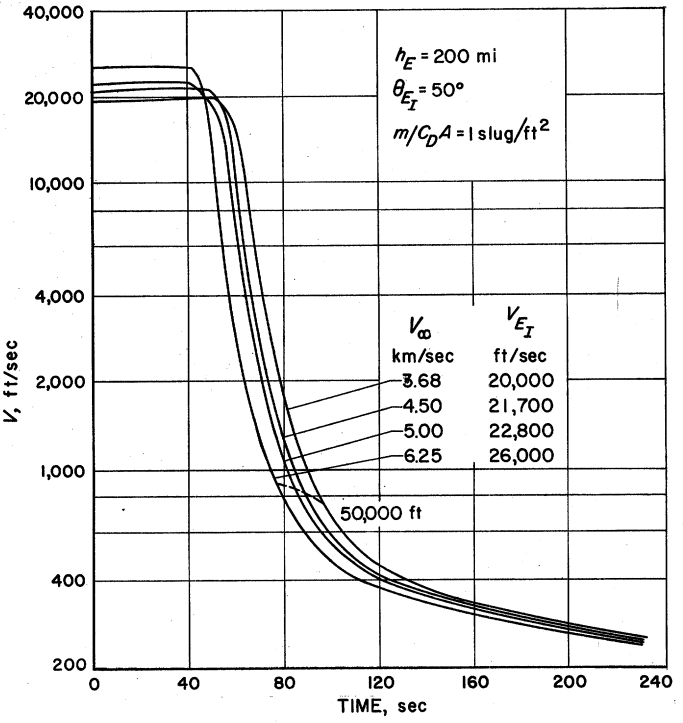

Figure 73. Mars entry, velocity history—effect of entry velocity

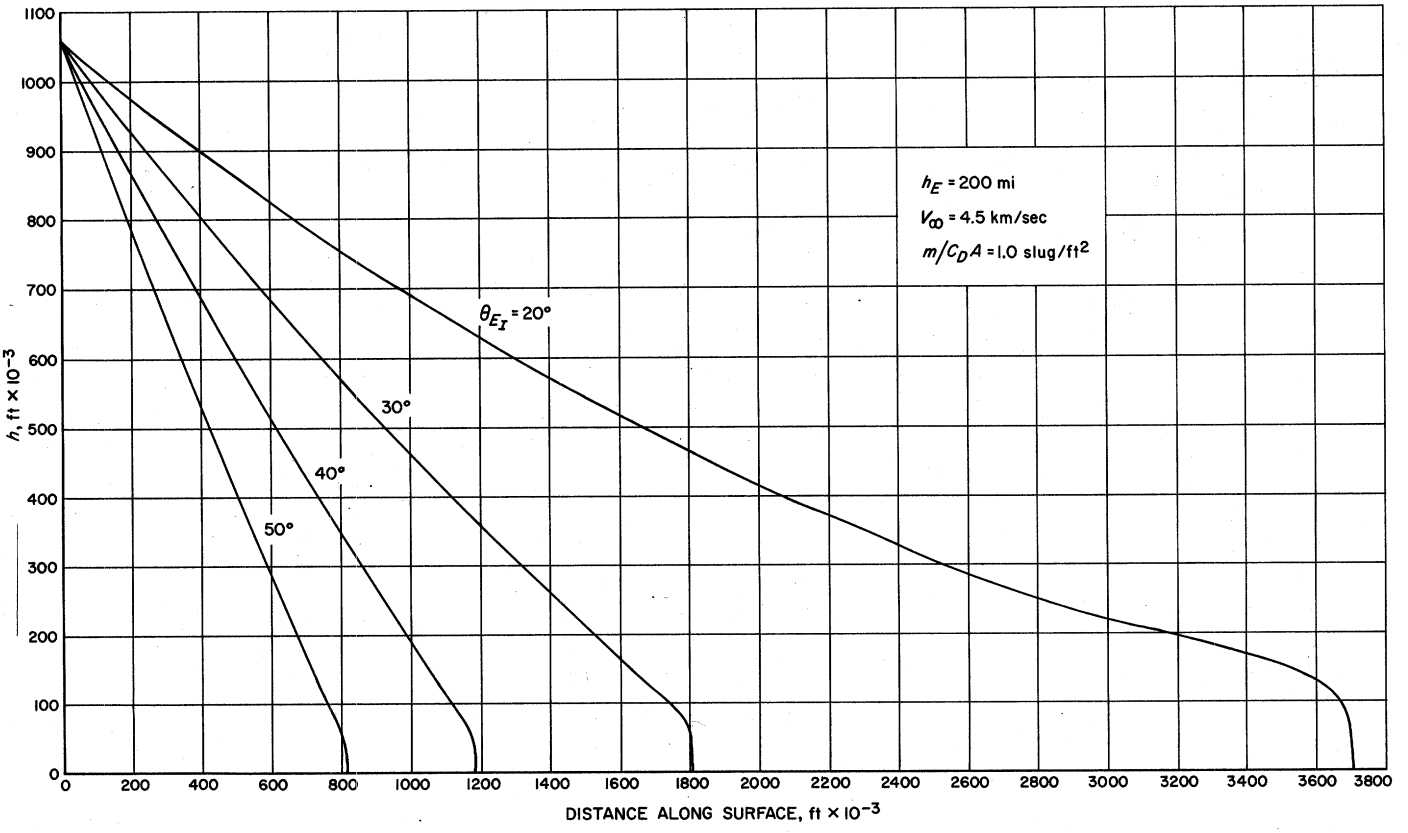

Figure 72. Mars entry, trajectory geometry—effect of entry angle

UNCLASSIFIED

UNCLASSIFIED

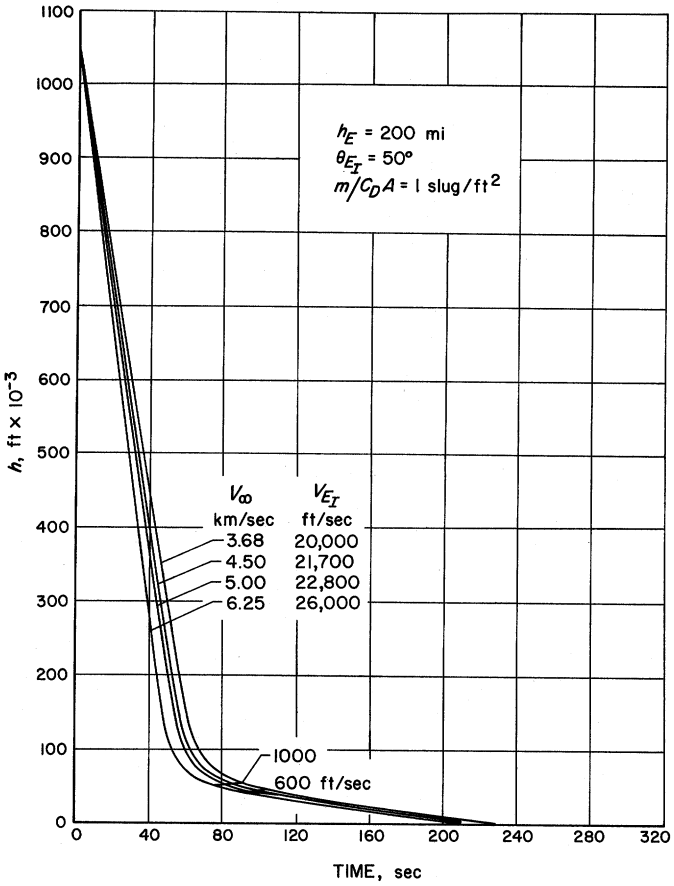

Figure 74. Mars entry, altitude history—effect of entry velocity

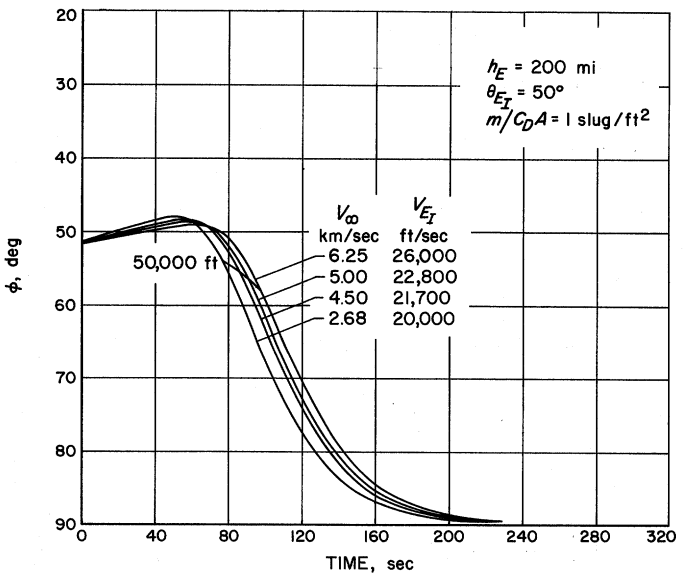

Figure 75. Mars entry, path-angle history—effect of entry velocity

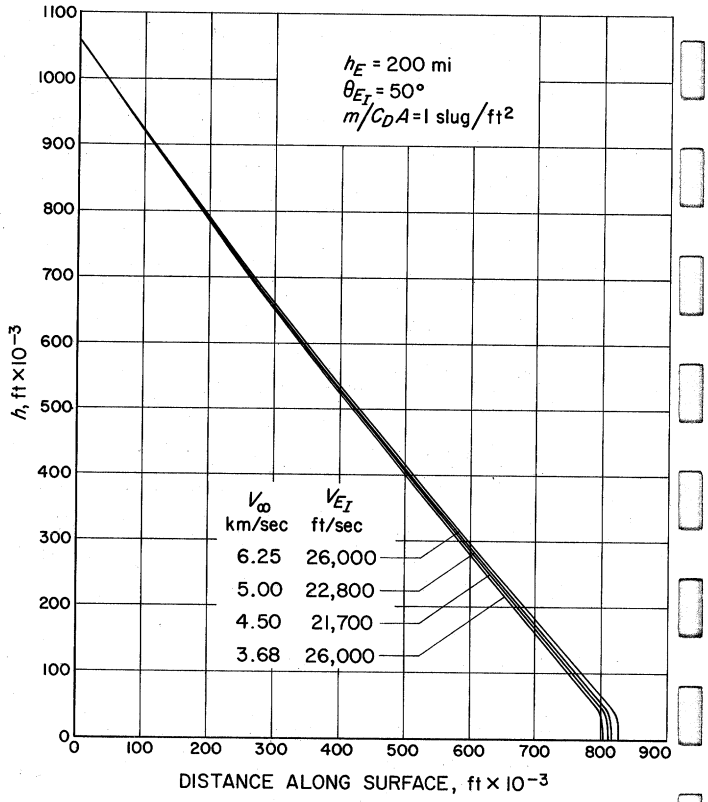

Figure 76. Mars entry, trajectory geometry—effect of entry velocity

(b) The total heat to be absorbed is a maximum for the shallowest entry, and is considerably above the value for 40 deg.*

(c) The Reynolds number controls the boundary layer transition and therefore fixes the heating rates (much higher for turbulent flow). A detailed analysis of Reynolds-number effects has not yet been made, but the possibility of laminar flow over at least some of the entry dispersion is good. The plots indicate that this would tend to occur towards the lower entry angles (lower *Re* at maximum heating); thus, some compensating effect to (2) may exist.

(d) Maximum deceleration is about 50 Earth *g*'s corresponding to a pressure loading on the projected frontal area of about 1300 lb/ft².

(e) The radiative gas-cap heating mode has not been analyzed in detail. However, it can be demon-

*These values of heating rates and total heat load are sufficient to show that a low-temperature ablating material will probably provide a minimum heat-shield weight.

UNCLASSIFIED

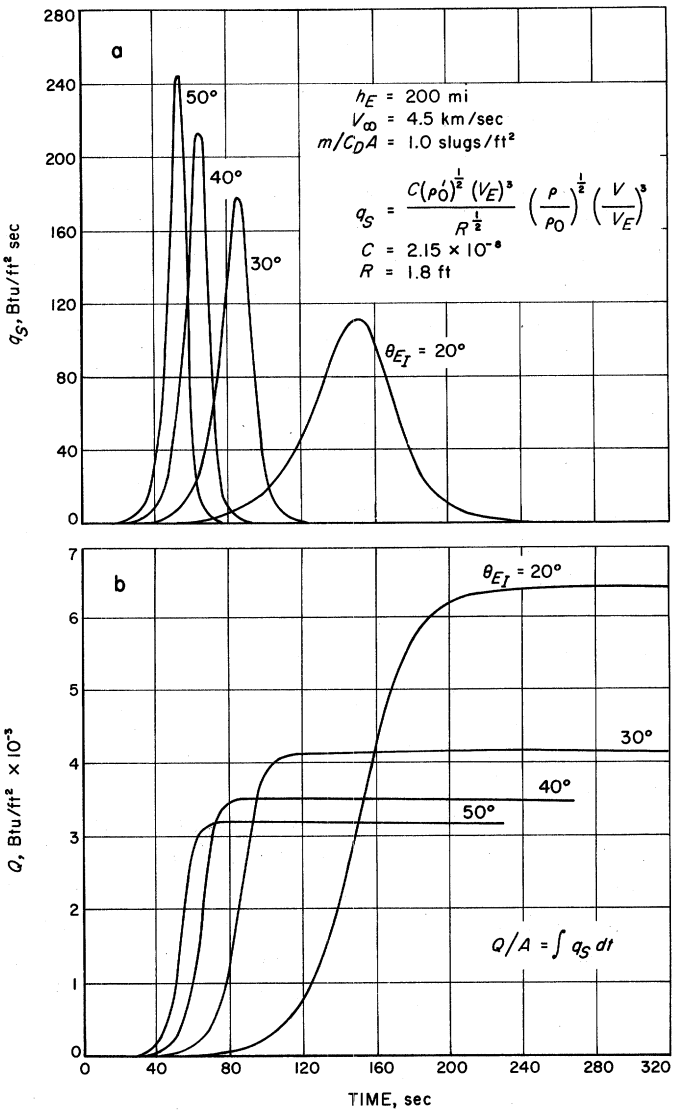

Figure 77. Mars entry, heating rate and total heat—effect of entry angle

strated to be quite small. If Lee's expression* is developed in the manner of Allen and Eggen,** the following equations result:

$$q_{R_{\max}} = 0.133R\left(\frac{\beta}{4.8\,\rho_0'}\frac{m}{C_DA}\frac{\sin\theta_E}{e}\right)^{1.3}\left(\frac{V_E}{10^4}\right)^{12.5}$$

$$\frac{V_{R_{\max}}}{V_E} = e^{-1/9.6}$$

$$h_{R_{\max}} = \frac{1}{\beta}\ln\left(\frac{4.8\,\rho_0'}{\beta}\frac{C_DA}{m}\frac{1}{\sin\theta_E}\right)$$

*Seifert, *op. cit.*, pp. 12–15.

**Allen and Eggen, *op. cit.*

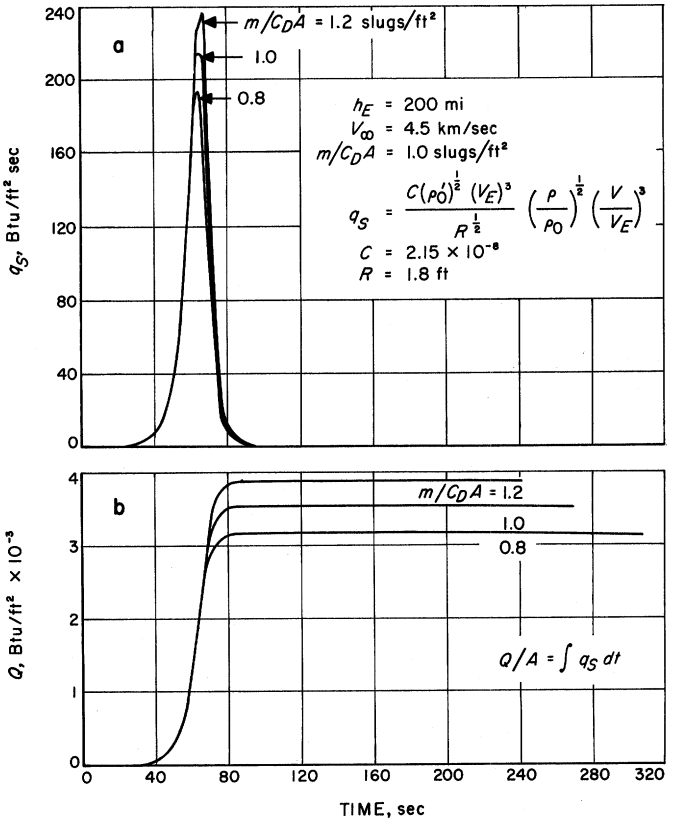

Figure 78. Mars entry, heating rate and total heat—effect of ballistic coefficient

As an example, let $V_E = 21{,}700$ ft/sec, $\theta_E = 52$ deg, $R = 1.5$ ft, then

$$q_{R_{\max}} = 2.2 \text{ Btu ft}^2/\text{sec}$$
$$V_{R_{\max}} = 19{,}500 \text{ ft/sec}$$
$$h_{R_{\max}} = 199{,}000 \text{ ft}$$

This shows that the radiation-heating maximum occurs at about the same time as the convective mode but is two orders of magnitude less for the case under consideration.

(3) Entry Dynamics and Stability

For the trajectories described above, the capsule was assumed to be a body acted upon by drag and gravity forces only. In reality, of course, both generalized forces and torques will be experienced, and the vehicle will undoubtedly perform pitching motions, although it will be trimmed to fly at zero lift. The constraints on this motion are as follows:

(a) The capsule must have on board an absolutely minimal active attitude-control system; preferably, none at all.

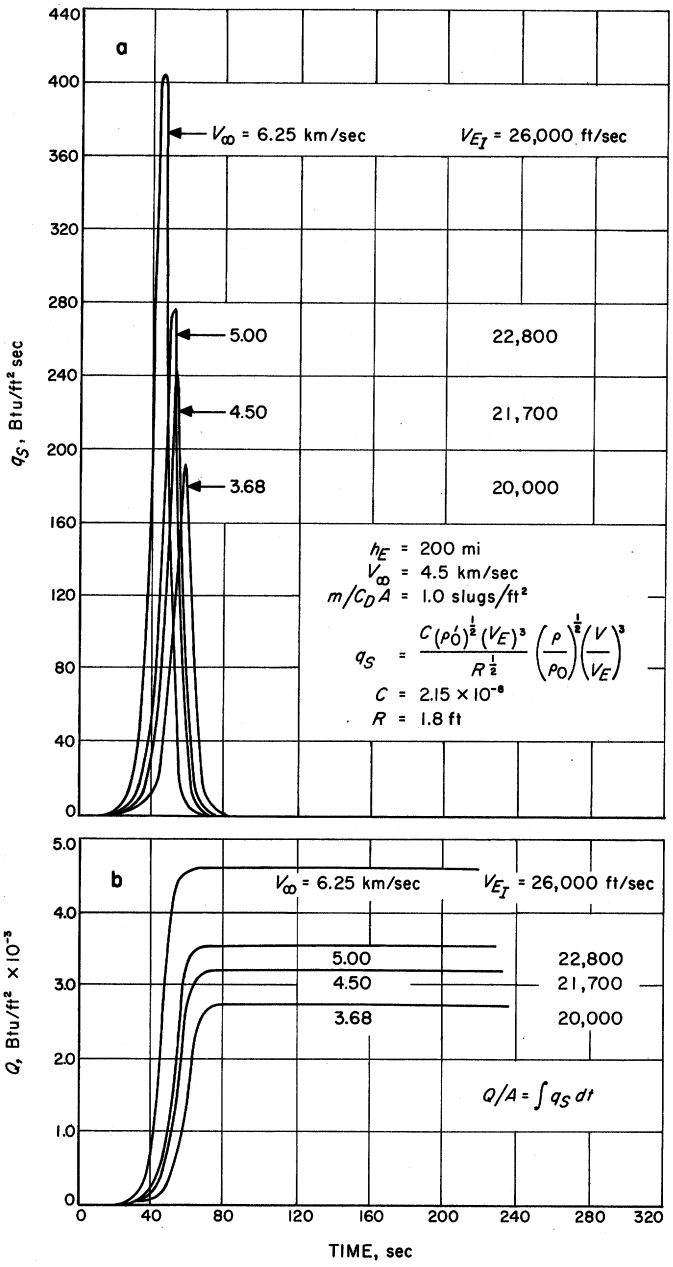

Figure 79. Mars entry, heating rate—effect of entry velocity

(b) The pitching motion during the heating pulse should not degrade the heat-shield design by more than a small percentage.

(c) The motion should be damped through most of the flight in the atmosphere, and if divergence cannot be completely prevented, it should be postponed until a Mach number of about 1.5 is reached.

The first point to be considered can be emphasized by asking the question: Can the capsule shape be designed so that the capsule will orient itself along the flight path from an arbitrary attitude and tumbling rate before atmospheric heating occurs? The capsule is released from the spacecraft about 22 hr before entry; hence, without on-board control there is no chance of maintaining an initial attitude. It is expected that a tumbling rate of 1 to 5 deg/sec will be generated by the separation, so that the capsule will hit the atmosphere with this same slow tumbling motion and at an arbitrary angle of attack anywhere between 0 and 180 deg. The reduced frequency of this motion, $\omega D/V \simeq 2 \times 10^{-5}$, is so small that no effect of the motion itself is to be expected. Only about half a revolution can occur between the onset of aerodynamic forces and the heating peak.

Therefore, the study resolves itself into a consideration of an arbitrary angle of attack. A preliminary study of this consideration has been made by Brofman* and will be summarized here. A body is represented by a sinusoidal moment curve,

$$C_m = C_{m_{\max}} \sin \alpha$$

$$C_{m_\alpha}(\alpha = 0) = C_{m_{\max}}$$

and with $C_L = 0$ (no lateral force) and no damping. The motion has been computed by an analog method, and the result can be summarized as follows: Let ϕ_D be the value of the oscillation envelope at divergence which occurs at the point of maximum acceleration for zero damping, and let ϕ_E be the angle of attack for entry. Then it is shown that a single function exists:

$$\frac{\phi_D}{\phi_E} K^{1/4} = f(\phi_E)$$

where

$$K = -\frac{C_{m_{\max}} \left(\frac{D}{\sigma}\right)^2}{DC_D \beta \sin \theta_E}$$

a static stability parameter > 200. Allen** gives the equivalent linearized result as

$$\frac{\alpha_D}{\alpha_E}\left(\frac{k_2}{k_0}\right)^{1/4} = \frac{e^{1/4}}{\sqrt{\pi}} = 0.725$$

*W. Brofman, "Tumbling Entry Analog Study," Jet Propulsion Laboratory, Pasadena, Calif.; unpublished memo.

**H. J. Allen, "Motion of a Ballistic Missile Angularly Misaligned with the Flight Path Upon Entering the Atmosphere and Its Effect Upon Aerodynamic Heating, Aerodynamic Loads, and Miss Distance," NACA TN 4048, 1957, Eq. 17d.

UNCLASSIFIED

UNCLASSIFIED

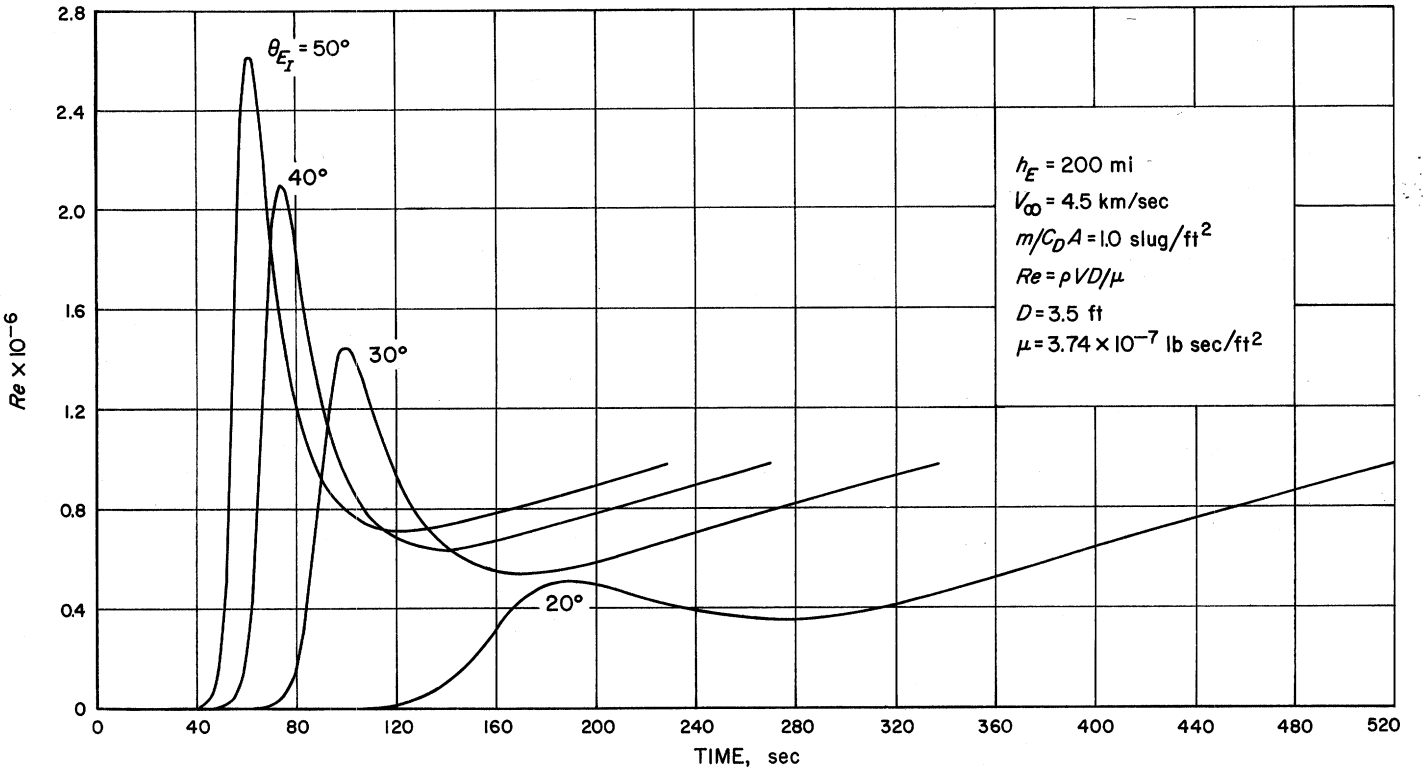

Figure 80. Mars entry, Reynolds number—effect of entry angle

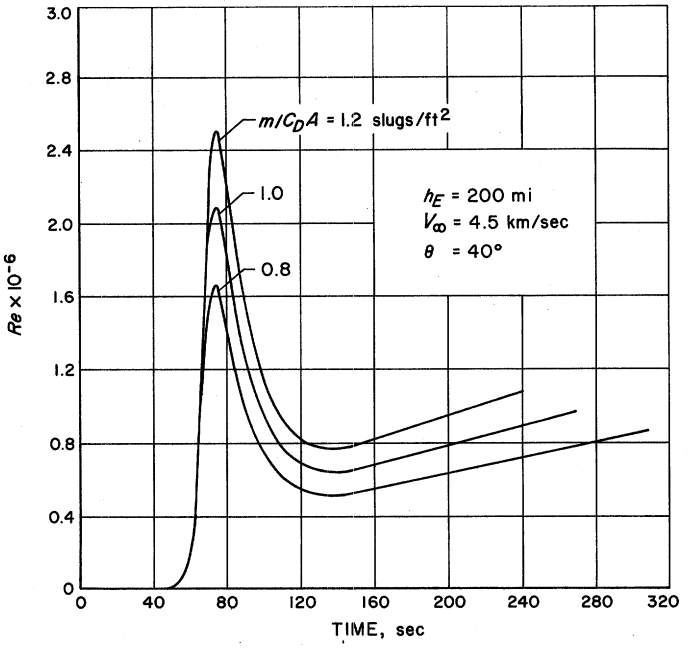

Figure 81. Mars entry, Reynolds number—effect of ballistic coefficient

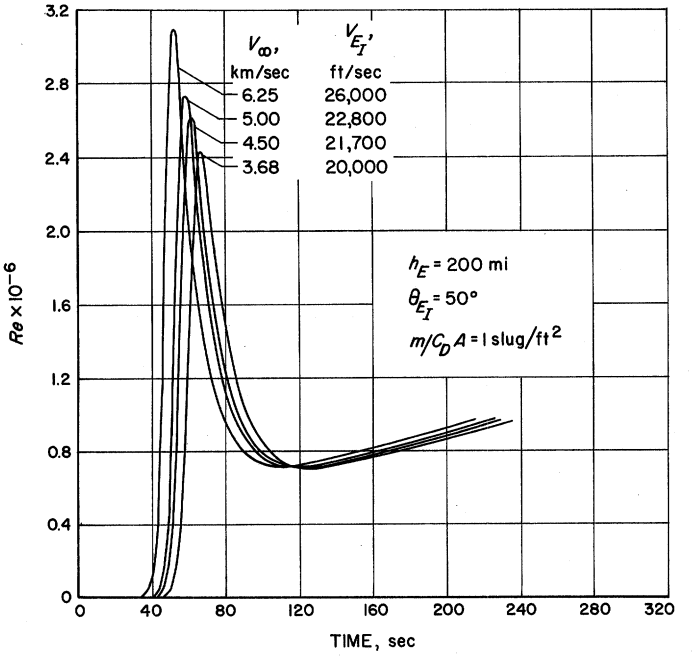

Figure 82. Mars entry, Reynolds number—effect of entry velocity

UNCLASSIFIED

UNCLASSIFIED

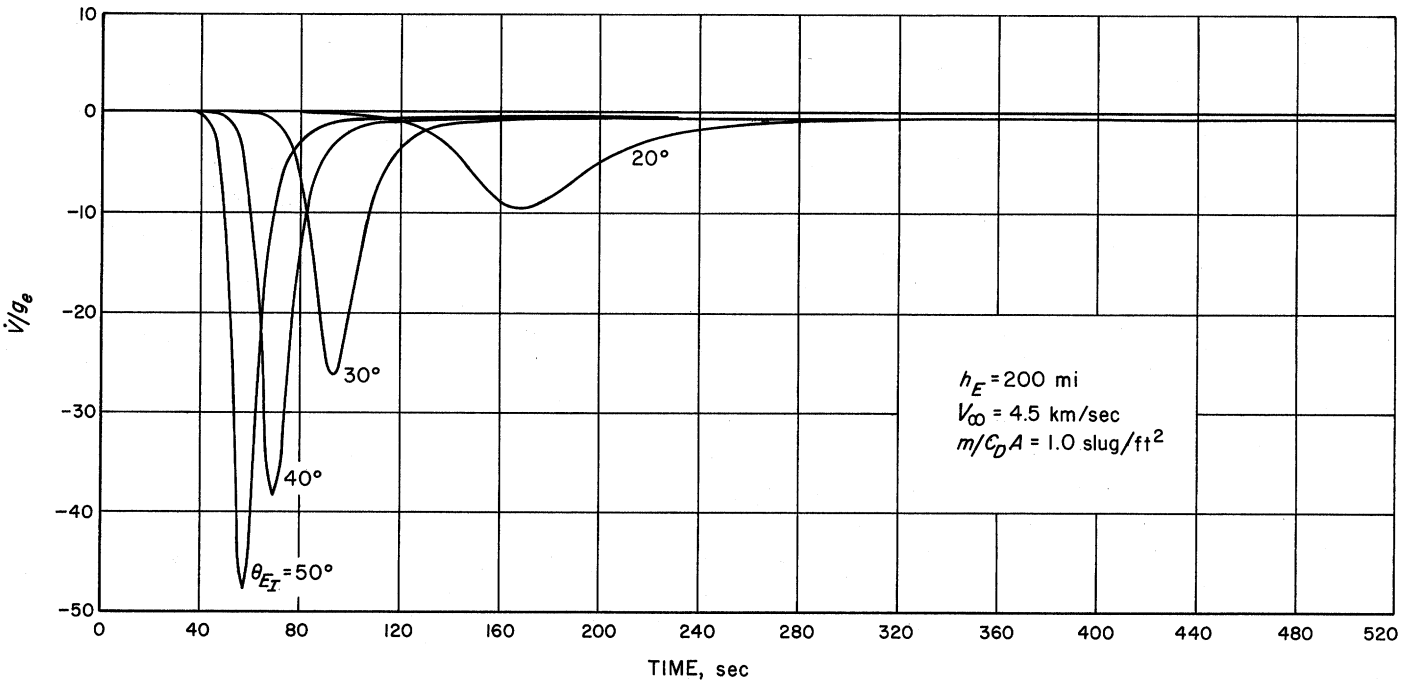

Figure 83. Mars entry, deceleration—effect of entry angle

where

$$\frac{k_2}{k_0} = -\frac{C_{m_\alpha}(\alpha = 0)\left(\frac{D}{\sigma}\right)^2}{2DC_D\beta \sin\theta_E} = \frac{K}{2}$$

Therefore, the analog result can be presented as

$$\frac{\frac{\phi_D}{\phi_E}}{\frac{\alpha}{\alpha_E}} = 1.64f(\phi_E)$$

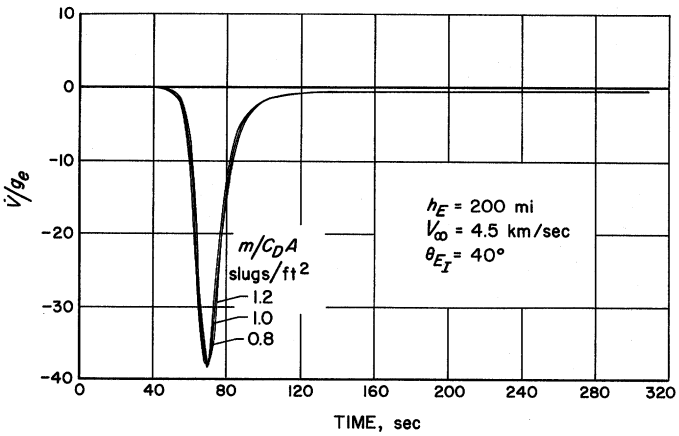

Figure 84. Mars entry, deceleration—effect of ballistic coefficient

This is shown in Fig. 86 for $0 \leqq \phi_E < \pi$.*

To show what this means to the present study, an example is given here: Let

$$C_{m_{\max}} = C_{m_\alpha}(\alpha = 0) = -0.2$$

$$\left(\frac{D}{\sigma}\right)^2 = 8$$

$$C_D = 0.8$$

$$D = 4 \text{ ft}$$

$$\beta = 2.37 \times 10^{-5}/\text{ft}$$

$$\theta_E = 40 \text{ deg}$$

then $k^{1/4} = 13.4$ and $\alpha_D/\alpha_E = 0.064$ at maximum deceleration. Fig. 86 shows that for 99% of the ϕ_E range,

$$\frac{\phi}{\phi_E} < \frac{2\alpha}{\alpha_E} < 0.128$$

Therefore, ϕ at maximum deceleration will be less than 23 deg for the example. The theory shows that ϕ at maximum heating is about 10% higher than ϕ at maximum deceleration for the zero-damping case, so that as a final result,

$$(\phi_{\max})_{\substack{\max \\ \text{heating}}} < 25 \text{ deg}$$

*The single curve cannot apply at $\phi_E = \pi$, since $\phi_D/\phi_E = 1$ here but correlates well to 179 deg.

UNCLASSIFIED

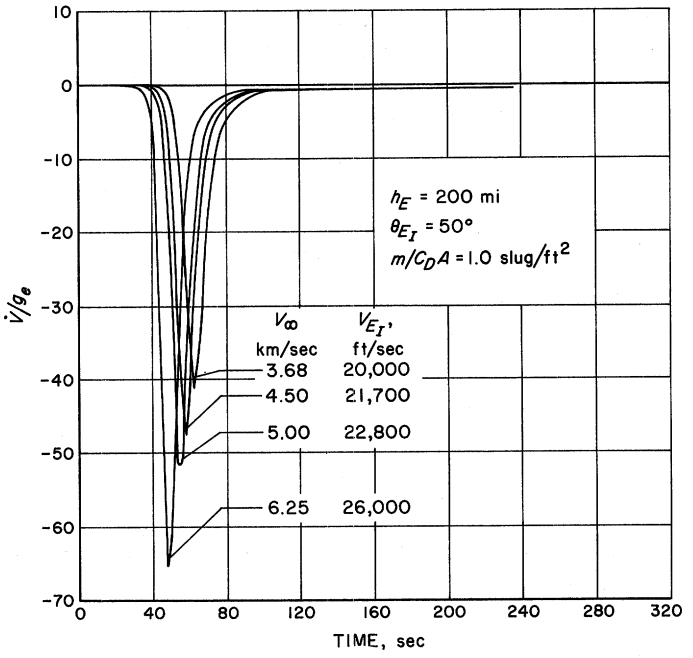

Figure 85. Mars entry, deceleration—effect of entry velocity

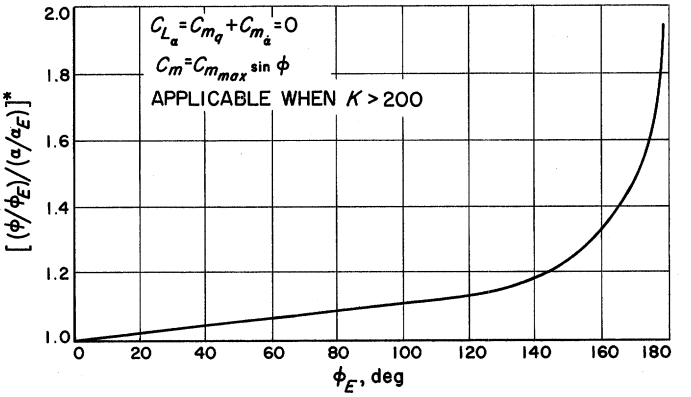

Figure 86. Entry-attitude-envelope function for large entry angles

for 99% of the entry attitudes. It is thought that this amount of motion will not degrade the heat-shield design appreciably, but a detailed analysis of the effect remains to be made. Also, of course, the motion analysis will have to be extended to bodies with lift and damping. Therefore, the conclusion presented here should be considered as encouraging to the uncontrolled entry, but not final.

(4) Other Methods of Entry Control

As alternates to the dependence on aerodynamic forces for initial attitude control, three other modes have been considered. They are:

(a) Spin-stabilization, with spinup at the time of capsule separation and de-spin, if necessary, just before entry.

(b) A one-axis attitude-control system using a Sun sensor and cold-gas reaction jets.

(c) A spherical-capsule configuration with a nondirectional heat shield and structure and c.g. offset.

The spin-stabilization technique has been studied in general terms,* and results can be stated as follows. The concept calls for separation from the spacecraft when in the cruise Sun-oriented attitude, so that the roll axis of the capsule is aligned in the Sun direction. This will correspond to a nominal value of $\alpha_{E_I} = 25$ deg with a dispersion from 40 to 12 deg. The capsule is spun to a selected rotational speed at release and is *not* de-spun before entering the atmosphere. Some de-spin may be necessary before parachute deployment, but this can be accomplished by aerodynamic devices. Thus, the method requires no on-board attitude control.

The envelope for the atmospheric motion of the vehicle can be described by the equation

$$\frac{\alpha(s)}{\alpha(s=0)} \simeq \sqrt{\frac{\frac{\pi a}{2}}{\tanh\frac{\pi a}{2}}}$$

where

$$a = \frac{\zeta}{\beta V_E \sin\xi \sin\theta_E}$$

ζ = tumbling rate created by separation

ξ = half-cone precession angle

s = spin rate

$$s = \frac{I_p}{I_z}\frac{\zeta}{\sin\xi}$$

and $\alpha(s=0)$ is taken from the paper by Allen.**

As an example, let $\alpha_E = 40$ deg and

$$\left.\frac{\alpha}{\alpha_E}\right|_{\substack{\max\\ \text{heating}}} = 0.06$$

*J. Lingerfelt, "Dynamic Considerations for a Spin-Stabilized Planetary Entry Capsule," Jet Propulsion Laboratory, Pasadena, Calif.; unpublished memo.

**H. J. Allen, *op. cit.*

UNCLASSIFIED

Then $\alpha|_{\text{max heating}} = 2.4$ deg; hence a value of $[\alpha(s)]/[\alpha(s=0)] = 4$ would be acceptable. From this value, a can be computed to be

$$a = 10$$

Let

$$\beta = 2.37 \times 10^{-5}/\text{ft}$$

$$V_E = 21{,}700 \text{ ft/sec}$$

$$\theta_E = 52 \text{ deg}$$

$$\xi = 5 \text{ deg}$$

$$\frac{I_z}{I_p} = 1.1$$

Then, an acceptable tumbling rate can be computed as $\zeta = 0.35$ rad/sec $\simeq 20$ deg/sec and the required spin rate is $s = 3.64$ rad/sec $\simeq 210$ deg/sec $= 35$ rpm.

Since separation tumbling rates of less than 5 deg/sec are realistic, it appears that very modest spin rates would be required to achieve control, and therefore the method should be considered as a practical alternate to the aerodynamic-oriented mode. One practical constraint is that I_z/I_p must be greater than, but close to, 1.0 for a good design. This assures damping of the precession if internal energy dissipation is present without increasing the stability parameter a unduly.

The other two alternates have not been studied in detail but, in view of the above analyses, definitely appear to be second choices. The Sun-sensor system appears feasible and has been estimated to weigh less than 15 lb but requires considerable additional mechanization on the capsule. The nondirectional approach is, in reality, a generalization of the aerodynamic attitude control and would require considerable weight penalty in heat shield and structure. Therefore, these approaches will not be discussed further but are simply presented as possibilities for the preliminary design.

(5) Dynamics During Entry

As mentioned previously, Allen* presents a definitive linearized analysis of the pitching motion during entry. No attempt will be made to summarize the results here, but the form of the motion and the parameters which influence it will be indicated.

The theory assumes that the aerodynamic coefficients are constant over the range of interest and that the weight of the body can be neglected when compared with the aerodynamic forces. Under these assumptions, three dimensionless parameters govern the motion:

(a) Trajectory parameter

$$k_0 = \frac{C_D A}{m} \frac{\rho_0'}{\beta \sin \theta_E}$$

(b) Dynamic-stability parameter

$$k_1 \simeq \frac{k_0}{4}\left[1 - \frac{C_{L_\alpha}}{C_D} + \frac{C_{m_q} + C_{m_{\dot\alpha}}}{C_D}\left(\frac{l}{\sigma}\right)^2\right]$$

(c) Static-stability parameter

$$k_2 = \frac{-k_0}{2\beta \sin \theta_E} \frac{C_{m_\alpha} l}{C_D \sigma^2}; \qquad k_2 > 0$$

Using these quantities, the motion can be clearly defined by three equations:

(1) Velocity relation

$$\frac{V}{V_E} = e^{-(k_0/2)e^{-\beta h}}$$

(2) Angle-of-attack envelope

$$\left(\frac{\alpha}{\alpha_E}\right)^* = \frac{e^{k_1 e^{-\beta h} + (\beta h/4)}}{\sqrt{\pi (k_2)^{1/4}}}$$

(3) Frequency

$$\frac{2\pi\omega}{\beta V_E \sin \theta_E} = \frac{V}{V_E}(k_2)^{1/2} e^{-\beta h/2}$$

The results show that during the entry, a rather slow, damped pitching oscillation will develop and will continue through heating and probably through maximum loading. At some altitude, defined by the equation $h = 1/\beta \ln(4k_1)$, a minimum amplitude will occur, and divergence will take place. (If divergence is to be avoided, k_1 must be less than ¼, but such a value may be difficult to achieve and is not really necessary.) After divergence starts, it will continue as the capsule decelerates to sonic speed. At this point, the analysis is no longer applicable because the aerodynamic coefficient will no longer be invariant. The frequency of the motion will increase to a maximum at the maximum loading point and will then decrease throughout the remainder of the motion, independent of the dynamic stability.

To illustrate the dynamics for the Mars capsule, a numerical example is presented here. The pertinent functional relationships are listed in Addendum 2, so that variations from the example can readily be studied.

*H. J. Allen, *op. cit.*

UNCLASSIFIED

The example inputs are:

$$C_{L_\alpha} = C_{m_q} + C_{m_{\dot\alpha}} = 0 \qquad \left(\frac{l}{\sigma}\right)^2 = 8$$

$$C_{m_\alpha} = -0.2 \qquad l = 4 \text{ ft}$$

$$C_D = 0.8 \qquad \theta_E = 52 \text{ deg}$$

$$\frac{m}{C_D A} = 1.0 \qquad V_E = 21{,}700 \text{ ft/sec}$$

These are suitable and technically feasible values. Then,

$$k_0 = 22.0$$

$$\frac{k_1}{k_0} = 0.25$$

$$\frac{k_2}{k_0} = 1.34 \times 10^4$$

For $k_1/k_0 = 0.25$, divergence occurs at maximum loading; therefore, this represents a somewhat special case. Table 28 shows results for maximum heating, maximum loading, and near-sonic velocity.

Table 28. Typical quantities during capsule entry

Parameters	Maximum heating	V_{max} and divergence	Near-sonic velocity
h, ft	176,000	130,000	54,000
V, ft/sec	18,350	13,150	1085
$(\alpha/\alpha_E)^*$	0.0750	0.0674	0.151
ω, cps	3.65	4.52	0.55

It is clear that if a body can be developed with the aerodynamic coefficients indicated here and if the entry angles can be kept small (<30 deg), or if the tumbling can be controlled, then the behavior of the body to near-sonic velocities can be considered entirely feasible.

One other point regarding entry bears mention. The interior of the capsule will have to be vented so that the internal pressure can build up in a manner which creates no unmanageable temperature or pressure environments for the equipment. It is thought that this is a straightforward problem requiring no active control, but no detailed study has been made at this writing, and it should be checked out early in the design.

(6) Configuration

*(a) **Heat shield and structure.*** The heat-shield configuration has been studied from an over-all point of view. The following statements summarize results to date.

1. The shield should be of the ablating type and will use one of the so-called low-temperature ablators which sublimate without forming a liquid phase. Teflon and polyethylene are typical materials.
2. The most effective configuration uses a small thickness of material which actually ablates, more of the same material which acts as insulation without ablating, and the load-carrying structure which acts as a final heat sink. These layers are balanced so that the structural temperature does not exceed a design figure (nominally, 600°F). If necessary, the equipment can be protected from the 600°F surface by an aluminum-foil radiation shield or by individual shielding. Conduction problems have not been considered to date.

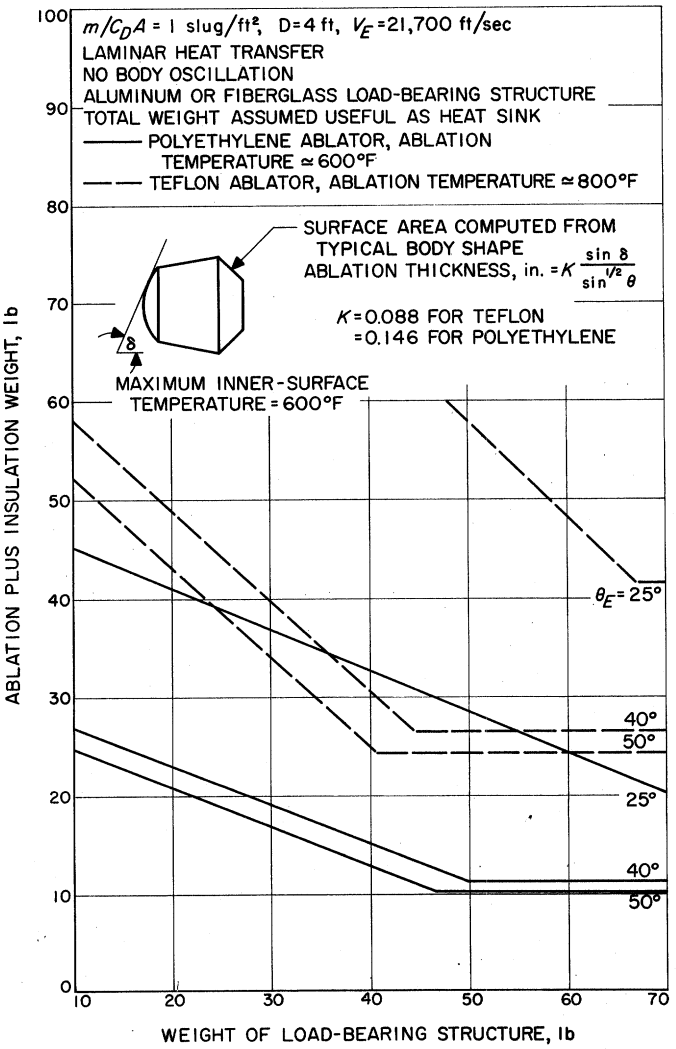

Figure 87. *Mariner B* entry capsule—heat-shield weights

3. Structural materials to take the aerodynamic loading have been studied only briefly. Aluminum and fiberglass are considered suitable from a heat-shield point of view, but a more detailed analysis will have to be made before final selection.

4. The effect of the entry-angle dispersion has been considered. Minimum weight corresponds to a 90-deg entry. The minimum angle applicable to heat-shield analysis is about 15 deg for the mission outlined here; this clearly involves a significant, but not prohibitive, weight penalty (see Fig. 87). Dispersion due to atmospheric properties and angle of attack have not yet been studied in detail. A preliminary estimate of atmosphere-dispersion effects is given in the general weight summary of Section IIIC-6.

5. Preliminary calculations show that the heat-transfer mode will be primarily laminar. However, the possibility of transition exists, and the effects of the subliming material are not clearly understood. A turbulent mode will again result in a requirement for more ablation material; hence, a further study is clearly indicated.

The weights calculated to date are summarized in Fig. 83. A preference for polyethylene is clearly indicated, and the effect of entry angle is shown.* A tabular comparison of possible ablation materials is shown in Table 29.

(b) Aerodynamic shape. Most of the previous discussion bears on the aerodynamic shape, but the major constraints will be listed here in summary as follows:

1. The size envelope is roughly a right-circular cylinder with a 4×4-ft dimension.

2. The drag coefficient has to be high enough to achieve a ballistic coefficient of about 1 slug/ft^2 with a weight of 300 lb.

3. The c.g. location must assure static stability $[C_{M_\alpha}(\alpha = 0) < 0]$ to the point of parachute deployment.

4. The body must be statically unstable near $\alpha_E = 180$ deg, so that a tumbling approach can be tolerated.

5. The lift-curve slope C_{L_α} should be greater than or equal to zero.

6. The dynamic-stability coefficient $C_{m_q} + C_{m_\alpha}$ should be less than zero if possible.

7. The base shape should be as flexible as possible, since both parachute cover and antenna may be incorporated into the base.

8. The forward-facing part of the body should not incorporate any very sharp corners because of the heat-shield requirements.

A detailed development of a shape to meet these requirements has been started, and specific results will be available for design. To indicate the general form, a shape is presented in Fig. 88 which theoretically performs correctly in the flight regime where modified Newtonian theory** can be used (higher Mach numbers). Experimental data found to date correlate reasonably well with the theory; it can be assumed that the final shape will resemble that shown here, unless other major constraints develop. The alternate base shapes shown produce about the same overturning moment and indicate that some latitude in the base shape is possible.

e. Final-Descent Performance

(1) Trajectory and Performance Requirements

The final-descent and landing performance is based on several requirements.

(a) A suitable period of time is to be provided for the major capsule experiments before landing.

(b) Landing velocity should be on the order of 50 ft/sec.

(c) Assuming a parachute is required, the opening shock loading should not exceed the entry loading.

*For details, see: J. M. Spiegel, "Design Study Graphs for Mars Atmospheric Entry Part II—Heat Shield Weights," Jet Propulsion Laboratory, Pasadena, Calif.; unpublished memo, October 1960.

For background literature, see:

Carl Gazley, Jr., "Atmospheric Entry of Manned Vehicles," Proceedings of the Manned Space Stations Symposium, Sponsored by the IAS with Cooperation of NASA and Rand, April 1960.

Leonard Roberts, "An Analysis of Ablation-Shield Requirements for Manned Re-entry Vehicles," NASA TR R-62, 1960.

M. C. Adams, "Recent Advances in Ablation," *ARS Journal*, Vol. 29, No. 9, September 1959.

M. C. Adams, William E. Powers, and Steven Georgian, "An Experimental and Theoretical Study of Quartz Ablation at the Stagnation Point," *Journal of Aero/Space Sciences*, July 1960.

Kenneth F. Stetson, "Deceleration and Heating of a Body Entering a Planetary Atmosphere from Space," Rand Report P-995, February 1957.

**J. D. Gray, "Drag and Stability Derivatives of Missile Components According to the Modified Newtonian Theory," AEDC-TN-60-191, November 1960.

Table 29. Typical low-temperature-ablation material characteristics[a]

Parameters	Teflon	Polycarbonate	Polyethelene	Fiberglass
Density ρ, lb/ft^3	131 to 144	75	57.5 to 59.5	112 to 122
Thermal conductivity k, Btu/ft sec °F	4.0×10^{-5}	3.1×10^{-5}	5.4×10^{-5}	4.2×10^{-5}
Specific heat c, Btu/lb °F	0.25		0.55	0.23
Ablation temperature T_a, °F	800	400	600	
$\rho k/c$	0.022		0.00575	0.0214
$(\rho k/c)^{1/2}(T_a - T_0)$	120		46	

[a]All materials considered to have good resistance to space vacuum and solar radiation.

(d) The descent should be approximately vertical and should not involve significant oscillating motion.

(e) Experiments should be constrained as little as possible by the capsule.

(f) The data-transmission system must operate at maximum bit rate during the descent period.

(2) Time to Descend

To illustrate the feasibility of meeting these constraints, the relation between time to descend and altitude must be known. Since the maneuver will begin somewhere near the tropopause, the function is presented here, assuming a constant lapse rate.

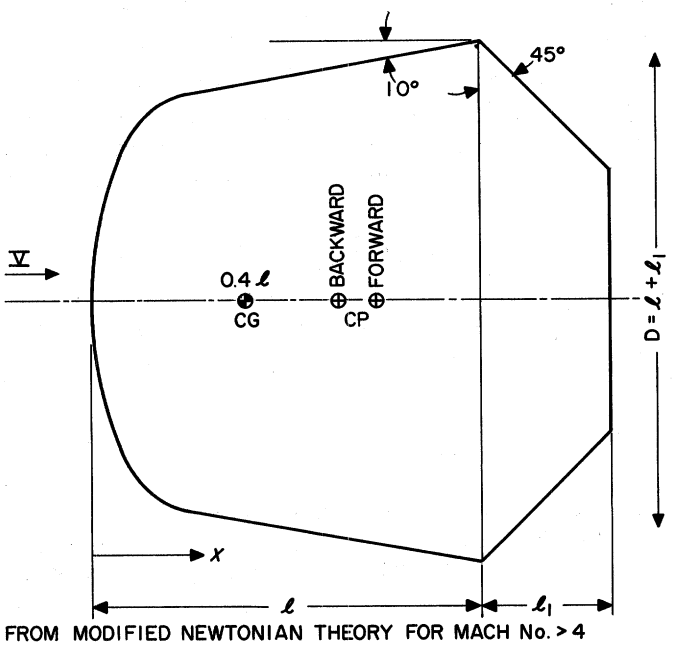

Figure 88. *Mariner B* typical-entry body configuration

For a vertical trajectory, the equation of motion is:

$$\frac{1}{\rho_0}\frac{dV^2}{dh} - \left(\frac{C_DA}{m}\right)_D \frac{\rho}{\rho_0}(h)\,V^2 + \frac{2g}{\rho_0} = 0$$

If a parachute is used, the first term of this equation is very small compared to the other two and can be neglected. Then the relation can easily be integrated to give:

$$V_0(t_0 - t_h) = \frac{1 - \left(1 - \frac{\Gamma}{T_0}h\right)^{\frac{(gM/R\Gamma)+1}{2}}}{\frac{\Gamma}{T_0}\frac{\frac{gM}{R\Gamma}+1}{2}}$$

and

$$\frac{V}{V_0} = \left(1 - \frac{\Gamma}{T_0}h\right)^{\frac{1-(gM/R\Gamma)}{2}}$$

These functions are plotted in Fig. 89 for the nominal Mars atmospheric values. Dispersions in Γ and T_0 will, of course, vary the result.

(3) Typical Parachute Design

The parachute must be chosen to give the proper terminal-velocity, opening-shock, and descent time, and the nominal altitude for deployment must be selected. The procedure required will be outlined briefly and numerical results given for the Mars case.

A probable selection for the main parachute is the Fist Ribbon Parachute.* It is somewhat heavier than other types but can be designed for higher opening speeds and is very stable (oscillations $< \pm 5$ deg).

*"United States Air Force Parachute Handbook," WADC TR 55-265, December 1956, p. 2-1-15.

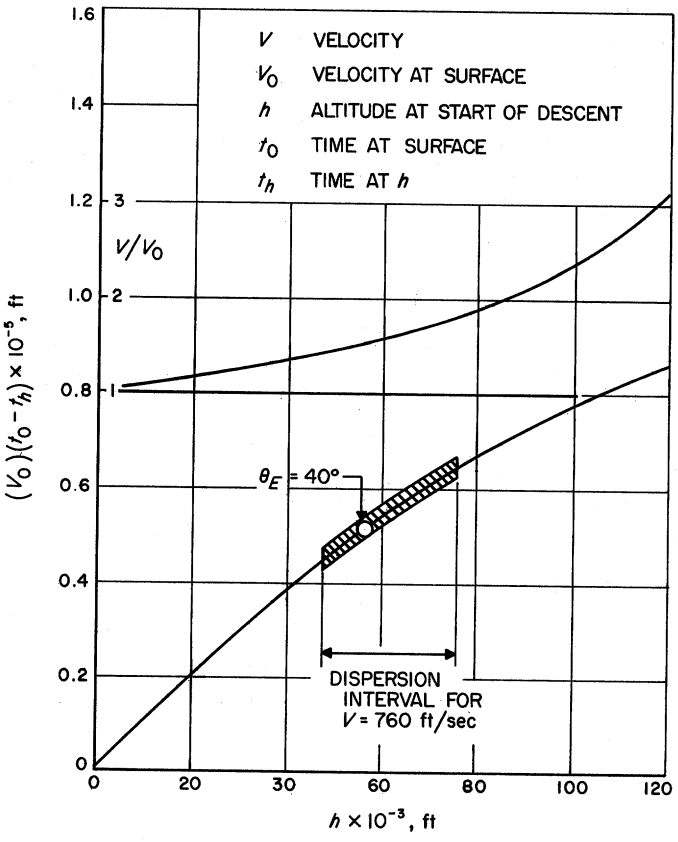

Figure 89. Time for a terminal-velocity descent on Mars

Two important design parameters, C_{D_s}/C_{D_p} and V_s/V_d must be selected. The first depends on parachute type and the second on type and opening performance.* The values for the capsule are

$$(C_{D_s}/C_D)_p = 1.05$$

$$V_s/V_d = 0.9$$

In terms of these quantities, a simple relation can be established between opening-shock loading and V_d/V_t:

$$\frac{\dot{V}_s}{g} = \frac{C_{D_s}}{C_D}\left(\frac{V_s}{V_d}\right)^2\left(\frac{V_d}{V_t}\right)^2$$

$$= 0.85\left(\frac{V_d}{V_t}\right)^2$$

Combining this with V/V_0 from the previous Section,

$$V_d = V_d\left(V_0, h, \frac{\dot{V}_s}{g}\right)$$

This function is plotted across the entry trajectories in Fig. 90 for two shock loadings, 50 and 35 Earth g's, and a surface terminal velocity of 50 ft/sec. A design point is chosen for a nominal parachute as shown in Fig. 90, and the results of this choice are shown in Table 30. The results demonstrate that such a design satisfies the performance requirements as presently understood.

Table 30. Final-descent quantities

Parameters	Design	Dispersion due to entry angle
Entry angle θ_E, deg	40	52 to 24
Deployment velocity V_d, ft/sec	760	—
Deployment altitude, ft	57,000	48,000 to 76,000
V_s/g_e	35	42 to 20
Time to land, min	17.3	14.4 to 21.7
Landing velocity, ft/sec	50	—

(4) Parachute Weight

For the terminal velocity at the surface of the planet, $(m/C_DA)_p = 0.0236$, which indicates a parachute of about 22.4-ft inflated diameter. The flat diameter $\simeq \sqrt{2}\,d = \sqrt{2} \times 22.4$ ft $= 31.9$ ft.

The Parachute Handbook* is the best source of weight information. To use this information, the Mars parachute must be scaled to an equivalent Earth parachute with the same mass, final velocity, and C_D. From this scaling,**

$$D_{e_p} = \frac{D_{m_p}}{1.99} = 16.0 \text{ ft}$$

The ribbon strength for the Earth parachute can be obtained from the Parachute Handbook.† Here,

$$\frac{F_0}{C_{D_0}A_0} = \frac{F}{W}\frac{m}{C_DA}g_e = 307 \text{ lb/ft}^2$$

This indicates that 400-lb ribbons are usable. The Earth weight, obtained from the Handbook,†† is 20 lb and the volume is 1500 in.^{3} Then, the Mars parachute should scale to

$$W_m = 16.2 \text{ lb}$$

$$V_m = 1220 \text{ in.}^3$$

*E. Pounder, "Parachute Inflation Process Wind-Tunnel Study," USAF TR No. 6117, GALCIT Report No. 536, April 1951.

**Ibid.*

***E. Pounder, "Basic Scaling Laws for Parachutes," Jet Propulsion Laboratory, Pasadena, Calif.; unpublished memo, March 1961.

†*Ibid.*, 5-3-3.

††*Ibid.*, 2-1-15.

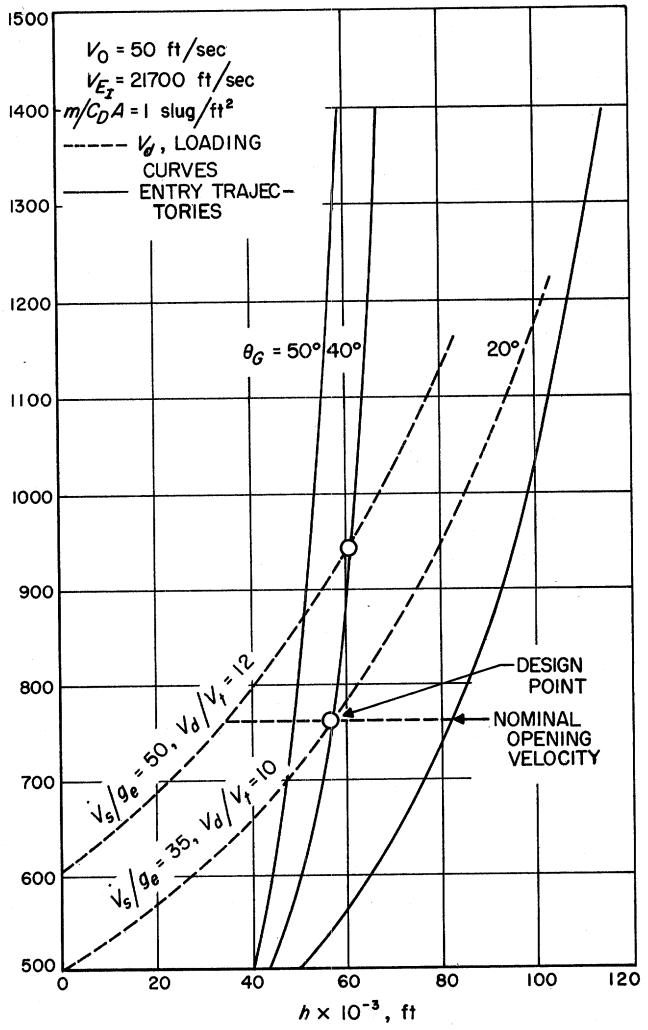

Figure 90. Parachute-opening load constraint

It would be wise to increase these numbers by 50% to account for loading uncertainties and the scaling problems.

Then, finally, the weight is 24.3 lb and the volume 1830 in.[3]

(5) Deployment Signal and Control

The parachute deployment on the capsule requires a guidance-and-control element to sense the proper conditions for deployment and carry out the maneuver. The basic problem is to determine the proper quantity to be sensed in order to minimize dispersion in velocity and altitude, including the effects of uncertainty in the atmosphere. The most straightforward approach is to consider the specific measurement of either velocity or altitude and determine the dispersion on the other.

Table 31. Errors for altitude-controlled parachute deployment

θ_E	$\left\lvert\frac{\Delta V}{V}\right\rvert_{\frac{\rho_0}{\beta}}$	$\left\lvert\frac{\Delta V}{V}\right\rvert_{\beta}$	$\left\lvert\frac{\Delta V}{V}\right\rvert_{h}$	$\left\lvert\frac{\Delta V}{V}\right\rvert_{\text{total}}$
24	0.316	0.950	0.634	1.185
40	0.313	0.705	0.470	0.903
52	0.315	0.599	0.399	0.786
90	0.301	0.477	0.318	0.648
θ_E	$\left\lvert\frac{\Delta q}{q}\right\rvert_{\frac{\rho_0}{\beta}}$	$\left\lvert\frac{\Delta q}{q}\right\rvert_{\beta}$	$\left\lvert\frac{\Delta q}{q}\right\rvert_{h}$	$\left\lvert\frac{\Delta q}{q}\right\rvert_{\text{total}}$
24	0.534	1.79	1.09	2.33
40	0.537	1.36	0.81	1.67
52	0.540	1.18	0.68	1.46
90	0 513	0.96	0.54	1.21

At the deployment point, the capsule is still decelerating fast enough so that the weight force can be neglected. Therefore, the errors can be studied by forming the derivative of the velocity function of the Allen and Eggen paper.* This can be written as

$$\frac{2}{H}\frac{dV}{V} - \frac{dV_E}{V_E} - \frac{d\frac{m}{C_DA}}{\frac{m}{C_DA}} + \frac{d\frac{\rho_0}{\beta}}{\frac{\rho_0}{\beta}} - \beta h\frac{dh}{h} + \frac{d\beta}{\beta} = 0$$

where

$$H = \frac{\rho_0}{\beta}\frac{C_DA}{m}\frac{e^{-\beta h}}{\sin\theta_E}$$

In general, errors in V_E and m/C_DA are very small and can be neglected. Without these terms, the expression relates errors in velocity, altitude, temperature (β), and pressure (ρ_0/β). To study the errors, the terms can be evaluated individually, and rms sums formed to show total errors.

Consider first the case in which h is measured with an accuracy of 10%. Table 31 shows corresponding errors in velocity and the resulting dynamic pressure for several entry angles of interest. The errors in β and ρ_0/β quoted previously are used; i.e.,

$$\left|\frac{\Delta\beta}{\beta}\right| = 15\%$$

$$\left|\frac{\Delta\frac{\rho_0}{\rho}}{\frac{\rho_0}{\beta}}\right| = 9\%$$

*Allen & Eggen, *op. cit.*

The indicated errors are so large that the use of the differential form is questionable; but it is clear that a system based on altitude measurement would create unacceptable velocity errors.

Now, assume that velocity is measured to 10%. Corresponding altitude and dynamic pressure errors are shown in Table 32.

Here, the errors are of realistic size, and a system based on a velocity measurement appears feasible. The indicated errors in altitude would not compromise the time of descent too seriously, and the dynamic-pressure error would produce a weight penalty on the parachute well within the pad already quoted. This is a fortunate result, since the measurement of velocity at high subsonic speeds is technically achievable, while the measurement of altitude (by radar altimeter perhaps) is prohibitive from both a weight and complication point of view.

A problem which will have to be considered in the detailed design should be mentioned here. Since the capsule parachute must be deployed subsonically, the body must fly through the transonic regime and reach the deployment point in a well-behaved manner. Both drag and stability can be expected to decrease during this period, and neither of these changes has been considered in the study to date. Several possibilities exist:

(a) The basic capsule shape may provide enough stability.

(b) Extendable fins might be used.

(c) If drag as well as stability is required, the parachute cover might be extended behind the capsule supersonically, or a small drogue chute might be included.

Deployment of such devices complicates the system, but it does not present any new or complex technical problems and should not degrade the general performance. In fact, a two-chute system may upgrade performance and should be considered in the detailed design.

Table 32. Errors for velocity-controlled parachute deployment

θ_E	$\left\lvert\frac{\Delta h}{h}\right\rvert_{\frac{\rho_0}{\beta}}$	$\left\lvert\frac{\Delta h}{h}\right\rvert_{\beta}$	$\left\lvert\frac{\Delta h}{h}\right\rvert_{\gamma}$	$\left\lvert\frac{\Delta h}{h}\right\rvert_{\text{total}}$
24	0.050	0.150	0.016	0.159
40	0.067	0.150	0.021	0.166
52	0.079	0.150	0.025	0.171
90	0.095	0.150	0.032	0.180
θ_E	$\left\lvert\frac{\Delta q}{q}\right\rvert_{\frac{\rho_0}{\beta}}$	$\left\lvert\frac{\Delta q}{q}\right\rvert_{\beta}$	$\left\lvert\frac{\Delta q}{q}\right\rvert_{\gamma}$	$\left\lvert\frac{\Delta q}{q}\right\rvert_{\text{total}}$
24	0	0.15	0.17	0.23
40	0	0.15	0.17	0.23
52	0	0.15	0.17	0.23
90	0	0.15	0.17	0.23

f. Conclusions and Major Problem Areas

A careful over-all study has been made of the general entry problem for Mars, and a specific mission has been considered within the general framework of the study. It is felt that the technical feasibility of this mission has been well established and that compliance with the first three guidelines in the introduction to this Section has been demonstrated.

As the study and design proceed into more detail, emphasis must be placed on certain problem areas to assure final success. The following are thought to be of special importance and are therefore listed specifically:

(1) Abort modes should be studied and data-recovery capability under aborting conditions maximized wherever possible.

(2) The atmosphere-model dispersions must be studied further, and the resulting constraints on the design must be fixed.

(3) The approach-attitude mode for the capsule must be fixed.

(4) The heat-transfer mode (laminar or turbulent) and the effects of angle-of-attack variations on the heat-shield design require further study.

(5) The capsule shape must be established. This requires a significant experimental effort and therefore may involve considerable lead times.

(6) The control system for the parachute and the general aerodynamic instrumentation requirements need more detailed study and definition.

(7) The parachute system requires special study and development; considerable lead time may be involved here.

(8) Capsule temperature control during the cruise mode and the mechanical capsule–spacecraft interface must be considered as basic constraints on the over-all spacecraft design.

UNCLASSIFIED

ADDENDA

1. Mars-Atmosphere Model

A model of the Mars atmosphere has been developed and is being used for the *Mariner B* landing study. It is proposed that the model be used for all such studies and that any revisions or additions be coordinated by JPL for purposes of consistency.

The model is defined by Table 33. The temperature–altitude relationship recommended is shown in Fig. 91 and the resulting density–altitude relationship in Fig. 92.

The density–altitude relationships can be expressed as follows:

Altitude 0 to 54,000 ft ($\Gamma = -215°$ *R/100,000 ft*)

$$\frac{\rho}{\rho_0} = \left[1 - \frac{\Gamma h}{T_0}\right]^{(g_0 M/R\Gamma)-1}$$

$$= [1 - 4.97 \times 10^{-6} h]^{2.497}$$

where h = altitude in ft.

Altitude above 54,000 ft (isothermal)

$$\frac{\rho}{\rho_0'} = e^{-\beta_T h}$$

where

$$\rho_0' = \rho_T e^{\beta_T h_T}$$

is a fictitious surface density for the isothermal part of the model and

$$\rho_0' = 4.09 \times 10^{-4} \text{ slugs/ft}^3$$

$$\beta_T = \frac{g_0 M}{RT_T} = 2.37 \times 10^{-5} \text{ 1/ft}$$

$$\rho_T = 1.136 \times 10^{-4} \text{ slugs/ft}^3$$

2. Summary of Motion Equations for the Entry Capsule

In an over-all consideration of entry-capsule feasibility, the motion of the capsule during the entry process is

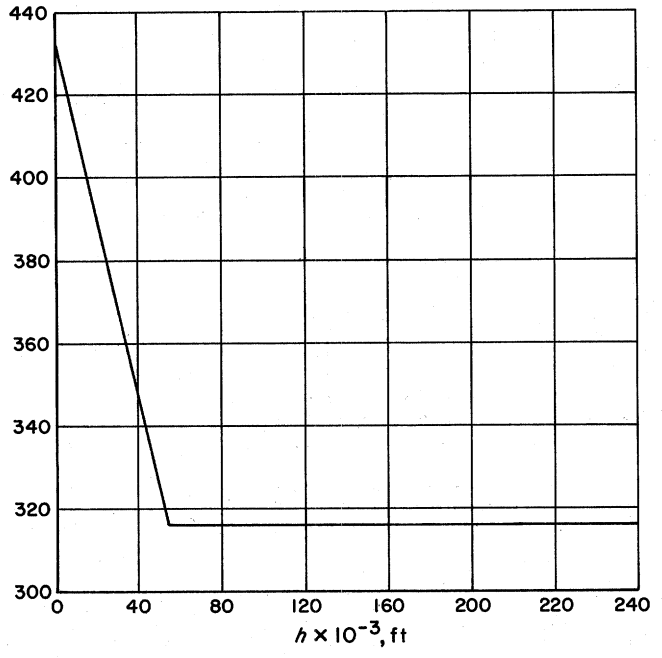

Figure 91. Mars-atmosphere model temperature vs altitude

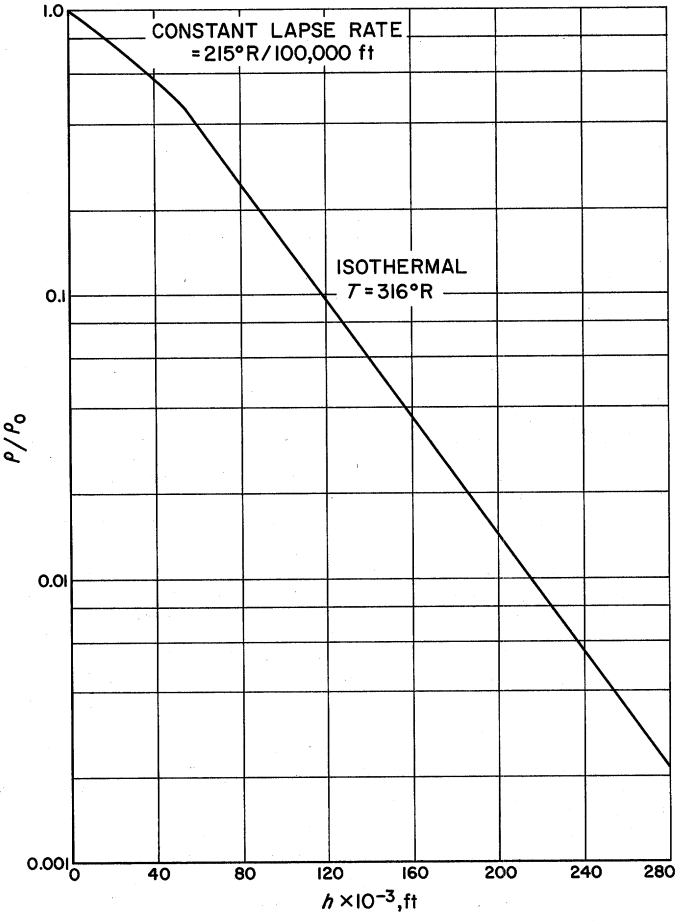

Figure 92. Mars-atmosphere model density vs altitude

UNCLASSIFIED

Table 33. Mars-atmosphere model

Footnotes	Symbol	Parameter	Minimum probable value	Accepted value	Maximum probable value	Units
1		relative abundance by volume				
		CO_2[a]	1.00	1.25	1.50	%
		A[a]	0.50	1.25	4.00	%
		N_2	94.50	97.50	98.50	%
3		relative abundance by weight				
		CO_2	1.54	1.94	2.33	%
		A	0.71	1.76	5.58	%
		N_2	92.14	96.30	97.73	%
	M	average molecular weight	28.236	28.365	28.733	—
4, 2	g_0	surface gravity	0.406	0.409	0.412	⊕
			398.2	401.2	404.1	cm sec^{-2}
			13.06	13.16	13.26	ft sec^{-2}
5, 2	P_0	surface pressure	0.0790	0.0888	0.0938	⊕
			80	90	95	millibars
			60.0	67.5	71.3	mm Hg
			1.160	1.305	1.378	lb $in.^{-2}$
			167	188	199	lb ft^{-2}
6	τ	total thickness	0.187	0.212	0.229	⊕
			1.495	1.698	1.831	km
			0.929	1.055	1.138	mi
7, 8, 2	T	mean temperature				
		surface	220	240	275	°K
			296	432	495	°R
		stratosphere	166	175.5	185	°K
			299	316	333	°R
9, 8, 12	ρ_0	surface density	0.0988	0.1279	0.1493	g l^{-1}
			1.92×10^{-4}	2.48×10^{-4}	2.90×10^{-4}	slugs ft^{-1}
10, 8	β	reciprocal scale height	0.0413	0.0570	0.0754	km^{-1}
			1.26×10^{-5}	1.74×10^{-5}	2.30×10^{-5}	ft^{-1}
11, 8	H	scale height (Earth-based)	13.4	17.5	24.0	km
			43.6	57.6	79.0	kft
			8.27	10.90	14.95	mi

[a]See footnote 2.

[1]CO_2 value from Seymour L. Hess, *Science*, 128, 811 (1958); A value from Gerard de Vaucouleurs, *Physics of the Planet Mars: An Introduction to Aerophysics*, Macmillan, New York, 1954, p. 127; N_2 value from assumption that no other component occurs significantly. An article by de Vaucouleurs in *The Exploration of Space*, edited by Robert Jastrow, Macmillan, New York, 1960, gives a CO_2 value of 2.2% and an A value of 4%, but the CO_2 value is very uncertain, and no error estimates are available for these values.

[2]Values of parameters so marked are taken as basic in the calculation of the values of all other parameters.

[3]Calculated from the volumetric abundances.

[4]From Krafft A. Ehricke, *Space Flight:* I. Environment and Celestial Mechanics, D. Van Nostrand, Princeton, 1960, p. 120–122. The range of values is caused here by the variation of gravity with latitude, resulting from both oblateness and centrifugal force. The accepted value is for 45° latitude, while the maximum and minimum values are for the poles and equator, respectively. The value used for Earth was $g_0 = 980.665$ cm sec^{-2}. Other sources give values centered around $g_0 = 0.383\oplus = 376$ cm sec^{-2}.

[5]Accepted value from A. Dollfus, *Supplement, Ann. d'Astrophys.*, No. 4, 1957 (quoted in Carl C. Kiess and K. Lassovzsky, *The Known Physical Characteristics of the Moon and Planets*, 1959). De Vaucouleurs (*Physics of the Planet Mars*, 1954) gives 85 millibars. The value used for Earth was $p_0 = 760$ mm Hg.

[6]From $[\tau g_0/Mp_0]\ \sigma^{\prime} = [\gamma g_0/Mp_0]\ \oplus$. The values used for Earth were $\tau = 7.991$ km and $M = 28.966$. The accepted STP thickness of CO_2 (and A) is 1.25% of τ, or 2120 cm.

[7]From de Vaucouleurs (*Physics of the Planet Mars*, 1954). The surface-temperature values apply to the equator and are averaged over the annual temperature cycle. The range in values is due to the daily temperature cycle. The stratosphere temperature is almost certainly constant. For plots of theoretical mean temperature vs altitude, latitude, time of day, and time of year, see de Vaucouleurs, pp. 135, 151, 156, and 159, respectively. All except the first are for the planetary surface, not the atmosphere.

[8]Evaluated at the surface and at the given surface temperatures.

[9]From $\rho_0 = p_0 M/RT$, where R is the universal gas constant, $R = 8.317 \times 10^7$ ergs $mole^{-1}$, $°K^{-1} = 4.973 \times 10^4$ ft lb (slug molecular weight)$^{-1}$ $°R^{-1}$.

[10]From $\beta = g_0 M/RT$. Carl Gazley, Jr. "Deceleration and Heating of a Body Entering a Planetary Atmosphere from Space," *Vistas in Astronautics*, Pergamon Press, New York, 1958, gives $\rho_0 = 1.93 \times 10^{-4}$ slugs ft^{-3} and $\beta = 1.15 \times 10^{-5}$ ft^{-1}. He also gives the abundance of CO_2 as 5%, but this is almost certainly an intentional overestimate.

[11]From $H = 1/\beta$. The 10-based scale height, H_{10}, is given by $MH_{10} = H$, where $M = \log_{10} e = 0.434294$.

[12]For an isothermal atmosphere at stratosphere temperature, probably a good approximation in the stratosphere, $\rho_0 = 3.39 \times 10^{-4}$ slugs ft^{-3} and $\beta = 2.38 \times 10^{-5}$ ft^{-1}.

Table 33. Mars-atmosphere model (cont'd)

Footnotes	Symbol	Parameter	Minimum probable value	Accepted value	Maximum probable value	Units
13, 8	C_p	specific heat at constant pressure	1.004 7.72	1.025 7.88	1.032 7.92	j g^{-1} °R Btu $slugs^{-1}$ °R
13, 8	γ	ratio of specific heats	1.3998	1.4023	1.4100	—
14, 8	Γ	dry adiabatic-lapse rate	3.857 2.115 11.17	3.914 2.146 11.33	4.027 2.208 11.66	°K km^{-1} °R kft °R mi^{-1}
15, 8	V_s	speed of sound	2.75×10^4 902	3.15×10^4 1033	3.69×10^4 1209	cm sec^{-1} ft sec^{-1}

[8] Evaluated at the surface and at the given surface temperatures.
[13] From *Tables of Thermal Properties of Gases*, National Bureau of Standards Circular 564.
[14] From $\Gamma = g_0/cp$.
[15] From $V_s^2 = \gamma p_0/\rho_0 = \gamma RT/M$.

most important. A linearized analysis of the entry behavior is presented by Allen,* and has been used for the study reported here. Pertinent relations taken or derived from Allen's work are listed here for the reader interested in the details of the analysis. The theory contains five major assumptions:

(a) Angular motion is small.

(b) An isothermal atmosphere exists.

(c) Nominal lift is zero.

(d) The weight of the body is neglected in the translation equation of motion.

(e) Aerodynamic coefficients are constant.

The summary is presented under the following headings:

(a) Motion parameters

(b) General equations

(c) Equations at maximum deceleration and frequency

(d) Equations at maximum stagnation-point heat transfer

(e) Equations at the point of divergence

(f) Equations at a near-sonic condition

The equations define the angle-of-attack envelope, the velocity and the frequency of the motion, as well as the related altitudes.

*H. J. Allen, *op. cit.*

a. Motion parameters

Trajectory parameter:

$$k_0 = \frac{\dfrac{\rho_0}{\beta \sin \theta_E}}{\dfrac{m}{C_D A}}$$

Dynamic-stability parameter:

$$\frac{k_1}{k_0} \simeq \frac{1}{4}\left[1 - \frac{C_{L_\alpha}}{C_D} + \frac{C_{m_q} + C_{m_{\dot\alpha}}}{C_D}\left(\frac{l}{\sigma}\right)^2\right]$$

Static-stability parameter:

$$\frac{k_2}{k_0} \simeq \frac{-1}{2\beta \sin \theta_E}\frac{C_{m_\alpha} l}{C_D \sigma^2}$$

b. General equations

Angle-of-attack envelope:

$$\left(\frac{\alpha}{\alpha_E}\right)^* = \frac{1}{\pi^{1/2}(k_2)^{1/4}} e^{k_1 e^{-\beta h} + (\beta h/4)}$$

Frequency:

$$\frac{2\pi\omega}{\beta V_E \sin \theta_E} = (k_2)^{1/2}\frac{V}{V_E} e^{-(\beta h/2)}$$

Velocity:

$$\frac{V}{V_E} = e^{(k_0/2)e^{-\beta h}}$$

UNCLASSIFIED

c. Equations for maximum deceleration and maximum frequency

$$h_a = \frac{1}{\beta} \ln k_0$$

$$\frac{V_a}{V_E} = e^{-1/2}$$

$$\frac{2\pi\omega_a}{\beta V_E \sin\theta_E} = \left(\frac{k_2}{k_0}\right)^{1/2} e^{-1/2}$$

$$\left(\frac{\alpha_a}{\alpha_E}\right)^* = \frac{e^{k_1/k_0}}{\sqrt{\pi}\left(\frac{k_2}{k_0}\right)^{1/4}}$$

d. Equations for maximum stagnation-point heat transfer

$$h_b - h_a = \frac{1}{\beta} \ln (3)$$

$$\frac{V_b}{V_a} = e^{1/3}$$

$$\left(\frac{\alpha_b}{\alpha_a}\right)^* = 3^{1/4}\, e^{-2/3\,(k_1/k_0)}$$

$$\frac{\omega_b}{\omega_a} = \frac{1}{\sqrt{3}} e^{1/3} = 0.807$$

e. Equations for divergence point

$$h_D - h_a = \frac{1}{\beta} \ln \frac{4k_1}{k_0}$$

$$\frac{V_D}{V_a} = e^{1/8\,[4\,(k_0/k_1)]}$$

$$\left(\frac{\alpha_D}{\alpha_a}\right)^* = \left(\frac{4k_1}{k_0}\right)^{1/4} e^{1/4-(k_1/k_0)}$$

$$\frac{\omega_D}{\omega_a} = \frac{e^{1/8\,[4-(k_0/k_1)]}}{\left(\frac{4k_1}{k_0}\right)^{1/2}}$$

f. Equations for near-sonic point

Let

$$\frac{V_c}{V_E} = 0.05 \qquad (1085/21{,}700, \text{ for instance})$$

Then,

$$h_a - h_c = \frac{1}{\beta} \ln (6)$$

$$\left(\frac{\alpha_c}{\alpha_a}\right)^* = \frac{e^{5k_1/k_0}}{6^{1/4}}$$

$$\frac{\omega_c}{\omega_a} = 0.05\,(6)^{1/2} = 0.122$$

Nomenclature

Quantities

A	projected frontal area, ft²
D	diameter, ft
g	acceleration due to gravity, ft/sec²
H	scale height $= RT/g_0M$, ft
h	altitude above planetary surface, ft
I_p	moment of inertia about pitch axis
I_z	moment of inertia about roll axis
K	planetary constant $g_0r_0^2$, ft³/sec²
l	length, ft
M	atmospheric molecular weight
m	mass, slugs
P	pressure, lb/ft²
Q	heat absorbed per unit area, Btu/ft²
q	heating rate per unit area dQ/dt, Btu/ft²/sec
q	dynamic pressure $\frac{1}{2}pV^2$, lb/ft²
R	universal gas constant
r	radius
S	perpendicular distance from center of planet to approach asymptote
s	spin rate about roll axis
T	temperature
t	time
V	velocity, ft/sec
W	weight, lb
α	angle of attack
β	reciprocal scale height $1/H$, 1/ft
Γ	lapse rate dT/dh (adiabatic value $= g_0/C_p$, where C_p = specific heat at constant measure)
ζ	tumbling rate (about pitch axis)
θ	trajectory path angle from local horizontal
ξ	precession half-cone angle
ρ	atmospheric density, slugs/ft³
ρ_0'	reference density for isothermal stratosphere

UNCLASSIFIED

σ radius of gyration about pitch axis; also standard deviation

Φ planetary central angle from approach-asymptote direction

ϕ angle of attack (used for tumbling study)

ω pitching frequency

Coefficients

C_D drag/$_qA$

C_L lift/$_qA$

C_{L_α} $dC_L/d\alpha$

C_m moment about c.g./$_qlA$

C_{m_α} $dC_m/d\alpha$

$C_{m_q} + C_{m_{\dot\alpha}}$ dynamic-stability derivative

C_N normal force/$_qA$

C_{N_α} $dC_N/d\alpha$

$k_{0,1,2}$ motion parameters (see Addendum 2)

m/C_DA ballistic coefficient, slugs/ft^2

Re Reynolds number based on free-stream conditions = $\rho V_1/\mu$

Subscripts

a capsule motion—maximum deceleration

b capsule motion—stagnation-point heat transfer

c capsule motion—near-sonic point

D capsule motion—divergence point

d parachute deployment

E entry condition (by definition, h_E = 200 mi)

e Earth quantity

I value in inertial coordinate system, fixed but not rotating with mass

m mass

p parachute

S stagnation-point conditions

s parachute-opening shock

t parachute terminal velocity

0 quantity at planetary surface

3. Space Science

R. W. DAVIES

(This Section is UNCLASSIFIED)

a. Martian-Atmosphere Experiments

It is interesting from both the scientific and engineering points of view to obtain information about the composition and the temperature, pressure, and density profile of the Martian atmosphere. At the present time, only carbon dioxide has been definitely identified in the Martian atmosphere; because of the interference of our own atmosphere, only upper limits have been set on other constituents. It should be noted that it is not necessary to make direct measurements of all the atmospheric constituents, since the abundance of some elements can be derived from the abundance of others, using known photochemical reaction rates and an assumed model atmosphere. The surface pressure has been determined to be between 70 and 100 millibars, and reliable maps of the sunlit-surface temperatures have been obtained.

Clearly, the most direct means of measuring local atmospheric parameters is by using the capsule. Furthermore, sensitive devices are required at two or more locations on the capsule in order to determine when the

UNCLASSIFIED

parachute is to be opened. The skin temperature of the entry vehicle will also be recorded, as well as some internal temperatures. After the deployment of the parachute, temperature and pressure measurements will be made at regular intervals; the density will be derived from these measurements. A serious problem is the measurement of height and velocity. A three-axis accelerometer should be flown for two reasons: first, to aid in determining the entry trajectory, and second, to measure scale height of the atmosphere. The connection between the pressure, temperature, and density and height can also be calculated if the molecular weight is assumed. A further check of the absolute altitude at several different times can be made from the photographs if distinct surface features are visible in several successive frames.

A direct measurement of the H_2, N_2, O_2, CO, CO_2, and CH_4 in the atmosphere can be made during the descent if a gas-chromatograph unit (described later in this Section) is flown.

b. Martian-Surface Investigations

Photographs taken from the capsule as it descends through the Martian atmosphere will complement those taken from the spacecraft. If the density of the Martian atmosphere is less than expected and the descent time is only 10 min, then the capsule can deliver at most 10^6 bits of information to the bus, corresponding to a maximum of ten 200×200-line pictures. A fairly straightforward optical system with a 7.5-cm lens and a 75-cm focal length could be used with a 150-line-per-centimeter image. This total system has a theoretical ground resolution of 10 cm from an altitude of 1 km. The area photographed would be approximately the size of a small suburban lot. The pictures taken during descent would be the limits of a set that begins with complete planetary coverage at 33-km resolution and converges to picture with a few centimeters resolution, a change in scale of more than 10^5.

Other possibilities for experiments which, directly or indirectly, would investigate the Martian surface are gas-chromatography and microscopy. The gas chromatograph appears at present to be the more feasible from the technological viewpoint. It does not require orientation, it weighs less than 10 lb, and it takes less than 10 w of power. It does not require a large information bandwidth.

The gas chromatograph would detect organic matter present in the atmosphere in the form of suspended particles, such as bacterial flora or organisms adsorbed on mineral-dust particles.

Samples of atmospheric dust would be drawn into a chamber in which organic compounds would be volatilized or pyrolized by controlled heating with thermite. The resulting volatile material would then be introduced into one or more chromatographic columns and identified by the characteristic retention times for each column. Pyrolytic decomposition of bio-organic materials produces volatiles such as H_2O, C_6H_6, acetonitrite, and acetone and would indicate the presence on Mars of a terrestrial type of biochemistry. In addition, the same instrument would be used to make quantitative and qualitative analyses of atmospheric gases.

A microscope system aboard the capsule would collect, concentrate, and observe with a vidicon microscope dust particles from the Martian atmosphere. The structure of these particles would be studied to determine if their morphology was indicative of micro-organisms.

A microscope system is currently being studied. The optical system will incorporate transmission, as well as color phase-contrast microscopy to obtain maximum visual efficiency. It will provide a field of view of 20-μ diameter at high magnification, while object fields of 100- and 500-μ diameter will make possible the examination of particles up to approximately 0.1 mm. The microscope image will be focused on a 400-line vidicon which will provide 0.2-μ resolution in the 20-μ field. Each picture, having 8 gray levels, will require 5×10^5 bits. The weight of this instrument would be less than 20 lb total and the instrument would be contained within a volume of 1 ft^3. It would require at least 7 w of continuous power.

It is believed that this would be an extremely exciting, but high-risk, experiment for *Mariner B*. It could be flown only by omitting the photographic system or by degrading drastically the quality of the microscope pictures. While neither alternative should be recommended without further study, it is felt that a simplified form of the microscope should not be excluded as possible capsule instrumentation.

Table 34. Compilation of capsule scientific experiments

Instrument	Weight, lb	Power, w	Stored information bits
Photographic system	12 to 20	5	10^5/picture
Pressure, temperature accelerometer	15 to 20	?	?
Gas chromatograph	<10	<10	20/sec
Multivator	<10	< 5	<20/sec
Microscope	20	7	5×10^5/picture

UNCLASSIFIED

A third experimental instrument, called a multivator, would suck up dust during descent and after impact, but instead of analyzing it chemically, would insert the dust into various solutions in order to detect fluorescence characteristics of organic matter of biological origin. It has been suggested that the multivator be developed as a shelf item which would be able to replace other instrumentation that cannot be made ready in time for the mission. At present, a multivator is being studied which weighs less than 10 lb, occupies around 250 in.^{3}, and requires less than 5 w of power.

Table 34 presents a compilation of the capsule experiments.

4. Communications

D. O. MUHLEMAN

(This Section is UNCLASSIFIED)

a. Introduction

The capsule-to-spacecraft communications link utilizes automatic phase-tracking loops, allowing communication in a relatively narrow bandwidth and removal of the doppler shift due to the relative motion of the capsule and spacecraft. As a consequence, it is fundamentally important to design the system to lock the communications link at separation and to minimize the probability of losing the locked link. For purposes of simplicity, omnidirectional antennas are used on both vehicles. A frequency of 135 mc was selected, which is sufficiently high to be reasonably unaffected by the Martian ionosphere, yet low enough to minimize the free-space path loss. A one-way link from capsule to spacecraft only is assumed.

The system has several modes of operation. At the time of separation, the system is operated without modulation at a radiated power level of 100 mw. This signal functions to keep the link in phase lock until shortly before the planetary entry. At this time, a timer switches the operation to 10 w of radiated power, and the modulation is turned on. This mode of operation will continue uninterrupted until about 50 min after impact, unless an accelerometer threshold detector senses an acceleration above a preset level; in that case, the modulation will be removed temporarily to allow carrier reacquisition in the spacecraft. After a nominal 50 min beyond impact, the time-controller will switch to a narrowband system with its associated transducers for the remainder of the experiments (maintaining the radiated 10 w).

b. Sequence of Events

A sequence of events pertinent to the communications problem will be presented before the system characteristics are discussed. The event numbers listed below correspond to the numbers in circles in Fig. 93 in which events are not drawn to scale. For purposes of this discussion, a nominal miss maneuver of 8000 km, with the capsule separating 22 hr before impact on Mars, was assumed.

① The capsule is split from the spacecraft at impact −22 hr. The spacecraft undergoes a maneuver of about 2 m/sec^2 approximately normal to the flight path. The 135-mc carrier is locked in the spacecraft, with the capsule radiating about 100 mw. The capsule tumbles in yaw or pitch at a rate less than 3 deg/sec. The carrier is not modulated.

② The capsule radiation power is switched automatically to the full 10 w, and the modulation is switched on. Transmission of scientific data begins.

③ High heating and acceleration is experienced, and the capsule becomes aerodynamically stable. It is assumed conservatively that the communications link is probably broken as a result of the high heating and ionization; the modulation is turned off (by an accelerometer) with a fail-safe switch (i.e., if the switch fails, the modulation is turned back on). The switch is designed such that it will close in a preset time (say, 10 sec). The loss of lock is detected automatically in the spacecraft, and the loop is put into an automatic-reacquisition mode. Since the total doppler shift due to the entry is not too great and is somewhat predetermined, the search range is not extensive. Acquisi-

UNCLASSIFIED

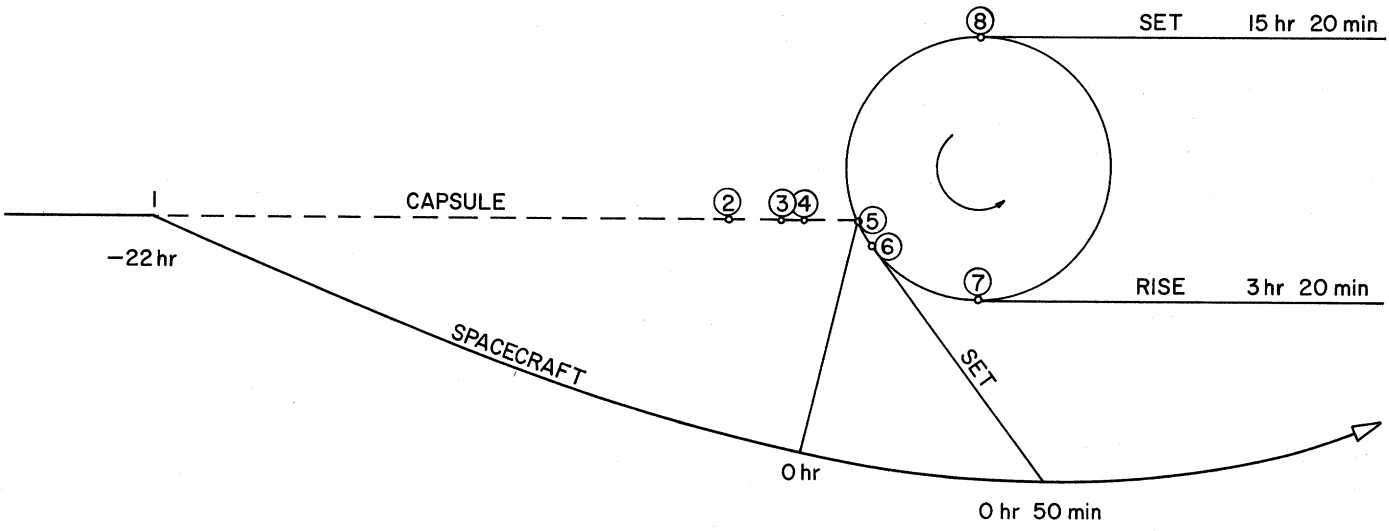

Figure 93. Communications sequence of events

tion must be assumed in the time interval during which the modulation is off (say, 10 sec), or the receiver may lock to a subcarrier after the modulation returns. In the event that lock is not lost, there is merely a loss of information (for 10 sec).

④ A few seconds after the end of maximum deceleration (about -40 g's) a parachute is deployed, creating another deceleration of approximately -40 g's. The communications link is so designed that this shock will not cause loss of lock. After the parachute is deployed, the scientific package takes pictures of the Martian surface which are read from the vidicon at a rate of 1/min and communicated to the spacecraft.

⑤ The capsule strikes the surface of Mars. If the shock is sufficient, the accelerometer will switch off the modulation and the automatic-reacquisition procedure is repeated.

⑥ The spacecraft appears to set below the Martian horizon about 50 min after impact. Before 3 hr 20 min after impact, the capsule communication system is automatically switched to the narrow-band system for measuring temperature, pressure, salinity, etc. (see Section IIIB-2).

⑦ At about 3 hr 20 min after impact, the spacecraft again rises over the same horizon because of the rotational motion of Mars. Automatic carrier acquisition is then achieved. If acquisition on a subcarrier occurs, a command-override system may be used to shift the frequency of the receiver local oscillator.

⑧ The spacecraft appears to set again at about 15 hr 20 min after impact, and the experiment is complete.

All automatic functions described above require careful investigation. In particular, a system for the auto-

Table 35. Capsule-to-spacecraft link (at impact)

Operating frequency	134 mc (λ = 2.22 m)
Communication distance	8×10^3 km (space loss = −154 db)
Total power radiated	10 w (40 dbm)
Over-all receiver temperature	1000° K
Omni-antenna gain, capsule	−1 db (±27 deg from pattern maximum)
Omni-antenna gain, spacecraft	−1 db (±27 deg from pattern maximum)
Polarization loss	3 db
System pad	7 db
Predetection bandwidth	4 kc
Tracking loop	
Power	0.5 w (27 dbm)
$2B_{L_0}$	44 cps
Data channel	
Power	9.5 w (39.8 dbm)
Phase modulation index $\Delta\omega$	2 rad
Modulation loss (carrier and subcarrier)	3.0 db
B_i (bandwidth)	510 cps
S/N	13 db

UNCLASSIFIED

UNCLASSIFIED

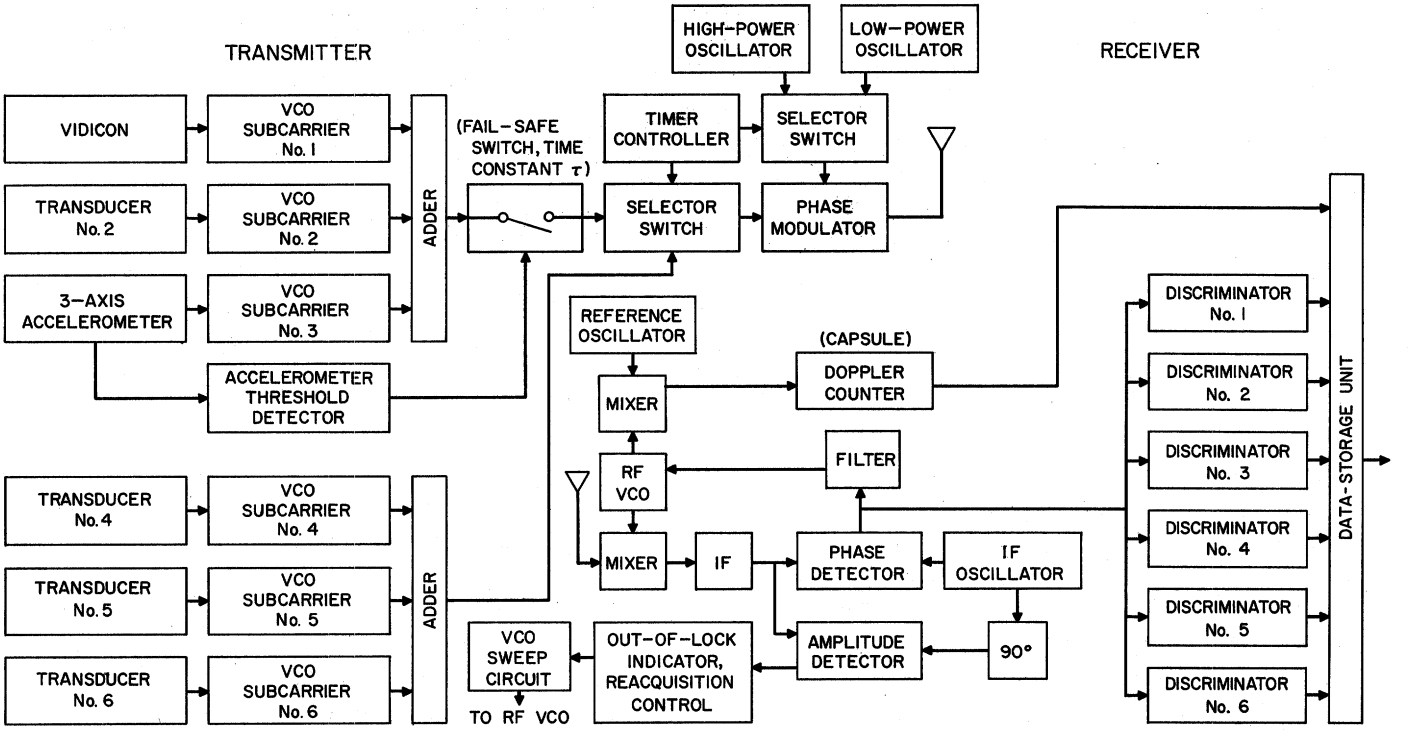

Figure 94. Capsule-to-spacecraft communication system

matic search and acquisition of a modulated carrier is believed to be a difficult task for a remotely operated receiver. Because of constraints on the weight and the desire for extreme simplicity with its associated good reliability in an unknown environment, a system employing FM–PM or FM–FM would probably be used. Such a system is presented schematically in Fig. 94.

The detailed system characteristics are described in Table 35. A fundamental requirement is that both the capsule and the spacecraft be assumed to have omnidirectional antennas for this link. (A detailed discussion on the capsule antenna follows.) Ten watts are radiated into the linearly polarized system. It is assumed that during the parachute descent the dipole antenna pattern will be oriented to within ± 27 deg of the plane of maximum signal strength. A similar assumption is made for the spacecraft dipole pattern, although this pattern is fixed relative to the attitude-controlled spacecraft. A modulation index of 2 rad will apparently allow a reasonable division of power between the carrier and signal sidebands, such that the significant sidebands will get through the 4-kc receiver front-end bandwidth. A modulation loss of 1.5 db must be accepted, and an additional 1.5-db loss was assumed for the subcarrier modulation. This results in a communications bandwidth of 510 cps, with a signal-to-noise ratio of $+13$ db.

The primary data requirement for the capsule is to transmit pictures with the following characteristics:

200 lines
200 elements per line
8 levels of gray
1 picture per minute

This can probably be achieved in the bandwidth available.

c. *Capsule Antenna*

For purposes of this study, it will be assumed that a dipole pattern can be created around the capsule. A suggested antenna system would be a loop antenna around the base of the capsule below the parachute area. The diameter of the capsule at this point is 1.1 m, which is a half wavelength at 135 mc and would determine the diameter of the loop. The major portion of the capsule, including the ablating material, scientific package, etc., is on the centerline in a direction toward Mars during the parachute descent of the capsule. The spacecraft is approximately at right angles to this line. Thus, the massive part of the capsule will not disturb the antenna pattern strongly in the communication direction. The landed orientation has not been determined and must be assumed

UNCLASSIFIED

UNCLASSIFIED

to be random. The capsule will tumble through random orientations before parachute opening.

The probability of the signal attenuation due to the orientation of the pattern may be computed by assuming that the pattern voltage is proportional to the sine of the angle measured from the null-axis of the dipole pattern. If the spacecraft is randomly oriented, then the probability of a signal attenuation of W db or more can be shown to be given by the expression*

$$P\,[w \leq W] = [1 - 10^{-w/10}]^{1/2}$$

This function is shown graphically in Fig. 95. For example, the probability of being down by more than 10 db is 5%, more than 20 db, 0.5%, etc. Thus, nulls deep enough to cause loss of lock are unlikely. It should be realized that considerable signal margin has been designed into the system presented here to track through the brief high-acceleration portions of the flight.

d. Narrowband Capsule System

As can be seen from Fig. 96 the transducer-modulation system will be switched to a narrowband system within a few hours after impact. The power level will be held to 10 w, and a noise bandwidth of 20 cps will be available for scientific data transmission for one Martian day.

*D. O. Muhleman, "The Communication Problem Associated With a Space Vehicle Split Into Two Vehicles in the Vicinity of Mars," Jet Propulsion Laboratory, Pasadena, Calif. (to be published).

Table 36. Capsule communications-weight breakdown

Components	Weight, lb
10-w 135-mc transmitter	—
Telemetry encoder	—
Omnidirectional antenna	—
Capsule	10

e. Communications-System Weight Breakdown

The capsule weight breakdown is presented in Table 36. The capsule system weight is 10 lb, which, of course, does not include power.

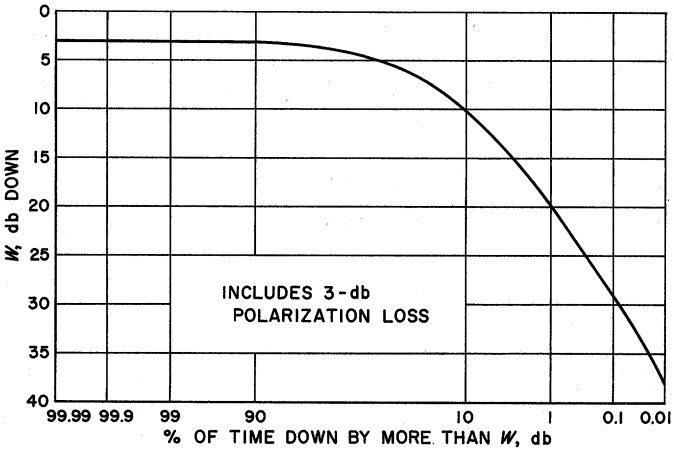

Figure 95. Null probability for a randomly oriented dipole-antenna pattern

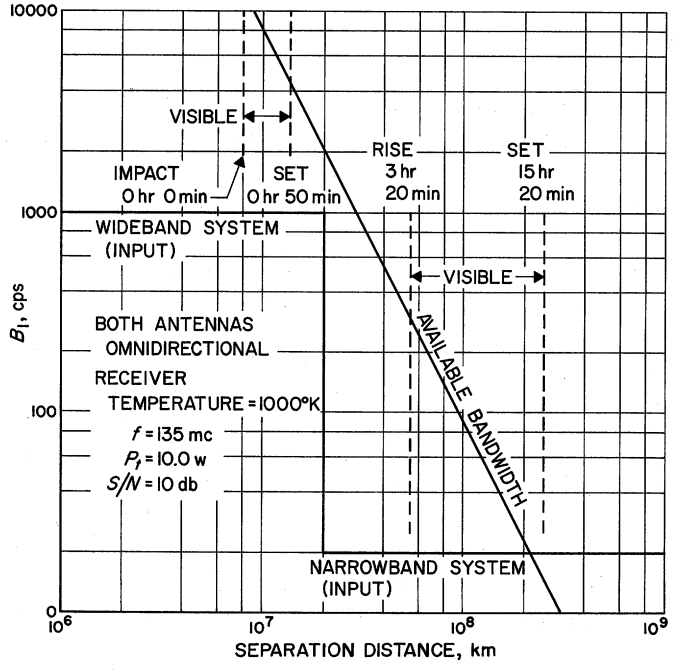

Figure 96. Available capsule noise bandwidth

UNCLASSIFIED

5. Power

T. W. KOERNER

(This Section is UNCLASSIFIED)

a. Power Requirements

Power requirements for the capsule are relatively simple compared to those of the spacecraft. Approximately 1.5 w of raw power are needed to operate a low-level transmitter for maintaining communication lock with the spacecraft during the interval from separation to capsule entry. The duration of this period is estimated to be slightly under 20 hr.

Shortly before capsule entry the scientific instruments and a higher-level transmitter are turned on. It is estimated that approximately 10 w of regulated power are required for the scientific instruments and about 65 w for the transmitter. Duration of this phase of operation is expected to be about 15.5 hr, after which the rotation of Mars eclipses the spacecraft and the capsule mission is considered to be completed. Assuming a conversion efficiency of 65%, the total capsule energy requirements are approximately 1800 whr.

Environmental conditions are somewhat more severe for the capsule than for the spacecraft because of the fairly high decelerations occurring at entry into the Martian atmosphere. Decelerations on the order of 35 to 50 Earth g's for periods of about 10 sec are expected.

b. System Description

The power system which appears most suitable for use in the capsule is a combination of a silver–zinc primary battery to supply the required total energy, a small converter to supply the low-level transmitter, and an inverter and set of transformer–rectifier units to deliver power to the scientific instruments and high-level transmitter. A timing device will be required in order to turn on the inverter at the proper time. The energy requirements of the timer are assumed to be negligible. A trickle charger will be required in the spacecraft in order to maintain the charge on the capsule battery. Power requirements of the trickle charger are estimated to be less than 1 w.

Table 37 shows the characteristics of the capsule power system and its components. The battery has been conservatively sized at 45 whr/lb in order to account for the high deceleration at entry into the Martian atmosphere.

Table 37. Power-system characteristics

System	
Weight	55 lb
Mode 1	
Power	1.5 w raw, 1 w regulated
Duration	20 hr
Mode 2	
Power	115 w raw, 75 w regulated
Duration	15.5 hr
Battery	
Type	Silver–zinc
Weight	40 lb
Capacity	1800 whr
Performance coefficient	45 whr/lb
Electrical-conversion system	
Weight	15 lb
Efficiency	65%
Performance coefficient	5 w/lb regulated

6. Configuration

J. DAVIS

(This Section is UNCLASSIFIED)

a. Introduction

There are a number of scientific and engineering experiments which cannot be performed adequately without penetration of the Martian atmosphere. The *Mariner B* capsule is designed to accomplish this task and collect pertinent data which are transmitted to the parent craft for processing and retransmission to Earth.

The configuration of the *Mariner B* capsule is based on the constraints developed by consideration of the number and order of desired experiments and the environmental constraints associated with entry.

Although independent in function, the capsule is closely tied to the parent-craft design through the common interacting constraints of total spacecraft weight, shroud envelope, and the assigned priorities of all proposed data and associated instruments. The assignment of relative merit and desirability to proposed instrumentation is a strong parameter in final achievement of an optimum spacecraft configuration. The generation and configuration implementation of such a priority schedule for space-exploration instrumentation is not a simple task. It must achieve an equitable balance between the gathering of engineering data required for advancement of planetary spacecraft technology and of data which would contribute to basic scientific knowledge.

The external geometry of a capsule is determined by the requirements of atmospheric entry.

The weight and size of the capsule for a given ballistic coefficient are primarily a function of the final instrument complement which is allocated for obtaining experimental data. The structure, ablation, and power weights associated with the instruments vary with the specific instruments selected, and addition or deletion of instrumentation affects the optimization of the capsule design. Therefore, many variations in capsule size and weight are possible, dependent on the specific compromise between desired experimentation, weight allocation, space limitation, and data priorities. The following configuration and integration discussion covers the range of possibilities and combinations for utilization of instrumentation in a Martian entry capsule, and presents one specific example from either end of that range. One configuration weighs 300 lb, is 4 ft in diameter, and incorporates more extensive experimentation, such as a vidicon, in addition to the basic instrumentation required for investigating the atmospheric properties. A second configuration weighing only 80 lb has a similar profile, scaled down to 21-in. diameter. This capsule, however, retains full capability for gathering the desired atmospheric-entry data. These combinations will be examined in detail in light of the design goals and constraints.

b. Design Goals

(1) Maximizing the probability of success in the overall planetary program.

(2) Exploration of the Martian atmosphere and surface with as complete and sophisticated an experiment package as possible within the limits of weight allocations and reliability.

One of the objectives of the future planetary program will be to place highly sophisticated packages on the surface of Mars in the gross-weight range of 3000 to 8000 lb. Any attempt at a Martian entry or landing mission must be preceded by sufficient knowledge of the atmospheric properties to allow the execution of a competent and efficient design, incorporating an acceptable instrument payload. One problem in achieving a maximum instrument payload for a given total spacecraft weight allocation is the uncertainty in the atmospheric parameters defined by the presently assumed atmospheric model. These uncertainties exhibit themselves in the entry-craft design by requiring greater weight allocations to ablation, insulation, structure, and parachute, since the design must assume the possible combination of the least attractive characteristics. This additional weight, if not in fact required, subtracts directly, significantly, and possibly prohibitively from the instrument payload. Decrease in these uncertainties promises more efficient weight allocation with respect to experimental payloads of future missions. Additionally, the scientific community holds extreme interest, as discussed in Section IIB, in examining those characteristics of Mars which relate to life processes. An entry-capsule design should be optimized toward contributing to the design goals in these specified areas of interest.

c. Design Constraints

The final capsule configuration must satisfy the following constraints:

(1) The capsule must be implemented in such a manner that it imposes minimum constraints on the potential success of the fly-by portion of the mis-

sion. For example, the minimum look-angle and miss-maneuver capability of the parent craft must be realized without regard to successful jettisoning of the capsule.

(2) The capsule must accommodate a sufficient instrument payload to justify that portion of the mission, with the final payload being selected from the list of recommended engineering and scientific instruments given in Section IIC, on the basis of assigned priority and capsule system compatibility.

(3) The capsule must provide for a data-communication link with the parent craft utilizing omnidirectional antennas only. Data must be transmitted to the parent craft as continuously as possible in order that failure during any phase may invalidate only the remaining portions of the capsule mission. For example, the acquisition of atmospheric data must not rely on the capsule surviving landing.

(4) The capsule must meet those constraints imposed on the entire spacecraft system design such as weight, shroud-envelope limitations, and launch and coast environments.

(5) The capsule must have an aerodynamic shape and ballistic coefficient which will accomplish the following:

(a) Aerodynamically arrest the tumbling and orient the capsule prior to the heating pulse. If passive orientation proves to be inadequate, pre-entry orientation will have to be established through spin–despin techniques or a simplified attitude-control system.

(b) Achieve and maintain stability throughout the entry phase until deployment of the parachute or drogue.

(c) Reduce the capsule velocity to that required for parachute or drogue deployment at a sufficient attitude for utilization of the descent experiments and the landing operation.

(6) The capsule must be capable of withstanding the effects of aerodynamic forces and heating and maintain an interior environment in which the instruments can survive.

(7) The capsule must provide a final-descent velocity which is compatible with the instrumentation and results in tolerable impact conditions.

(8) The capsule, to utilize post-landing experimentation, must absorb the energy of landing without exceeding the maximum acceleration loading allowable for the payload.

(9) Post-landing experimentation, monitoring, and data-transmission must be accomplished without reorientation from the final random position of rest.

(10) Sterilization must be accomplished. All components of the spacecraft system which enter the atmosphere must be void of viable organisms.

d. Configuration

Figures 97 and 98 indicate a typical arrangement of capsule subsystems satisfying the design constraints.

The capsule shape and size as shown in Figure 99 satisfies the ballistic-coefficient requirements for a 300-lb capsule. A monocoque RF transparent fiberglass structure provides support for the ablation and insulation material and resists the aerodynamic forces. Ablation techniques for cooling the capsule were selected over full heat-sink methods because of the weight advantage. The fiberglass structure, however, does act as a heat-sink, reducing the amount of insulation material that would otherwise be required. Were not RF transparency necessary, better heat distribution would be obtained with a material of higher thermal conductivity.

This design presumes that the complete heat shield, including structure, ablation, and insulation, must be intact and separated in one piece if such separation is required. If subsequent investigation shows that the ablation surface and/or the monocoque structure may be violated with seams, joints, or hatches, the interior design may be simplified in several areas.

The total c.g. must be kept as far forward of the center of pressure as possible to insure static stability in the forward direction and instability in the reverse direction. Instability in the reverse direction is required to aid the aerodynamic orientation during the initial phases of entry.

For reasons of the c.g. position requirement, the batteries, converters, transmitter, experiments, and electronics are positioned very near the nose. The ablation coating, although thickest at the nose and stagnation point and tapering off toward the skirt, does not enhance the c.g. position, since the ablating process tends to shift the c.g. aft during or before critical stability periods.

If the capsule is to impact the surface with the same orientation held during entry, the integration of the landing absorber, shown here as a ring of crushable structure, and allowance for its excursion further complicate equipment placement for acceptable c.g. locations.

UNCLASSIFIED

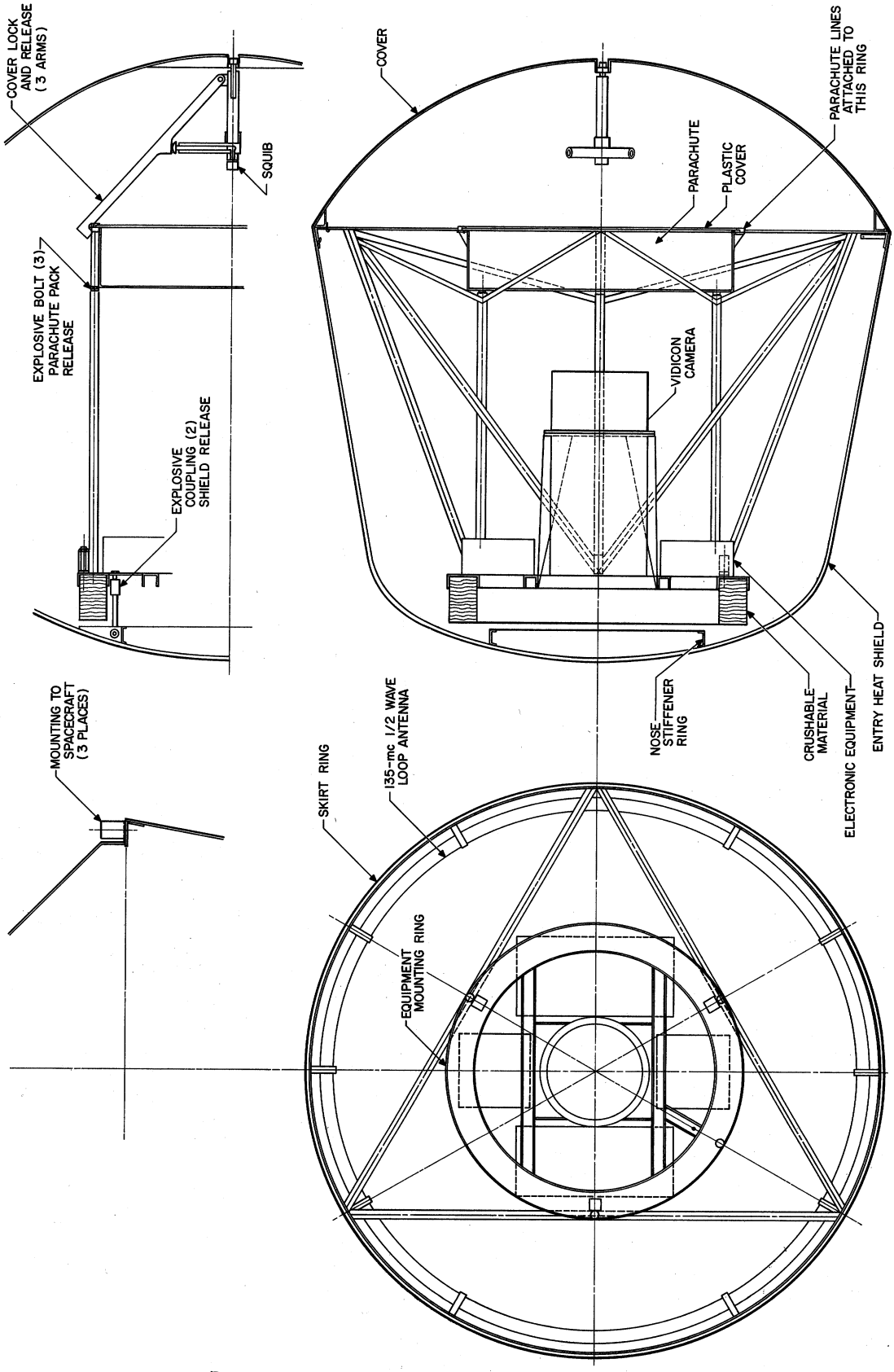

Figure 97. Three-hundred-pound entry capsule

UNCLASSIFIED

UNCLASSIFIED

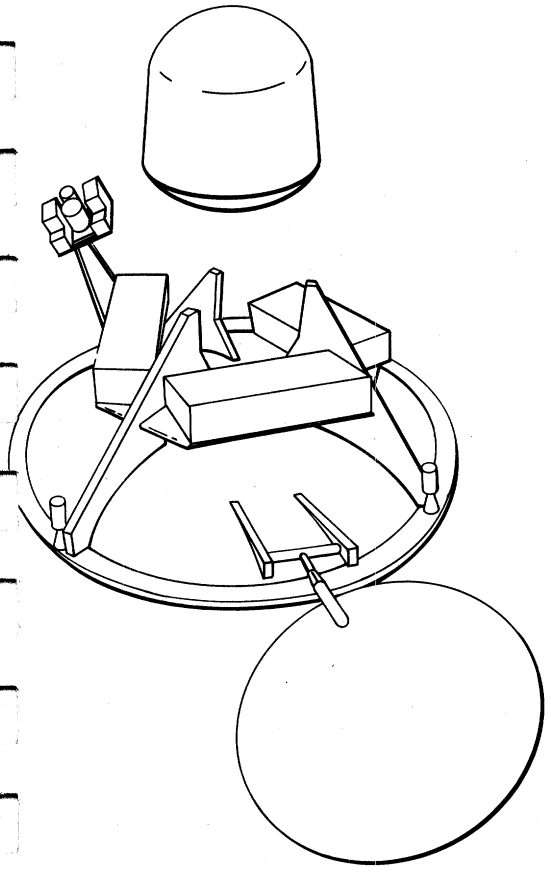

a. SPACECRAFT AND CAPSULE JUST AFTER POINT OF CAPSULE RELEASE

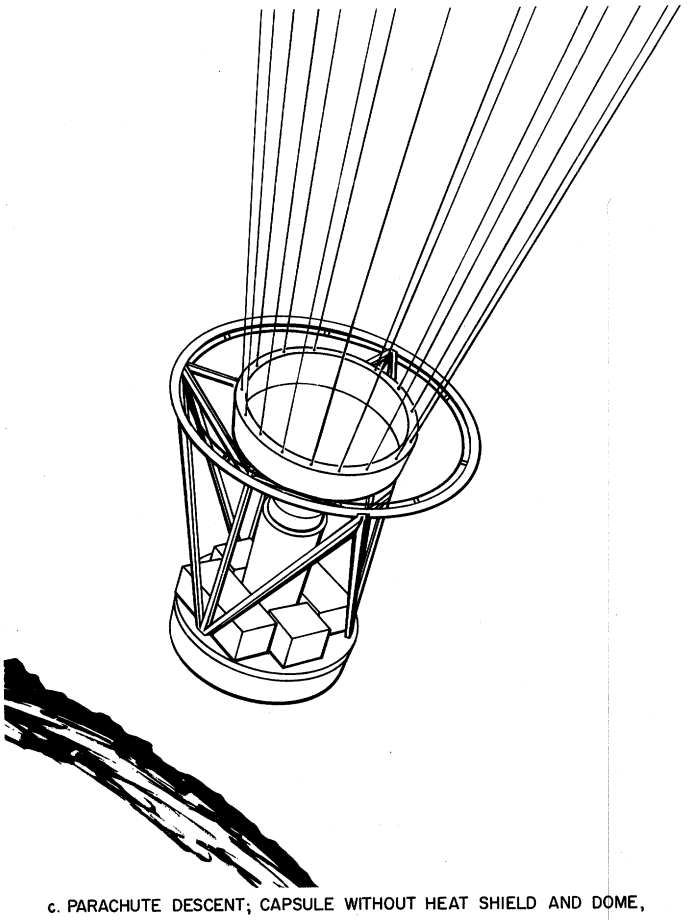

c. PARACHUTE DESCENT; CAPSULE WITHOUT HEAT SHIELD AND DOME, HANGING FROM 35-ft PARACHUTE

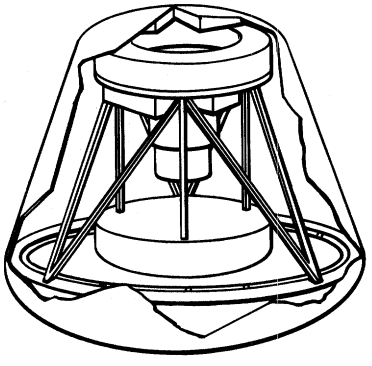

b. ENTRY; 3-DIMENSIONAL, CUTAWAY SHIELD AND DOME COVER

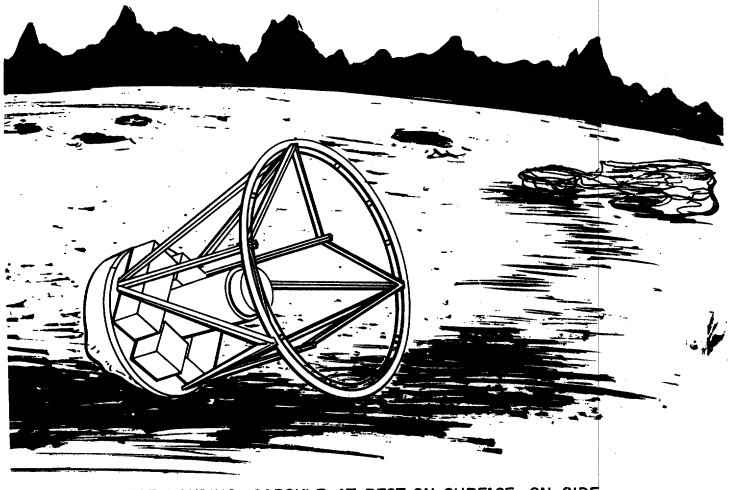

d. POST LANDING; CAPSULE AT REST ON SURFACE, ON SIDE, WITHOUT PARACHUTE OR PARACHUTE CONTAINER

Figure 98. Artist's rendition of capsule

UNCLASSIFIED

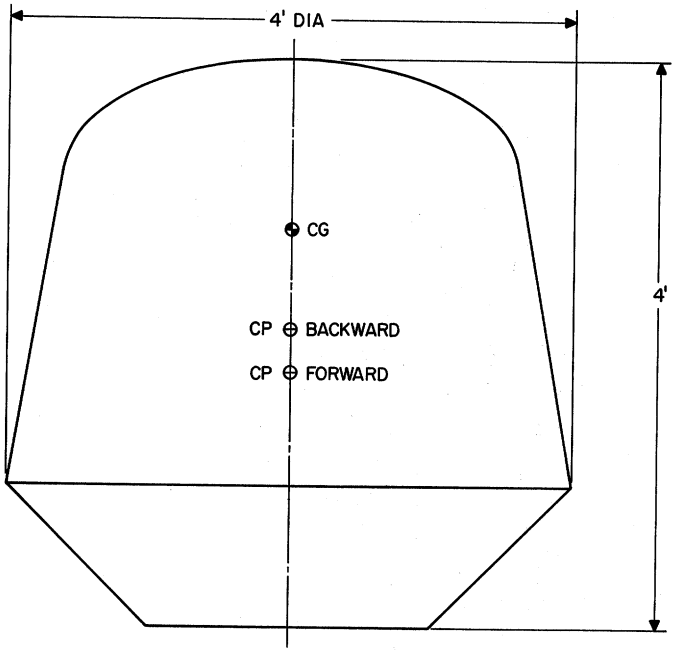

Figure 99. Aerodynamic profile of entry capsule

A parachute for reducing the final-descent velocity to approximately 45 ft/sec is positioned for deployment after jettisoning the aft fiberglass dome cover. The shroud-line loads are carried through the vertical truss members directly to the equipment-mounting ring.

The capsule must be capable of selecting the proper time during entry to deploy the parachute. Weight and simplicity constraints rule out an altimeter, and a full timer or parent-craft command initiation appears to be impractical. The most encouraging approach to date is to sense in the capsule a specific aerodynamic phenomenon associated with entry, such as maximum acceleration. and use a timed command based on this phenomenon to initiate parachute deployment.

The truss structure transmits the loads from the skirt ring and monocoque structure to the forward equipment ring. The monocoque structure is held in place by explosive tension ties between the nose-stiffener ring and the forward equipment ring.

The equipment ring supports the batteries, converters, experiments, and crushable structure.

The loop antenna for the 135 Mc communication link is accommodated geometrically inside the skirt hoop. This position requires that the heat shield and dome cover be RF-transparent and the effects of the remaining structure on the radiation pattern be determined.

At parachute deployment, load on the shroud-line-attach points initiates the heat-shield explosive tensio ties jettisoning the monocoque structure, remaining abla tion, and insulation. This sequence provides viewing access for the vidicon camera, reduces descent and land ing weight, and simplifies temperature and pressur measurements by exposing the interior of the capsule to the atmosphere and its ambients.

The vidicon may then take pictures of increasingl higher resolution as the capsule approaches the surface.

This mode is maintained until first surface impact when the parachute/attach ring is separated from the truss structure. This is done both to keep the capsule from being dragged over the terrain by surface wind and to lessen the likelihood of the parachute settling o the capsule.

Both the vertical and (unknown) horizontal component of the landing energy must be absorbed, bringing th capsule to a random position of rest.

The landing decelerations encountered, assuming 4 ft/sec descent velocity and 2 in. of perfect crushing would be on the order of 200 g's.

With the restraint, under the dictate of simplicity, tha post-landing monitoring of experiments be accomplished without reorientation of the capsule, utilization during that phase of the vidicon, anemometer, and salinity experiments is limited. The capsule weight-breakdown chart (Table 38) lists the estimated weights for the subsystems in the described configuration.

The recommended capsule experiments and the se quence of events have shown that a large portion of the anticipated scientific and engineering data from the higher-priority instruments is gathered and relayed to the parent craft during the entry and parachute-descent

Table 38. Capsule weight breakdown

Subsystems	Weight, lb
Monocoque structure (fiberglass)	86
Internal structure	25
Landing-energy absorber	10
Battery and converters	55
Transmitter and antenna	10
Parachute	24
Ablation and insulation	30
Miscellaneous hardware	10
Instrument payload	50
Total	300

phase. In order to gather and transmit data after landing, the capsule must be designed to survive that landing without prior knowledge of the horizontal velocity or of the surface conditions. The high-risk and obvious difficulties in implementing with confidence for the post-landing phase, with the relatively small portion of data to be gained, have indicated that primary emphasis should be directed toward success during the entry and descent portions of the mission.

e. Special Problems

(1) Sterilization

The implications of the potential sterilization requirements continue to pose design problems in *Mariner B* missions. With the midcourse propulsion system mounted on the parent craft, the spacecraft must fly an intercept trajectory with the planet at the time of capsule release. Failure to execute the miss-maneuver would result in entry of the atmosphere by the parent craft. This possibility, with its attendant sterilization requirements for the complete spacecraft, must be considered.

If it is determined that the capsule only must be sterile, the problem of maintaining final surface sterility while mated to a non-sterile spacecraft and shroud must be met. The split *Centaur* shroud does not lend itself as readily to gas sterilization as the *Agena* shroud. This problem will require special attention at a later date.

(2) Aerodynamic Entry

Once the nominal weight allocation for the capsule has been determined, the most severe remaining configuration constraint is imposed by the profile required for successful aerodynamic entry. A specific shape coupled with a given entry angle, velocity, and atmospheric model, carries with it attendant requirements for discrete structural characteristics, location of c.g. insulation and ablation protection.

Once the shape is determined, a parachute-deployment system and landing-energy absorber must be adapted to this rather inflexible design, with the remaining volume allocated to the power source, attitude control (if required), communications, instrument payload, and supporting structure. Therefore, a significant portion of the capsule equipment-design effort is constrained by, and must follow, the design development and final selection of the capsule aerodynamic shape. This shape must be studied and evaluated prior to the initiation of preliminary design. Passive attitude orientation, heating, and acceleration must be included as part of the evaluation.

(3) Others

Other problems which must be investigated include instrumentation techniques for gathering pressure and temperature during entry and techniques for determining proper time for parachute deployment.

f. Minimal Capsule

The implications of the *Mariner B* weight picture as evidenced by the weight breakdowns given earlier in this Section, and the extreme importance associated with gaining more accurate Martian atmospheric data, have prompted an investigation into the utilization of a "minimal" entry capsule.

Although time did not allow for formal treatment of the proposal by the study committee, it has been considered with respect to entry dynamics and heating, communications, configuration, and spacecraft integration, and is included in this Report.

With a ballistic coefficient (m = mass, C_D = coefficient of drag, A = maximum cross-sectional area), fixed by parachute-deployment constraints, any increase in weight due to elimination of equipment or structure may be accompanied by a decrease in capsule size, ablation weight, and parachute weight. Therefore, the weight of the capsule is significantly reduced by deleting lower-priority experiments and simplifying functional requirements.

Consideration of the possibility of de-emphasizing landing survival as discussed in Part I for the 300-lb capsule is a first step in reducing capsule weight. Trade-off of this type between weight and functional capabilities is further considered in the following discussion to determine the limit of simplification within which a useful capsule mission can still be maintained.

It appears possible that a capsule which retains full capability for gathering the desired atmospheric-entry data can be implemented for as little as 80 lb.

Figure 100 and the weight breakdown in Table 39 depict the schematic implementation of such a minimal capsule. The diameter, maintaining $m/C_DA = 1$, is scaled down to 21 in. The terminal velocity with a 3- to 4-ft-diameter balloon drogue would be approximately 250 to 300 ft/sec, with an impact acceleration of 3000 to 5000 g's. The information which could be gained from such a capsule would be axial, pitch, and yaw accelerations, stagnation and base pressures, and recovery and internal temperatures during entry. These measurements should make possible the determination of the entry trajectory,

Table 39. Minimal capsule weight breakdown

Subassemblies	Weight, lb
Monocoque structure (fiberglass) and internal structure	20
Landing-energy absorber	5
Battery and converters	17
Transmitter and antenna	8
Drogue balloon	10
Ablation and insulation	10
Miscellaneous hardware	3
Instrument payload	7
Total	80

variation of atmospheric density and temperature with attitude, and heat-shield performance.

Monitoring of impact accelerations and ambient surface temperature and pressure could be attempted with the addition of approximately 5 lb of crushable structure.

Table 40 indicates the ablation and insulation weight requirements for three sizes of capsules as a function of the optimistic, nominal, and pessimistic values of the atmospheric parameters as listed in the Notes of the Table for an isothermal atmosphere. This range of uncertainty, when applied to larger capsules, spans the transition point from laminar to turbulent flow, and consequently increases the heat transfer. This transition point exerts an additional strong parameter on ablation requirements. The entry angle of 25 deg, used for the 4000-lb case, corresponds to incipient boundary-layer transition. (A higher angle would increase the probability of transition.)

Table 40. Effect of atmospheric uncertainties on ablation plus insulation weights
(Based on Alderson's Atmospheric Model)

Capsule weight, lb (Earth)	100	300	4000
Maximum diameter, ft	2	4	12.6
Drag coefficient	1.0	0.75	1.0
Entry angle, deg	40	40	25
Nominal laminar			
W_h, lb	3.9	11.2	76
% W	3.9	3.7	1.9
g's	38	38	25
Pessimistic laminar			
W_h, lb	6.2	18.9	250
% W	6.2	6.3	6.3
g's	28	28	18
Nominal turbulent			
W_h, lb		20.1	204
% W	Turbulent flow very unlikely	6.7	5.1
g's		38	25
Pessimistic turbulent			
W_h, lb		30.7	375
% W	Turbulent flow very unlikely	10.2	9.4
g's		28	18
Optimistic laminar			
W_h, lb	3.3	9.4	64
% W	3.3	3.1	1.6
g's	50	50	33

1. Ablation and insulation material assumed to be polyethylene.
2. Load-bearing structure taken as 60 lb for 300-lb capsule, and scaled accordingly for 100-lb and 4000-lb cases. (Used for estimating structural heat sink capabilities only.)
3. $(m/C_DA) = 1$ slug/ft^2.
4. Maximum internal skin temperature = 600°F.
5. W_h = Ablation + insulation weight.
6. m = Entry mass of capsule.
7. B = Inverse scale height.

$B_{nom} = 2.37 \times 10^{-5}$ ft$^+$ $T_{nom} = 316°R$
$B_{pes} = 1.73 \times 10^{-5}$ ft$^+$ $T_{pes} = 299°R$
$B_{opt} = 3.16 \times 10^{-5}$ ft$^+$ $T_{opt} = 330°R$

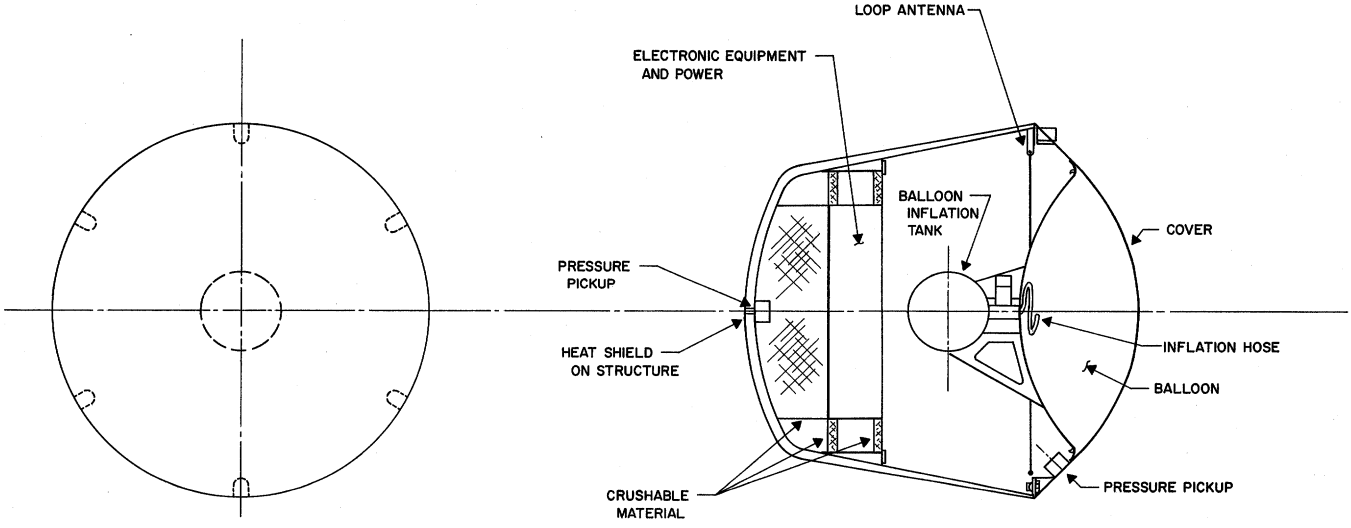

Figure 100. Configuration schematic of 80-lb entry capsule

UNCLASSIFIED

The information in Table 40 points out the fact that for a 100-lb capsule, the optimistic and pessimistic ablation and insulation requirements are 3.3 and 6.2 lb respectively. This represents a penalty of 2.9 lb in designing for the pessimistic value and only 9.1 lb in doubling the value for safety factor.

Comparing this with a 4000-lb capsule, as might be used on *Voyager*, the optimistic and pessimistic values are 64 and 375 lb. The potential weight penalty in this case is 311 lb for a pessimistic design or 686 lb for a safety factor similar to that proposed for the 100-lb capsule.

A minimal capsule, then, because of its weight advantage, enhances the possibility of including a capsule on the *Mariner A* mission, provides data for decreasing the uncertainties in the atmosphere parameters, and promises greater payloads and higher probabilities of success on future missions to Mars.

g. Conclusions

In the preliminary configuration studies conducted on the *Mariner* entry capsule, representative capsule shapes of nominal ballistic and drag coefficients were introduced for feasibility determination. The incorporation and implementation of selected groups of capsule functions and equipments, into a specific shape of the shape class considered, and within the capsule weight range, is judged to be technically feasible and reasonable for the mission described.

It is seen that there are available many possibilities of capsule size and weight, between 75 and 300 lb, depending upon the sophistication of the instrumentation program selected. Since the capsule must be defined early in the preliminary design phase, one possible consideration is that of carrying the design of both an optimistic capsule and a minimal capsule, with the necessary adaptors to mate either to the parent craft at a later point in the design.

In line with the design goals, a small entry probe in the 75- to 300-lb class is particularly well adapted to an initial entry mission, since it permits large excursions from a maximum-efficiency design in order to gain independence from uncertainties in atmospheric properties, entry angle, stability criteria, etc., without imposing prohibitive weight penalties.

UNCLASSIFIED

APPENDIXES

APPENDIX A

Capsule Propulsion

R. R. BRESHEARS

(This Section is UNCLASSIFIED)

1. Introduction

Rather than placing the spacecraft on a trajectory which will impact Mars, separating the capsule, and then deflecting the spacecraft to fly by, an alternative scheme is to aim the spacecraft to miss Mars by the desired altitude and then to deflect the capsule to enter the Martian atmosphere. This scheme requires propulsion aboard the capsule, and possibly some form of attitude control.

Although this concept complicates the capsule design and may impose certain requirements on guidance and control during the ejection sequence, there may be some benefits over the other scheme. First, there is a propulsion-weight saving, because the deflection impulse would be applied to the capsule which weighs about 300 lb, rather than to the heavier spacecraft which weighs 1600 to 1700 lb. Second, since the flyby is regarded as the major mission and the capsule is secondary, the mission would have greater assurance of success if the spacecraft were pointed to miss the target planet. Finally, this may influence the operationally difficult problem as to whether the spacecraft need be sterilized.

There are three alternatives in accomplishing a propulsive-capsule design:

a. Deflection motor on capsule with spin-stabilization
   (1) With de-spinning
   (2) Without de-spinning

b. Deflection motor on capsule with active attitude-control system.

c. Complete midcourse, approach, and deflection propulsion system on capsule.

2. Discussion of Alternate Schemes

a. The presently proposed method of deflecting the spacecraft to miss by imparting an impulse velocity of 127 m/sec requires approximately 91 lb of propellant (hydrazine) plus an additional 10 lb of tankage. Preliminary calculations for a spin-stabilized capsule deflected by the same velocity increment of 127 m/sec could save up to 79 lb in spacecraft weight. The estimated total weight to accomplish this sort of maneuver is 22 lb, which includes two solid-propellant spin rockets, the solid-propellant deflection rocket, a sequencer and power supply, plus attachments and structure. Figure A-1 shows one possible configuration which incorporates this scheme. The ejection sequence would be as follows:

(1) Orient spacecraft

(2) Separate capsule

(3) Spin capsule

(4) Fire deflection rocket

(5) De-spin capsule (optional) and separate rocket motor (optional)

The deflection impulse is applied at nearly right angle to the spacecraft velocity vector. This direction minimizes the effect of errors or uncertainties in direction and represents the most efficient use of propellant. A possibly undesirable situation resulting from this scheme is that the capsule will begin entry with the roll axis about 80 deg to the velocity vector. It is not now known whether the capsule can re-orient itself soon enough after atmospheric entry to prevent excessive heating of the capsule base, which may not have enough ablation protection.

UNCLASSIFIED

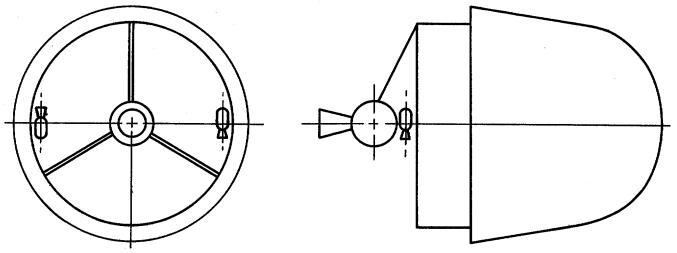

Figure A-1. Typical capsule configuration with solid-propellant spin and deflection rockets

If total impulse control is required, this can be put on the deflection motor at a small cost in propulsion weight, although at the expense of increased weight for the velocity-measurement system. The de-spinning may be done by releasing the empty spin rockets in a "yo-yo" transfer of angular momentum. By proper design of the "yo-yo," a low spin rate may be retained by the capsule to achieve even ablation and additional stability.

The option of not de-spinning the capsule, and therefore not allowing the capsule to right itself aerodynamically, may be taken. In this case, the capsule would be aimed at the proper entrance angle and the deflection rocket fired at this angle. This requires a much higher velocity increment, although a small weight saving of about 5 lb over the system of deflecting the spacecraft still results. There is a possible advantage in this case when the capsule is accelerated in the general direction of the planet, because the capsule would impact about 2 hr before the spacecraft flies by. The distance separating the two is about 30,000 km at capsule encounter.

Compromise orientations of the capsule-deflection thrust between the most efficient and this alternative are possible. The compromise will result in less weight saving but a better entrance angle into the atmosphere.

It appears that the pointing accuracy for the capsule needs to be high in this case. A pointing error of 1 deg would result in an error of ±630 km in the capsule impact location. This is the same order of magnitude as the error due to the approach corrections. The approach corrections may have to be made closer to the plane than presently contemplated, which means additional approach-correction propellant.

b. If the capsule has an active attitude-control system (employing, for instance, jet vanes on the rocket motor), this would eliminate spin-stabilization, use the propellant most efficiently, and still maintain a desirable entrance angle, now at the expense of additional attitude-control weight and complexity.

c. The third alternative design incorporates the entire midcourse-, approach-, and deflection-propulsion system (a restartable hydrazine monopropellant engine) on board the capsule. (See Appendix B for a typical configuration using this scheme.) This increases the total capsule weight (which must now include some control and sequencing hardware) at the time of capsule deflection and decreases the possible weight saving.

3. Conclusion

The alternative of deflecting the capsule rather than the spacecraft has advantages of weight savings and ensuring a spacecraft miss of the planet, but raises concomitant problems. A detailed study of the constraints and problems related to the encounter trajectory, guidance and control, and propulsion must be conducted to establish the feasibility of capsule deflection and to determine the optimum scheme of achieving it.

UNCLASSIFIED

UNCLASSIFIED

APPENDIX B

Alternate Spacecraft Configurations

T. A. COOK

(This Section is UNCLASSIFIED)

Although only two configurations were discussed in Section IIIB-8, there are many that may be suitable for the *Mariner B* mission. Sixteen different configurations were considered in this study, and are shown in the accompanying figures.

At the beginning of the study, it was estimated that the midcourse-propulsion system would weigh about half as much as the capsule. With respect to these two elements, the lightest structure would result from placing the capsule closer to the booster than the propulsion system. This was done in Fig. B-1. A 10.5-ft^3 volume for electronics was provided between the propulsion system and the capsule. One hundred square feet of solar cells on folding panels are used for power.

By placing the capsule forward, as shown in Fig. B-2, and changing from a single motor on the centerline to four motors off the centerline, it is possible to put a 6-ft high-gain antenna on the axis of symmetry.

By moving the capsule further forward, it is possible to have both a single motor and a 6-ft antenna on the centerline (Fig. B-3). In order to stay within the nose-fairing envelope, it was necessary to move the electronics volume off the centerline to a "donut" around the midcourse motor. Flat solar panels with foldable reflectors were used for power.

In Figure B-4, the high-gain antenna is moved off the centerline and the electronics are moved into the centerline.

Figure B-5 is similar to Fig. B-4, but a shorter over-all length is achieved by folding the antenna feed.

An attempt was made in Fig. B-6 to find the largest possible volume for electronics. Accessibility and temperature control were important factors in the selection of the large annular configuration shown.

Figure B-7 is similar to Fig. B-6, but the antenna has been moved forward and onto the centerline. With this antenna position, a foldable feed is not necessary, but the antenna-articulating structure is complicated.

Figure B-8 shows an arrangement of the *Mariner B* elements on a triangular structure. In this configuration, the electronics are packaged within the basic structure. Placing solar panels 120 rather than 180 deg apart leaves considerable room for antenna movement but severely restricts the planet boom.

To improve the look-angle problem created in Fig. B-8, the power system was changed from solar panels to the solar concentrator shown in Fig. B-9. Location of the concentrator on the centerline substantially increases the field of action of the articulated members, but unless the midcourse-motor axis is not coincident with the roll axis, a multi-motor system off the centerline must be used. This configuration is discussed in Section IIIB-8.

Figure B-10 shows a modified *Mariner A* structure with the *Mariner A* planet boom, midcourse motor, and antenna. This configuration is also discussed in Section IIIB-8.

Figures B-11 and B-12 show the configurations of Fig. B-9 and B-10, respectively, modified by placing the midcourse motor on the capsule so that the capsule and midcourse motor are separable as a unit. The consequences of the arrangement are discussed in Appendix A.

Figure B-13 illustrates a method of incorporating two 6½-ft-diameter solar concentrators. Figure B-14 shows a method of mounting four 5-ft-diameter concentrators.

Figure B-15 shows three elliptic paraboloids—one for communication, and the other two for solar concentration. This configuration was developed from a triangular basic structure.

The dimensions of flat solar panels depend on the area required, the diameter of the nose fairing, the slope of the nose fairing, the height of support structure available, the angle between the panels and the centerline, and on the distance from the base of the panels to the centerline. To minimize the distance from the centerline to the tip of the panel when unfolded, the distance to the base when folded should be a minimum. This results in wider panels, since the full diameter of the nose fairing can be utilized. Figure B-16 shows a configuration with solar panels stowed and extended along the centerline.

UNCLASSIFIED

UNCLASSIFIED

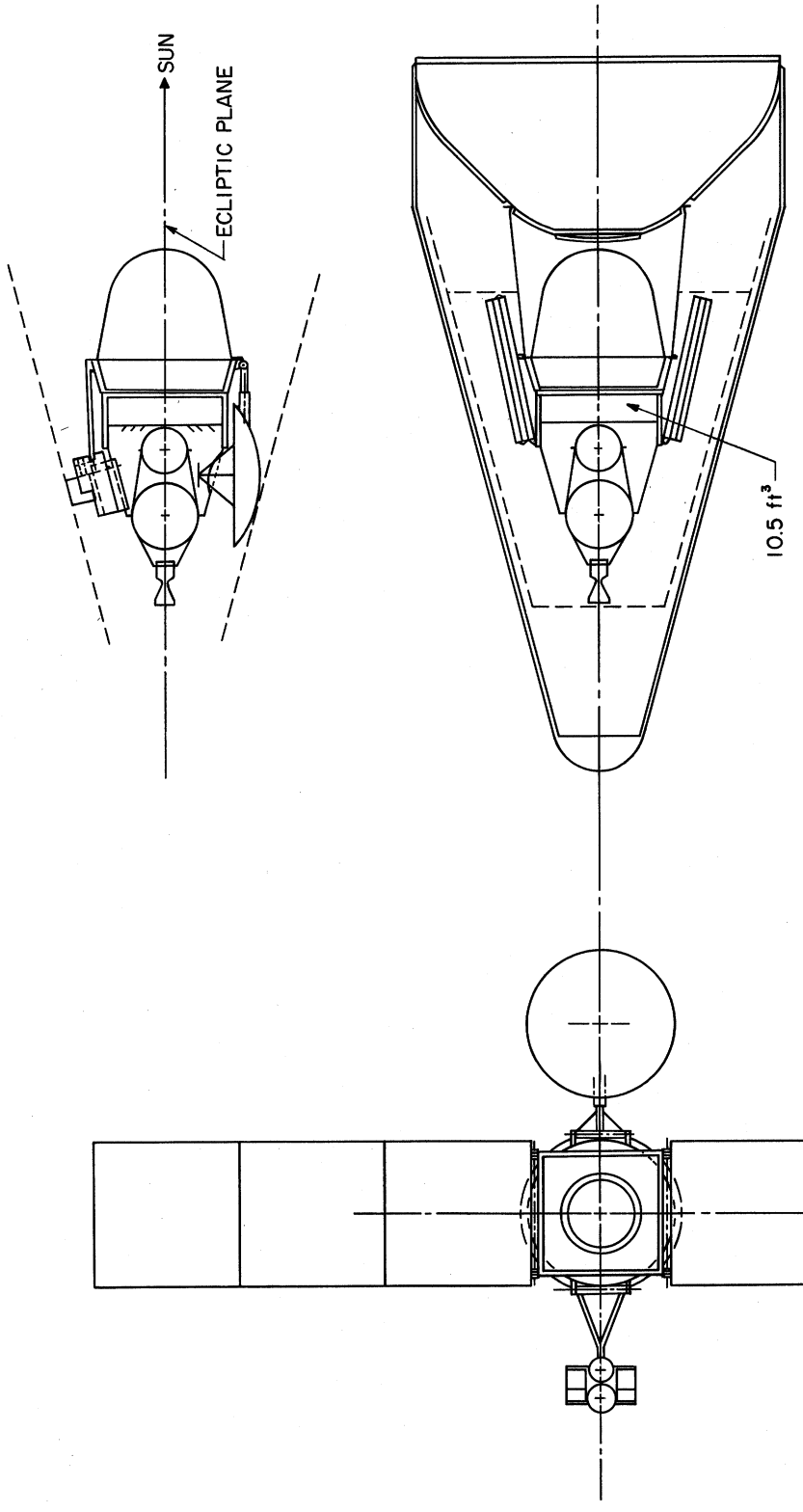

Figure B-1. Capsule aft

UNCLASSIFIED

UNCLASSIFIED

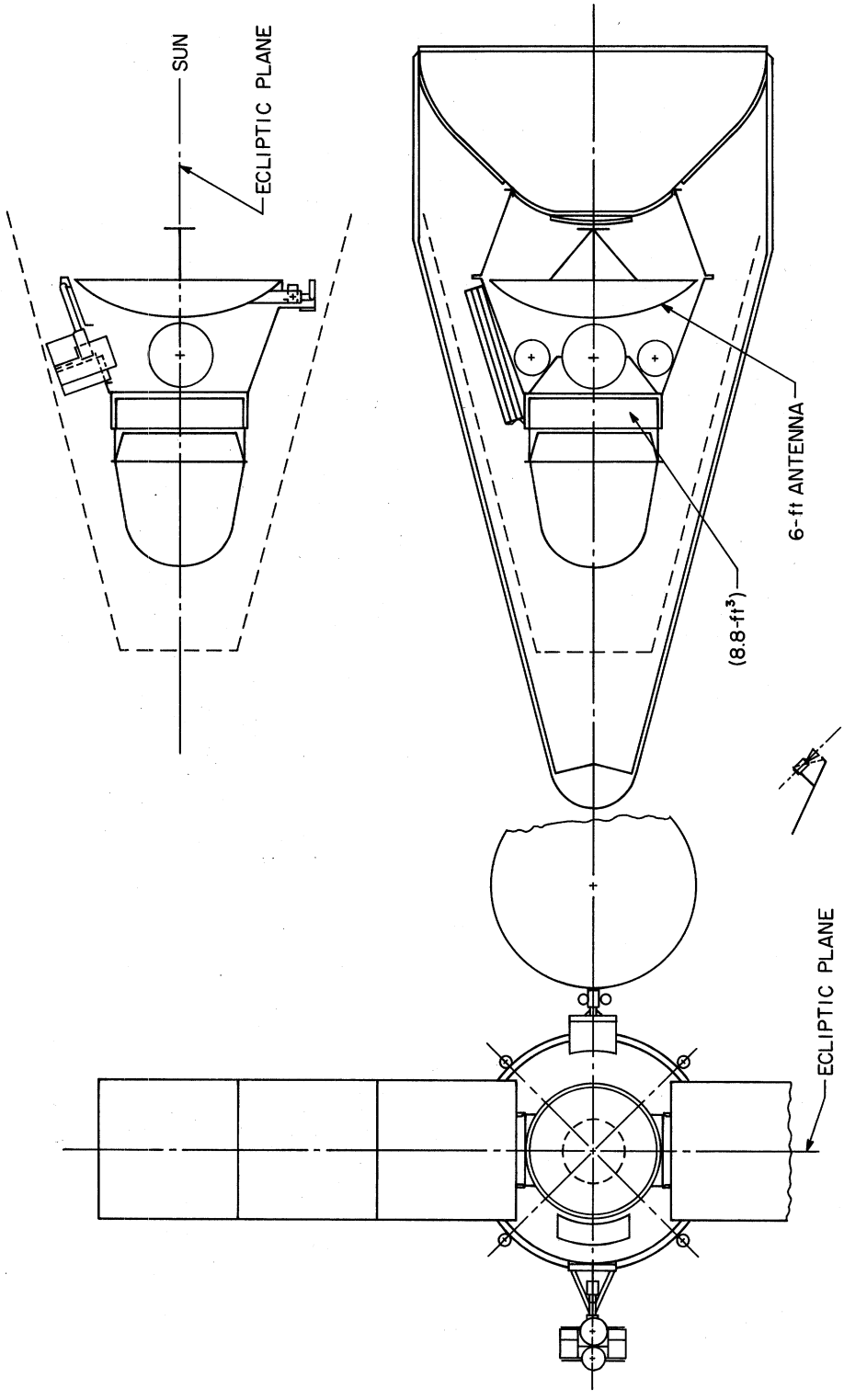

Figure B-2. Capsule forward, antenna on centerline, four motors

UNCLASSIFIED

UNCLASSIFIED

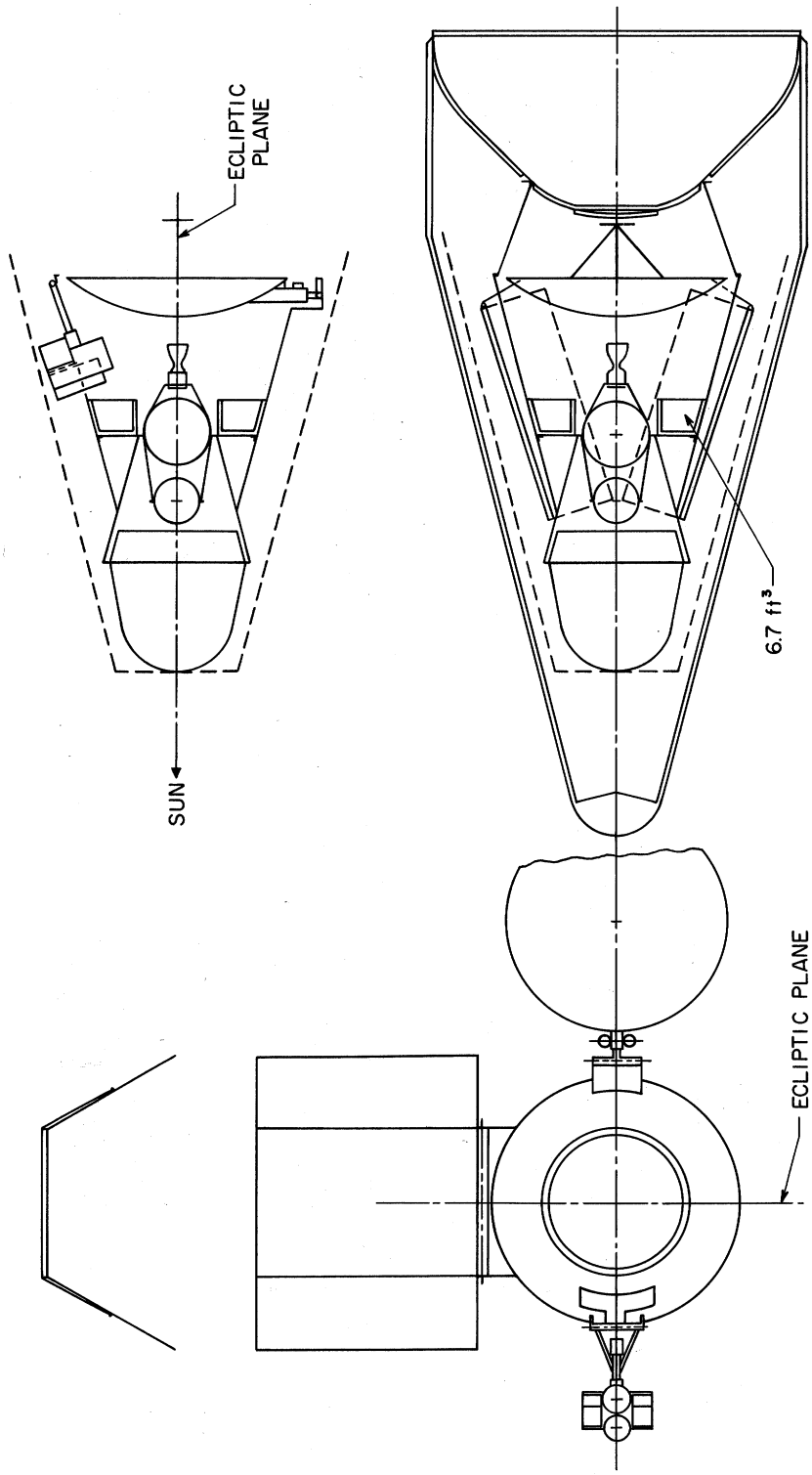

Figure B-3. Capsule forward, antenna on centerline, single motor, panels with reflectors

UNCLASSIFIED

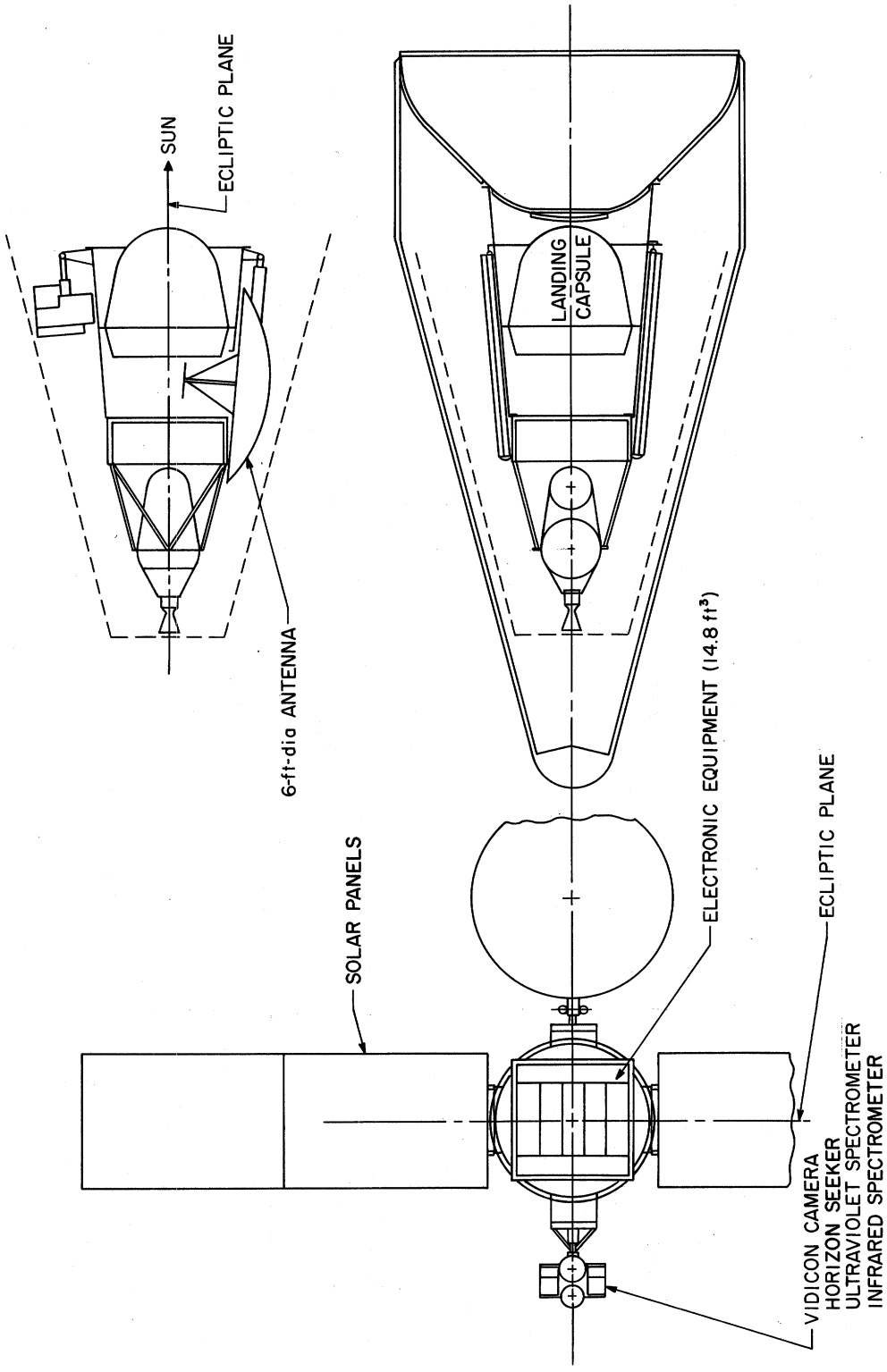

Figure B-4. Antenna off centerline, electronics on centerline

UNCLASSIFIED

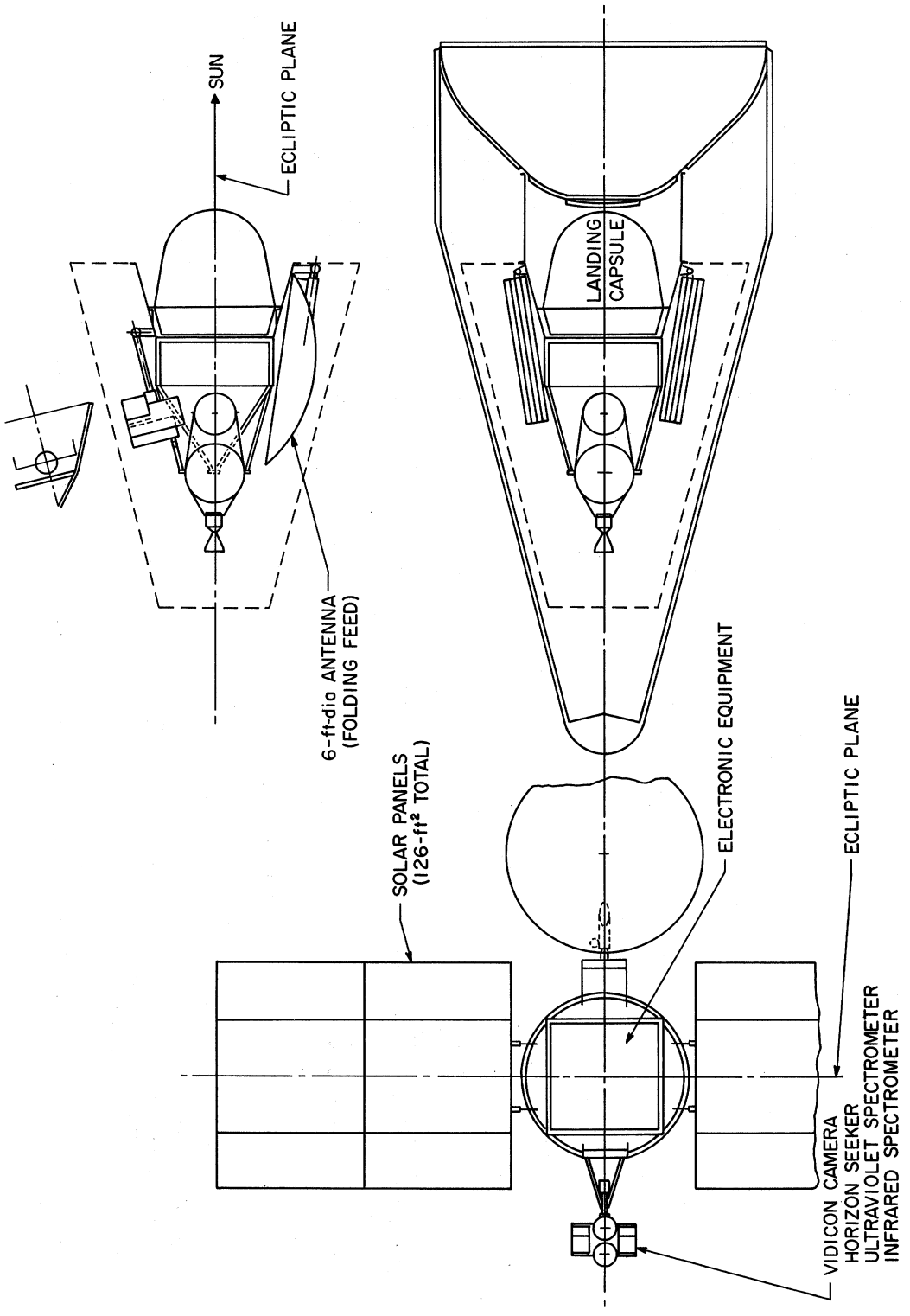

Figure B-5. Foldable feed on antenna

UNCLASSIFIED

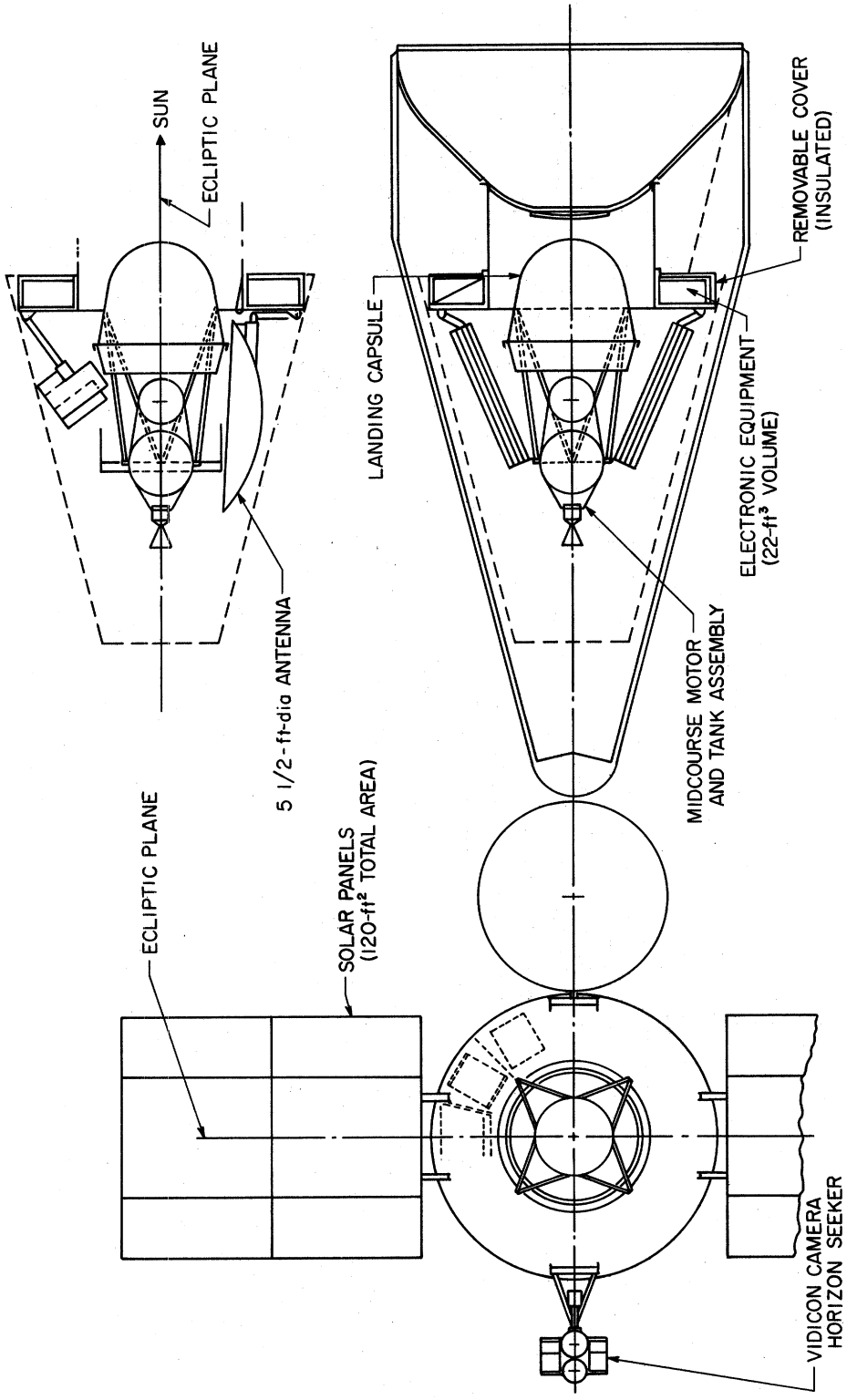

Figure B-6. Largest electronics volume

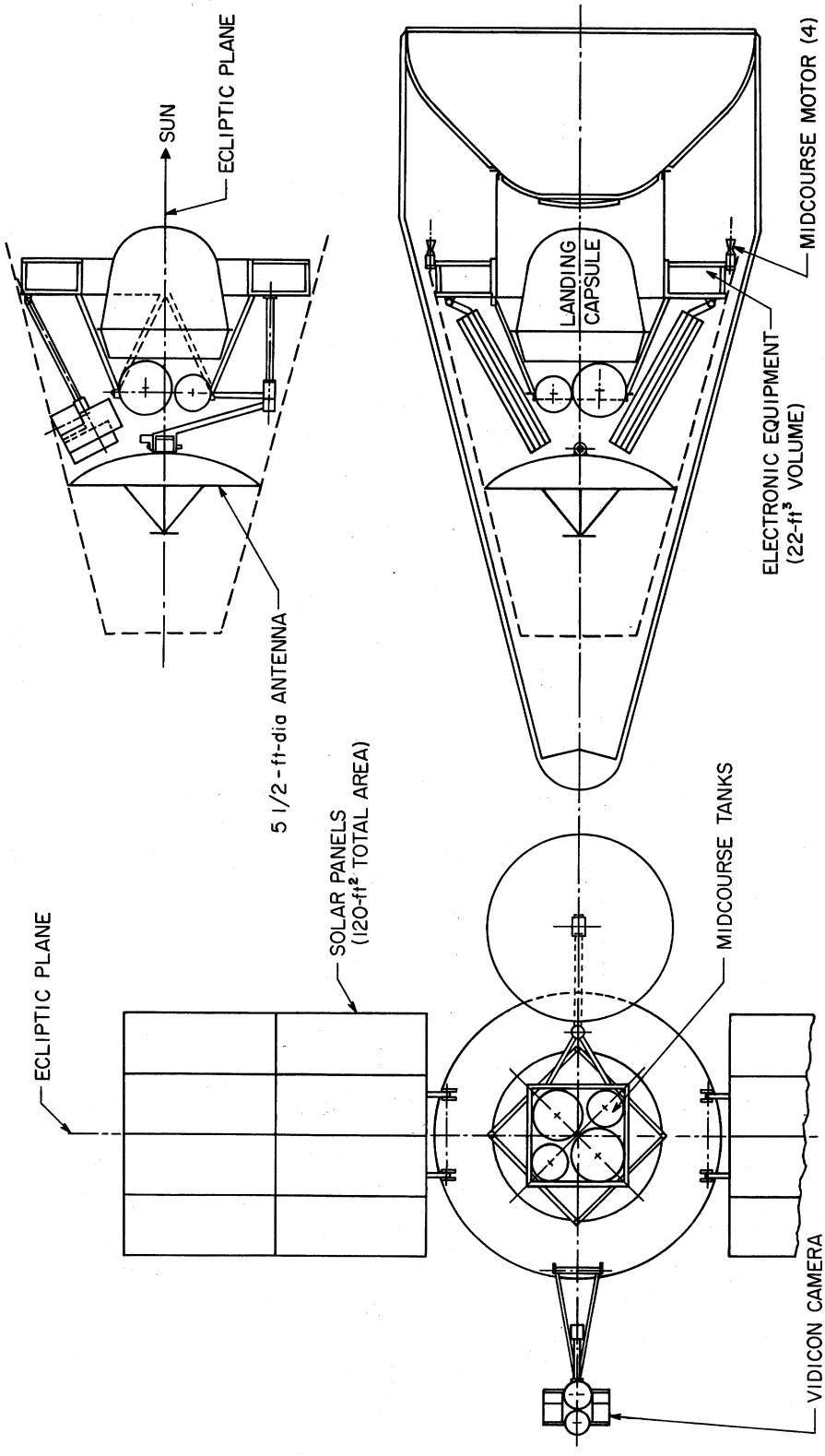

Figure B-7. Antenna forward, four motors

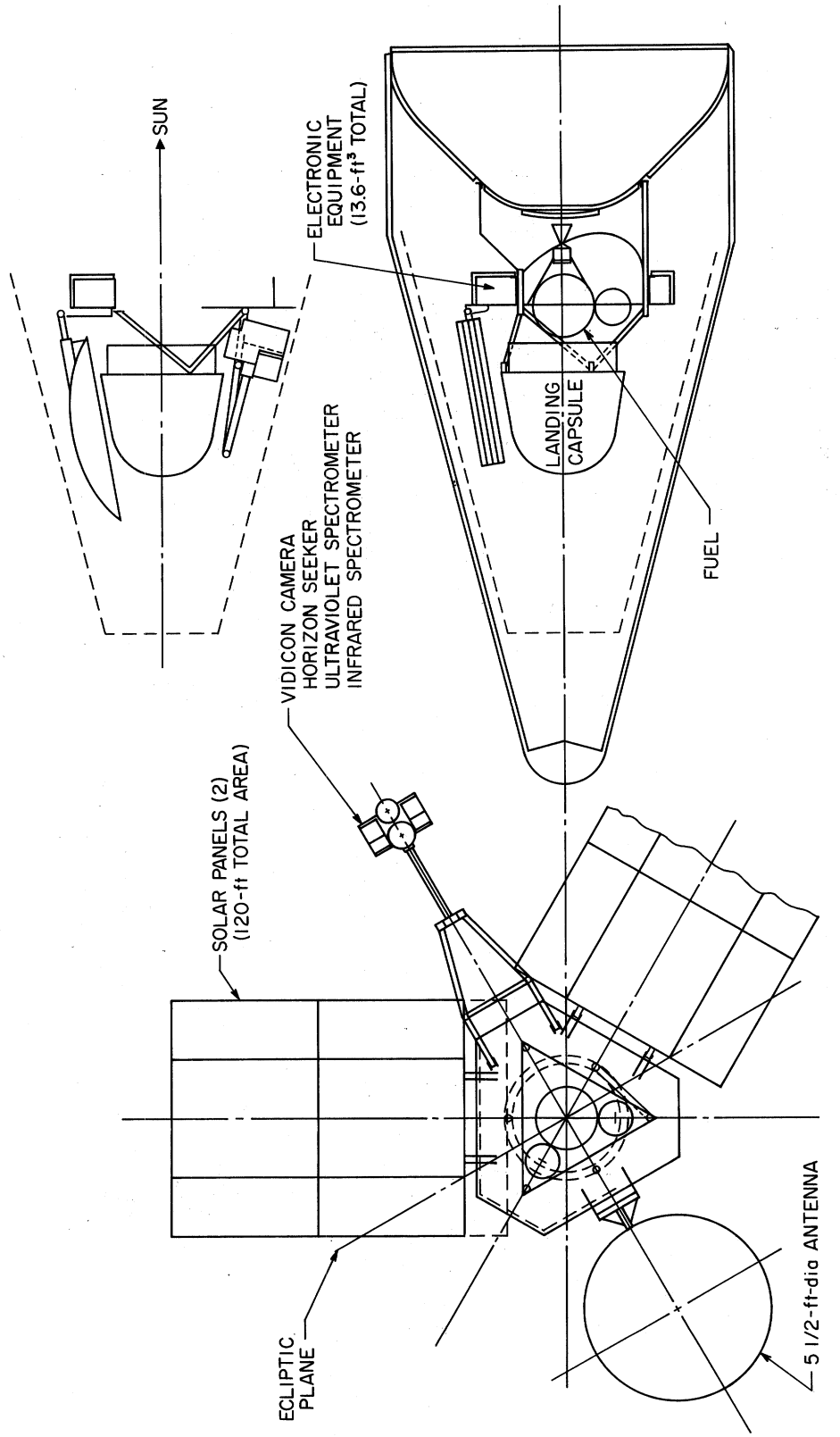

Figure B-8. Triangular structure with solar panels

UNCLASSIFIED

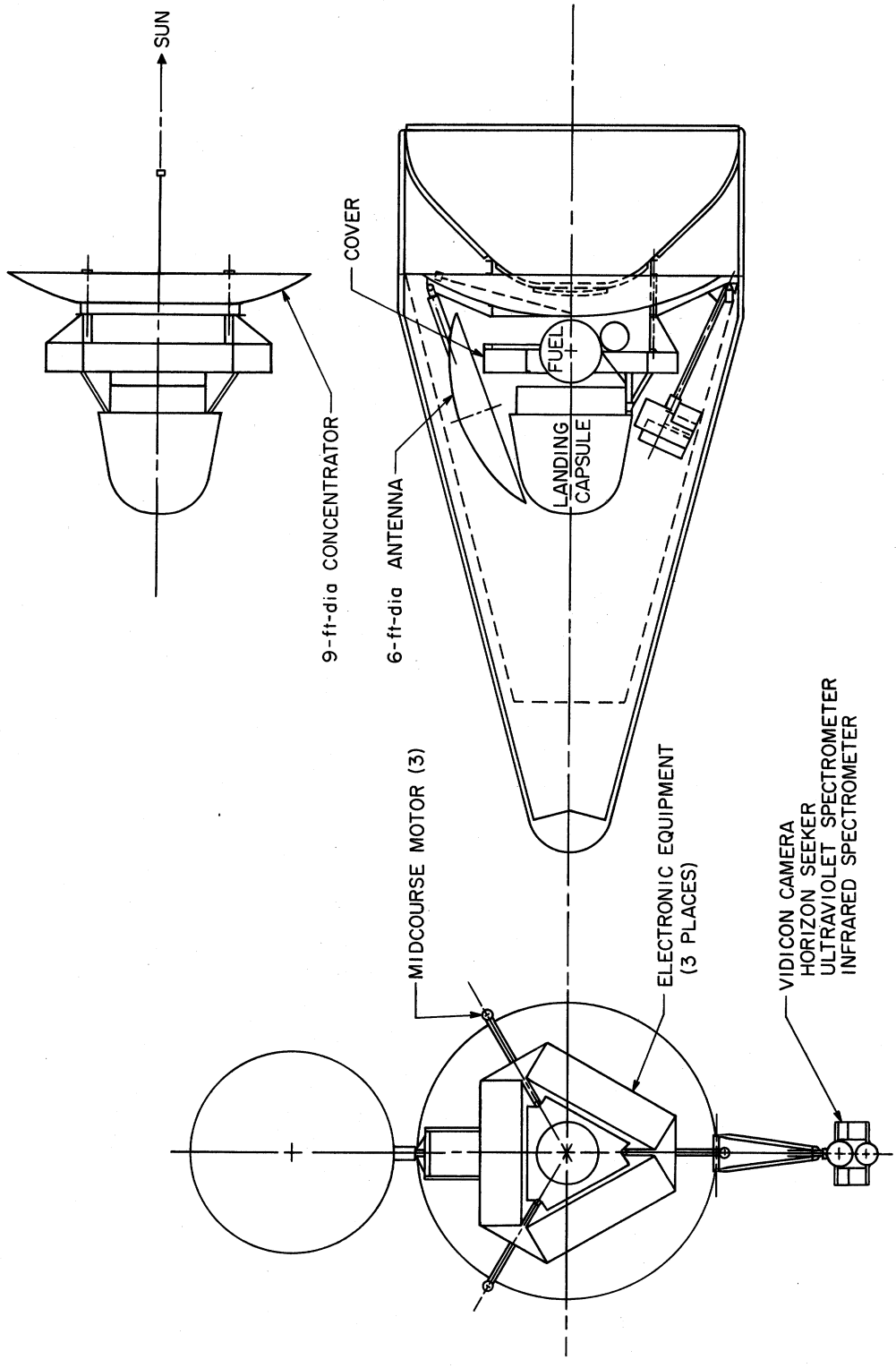

Figure B-9. Triangular structure with single fixed solar concentrator

UNCLASSIFIED

UNCLASSIFIED

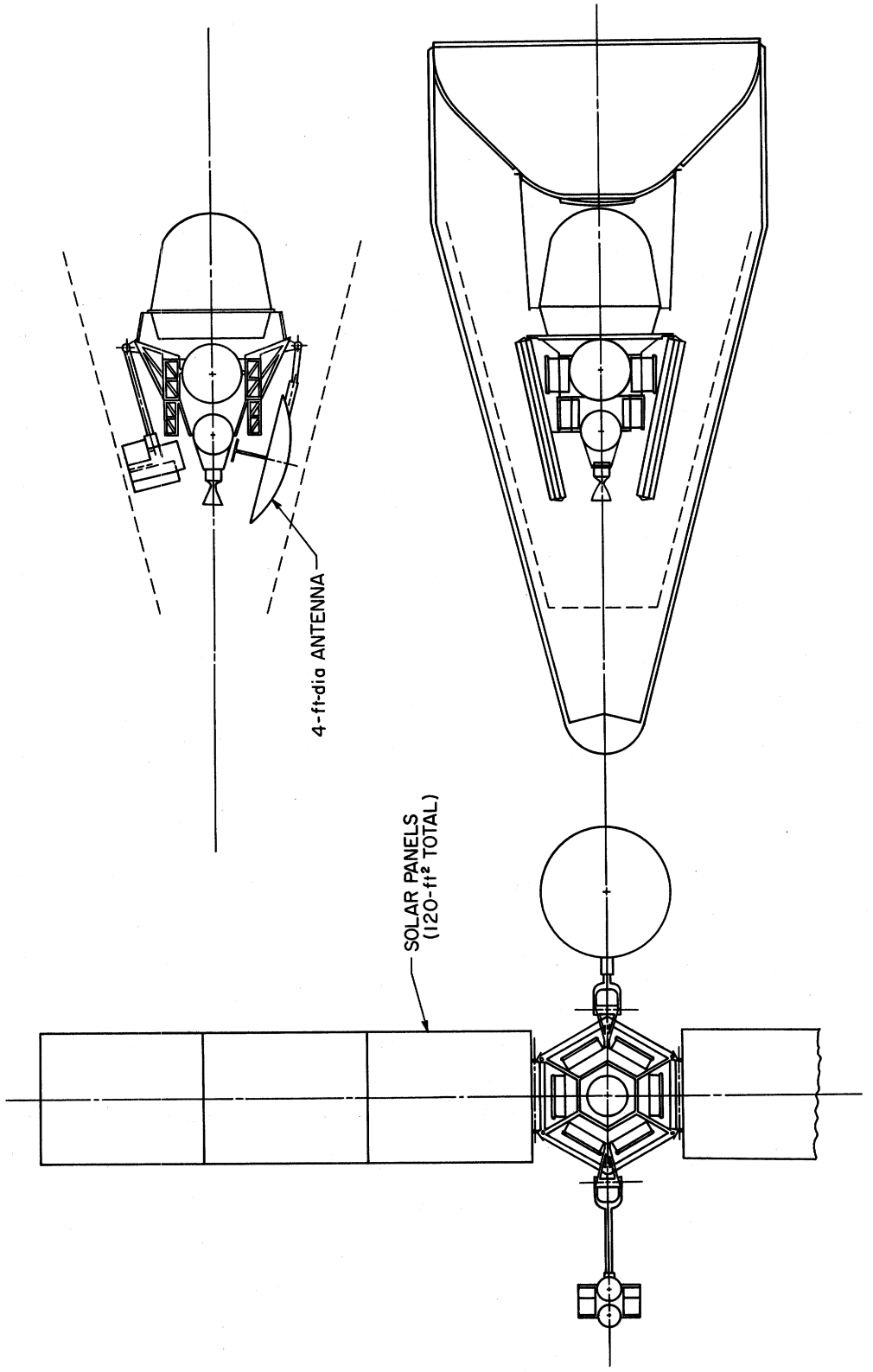

Figure B-10. Modified *Mariner A*

UNCLASSIFIED

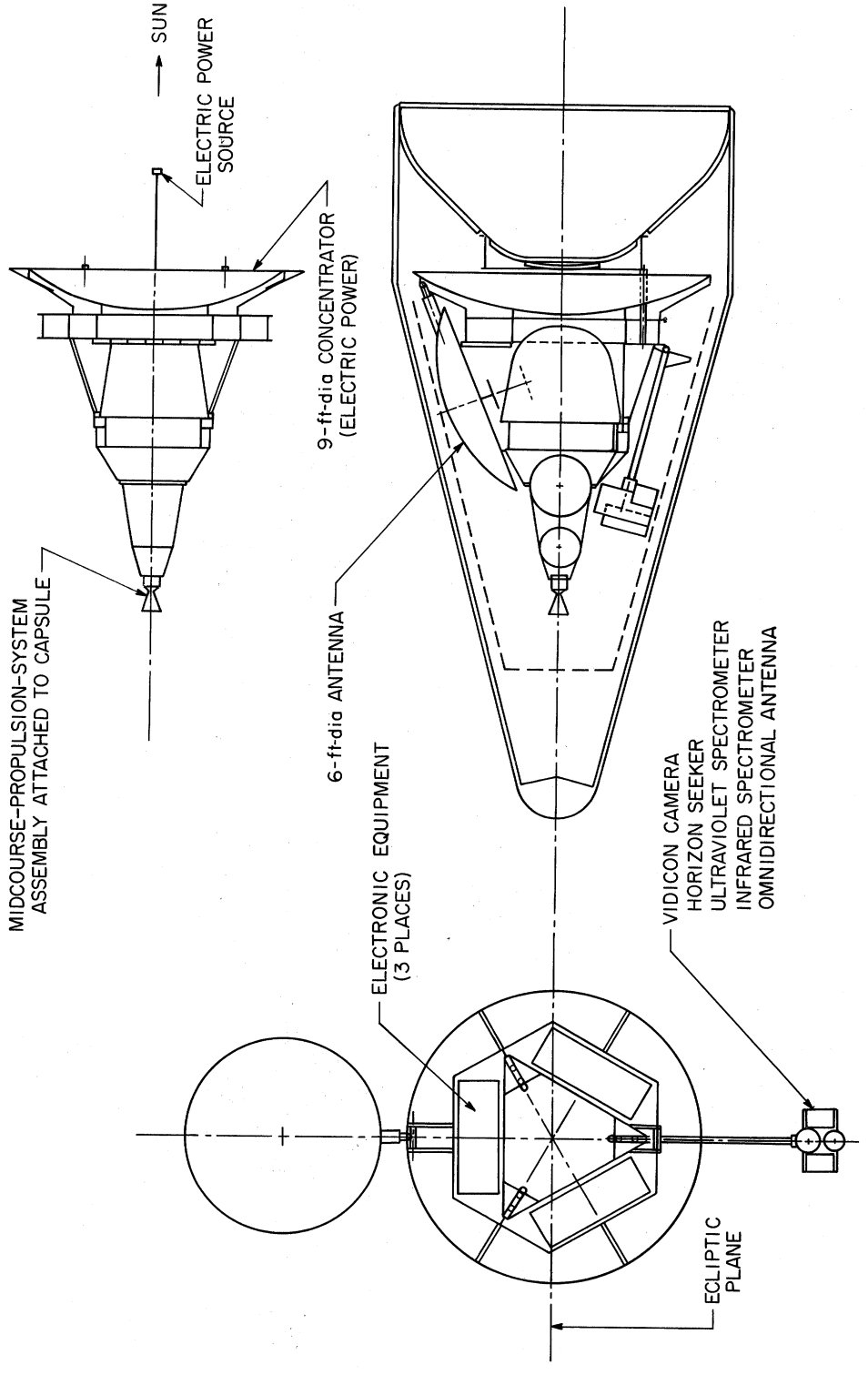

Figure B-11. Triangular structure with single fixed solar concentrator and motor on capsule

UNCLASSIFIED

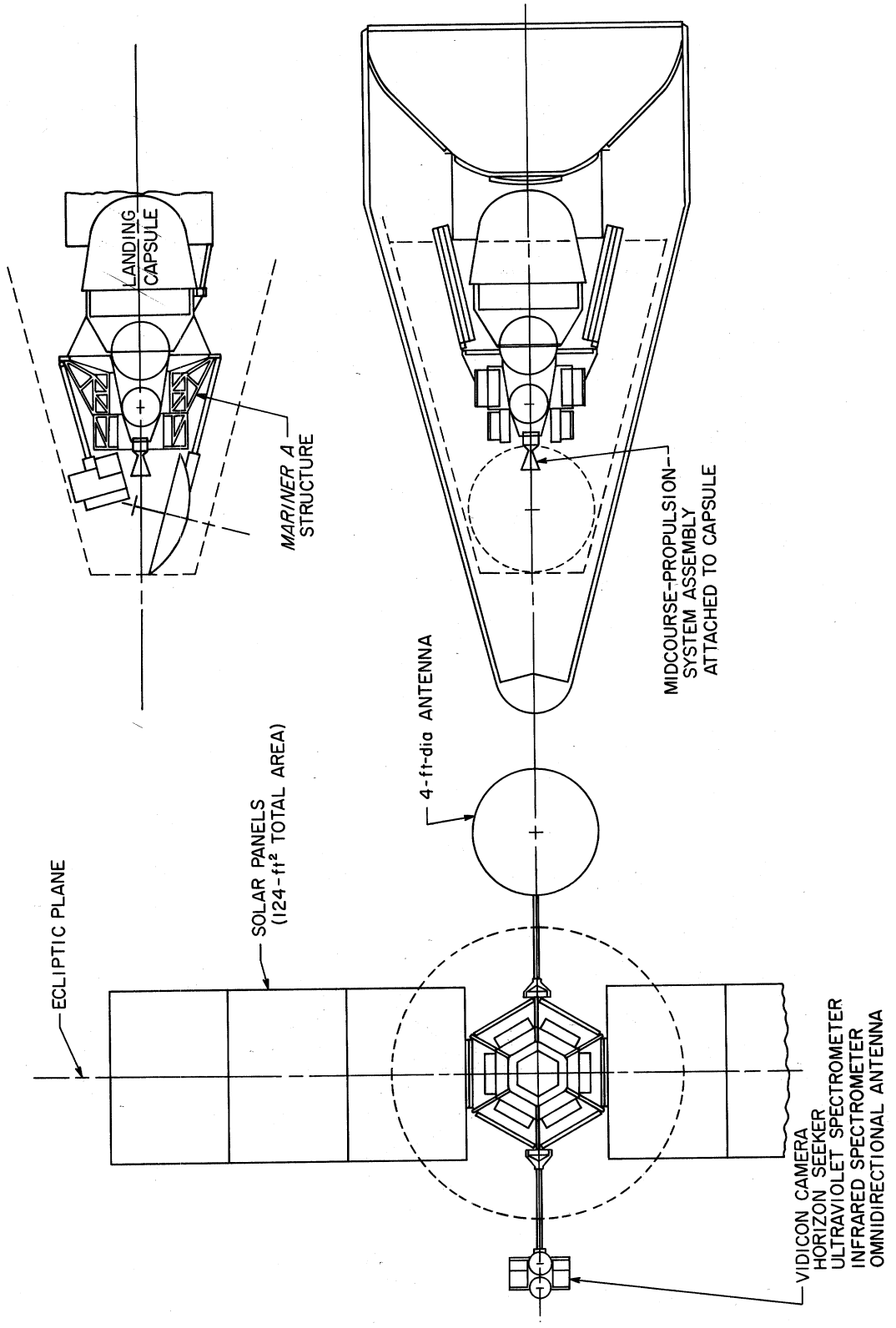

Figure B-12. Modified *Mariner A* with motor on capsule

UNCLASSIFIED

UNCLASSIFIED

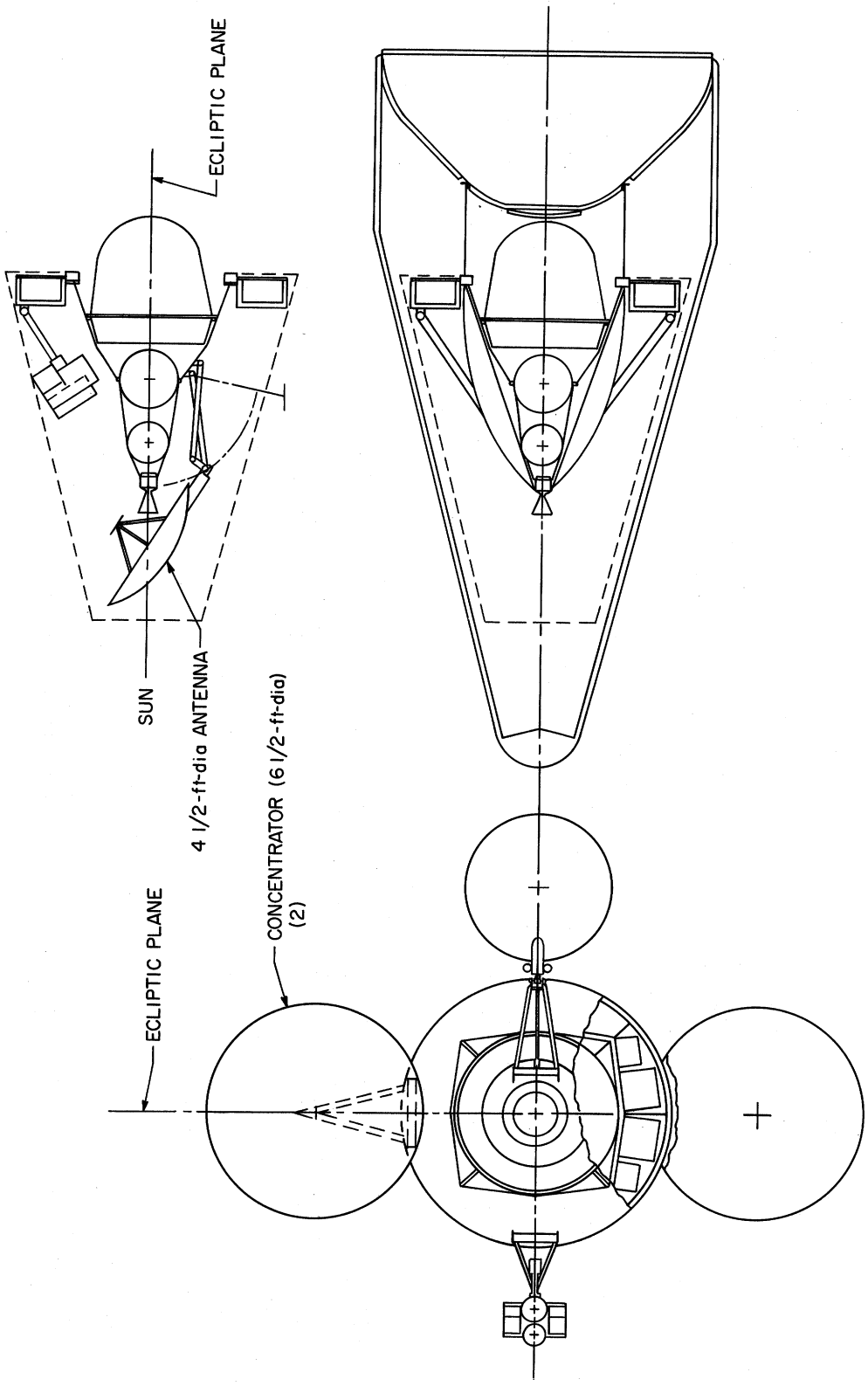

Figure B-13. Two large movable solar concentrators

UNCLASSIFIED

UNCLASSIFIED

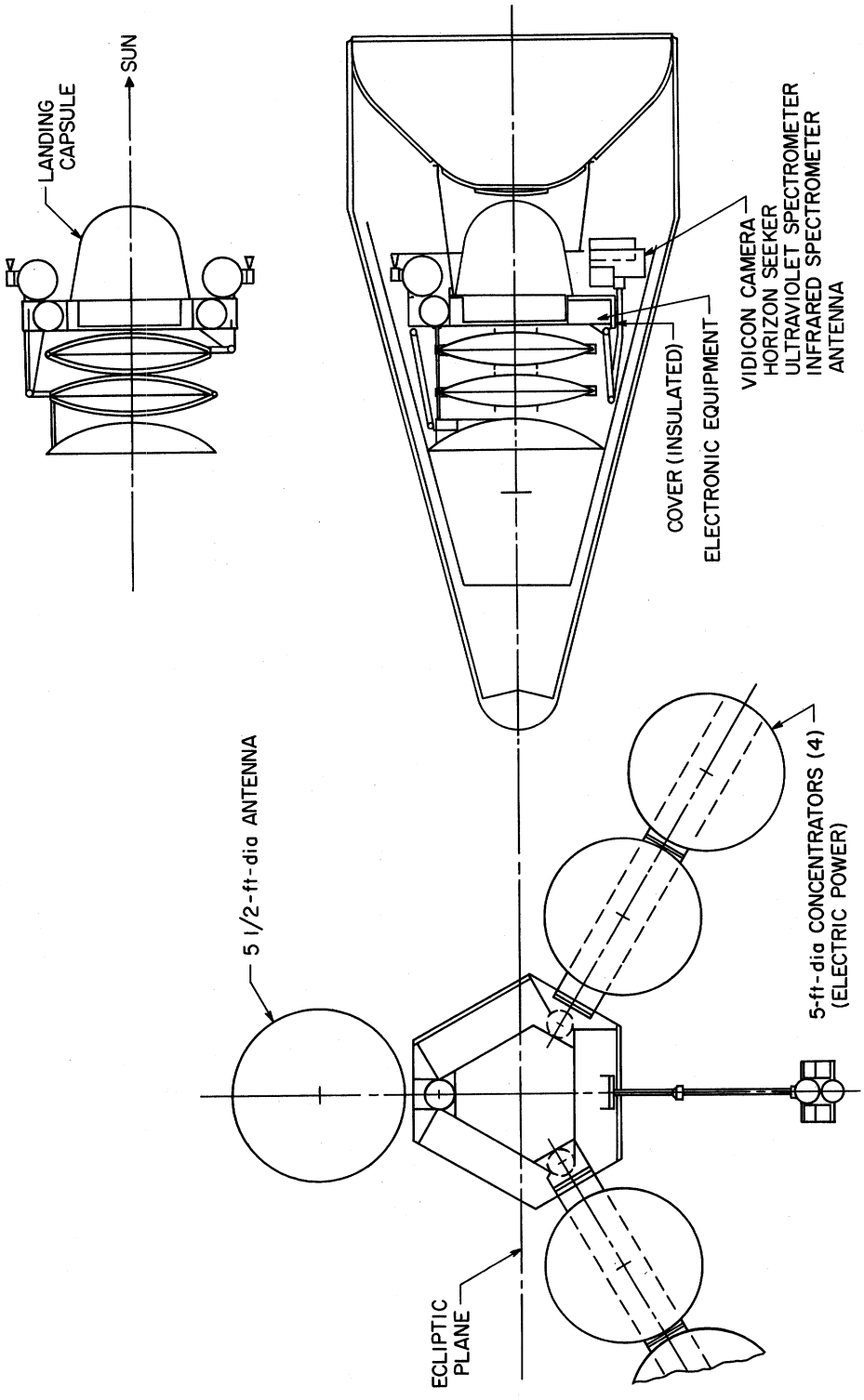

Figure B-14. Four movable solar concentrators

UNCLASSIFIED

UNCLASSIFIED

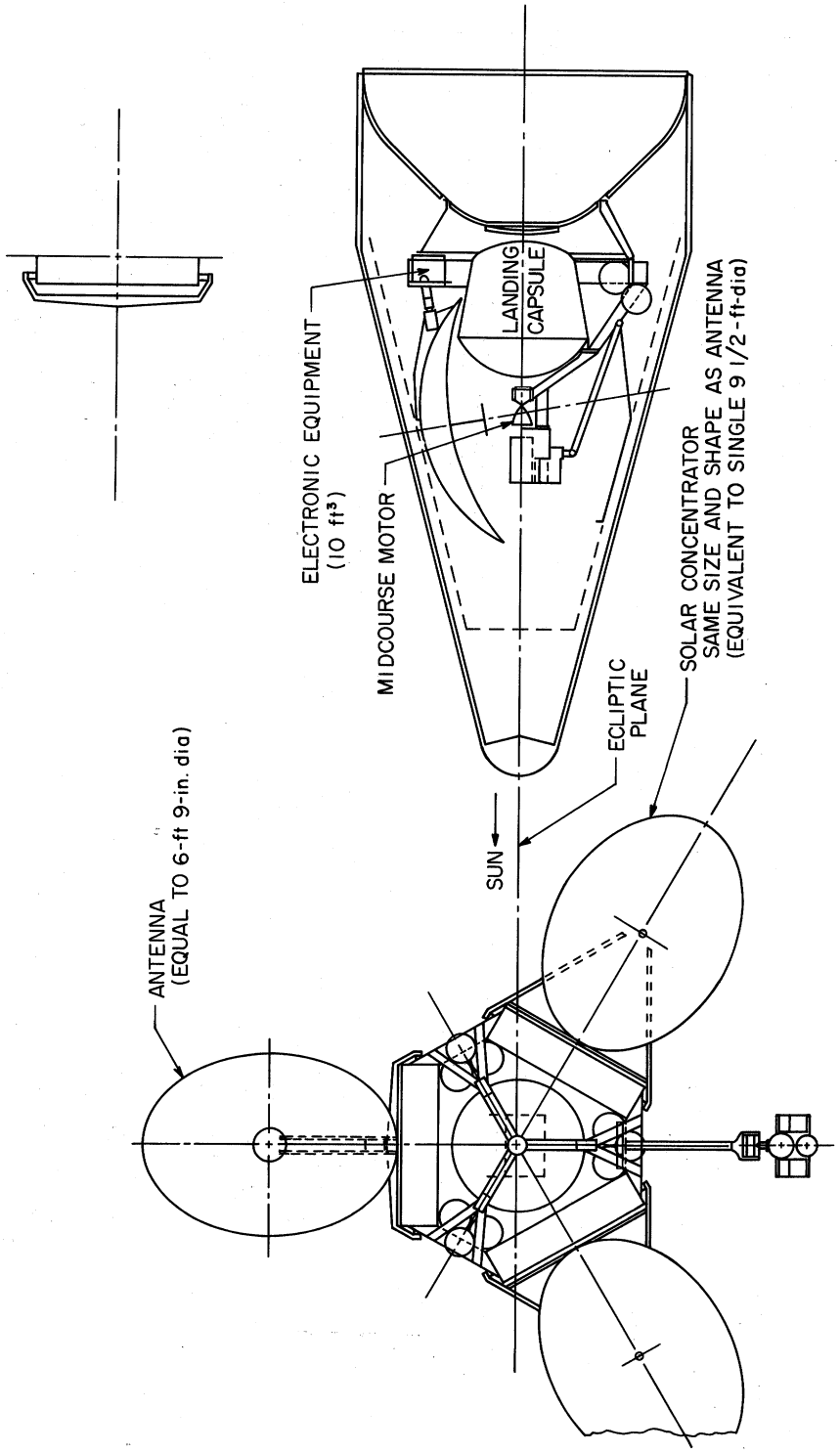

Figure B-15. Triangular structure with elliptic paraboloid concentrators and antenna

UNCLASSIFIED

UNCLASSIFIED

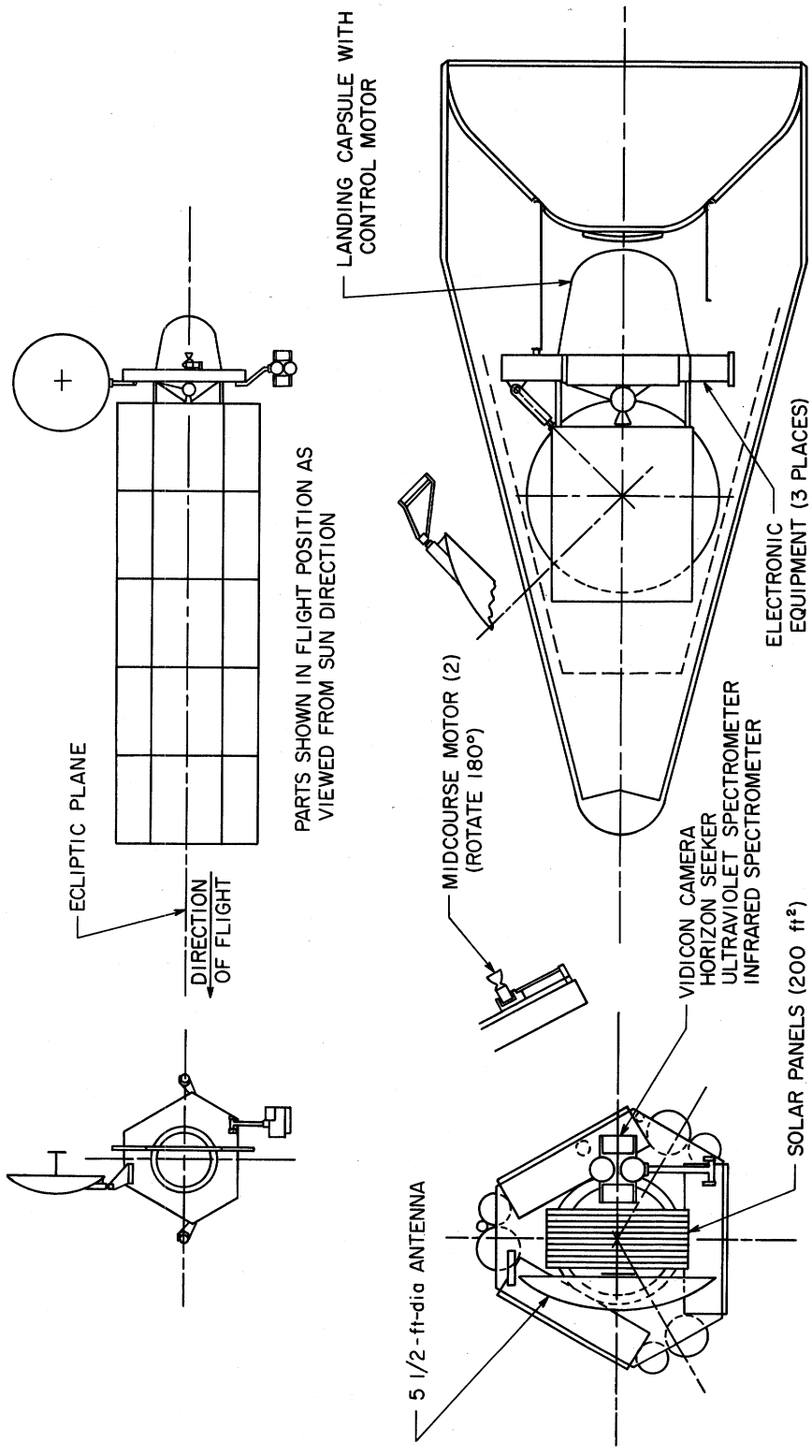

Figure B-16. Solar panels stowed along centerline

UNCLASSIFIED

UNCLASSIFIED

[redacted]

[redacted]

Classification Changed to
UNCLASSIFIED
Authority
Executive Order #11652
Date 7-30-1975 By Q. Castain

[redacted]

UNAUTHORIZED
CRIMINAL SANCTIONS
LOG-M01687

[redacted]

UNCLASSIFIED